University of Alberta

Characterization of asphaltene molecular structures by cracking under hydrogenation conditions and prediction of the viscosity reduction from visbreaking of heavy oils

by

Rosa Imelda Rueda Velásquez

A thesis submitted to the Faculty of Graduate Studies and Research
in partial fulfillment of the requirements for the degree of

Doctor of Philosophy
in
Chemical Engineering

Department of Chemical and Materials Engineering

Spring 2013
Edmonton, Alberta

Abstract

The chemical building blocks that comprise petroleum asphaltenes were determined by cracking samples under conditions that minimized alterations to aromatic and cycloalkyl groups. Hydrogenation conditions that used tetralin as hydrogen-donor solvent, with an iron-based catalyst, allowed asphaltenes from different geological regions to yield 50-60 wt% of distillates (<538°C fraction), with coke yields below 10 wt%. Control experiments with phenanthrene and 5α-cholestane confirmed low hydrogenation catalytic activity, and preservation of the cycloalkyl structures. Quantitative recovery of cracking products and characterization of the distillates, by gas chromatography-field ionization–time of flight high resolution mass spectrometry, displayed remarkable similarity in molecular composition for the different asphaltenes. Paraffins and 1-3 ring aromatics were the most abundant building blocks. The diversity of molecules identified, and the high yield of paraffins were consistent with high heterogeneity and complexity of molecules, built up by smaller fragments attached to each other by bridges. The sum of material remaining as vacuum residue and coke was in the range of 35-45 wt%; this total represents the maximum amount of large clusters in asphaltenes that could not be converted to lighter compounds under the evaluated cracking conditions.

These analytical data for Cold Lake asphaltenes were transformed into probability density functions that described the molecular weight distributions of the building blocks. These distributions were input for a Monte Carlo approach that allowed stochastic construction of asphaltenes and simulation of their cracking reactions to

examine differences in the distributions of products associated to the molecular topology. The construction algorithm evidenced that a significant amount of asphaltenes would consist of 3-5 building blocks. The results did not show significant differences between linear and dendritic molecular architectures, but suggested that dendritic molecules would experience slower reaction rates as they required more breakages to reach a given yield of distillates.

Thermal cracking of asphaltenes in heavy oils and bitumens can dramatically reduce viscosity, enabling pipeline transportation with less solvent addition. The viscosities of the products from visbreaking reactions of two different heavy oils were modeled with lumped kinetics based on boiling point pseudo-components, and with the estimation of their individual fluid properties. The model was tuned with experimental viscosity data, and provided estimations of viscosities at different temperatures with absolute average deviations lower than 31%.

Acknowledgements

First and foremost, I would like to express my deepest gratitude to Dr. Murray R. Gray. His extraordinary experience and knowledge have always been admirable, and it has been an honor and a privilege for me to have worked under his mentorship and guidance. I am very grateful for his continuous support and encouragement, and his valuable comments and suggestions to my work. Thanks to his help and diligence this work has been possible.

I would also like to extend my appreciation to my committee members: Dr. Natalia Semagina, and Dr. Jeffrey M. Stryker for the fruitful discussions and suggestions to my experimental work. I highly appreciate the valuable suggestions and ideas from Dr. Semagina during the preparation and evaluation of the iron-based catalyst.

Special thanks are due to Dr. Yadollah Maham for his collaboration and thoughts regarding the thermal gravimetric analysis of some samples during this study. I am also grateful for his advice and support.

I wish to acknowledge the help and assistance provided by Ms. Tuyet Le, Dr. Kavithaa Loganathan, Ms. Lisa Brandt, Dr. Xiaoli Tan, Mr. Keith Draganiuk, Ms. Lynette Hussain, and to the summer student Peiwen Wang. Their technical support and contribution to my experimental work have been extremely appreciated. I also owe my gratitude to Dimitre Karpuzov and Shihong Xu from the Alberta Centre for Surface Engineering and Science (ACSES) for their assistance.

My special thanks are extended to Imperial Oil and the Centre for Oil Sands Innovation - COSI, for the financial support to this project. I am especially grateful to ExxonMobil Research and Engineering Co. for the analysis performed in their facilities. Those results represented an important piece of information in this study.

I would like to express my very great appreciation to Dr. Mainak Ghosh and Dr. Amitava Sarkar, from Imperial Oil, and to Dr. Howard Freund, Dr. Kuangnan Qian, Dr. William N. Olmstead, and Dr. David Rennard, from ExxonMobil Research and Engineering Co., for their valuable feedback to my work throughout the course of this project.

Thanks go also to the Colombian National Oil Company - Ecopetrol S.A., and to some of my former colleagues in this company for providing samples of vacuum residue of Colombian heavy oils.

I want to offer my special thanks to Mr. Jose Zacharia for his help and technical assistance. I am particularly grateful to Dr. Merlyn X. Pulikkathara for her exceptional and unconditional help, support and advice. I am really short in words to express my gratitude to her.

During this time, I have also had the opportunity to interact with many brilliant and friendly people. My sincere appreciation is extended to some of the former Ph.D. students in our group: Dr. Arash Karimi, Dr. Ali Alshareef, Dr. Reza Bagheri, and Dr. Marzie Derakhshesh. Their advice, support, encouragement, the fruitful conversations, and their friendship have been invaluable.

Dr. Cedric Laborde-Boutet, postdoctoral researcher, provided me with very valuable suggestions for my simulation work. His comments and advice are highly acknowledged.

My heartfelt gratitude goes to my beloved family for their constant moral support, and motivation. My mom, dad, sister, brothers, nephews, and nieces have been such a blessing in my life. My special thanks go to my uncle Alvaro Rueda and his wife for their incommensurable and constant support and generosity.

I am deeply in debt to Alice and Rene Loe, my former landlords. Not enough words to thank all their invaluable help, advice, and kindness.

I want to express my appreciation to the wonderful friends I have met in Edmonton, and to those who always keep in touch and have played an important role during my career as well as my life. They are: Silvia, Kelly, Gustavo, Carolina, Somayeh, Alfonso, Lina, Carolina F., Héctor, Sabereh, Juan Pablo, Eliana, Libardo, Laura, Samuel, Jose Luis, Mariangel, Roberto, Luis Carlos, Lisa, Mingyang, Weida, Shanshan, and my dear friends from the praying group. I cannot really count one by one all the wonderful people who have shared their time and generosity with me.

Last but not least, thanks to God for the infinite blessings in my life.

Table of contents

List of Tables

List of Figures

List of Symbols, Nomenclature and Abbreviations

(Context dependent)

References are related to Chapter 5.

Greek Letters

α = positive empirical constant in Shu et al.[12] liquid mixture viscosity equation

η = kinematic viscosity, cSt or m^2/s

μ = dynamic viscosity, cP or Pa.s

ρ = density, kg/m^3

τ = residence time, h or min

Nomenclature

a = parameter in Mehrotra[24] viscosity correlation

= adjustable parameter for the viscosity of the vacuum residue fraction

= stoichiometric coefficient in kinetic model introduced by Ayasse et al.[17]

a_{ij} = binary parameter in Modified Andrade equation[38]

A = parameter in Andrade or de Guzman[34] viscosity correlation

= parameter in Vogel[35] viscosity correlation

= adjustable parameter in Riazi[40] method

= parameter in API Procedure 6A3.5[42]

b = adjustable parameter for the viscosity of the vacuum residue fraction

= stoichiometric coefficient in kinetic model introduced by Ayasse et al.[17]

b_1 = parameter in ASTM[36] or Walther equation[37]

b_2 = parameter in ASTM[36] or Walther equation[37]

b_{ij} = binary parameter in Modified Andrade equation[38]

B = parameter in Andrade or de Guzman[34] viscosity correlation

= parameter in Vogel[35] viscosity correlation

= adjustable parameter in Riazi[40] method

= parameter in API Procedure 6A3.5[42]

c = stoichiometric coefficient in kinetic model introduced by Ayasse et al.[17]

c_{ij} = binary parameter in Modified Andrade equation[38]

C = parameter in Vogel[35] viscosity correlation

= parameter in API Procedure 6A3.5[42]

D = parameter in API Procedure 6A3.5[42]

d_{ij} = binary parameter in Modified Andrade equation[38]

Denl = liquid density in API Procedure 6A3.5[42], lb_m/ft^3

Distillates = distillates concentration, kg/m^3

E = parameter in API Procedure 6A3.5[42]

f = mole or mass fraction

= adjustable parameter in ASTM Liquid Mixture Viscosity[39]

Gas Oil = gas oil concentration, kg/m^3

k', k'_1, k'_2 = rate constants in kinetic models with stoichiometric coefficients, h^{-1}

k_1-k_5 = rate constants in kinetic models, h^{-1}

k_{123} = lumped kinetic rate constant, h^{-1}

k_{45} = lumped kinetic rate constant, h^{-1}

k_{ij}, k_{ji} = symmetric binary parameter in ASPEN Plus™ - Aspen Liquid Mixture Viscosity[38] correlation

l_{ij}, l_{ji} = antisymmetric binary parameter in ASPEN Plus™ - Aspen Liquid Mixture Viscosity[38] correlation

M = molar mass, kg/kmol

$\bar{M}$ = average mixture molar mass, kg/kmol

MeABP = Mean average boiling point, °R

n = number of experimental measurements

= number of reactions

Naphtha = naphtha concentration, kg/m^3

SG = specific gravity

SG_0 = adjustable specific gravity parameter in Riazi[40] method

t = reaction residence time, h

T = temperature, K

T_b = mean boiling point or 50% boiling point, K

T_0 = adjustable temperature parameter in Riazi[40] method

VR = vacuum residue concentration, kg/m^3

w = mass fraction

W = mass fraction

x = mole fraction

x_c = cumulative weight or volume fraction

X = parameter in Shu et al.[12] liquid mixture viscosity equation

= mole fraction or mass fraction

= vacuum residue conversion

Subscripts

0 = initial value, initial concentration

A = component A

av = average

i = component i in a mixture

exp = experimental

F = feed, original heavy oil

fi = fraction or pseudo-component i

j = component j in a mixture

m = liquid mixture

pred = prediction

VR = vacuum residue

Abbreviations

1-MN = 1-methylnaphthalene

AAD = average absolute deviation

ABP = average boiling point

DHA = 9,10-dihydroanthracene

DHP = 9,10-dihydrophenanthrene

ECS = extended corresponding states method

FBP = final boiling point

G = gas

GLN = gasoline

HO = heavy oil

IBP = initial boiling point

LC = liquid crystal

LGO = light gas oil

MCR = microcarbon residue

Py = pyridine

Q = quinoline

SG = specific gravity

SimDist = simulated distillation analysis

SSR = sum of squared errors

TGA = thermal gravimetry analysis

THQ = 1,2,3,4-tetrahydroquinoline

TN = tetralin (1,2,3,4-tetrahydronaphthalene)

Tol = toluene

UofA = University of Alberta

UOP K = UOP (or Watson) K characterization factor

VGO = vacuum gas oil

VR = vacuum residue

1 Introduction

A confluence of different factors has made the world consider heavy oils and bitumen as important actors in the energy basket. These alternative oil sources have become more attractive as the world oil demand increases, and the depleting conventional and lighter oil sources are traded in the market at high prices as valuable commodities. Massive deposits of natural bitumen are present in Canada, and of extra heavy oil in Venezuela, with remaining reserves of 26.8[1] and 9.2[2] billion cubic meters (10^9 m^3), respectively.

However, as oil becomes heavier, the different operations of extraction, processing and transportation become more challenging[3] due to higher viscosities and densities, increasing heteroatom content, higher aromaticity (which is in accordance with lower hydrogen content), and most significantly due to the increased concentration of asphaltenes.

Asphaltenes, defined as the toluene soluble, but *n*-alkane insoluble fraction of oil, constitute the most complex material present in petroleum. These dark brown to black solids[4] are characterized by their high density, reported around 1,200 kg/m^3,[5, 6] high content of sulphur, nitrogen, oxygen, and metals (Ni and V), low H/C ratios, and high aromaticity, with reported fractions of aromatic carbon in the range of 0.43 to 0.69.[5, 7] Calemma et al.[5] evaluated asphaltenes from different sources, and the elemental composition revealed contents spanning 1.9–10.8 wt% for sulphur, 1.0-1.9 wt% for nitrogen, and 0.8-6.2 wt% for oxygen (estimated by difference). Heavy oils and bitumens can exhibit a wide range of

asphaltene concentrations, and published data show that yields of *n*-C_5 asphaltenes greater than 20 wt% can even be expected.[6]

Many problems arise from the presence of asphaltenes in oil. Some of these issues have been summarized by Speight,[4] and comprise a wide range of upstream and downstream operations. Thus, the flocculation and or sedimentation of asphaltenes have been found to be related to different types of fouling that affect flow assurance, mainly because of the plugging and deposition during oil extraction and transportation,[4] and that also compromise refining operations because of the formation of coke.[3]

Speight[4] also mentioned other issues associated with asphaltenes, such as the precipitation and formation of deposits during the storage of crude oil and products, and also during blending operations, as a result of their destabilization in the medium. Due to their capability to form emulsions, asphaltenes can also contribute to water contamination of crude oil, via water-in-oil emulsions. Furthermore, their high concentration in fuel oils leads to poor combustion properties.

Asphaltenes have also been an important factor to consider in catalytic processing. These large and complex molecules can plug the catalyst pores, or form deposits of coke on the catalyst surface, hindering the access of the molecules to the active sites,[8] and therefore can cause catalyst deactivation. Moreover, their high heteroatom content can lead to deactivation by poisoning or metals deposits.[9, 10]

These difficulties seem independent of the content of asphaltenes in the oil. In production, asphaltene precipitation has demonstrated to be more problematic in light crude oils, with low asphaltene content, than in heavier crude oils.[11] However as their concentration increases due to processing or, as mentioned before, by the progressing interest in heavier oil sources, viscosity and processing issues are exacerbated.

The economic implications of these production and processing issues can partly explain why asphaltenes have been a focus of attention for many decades. In general, the chemical composition and structure determines the properties of the materials;[12] therefore, it is expected that a better knowledge of the composition of asphaltenes can lead to a better understanding of their behavior and eventually solutions could be proposed to mitigate these problems. However, the identification as a solubility class makes them encompass a broad range of compounds that can precipitate out from the oil medium not only by insolubility, but also by coagulation of nanoaggregates,[13] similar to colloidal suspensions. This heterogeneity is at the same time a source of uncertainty in the determination of their molecular composition.

The difficulties in analysis due to the high complexity of asphaltenes, high molecular weight and aromaticity, are aggravated by their high tendency to aggregate in solution.[14] These characteristics hinder the efforts to compile a complete molecular description that can explain the observed complex behavior and that also demonstrates consistency with the data obtained from their

processing.[15] This molecular description should then include not only the size distribution, but also the architecture of the molecules.

Thus, the continuing debate around asphaltenes has been the result of dissimilar experimental observations that have led to the formulation of contrasting conclusions regarding the predominant molecular motifs. Yen et al.,[16, 17] later supported by Mullins and coworkers,[18-20] have described asphaltenes as single large polycyclic aromatic hydrocarbons (PAHs) with naphthenic and peripheral alkyl substituents. This molecular representation was accompanied by a hierarchical model to explain asphaltenes aggregation, where the molecular stacking was mainly attributed to π-π interactions between the aromatic sheets. However, the analytical techniques, the instrumental calibration, and the interpretation of the results that led to propose and support this "island" model have been questionable.[21, 22]

In contrast, the identification of diverse smaller molecules in the distillable products from the cracking of asphaltenes, including aromatic, naphthenic, and heteroatomic compounds,[23, 24] led to the "archipelago" model. Thus, the description of asphaltenes built up by smaller molecules linked by alkyl and thioether bridges[25, 26] was able to reconcile the observations made during thermal processing of asphaltenes.[15] For example, the thermal cracking approach reported by Karimi et al.[7] yielded 15-20% of analyzable material and the characterization of this fraction confirmed the existence of archipelago structures in asphaltenes.

The supramolecular assembly model proposed by Gray et al.,[13] provided a different perspective to gain a better understanding of this complex material.

Consistent with the archipelago type of molecules, the aggregation of asphaltenes was explained due to the individual contributions of different interactions including the following: hydrogen bonding, acid-base interactions, metal coordination, hydrophobic pockets promoted by cycloalkyl and alkyl groups, and also due to π-π stacking. This last one had been thought to be the main factor in the formation of asphaltene clusters, according to the island model.

At this point, the abundant literature around asphaltenes has indicated that more definite conclusions could be drawn if a significant fraction of the asphaltenes could be properly characterized. However, when it comes to such complex systems, it is important to ensure that the analytical methods are properly calibrated and can yield meaningful results. This is not a straightforward task for asphaltenes since most of the available techniques are calibrated for lighter fractions in the distillable range. Additionally, the yield of distillable compounds from thermal cracking of asphaltenes is limited by the high yields of coke.[7, 27]

Thus, this research work was intended to characterize the molecular structures present in asphaltenes by cracking under hydrogenation conditions. The use of tetralin as hydrogen-donor solvent and a catalyst with mild hydrogenation activity, i.e. an iron-based catalyst, in a hydrogen atmosphere, provided favorable conditions to suppress the coke formation and obtain high yields of distillates. Control experiments with model compounds confirmed the preservation of the ring structures under the reaction conditions. The reactions performed in 15 ml stainless steel batch microreactors allowed quantitative recovery of the cracking products, and provided enough sample for the characterization analysis. A

calibrated high resolution GC-MS method was used for the identification and quantification of the molecules present in the distillable fraction of the liquid products. Thus, this approach provided quantitative and reliable results, and the results recognized an important presence of bridged structures in asphaltenes.

This thesis has been organized in seven chapters, and four of them contain individual research studies presented in paper format with their own bibliography. Chapter 1 was designed to introduce the research topics covered in the thesis, and provide the reader with an overall description and background to understand the scope and significance of this work.

Chapter 2 presents the experimental work carried out to characterize the molecular structures present in asphaltenes by cracking under hydrogenation conditions. This study constitutes the second phase of a project for bitumen characterization sponsored by the Centre for Oil Sands Innovation (COSI) at the University of Alberta, and was made in partnership with ExxonMobil Research and Engineering Co. A version of this work has been submitted for publication in a peer-reviewed scientific journal.

Chapter 3 examines different solvents, with and without hydrogen-donation capacity, during the cracking of asphaltenes under hydrogenation conditions. These solvents are compared in terms of coke yield with the reactions in presence of tetralin, which was chosen as the hydrogen-donor solvent in the study presented in Chapter 2.

According to the evidence of significant amounts of bridged-structures, a Monte Carlo simulation was developed to gain insight into the molecular

architecture. Thus, in Chapter 4, the distribution of products from the cracking of asphaltene molecules that were constructed stochastically with linear and dendritic topologies are compared to the available experimental data from Chapter 2. This chapter also describes the generation of the probability density functions (PDFs), required as input for the simulation, and the approach that was used to construct and crack populations of asphaltenes conveniently represented in matrix form.

Chapter 5 moves away from the study of asphaltenes, but deals with one of the main challenges that the oil industry faces with the growing interest in heavy oils: pipeline transportability. Viscosity reduction via visbreaking is evaluated by the development of a fluid model, based on boiling point pseudo-components, which is coherent with the high complexity of heavy oils.

The relation between these separate studies is evidenced in the synthesis presented in Chapter 6, and the conclusions and recommendations are summarized in Chapter 7.

Appendix 1 illustrates the heating curves for the batch microreactor at different temperature set points, which correspond to the reaction temperatures of the experiments presented in Chapters 2, 3, and 5. Appendix 2 briefly describes the main inconveniences that hampered the aromaticity estimations of the reaction products by NMR analysis. A third appendix summarizes the correlations found for different measured or estimated variables involved in the study about asphaltenes characterization presented in Chapter 2. The routines programmed in MATLAB® (Version R2011b, The MathWorks, Inc., USA), for the Monte Carlo

simulation discussed in Chapter 4, are described in Appendix 4, including a brief explanation of the inputs and outputs, and the lines of code.

1.1 References

1. Energy Resources Conservation Board. *Alberta's Energy Reserves 2011 and Supply/Demand Outlook 2012–2021, ST98-2012;* Calgary, AB, Canada, 2012; pp 290.
2. World Energy Council. *2010 Survey of Energy Resources;* London, United Kingdom, 2010; pp 618.
3. Wiehe, I. A. *Process chemistry of petroleum macromolecules;* CRC Press: Boca Raton, FL, 2008; pp 427.
4. Speight, J. G. Petroleum asphaltenes - Part 1: Asphaltenes, resins and the structure of petroleum. *Oil and Gas Science and Technology - Rev. IFP* **2004**, *59*, 467-477.
5. Calemma, V.; Rausa, R.; D'Antona, P.; Montanari, L. Characterization of asphaltenes molecular structure. *Energy & Fuels* **1998**, *12*, 422-428.
6. Akbarzadeh, K.; Alboudwarej, H.; Svrcek, W. Y.; Yarranton, H. W. A generalized regular solution model for asphaltene precipitation from n-alkane diluted heavy oils and bitumens. *Fluid Phase Equilibria* **2005**, *232*, 159-170.
7. Karimi, A.; Qian, K.; Olmstead, W. N.; Freund, H.; Yung, C.; Gray, M. R. Quantitative Evidence for Bridged Structures in Asphaltenes by Thin Film Pyrolysis. *Energy & Fuels* **2011**, *25*, 3581-3589.

8. Trejo, F.; Ancheyta, J.; Centeno, G.; Marroquin, G. Effect of hydrotreating conditions on Maya asphaltenes composition and structural parameters. *Catalysis Today* **2005**, *109*, 178-184.

9. Furimsky, E. Selection of catalysts and reactors for hydroprocessing. *Applied Catalysis A: General* **1998**, *171*, 177-206.

10. Furimsky, E.; Massoth, F. E. Deactivation of hydroprocessing catalysts. *Catalysis Today* **1999**, *52*, 381-495.

11. de Boer, R. B.; Leerlooyer, K.; Eigner, M. R. P.; van Bergen, A. R. D. Screening of Crude Oils for Asphalt Precipitation: Theory, Practice, and the Selection of Inhibitors. *SPE Production & Facilities* **1995**, *10*, 55-61.

12. Speight, J. G. *The chemistry and technology of petroleum;* CRC Press/Taylor & Francis: Boca Raton, FL, 2006.

13. Gray, M. R.; Tykwinski, R. R.; Stryker, J. M.; Tan, X. Supramolecular Assembly Model for Aggregation of Petroleum Asphaltenes. *Energy & Fuels* **2011**, *25*, 3125-3134.

14. Savvidis, T. G.; Fenistein, D.; Barré, L.; Béhar, E. Aggregated structure of flocculated asphaltenes. *AIChE Journal* **2001**, *47*, 206-211.

15. Gray, M. R. Consistency of Asphaltene Chemical Structures with Pyrolysis and Coking Behavior. *Energy & Fuels* **2003**, *17*, 1566-1569.

16. Dickie, J. P.; Yen, T. F. Macrostructures of the asphaltic fractions by various instrumental methods. *Analytical Chemistry* **1967**, *39*, 1847-1852.

17. Yen, T. F. Structure of Petroleum Asphaltene and Its Significance. *Energy Sources, Part A: Recovery, Utilization, and Environmental Effects* **1974**, *1*, 447-463.

18. Groenzin, H.; Mullins, O. Asphaltene molecular size and structure. *J. Phys. Chem. A* **1999**, *103*, 11237-11245.

19. Groenzin, H.; Mullins, O. C. Molecular Size and Structure of Asphaltenes from Various Sources. *Energy & Fuels* **2000**, *14*, 677-684.

20. Mullins, O. C. The Modified Yen Model. *Energy & Fuels* **2010**, *24*, 2179-2207.

21. Strausz, O. P.; Mojelsky, T. W.; Lown, E. M. The molecular structure of asphaltene: an unfolding story. *Fuel* **1992**, 71, 1355-1363.

22. Strausz, O. P.; Safarik, I.; Lown, E. M.; Morales-Izquierdo, A. A critique of asphaltene fluorescence decay and depolarization-based claims about molecular weight and molecular architecture. *Energy & Fuels* **2008**, *22*, 1156-1166.

23. Payzant, J. D.; Lown, E. M.; Strausz, O. P. Structural units of Athabasca asphaltene: the aromatics with a linear carbon framework. *Energy & Fuels* **1991**, *5*, 445-453.

24. Strausz, O. P.; Mojelsky, T. W.; Faraji, F.; Lown, E. M.; Peng, P. Additional Structural Details on Athabasca Asphaltene and Their Ramifications. *Energy & Fuels* **1999**, *13*, 207-227.

25. Ignasiak, T.; Kemp-Jones, A.; Strausz, O. P. The molecular structure of Athabasca asphaltene. Cleavage of the carbon-sulfur bonds by radical ion electron transfer reactions. *J. Org. Chem.* **1977**, *42*, 312-320.

26. Murgich, J.; Abanero, J. A.; Strausz, O. P. Molecular Recognition in Aggregates Formed by Asphaltene and Resin Molecules from the Athabasca Oil Sand. *Energy & Fuels* **1999**, *13*, 278-286.

27. Savage, P. E.; Klein, M. T.; Kukes, S. G. Asphaltene reaction pathways. 3. Effect of reaction environment. *Energy & Fuels* **1988**, *2*, 619-628.

2 Characterization of pendant groups obtained by cracking of asphaltenes under favorable hydrogenation conditions[1]

2.1 Introduction

The study of asphaltenes is challenged by the complex character of this material, which is defined as the oil fraction soluble in toluene, but insoluble in paraffinic solvents such as *n*-pentane or *n*-heptane. This solubility definition of asphaltenes encompasses a heterogeneous material obtained by processes that include precipitation due to solubility, through non-selective coprecipitation, and coagulation of nanoaggregates.[1, 2] One of the most remarkable characteristics of asphaltenes is their liability to aggregate in solution, which hampers the molecular analysis by mass spectrometric techniques,[1] the determination of molecular weight, and other structural features. Nevertheless, the asphaltene fraction correlates with a range of production and processing problems in the petroleum industry, and this makes their study a relevant topic.

The molecular architecture of asphaltenes has been a matter of discussion for many decades, yet so far there is not a general consensus regarding the predominant structures. Yen and coworkers[3, 4] proposed a model consisting of single alkylated cores, constituted by aromatic and naphthenic rings fused

[1] A version of this chapter has been submitted for publication as: Rueda-Velásquez, R. I.; Freund, H.; Qian, K.; Olmstead, W. N.; Gray, M. R. Characterization of Asphaltene Building Blocks by Cracking under Favorable Hydrogenation Conditions. *Energy & Fuels* **2012**

together. The presence of alkyl chains would explain the stability of asphaltenes in oil, and the π-π interactions between the aromatic sheets was taken as the driving force for the formation of aggregates. Dickie and Yen[4] depicted asphaltene molecules as large aromatic sheets with more than 100-300 carbon atoms. This type of structure, also known as the island model, has also been supported by Mullins[5] and coworkers (Groenzin et al.[6, 7]), who used fluorescence depolarization measurements to emphasize alkyl polycyclic aromatic hydrocarbons (PAHs) as the main motif in asphaltenes, but they suggested much smaller molecules in the range of 500-1000 amu. However, the conclusions from this work are still controversial. Questions have been raised on proper calibration, instrumental limitations, and interpretation of the results.[8]

Several studies have indicated the presence of a range of aromatic ring sizes in the asphaltene fraction. Calemma et al.[9] used a variety of analytical methods on asphaltenes from different sources, and suggested a representation of asphaltenes as clusters of polycondensed groups comprised of 5 to 7 fused rings, joined by alkyl and heteroatomic bridges. In a later study, involving the use of pyrolysis-GC/MS analysis, smaller aromatic units were identified, leading to a new description of asphaltenes as polyaromatic and hydroaromatic units with 1 to 10-20 rings, joined by aliphatic bridges.[10] The thermolysis reactions conducted at mild conditions by Strausz et al.[11-13] produced alkyl-substituted mono- to penta-cyclic aromatic structures which should be present in the original asphaltenes as were identified, and suggested that the aromatic condensation could not be as high

as proposed by Yen et al.[3] Speight[14] pointed out that polynuclear aromatic systems with more than 10 rings would be unlikely in asphaltenes.

Cracking of asphaltenes yields a diverse variety of molecules, including aromatics, naphthenes, saturates, and heteroatomic compounds,[12, 13, 15] which would be present as substructures in the parent components, since these structures cannot be formed from the cracking and rearrangement of large aromatic clusters under mild thermolysis conditions.[16] This observation from the processing of asphaltenes could not be reconciled with a model based only on large, and highly condensed aromatic cores, substituted with side chains; it was rather more consistent with asphaltenes representations consisting of diverse aromatic units with aliphatic chains, attached to each other by bridges.[17]

Wiehe[18] introduced a simple, but useful representation for the molecules in petroleum residua and asphaltenes consisting of different combinations of core and pendant building blocks, joined by thermally labile bonds. During cracking, the pendant building blocks could be split off, while the cores would remain nonvolatile. This model provided a mechanism for coke formation, but did not provide any information regarding the size of the cores and pendant groups. Wiehe suggested, as next step, the introduction of a distribution of species that could replace the core and pendant building blocks.

Cracking of asphaltenes under hydrogenation conditions enhances the yields of distillates and lowers production of coke compared to thermal cracking. Savage et al.[19] observed that cracking in the presence of hydrogen alone, without addition of catalyst or solvent, yielded similar amounts of coke and maltenes as

those reactions performed in an Argon atmosphere. However, the introduction of hydrogen-donor solvents into the reaction system led to higher selectivities to maltenes, and the further addition of a hydrotreating catalyst could maintain this high selectivity even at high conversions. Gray et al.[20] suggested that the capacity of hydrogen-donor solvents to suppress coke formation is a consequence of their ability to react with olefins, which can otherwise undergo polymerization reactions and lead to the formation of coke.

Conventional industrial catalysts for hydrogenation of heavy petroleum fractions consist of Mo promoted by either Ni or Co, and supported on γ-alumina, zeolites, or silica. These active materials can significantly change the molecular structures present in the processing feed by desulphurization, denitrogenation and hydrogenation of molecules.[21] This excessive hydrogenation activity is undesirable if we wish to use cracking to explore the range of the original structures present in asphaltenes. Ranganathan et al.[22] patented an iron-based catalyst supported on coal that showed good ability to suppress the formation of coke, while exhibiting mild activity towards hydrodesulphurization and hydrocracking.

The objective of this study was to maximize the conversion of asphaltenes by thermal cracking to their constituent ring substructures. The term “pendant groups”, introduced by Wiehe[18] to group together any material that could be cracked off the residue molecules is used here interchangeably with the term “building blocks”. They both denote cracked fragments from asphaltenes, but do not denote any particular size or structure. Based on the known thermal chemistry

of petroleum components, both aromatic and cycloalkyl building blocks may be obtained by breaking bridging linkages. In this study, we selected an iron-based catalyst with a modest activity for hydrogenation to suppress the formation of coke as described by Ranganathan et al.,[22] combined with a hydrogen atmosphere and a hydrogen-donor solvent. The objective was to obtain a high selectivity to distillates at high conversion of asphaltenes, while ensuring minimal change of the ring structures in the cracked fragments. The product material in the distillate range (< 538°C), which constitutes the analyzable fraction from the reaction products, was quantitatively recovered and analyzed by gas chromatography – field ionization – time of flight high resolution mass spectroscopy to identify the building blocks and their abundance.

2.2 Materials and Methods

2.2.1 Catalyst and model compounds

The catalyst was iron sulphate ($FeSO_4.7H_2O$, ≥ 99%, from Fisher Scientific, Mississauga, ON) supported on Coal Valley sub-bituminous coal. The proximate and ultimate analyses of this coal are shown in Table 2-1. The standard methods used for these analyses were: ASTM D3172 for Proximate Analysis, ASTM D3173 for Moisture content, ASTM D3174 for Ash Content, and Test Method ASTM D3175 for Volatile Matter Content.

The model compounds evaluated consisted of the aromatic compound phenanthrene (> 96%, HPLC grade from Sigma Aldrich), and the naphthenic compound 5α-cholestane (≥ 97%, GC grade from Sigma). 1,2,3,4-

tetrahydronaphthalene (99%, ReagentPlus® from Sigma Aldrich), also known as tetralin, was used as a hydrogen-donor solvent in the thermal cracking reactions.

Table 2-1. Proximate and ultimate analyses of sub-bituminous Coal Valley

Proximate Analysis	
Moisture, wt%	6.3
Ash, wt%	10.3
Volatile Matter, wt%	34.6
Fixed Carbon, wt%	48.8
Ultimate Analysis	
Carbon, wt%	61.2
Hydrogen,wt%	4.2
Nitrogen, wt%	1.3
Sulphur, wt%	0.5

2.2.2 Asphaltenes

Asphaltenes from different sources were evaluated. Athabasca asphaltenes obtained by precipitation in a pilot plant with *n*-pentane were used as received, and are referred to hereinafter as Athabasca industrial *n*-C_5 asphaltenes. These asphaltenes were available in large amounts and were also used as source of *n*-C_7 asphaltenes. The yields of *n*-C_5 and *n*-C_7 asphaltenes from this sample were 68% and 59%, respectively. Cold Lake *n*-C_7 asphaltenes were provided by ExxonMobil Research and Engineering, and were used as received. Maya, Safaniya, Athabasca and Venezuelan *n*-C_7 asphaltenes were obtained by precipitation in *n*-heptane from crude oil or vacuum residue samples. Thus, the

paraffinic solvent was mixed in a ratio of 40:1 solvent to vacuum residue from each one of these different origins, or also to Athabasca industrial *n*-C_5 asphaltenes. The mixture was stirred for 24 hours with a magnetic stir bar, and then the asphaltenes were filtered out under vacuum using a 0.22 µm pore size filter paper (Millipore). The asphaltenes were dried at room temperature and collected 48 hours later.

Gudao *n*-C_7 asphaltenes, obtained from a Chinese waxy crude, were precipitated following the standard procedure described by ASTM D6560 which includes reflux with hot *n*-heptane to separate the waxy compounds from the asphaltenes. The mixture 30:1 *n*-heptane to Gudao vacuum residue was boiled under reflux for one hour, and after cooling for 90 minutes, the sample and the rinsings of the flask with hot *n*-heptane were poured through a filter paper Whatman Grade 42, 90 mm diameter. The filter paper and its contents were placed in a reflux extractor and refluxed with *n*-heptane for one hour. The asphaltenes recovered on the filter paper were dried at room temperature for 48 hours, and then collected.

2.2.3 Preparation of catalyst

The catalyst was made following the procedure described by Ranganathan et al.[22] with minor modification. The coal was ground and passed through a 100 mesh screen. The <100 mesh size particles were mixed in a 1:1 mass ratio with distilled water. $FeSO_4.7H_2O$ was added slowly to achieve an $FeSO_4$ concentration of 30% by weight in the catalyst. The stirring provided by a magnetic bar was

maintained for two hours, and then the mixture was evaporated under vacuum at 60˚C to remove most of the water. The rotary movement during the water removal ensured continuous mixing, and thus a better dispersion of the active metal on the surface of the coal. The remaining moisture was removed by drying under vacuum at 60°C for 80 hours in oven. The dried material was ground with mortar and pestle to obtain catalyst particles < 100 mesh size.

Catalyst, coal, and $FeSO_4.7H_2O$ were analyzed in a thermogravimetric analyzer (TherMax 400 Cahn from Thermo Scientific). The software programs Thermal Analyst – Data Acquisition for TherMax Version 3.0.0.0 TM and Thermal Analyst – Analysis Version 1.3.2.2 by Thermo Cahn Instruments were used to collect and postprocess the TG data, respectively. Samples of approximately 50 mg of catalyst and coal were analyzed by the same method, consisting of an initial isothermal step at 21°C, followed by a dynamic step with a heating rate of 50°C/min with start temperature of 21°C and end temperature of 430°C, and a final isothermal step at 430°C. A constant air flow of 80 ml/min at atmospheric pressure was used for this method.

2.2.4 Cracking of model compounds

Phenanthrene ($C_{14}H_{10}$) and 5α-cholestane ($C_{27}H_{48}$) were thermally cracked in the presence of tetralin ($C_{10}H_{12}$) at mild conditions, 430°C for 45 minutes, and at more severe conditions, 450°C for 3 hours. These reactions were made in the presence and absence of catalyst, and at hydrogen pressure of 4.1 MPa at ambient

temperature. The catalytic reactions contained 2% by weight of catalyst on a total mass basis.

The reactions were carried out in 15 ml stainless steel microreactors. This batch reactor is made of nominal ¾ in. stainless steel tubing, connected to Swagelok fittings. The main body is a 2 ½ in. long tube (3/4 in. OD, 1/16 in. thickness) connected to a bored-through reducing union, ¾ x ¼ in., and capped on the other end. The reducing union has a reducer tube attached, ¼ x 1/8 in., which is connected to a bracket consisting of three parts: a 1/8 in. bonnet needle valve, a two-piece ½ in. thick bracket made of 6061 Aluminum, and a stem of appropriate length to ensure complete immersion of the microreactor into the sand bath, consisting of 1/8 in. tube with ferrules attached on both ends.

In the 15 ml microreactors, approximately 3.5 grams of total sample were loaded. The individual concentrations of phenanthrene and cholestane in tetralin were approximately 1.6 wt%, and the amount of catalyst (in the catalytic reactions) was 2 wt% on total mass basis. Five 3/16 in. stainless steel balls were introduced in the microreactor in order to improve the mixing provided by the vertical agitation. Leak testing was done by connecting the system to a regulated high pressure cylinder. After verifying of the absence of leaks, the apparatus was purged three to five times with hydrogen; thus, the air inside the microreactor was displaced by the gas used in the reaction. Then, the system was pressurized with hydrogen at 4.1 MPa at ambient temperature.

The microreactor was attached to the mechanical shaking system and plunged into the preheated sand bath. The isothermal conditions during the

reaction were provided by a fluidized sand bath (Tecam model SBS-4, Cole-Parmer).

2.2.5 Characterization of feed and products from the reaction of model compounds

The liquid sample was quantitatively recovered from the microreactor and the conversion of each compound was determined by GC analysis (Agilent Technologies 7890A GC System, New Castle, DE), equipped with FID detector and an HP-PONA 50 m x 0.200 mm x 0.50 µm column. The oven was programmed at 30°C for 10 minutes, followed by a ramp from 30°C to 300°C at 10°C/min, with helium as carrier gas at 1.1 ml/min, with a split flow of 224.1 ml/min and pressure of 32.72 psi. The FID detector operated at 250°C with hydrogen and air flows of 30 and 250 ml/min, respectively. The vials for the analysis contained samples diluted to concentrations of approximately 1.5 wt% in methylene chloride (99.9%, stabilized HPLC grade from Fisher Scientific), and n-octane (≥ 99.5%, puriss p.a. grade from Sigma Aldrich) was used as internal standard.

The liquid products from the reaction were also analyzed by GC-MS (Trace GC Ultra coupled to a DSQ II unit from Thermo Fisher Scientific, Mississauga, ON). The GC-MS had a TR-5 GC Column, 7 m length, 0.32 mm ID, and 0.25 µm film thickness. The software Thermo Fisher Scientific Xcalibur 2.0.7, DSQ 2.0.1, and Trace GC Ultra 2.0, were used for operation of the instrument and analysis of the data. The oven was set at 40°C for 1 minute,

followed by a heating rate at 10°C/min until 310°C. The equipment was operated in splitless mode with a flow of 50 ml/min, with helium as carrier gas at 1 ml/min. The samples were analyzed diluted in methylene chloride (99.9%, stabilized HPLC grade from Fisher Scientific) at concentrations of approximately 1.5 wt%, and they were injected manually using a microsyringe.

2.2.6 Cracking of asphaltenes under hydrogenation conditions

The reactions took place in the presence of the hydrogen-donor solvent tetralin, obtained from Sigma Aldrich as ReagentPlus®, 99%. The catalyst prepared by supporting $FeSO_4$ on sub-bituminous coal, as explained previously, was also introduced in the reaction system, aiming to suppress coke formation, while ensuring minimal change of the molecular structures due to its low activity for hydrogenation. Hydrogen gas was obtained from Praxair with specifications of ultra-high purity, 100.00% (Purity Grade: 5.0).

The reactions were carried out in 15 ml stainless steel batch microreactors, described previously and also used for the reactions of model compounds. The reactors were loaded with approximately 4 grams of total sample, including asphaltenes, tetralin, and catalyst. Five 3/16 in. stainless steel balls were also loaded into the microreactor to provide better mixing. The system was pressurized with hydrogen at 4.1 MPa at ambient temperature, after the verification of the absence of leaks, and the purge of the system three to five times with hydrogen gas.

After the reaction, the gases were released into a 1 liter gas bag and analyzed by GC-TCD (SRI 8610C GC unit from SRI Instruments, Torrance, CA), equipped with thermal conductivity detector and two 6-feet silica gel columns, and operated with the software PeakSimple Version 3.56 (licensed by SRI Inc.). The temperature program consisted of an isothermal step at 50ºC for 4 minutes, followed by a ramp of 10°C/min to reach 220°C, and a final isothermal step at 220°C for 20 minutes.

The liquids were filtered under vacuum to remove the coke and the catalyst, using a 0.22 µm pore size filter paper (Millipore), and rinsing the microreactor several times until constant mass with methylene chloride. The filter paper and contents were dried in an oven at 80ºC for 24 hours, and then weighed. The liquid products were recovered after the removal of methylene chloride by evaporation in a rotary evaporator (Rotavapor Buchi R215).

Part of this liquid sample, approximately 1.5 g, was mixed in a ratio of 40:1 *n*-heptane to sample, and sonicated for one hour in a sonicator (Aquasonic Ultrasonic Cleaner, VWR Scientific, Model 150HT, frequency 50/60 Hz). This mixture was filtered 24 hours later under vacuum using a 0.22 µm pore size filter paper (Millipore), and rinsing with *n*-heptane. These asphaltenes recovered on the filter paper were dried in an oven at 80ºC for 24 hours. Likewise, the same procedure was followed with a mixture of asphaltenes feed and tetralin, with the same ratio used in the reaction, in order to take into account the effect of tetralin on the solubility of the mixture, and thus get an estimation of the conversion of *n*-C_7 insolubles.

Another sub-sample of the liquid products, approximately 0.4 g, was evaporated for four hours at 10 mbar, and 90-93 ºC, in order to get a tetralin-free sample that could be analyzed by Simulated Distillation (SimDist). These results, together with the analysis of the asphaltenes feed by SimDist, provided an estimation of the conversion of the vacuum residue fraction.

These reactions for mass balance purposes were made by duplicate or triplicate with each one of the asphaltenes, and separate reactions, under the same conditions, were also made to recover the liquid products with minimal loss of light compounds to be analyzed by a high resolution GC-MS analysis. These liquid samples were collected directly from the microreactor, removing coke by filtration with syringe filters.

Blank reactions, where only catalyst and tetralin were loaded into the microreactor, were performed to estimate the approximate amount of catalyst that is not recovered by filtration after reaction, and the amount of *n*-C_7 insolubles produced from the sub-bituminous coal. These results were taken into account in the mass balances.

2.2.7 Characterization of the asphaltenes and products

The asphaltenes and their tetralin-free liquid products were analyzed by SimDist according to the ASTM D5307 method in a Varian 450-GC Gas Chromatograph (Bruker Ltd., Milton, ON), operated with an Agilent Capillary Column WCOT Ultimetal (L (m) x ID (mm) x OD (mm): 5 x 0.53 x 0.80) with film thickness of 0.09 µm. The temperature program in the column oven consisted

of an isothermal step at 35 ºC for one minute, followed by a ramp of 20 ºC/min up to 400 ºC, and a final isothermal step at 400 ºC, with a total process time of 45 minutes. Samples were prepared by dilution in carbon disulfide (CS_2) at approximate concentrations of 1.5 wt%. Two vials were prepared per sample, one of them containing approximately 0.3 wt% of an ASTM D5307 internal standard (SUPELCO Analytical), consisting of a mixture of hydrocarbons C_{14}-C_{17}. A volume of 0.20 µL was injected for each analysis. The unit was operated with the software Galaxie Chromatography Data System Version 1.9.302.530, and the chromatograms were processed and integrated with the software SimDist – Varian Galaxie Version 6.5.45.

The elemental compositions of the asphaltenes were determined in an Elementar vario MICRO CUBE unit (Elementar Americas, Inc., Mt. Laurel, NJ), operated with the software VarioMICRO V1.9.5 2/12/2010 (Copyright © 2004 by elementar Analysensysteme GmbH). The liquid products from the reaction were analyzed in the Department of Chemistry of the University of Alberta in a Carlo Erba CHNS-O EA1108 Elemental Analyzer.

XPS analyses of asphaltenes, and catalyst before and after reaction, were performed at the Alberta Centre for Surface Engineering (ACSES) at University of Alberta, in an Axis 165 X-ray Photoelectron Spectrometer from Kratos Analytical.

Microcarbon Residue (MCR) and ash content of asphaltenes and their liquid products were approximated by TGA analysis in a TherMax 400 Cahn Thermogravimetric Analyzer (Thermo Fisher Scientific, Waltham, MA). Samples

of 10-13 mg were subjected to a heating program, consisting of an isothermal step at 21.8 ºC for 10 minutes, followed by a ramp of 5 ºC/min up to 500 ºC, and an isothermal step at 500 ºC for 2 hours, with Argon flowing at 50 mL/min. The TGA residue at this point was reported on ash-free basis, approximating the MCR content obtained by the method ASTM D4530. Subsequently, gas was shifted to air with a flow of 50 mL/min, and the temperature was kept at 500 ºC for two hours (5 hours for Cold Lake *n*-C_7 asphaltenes). The residual mass was reported as the ash content.

The liquid products recovered after the reaction, without any further treatment other than filtration with a syringe filter, were analyzed by gas chromatography – field ionization – time of flight high resolution mass spectroscopy (GC-FI-TOF HR MS) technique described by Qian et al.[23] Hydrocarbon compounds with boiling points < 538°C were separated by boiling point, ionized, resolved, and accurately identified, providing a reliable speciation of the molecules present in the distillates fraction of the liquid products from the asphaltenes reactions.

Tetralin conversion was determined by GC-FID analysis of the light fraction (< 343 ºC) obtained by distillation of the liquid products in a Model 800 Micro Distillation System (B/R Instrument Corporation, Easton, MD) operated with the software M690 PC Interface. Tetralin and naphthalene were identified and quantified in a 7890A GC System from Agilent Technologies (New Castle, DE), using a HP-PONA column, 50 m x 0.200 mm x 0.50 µm. The analyses were made in split mode, with a split ratio of 200:1, and total flow of 224.1 mL/min.

The column oven was programmed at 30 ºC for 15 minutes, followed by a ramp of 10 ºC/min up to 300 ºC, and a hold time of 20 minutes at 300 ºC, for a total run time of 62 minutes. The samples were prepared at concentrations of 1.5 wt% by dilution in methylene chloride (Stabilized HPLC Grade, Fisher Scientific, 99.9%), and using *n*-octane (Sigma Aldrich, puriss. p.a. ≥ 99.5%) as internal standard.

2.3 Results and Discussion

2.3.1 Catalyst composition

The TGA analyses of the coal and the catalyst in the oxidative atmosphere allowed the estimation of the amount of iron sulphate supported on the coal after the wet impregnation process. The TGA results showed an ash content of 12.5 wt% in the coal, and 37.0 wt% in the initial catalyst. These results indicated a loading of iron sulphate ($FeSO_4$) on coal of 28 wt%, which gives a loading of iron as metal of 10.3 wt% of the initial catalyst.

2.3.2 Conversion of model compounds and characterization of products

GC-FID analysis of the reaction mixture before and after the reaction provided a quantitative estimation of the conversions of the model compounds, and also allowed the estimation of the amount of naphthalene produced by dehydrogenation of tetralin, as reported in Table 2-2. The conversion for each compound *i* was estimated with the following equation:

$$\text{Conversion}_i = \frac{(\text{initial mass})_i - (\text{final mass})_i}{(\text{initial mass})_i} * 100\% \qquad (2\text{-}1)$$

The reactions at mild conditions (430°C and for 45 minutes) showed lower conversions than the reactions performed at the severe conditions (450°C and for 3 hours). Phenanthrene and tetralin showed significantly higher conversions in the presence of catalyst than in the non-catalytic reactions. By contrast, 5α-cholestane exhibited similar conversions in the reactions with and without catalyst. The amount of naphthalene produced by dehydrogenation of tetralin was also quantified, and in most of the reactions represented approximately 22% of the total conversion of tetralin. Some activity of the reactor surface cannot be ruled out in these experiments.

Table 2-2. Conversions of phenanthrene and 5α-cholestane by cracking in presence of tetralin and hydrogen, estimated from GC-FID results

Conversions (%)	**T = 430°C, τ = 45 min**		**T = 450°C, τ = 3 hours**	
	No catalyst	**2% catalyst**	**No catalyst**	**2% catalyst**
Phenanthrene	3.4	9.1	15.2	24.4
5α-cholestane	9.8	8.6	48.9	57.0
Tetralin	2.2	2.9	8.3	12.3
Tetralin conversion to naphthalene	0.5	0.7	1.1	2.6

GC-MS results provided information about the compounds formed from the reactions of phenanthrene, 5α-cholestane and tetralin. Phenanthrene (represented as P), gave the main identified product with a mass/charge ratio (m/z) of 180; this compound has the form of the partially hydrogenated species H_2P, and would correspond to 9,10-dihydrophenanthrene ($C_{14}H_{12}$), as observed in previous studies.[24-28] Three other minor products were identified; one of them

with m/z of 182 that can be attributed to the compound 1,2,3,4-tetrahydrophenanthrene ($C_{14}H_{14}$) which has the form of H_4P. The partially hydrogenated species H_6P, with m/z of 184 and molecular formula $C_{14}H_{16}$, was observed eluting next to the previous compound. The third identified product had also m/z of 180 and would correspond to 1,2-dihydrophenanthrene with molecular formula $C_{14}H_{12}$, and constitutes one of the isomers of the species H_2P. Highly hydrogenated species, such as octahydro- and perhydrophenanthrene, were not observed in the products at the reaction conditions evaluated.

Figure 2-1 illustrates these results, showing the peaks for phenanthrene and each one of the compounds identified by GC-MS. The non-labeled peaks in the picture are minor byproducts from the reaction of tetralin.

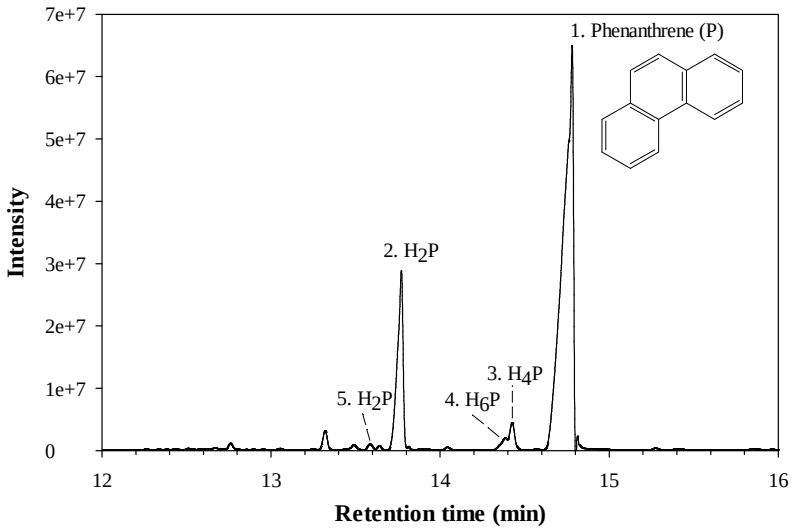

Figure 2-1. GC-MS chromatogram obtained in splitless mode analysis, showing the peaks for phenanthrene and its products from the cracking under hydrogenation conditions, at 450°C, residence time of 3 hours, and 2 wt% catalyst.

Phenanthrene has been widely used as model compound in the study of coal liquefaction. As observed by Chadha et al.[24] and Suzuki et al.[25] in their experiments with phenanthrene and other model compounds, iron-based catalysts demonstrated mild activity for hydrogenation. Chadha and coworkers[24] studied mixtures of pyrite and pyrrhotite as catalysts for the reactions of hydrogenation and hydrogen shuttling in the presence of tetralin. They obtained conversions of phenanthrene of up to 19%, at reaction conditions of 400°C, H_2 pressure of 1000 psig at ambient temperature, residence time of 30 minutes, and concentrations of catalyst of 12.5 wt% on total mass basis, and detected only 9,10-dihydrophenanthrene and 1,2,3,4-tetrahydrophenanthrene in the products.

Suzuki and coworkers[25] conducted experiments with different iron-based catalysts, at 375°C, H_2 pressure of 5 MPa, and with reaction time of 60 minutes. In the reactions of phenanthrene with FeS_2, the amount of catalyst used was 0.25 mmol or approximately 0.5 wt% on a total mass basis, and the reported conversion was 14.4%, with detection of the two hydrophenanthrene compounds also identified by Chadha et al.[24]. They observed products with higher hydrogenation degree when more active catalysts were used, as also reported by Nuzzi[26] with Ni catalysts, by Benbenek et al.[27] when Ni and Pd-based catalysts were evaluated under different conditions, and by Bate and coworkers[28] with bimetallic and monometallic catalysts made of Ni, Co, Mo, W, and Zn.

Thermal cracking accounted for the conversion of 5α-cholestane, with products identified by GC-MS that included species formed by cracking of the side chain and/or dehydrogenation of the sterane ring, without formation of

aromatization derivatives. Some of the main identified products are shown in Figure 2-2.

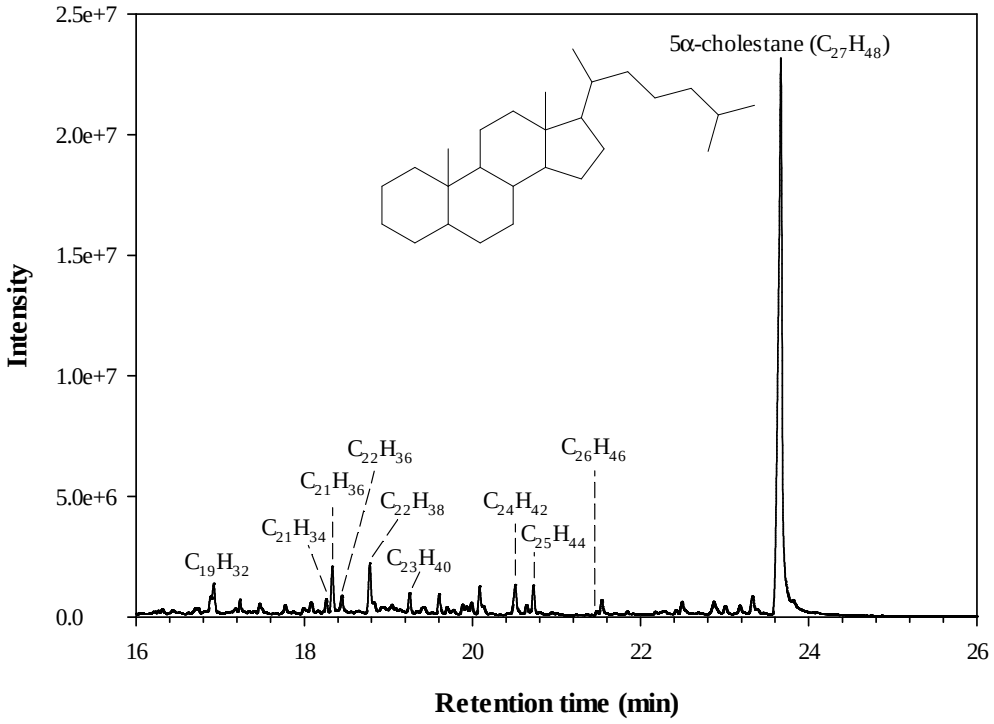

Figure 2-2. GC-MS chromatogram obtained in splitless mode analysis, showing the peaks for 5α-cholestane and some of its products from the cracking under hydrogenation conditions, at 450°C, residence time of 3 hours, and 2 wt% catalyst.

5α-cholestane is considered as one of the typical representatives of the naphthenic biomarkers, but little data about the cracking of this compound and its products have been published. One of these few studies was made by Carlson and coworkers[29] who evaluated the reaction of this hydrocarbon in the presence of palladium on carbon catalyst, under vacuum at 300°C, and identified by GC-MS

products formed by isomerization, dehydrogenation, C-C bond cracking, migration and loss of the methyl groups, and other molecular rearrangements. The main steroidal products involved the products $C_{18}H_{18}$, $C_{26}H_{32}$, $C_{26}H_{34}$, $C_{26}H_{36}$, $C_{27}H_{40}$, and $C_{27}H_{42}$, with their respective isomers.

Kissin[30] studied the cracking of 5α-cholestane at 300°C, obtaining conversions of circa 50% with residence time of 240 hours, and 85% with reactions for 355 hours in the presence of kaolin. The main observation from his experiments was that very small amounts of light naphthenic compounds, with one or two rings, are formed from the cracking of this steroid, preserving its ring structure, the same as observed in this study.

From the reaction of tetralin ($C_{10}H_{12}$), three main products were identified: naphthalene ($C_{10}H_8$) produced by dehydrogenation, the isomer 1-methylindane ($C_{10}H_{12}$) formed by ring contraction, and *n*-butylbenzene ($C_{10}H_{14}$) by ring opening. The formation of these three compounds during thermolysis and hydrogenolysis reactions was also reviewed and presented by Poutsma et al.[31]. From the GC-FID results, it was found that the conversion of tetralin to naphthalene represented around 22% of the total conversion of tetralin, except for the reaction at severe conditions without catalyst, where the conversion of tetralin to naphthalene accounted for 14% of the total conversion of tetralin.

The conversions of tetralin to 1-methylindane and *n*-butylbenzene, shown in Table 2-3, were estimated using the same response factor calculated for tetralin, and it was found that the selectivity of tetralin to 1-methylindane was higher in the non-catalytic reactions, accounting for 17 and 28% of the total conversion of

tetralin in the reactions at mild conditions, with and without catalyst respectively, and similarly for 37 and 48% in the higher severity reactions. Likewise, the presence of catalyst did not favor the selectivity of tetralin towards *n*-butylbenzene, as shown by the values of 10 and 18% for the low severity reactions, with and without catalyst respectively, and in the case of the reactions at high severity, where the conversion to *n*-butylbenzene accounted for 19 and 25% of the total conversion of tetralin. The selectivity towards each product *i* was estimated with the following equation:

$$\text{Selectivity}_i = \frac{\text{Yield}_i}{\text{Conversion}} = \frac{(\text{mass product})_i}{\text{total mass of products}} * 100\% \qquad (2\text{-}2)$$

Table 2-3. Yields and selectivities estimated for the main products from the reaction of tetralin, formed by ring contraction, dehydrogenation, and ring opening.

Yields and (*selectivities*), (%)	**T = 430°C, τ = 45 min**		**T = 450°C, τ = 3 hours**	
	No catalyst	**2% catalyst**	**No catalyst**	**2% catalyst**
1-methylindane	0.6 (*28*)	0.5 (*17*)	4.0 (*48*)	4.5 (*37*)
Naphthalene	0.5 (*22*)	0.7 (*22*)	1.1 (*14*)	2.6 (*21*)
n-butylbenzene	0.4 (*18*)	0.3 (*10*)	2.1 (*25*)	2.4 (*19*)

The conversions and selectivities from the non-catalytic reactions of tetralin, at mild and severe conditions, are very similar to the values reported by de Vlieger et al.[32] for the experiments conducted at 400 and 450°C, in H_2 atmosphere at 10 MPa (at reaction temperature).

2.3.3 Characterization of asphaltenes

The elemental compositions of the asphaltenes evaluated in this study are shown in Table 2-4. These results indicated similar values for carbon and hydrogen, and more significant differences were observed for nitrogen and sulphur contents, which fluctuated in broader ranges of 1.6-2.3% and 6.1-8.3%, respectively, for the set of *n*-C_7 asphaltenes. The elemental composition of Cold Lake *n*-C_7 asphaltenes is slightly different compared to the other samples because of its high ash content, as shown in Table 2-5.

Table 2-4. Elemental composition and aromaticity (f_a) of asphaltenes samples

Asphaltenes	**C**	**H**	**N**	**S**	**H/C (molar ratio)**	***Aromaticity f_a**
Athabasca ind. *n*-C_5	81.6	8.5	1.4	7.7	1.25	-
Athabasca *n*-C_7	81.5	7.6	1.6	8.0	1.11	0.50
Cold Lake *n*-C_7	77.6	7.6	1.6	8.3	1.17	0.46
Gudao *n*-C_7	81.6	8.4	2.1	6.3	1.23	-
Maya *n*-C_7	82.1	7.7	1.8	7.5	1.12	0.50
Safaniya *n*-C_7	82.0	7.7	1.5	7.9	1.12	0.51
Venezuelan *n*-C_7	81.8	8.0	2.3	6.1	1.17	0.43

* Aromaticity values reported by Karimi et al.[15]

The last column in Table 2-4 gives the experimental values for aromaticity (f_a) reported by Karimi et al.[15] for the same set of asphaltenes samples, evaluated by ^{13}C NMR analysis. The aromaticity values are in the narrow range of 0.43 to 0.51 for the *n*-C_7 asphaltenes evaluated, but lower aromaticity values would be

expected for Gudao *n*-C_7 and Athabasca industrial *n*-C_5 asphaltenes because of their higher hydrogen content.

The ash and pyrolysis residue contents of the asphaltenes are given in Table 2-5. The pyrolysis residue by TGA approximates the MCR content. These values are similar for the various samples of *n*-C_7 asphaltenes, ranging between 41 and 48%, with the exception of Gudao that exhibited a significantly lower value of 38.1%. Ash contents were below 1.3%, excluding Cold Lake *n*-C_7 asphaltenes. These ash values were accounted for in mass balances, considering this content as inert material in the cracking reactions.

Table 2-5. TGA Results: MCR and ash content of asphaltenes samples

Asphaltenes	TGA residue*, wt%	Ash content, wt%
Athabasca industrial *n*-C_5	34.0	1.0
Athabasca *n*-C_7	46.3	0.7
Cold Lake *n*-C_7	41.3	4.8
Gudao *n*-C_7	38.1	0.4
Maya *n*-C_7	46.5	1.1
Safaniya *n*-C_7	48.0	0.9
Venezuelan *n*-C_7	42.2	1.3

* TGA residue at 500°C approximates the microcarbon residue (MCR) content determined by method ASTM D4530

The set of asphaltenes samples were also analyzed by XPS in order to get additional information that could indicate some significant differences among the various asphaltenes. The deconvolution of the S2p peak for aliphatic and aromatic sulphur, into their 3/2 and 1/2 components, with an area ratio of 2/1 and a relative

position separation of 1.18 eV, provided a quantitative measure of sulphur speciation. The relative position between the S2p 3/2 peaks for the aromatic and aliphatic sulphur was set at 0.7 eV, as proposed by Siskin et al.[33]. For example, the sulphur 2p peak for Cold Lake *n*-C_7 asphaltenes and its curve-resolution components are shown in Figure 2-3.

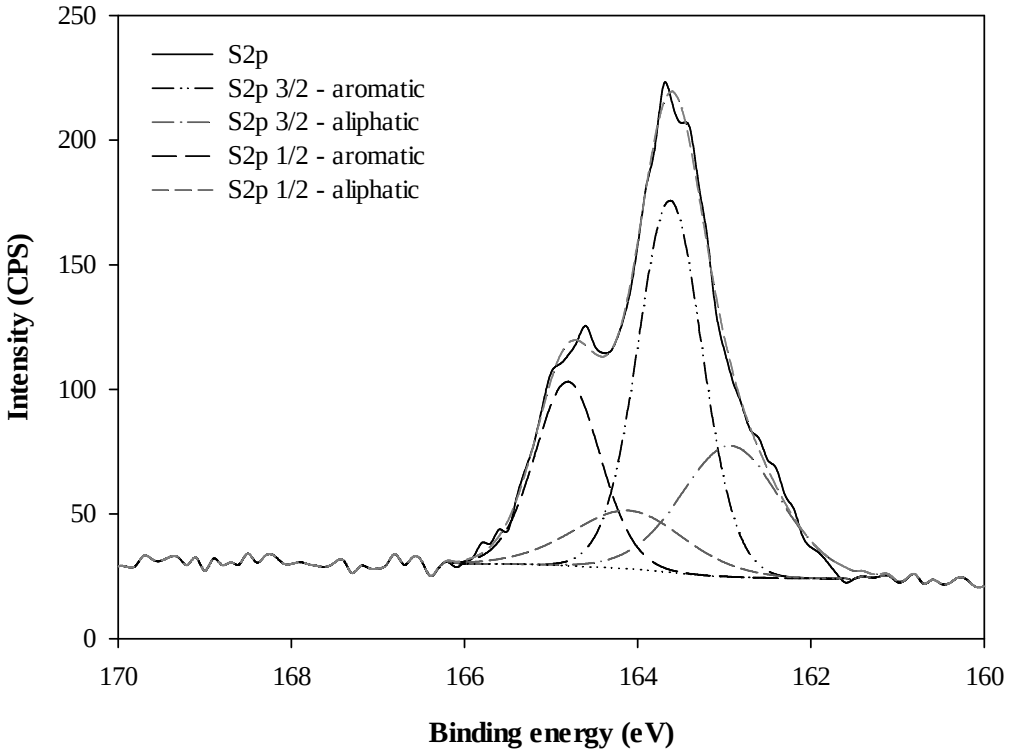

Figure 2-3. XPS spectrum of sulphur 2p and its curve-resolution results for Cold Lake *n*-C_7 asphaltenes

As presented in Table 2-6, sulphur speciation results indicate more significant differences among asphaltenes than MCR content or elemental composition, because aliphatic sulphur varies between a broad range of 14 to

35%. Safaniya *n*-C_7 asphaltenes is the sample with the lowest aliphatic sulphur, and at the same time with the highest MCR content.

Table 2-6. XPS Curve-Resolution results for sulphur speciation

Asphaltenes	**mole %**	
	Aliphatic	**Aromatic**
Athabasca industrial *n*-C_5	23	77
Athabasca *n*-C_7	19	81
Cold Lake *n*-C_7	35	65
Gudao *n*-C_7	35	65
Maya *n*-C_7	22	78
Safaniya *n*-C_7	14	86
Venezuelan *n*-C_7	28	72

2.3.4 Selection of reaction variables that maximize yield of distillates with minimal coke

A set of reactions at different conditions was performed in order to find the most favorable conditions for minimal coke and maximal yield of products in the distillates range. The hydrogenation conditions, provided by a hydrogen atmosphere, combined with a hydrogen-donor solvent, and an iron-based catalyst with mild activity for hydrogenation intended to suppress the formation of coke, while preserving the ring structures of the asphaltenes fragments.

The major role of the hydrogen-donor solvent in the control of the coking reactions has been attributed to the reaction of the hydroaromatic solvent with the

olefins formed during thermal cracking (Gray et al.[20]). Thus, the elimination of olefins reduces the polymerization reactions that lead to the formation of coke.

The iron-based catalyst was selected for the reaction to avoid the excessive hydrogenation that would be provided by the molybdate catalysts promoted by either Ni or Co, supported on γ-alumina, zeolites, silica or silica-aluminates, which are conventionally used during hydroprocessing (Furimsky et al.[34]). In the patent by Ranganathan et al.[22], the iron sulphate catalyst, in concentrations of 0.1-5 wt%, showed very mild activity towards hydrodesulphurization and hydrocracking, but appeared to be extremely effective as coke suppressor.

XPS analysis of the fresh catalyst, and of the catalyst recovered together with the coke after the reaction of Cold Lake *n*-C_7 asphaltenes, shown in Figure 2-4 and Figure 2-5, demonstrated the presence of sulphate as the only sulphur species in the fresh catalyst, with the peak of S2p 3/2 in the characteristic range of binding energies for sulphate between 168-171 eV. The presence of organic sulphur from the coal was not observed in the fresh catalyst which could be due to the effect of the iron sulphate coating. The deconvolution of the results for the sample recovered after the reaction exhibited the presence of different sulphur species, including aliphatic (sulphide), sulphite, sulphate, and aromatic (thiophenic) sulphur.

Jimenez et al.[35] analyzed coke samples by XPS, and reported the thiophenic sulphur as the most abundant one. Sulphide species were not present in coke, and this could be due to its labile character under thermal cracking conditions. Therefore, the sulphide peak observed in the sample after the reaction

could be mainly attributed to the in-situ formation of iron sulphide from the reaction of iron sulphate with H_2S, following the equation shown below. Thus, iron sulphide would catalyze the reactions, with a mild activity for hydrogenation as already observed in previous studies.[36, 37]

$$FeSO_4 + H_2S \rightarrow FeS + H_2SO_4 \quad (2\text{-}3)$$

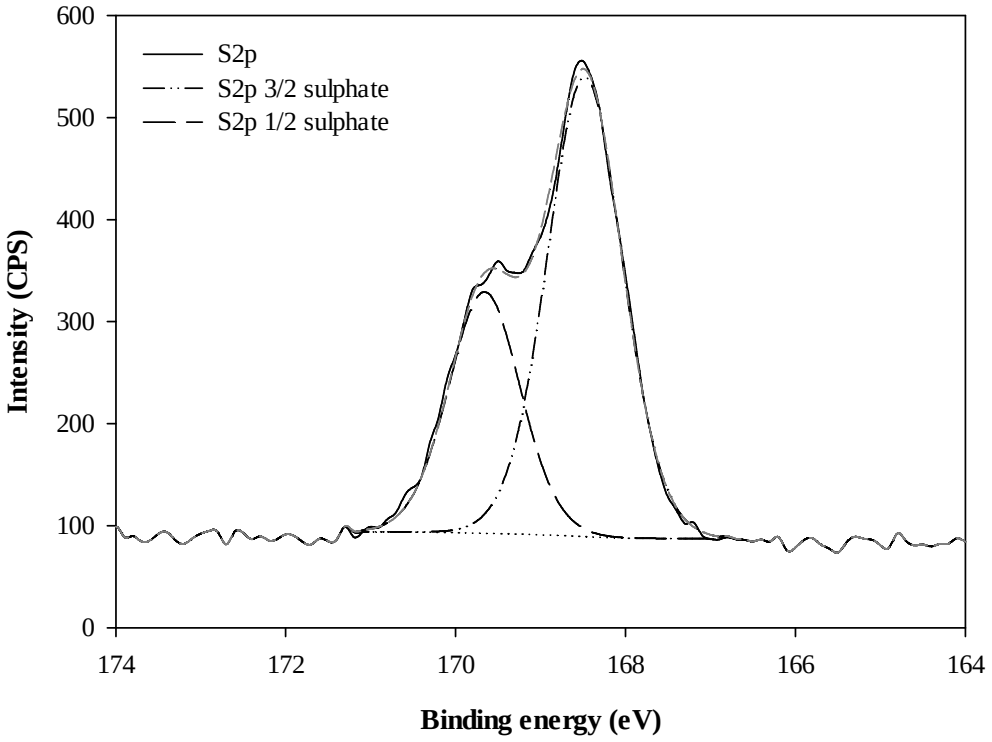

Figure 2-4. XPS spectrum of sulphur (2p) and its curve-resolution results for fresh catalyst

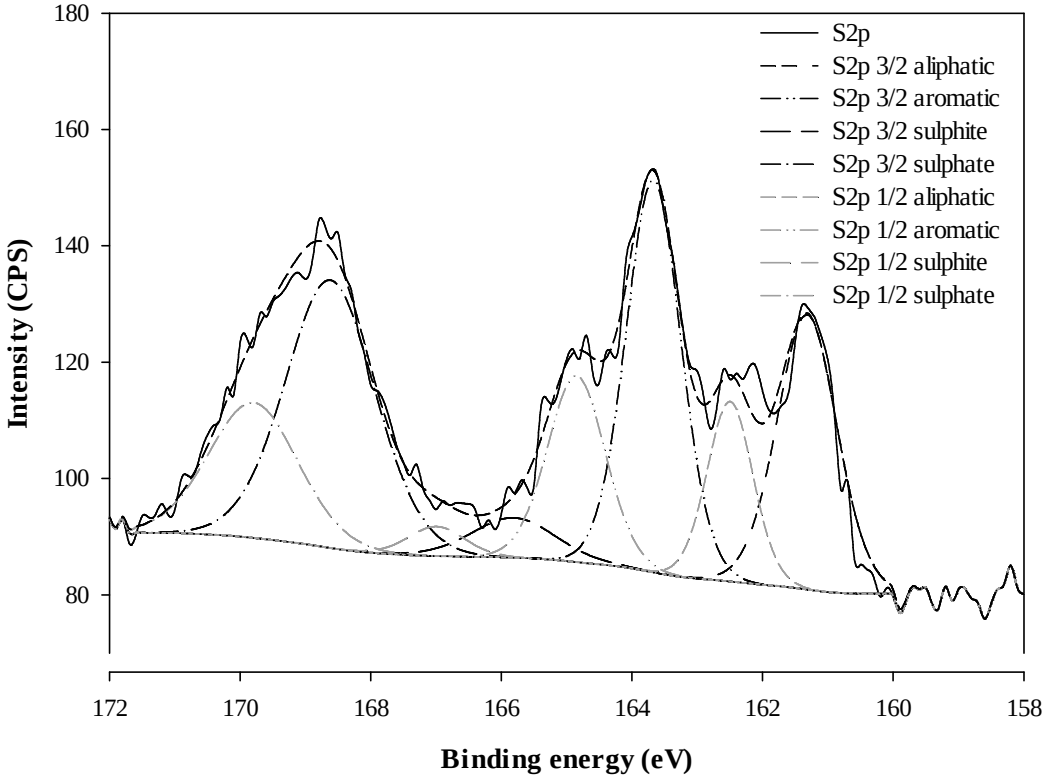

Figure 2-5. XPS spectrum of sulphur (2p) and its curve-resolution results for sample of catalyst after reaction recovered together with the coke from the reaction of Cold Lake *n*-C_7 asphaltenes at 450°C, residence time of 3 hours, tetralin/asphaltenes ratio of 2.5/1, and 2 wt% catalyst

The reactions were made with Athabasca industrial *n*-C_5 asphaltenes, and variables such as temperature, residence time, tetralin/asphaltenes ratio, and concentration of catalyst were evaluated. Figure 2-6 shows the yields and the conversion of the vacuum residue fraction for those conditions where the yield of distillates was above 50 wt%, with tetralin/asphaltenes ratio of 2/1 and 2% catalyst. The reaction at 450 °C with residence time of 3 hours provided the most

favorable conditions, providing significant amounts of distillates with relatively low yields of coke.

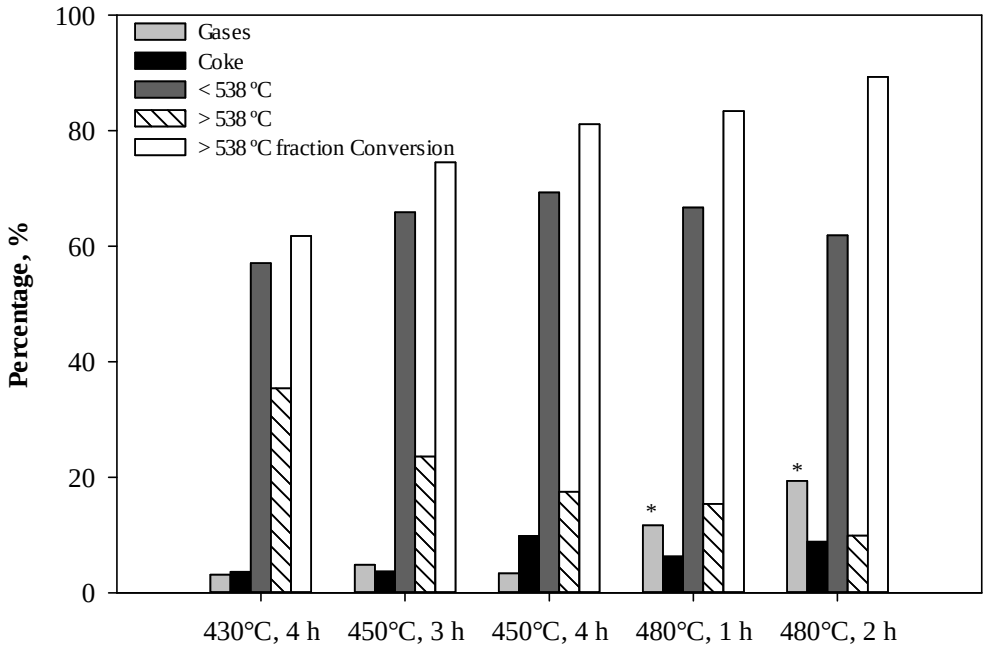

* Estimated gas yields. Concentrations out of calibration range in GC-TCD unit.

Figure 2-6. Yields and conversions from reactions of Athabasca industrial *n*-C_5 asphaltenes with tetralin/asphaltenes ratio of 2/1, 2% catalyst, and at different temperatures and residence times that provided high yield of products in the distillates range.

Experiments with tetralin/asphaltenes ratio of 3/1 did not provide significant improvements in terms of coke reduction or higher yields of distillates. The experiments with *n*-C_7 asphaltenes were made with tetralin/asphaltenes ratio of 2.5/1, and approximate calculations using Peng-Robinson equation of state suggested that 58% of the solvent mass would stay in the liquid phase, under the

reaction conditions of 450°C and hydrogen pressure of 4.1 MPa (measured at room temperature).

Likewise, in order to evaluate the catalyst and its appropriate concentration in the reaction system, four reactions were executed: without catalyst, with 2 wt% of sub-bituminous coal (catalyst support, without Fe), and with 2 and 5 wt% of catalyst. As shown in Figure 2-7, the two non-catalytic reactions had higher coke yields, and by increasing the amount of catalyst we did not observe a significant improvement in the reduction of coke. The yields of distillates were very similar for the four reactions, with differences of less than 1.5%. Therefore, amounts of 2 wt% of catalyst in the reaction system were used to get some reduction of coke yield.

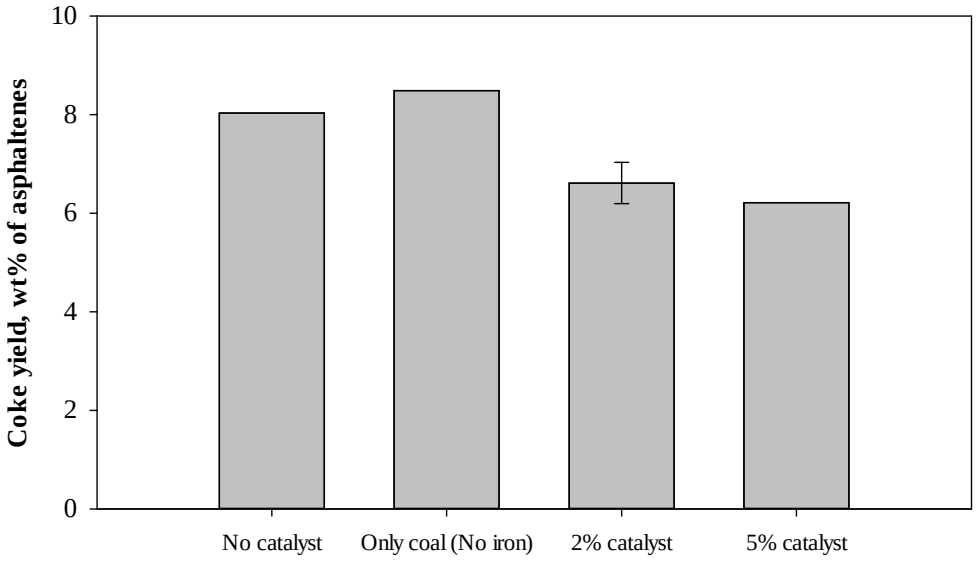

Figure 2-7. Coke yields from the reactions of Athabasca industrial *n*-C_5 asphaltenes, at 450°C, 3 hours, and tetralin/asphaltenes ratio 2/1

2.3.5 Reactions of asphaltenes from different geological origins

The set of *n*-C_7 asphaltenes were reacted under the same conditions, with temperature of 450°C, residence time of 3 hours, tetralin/asphaltene ratio of 2.5/1, and with 2 wt% of iron-based catalyst in the system. Mass balances were all above 97%, the yields of distillates were between 50 to 61%, and the production of coke was less than 10% of the initial mass of asphaltenes, as shown in Figure 2-8.

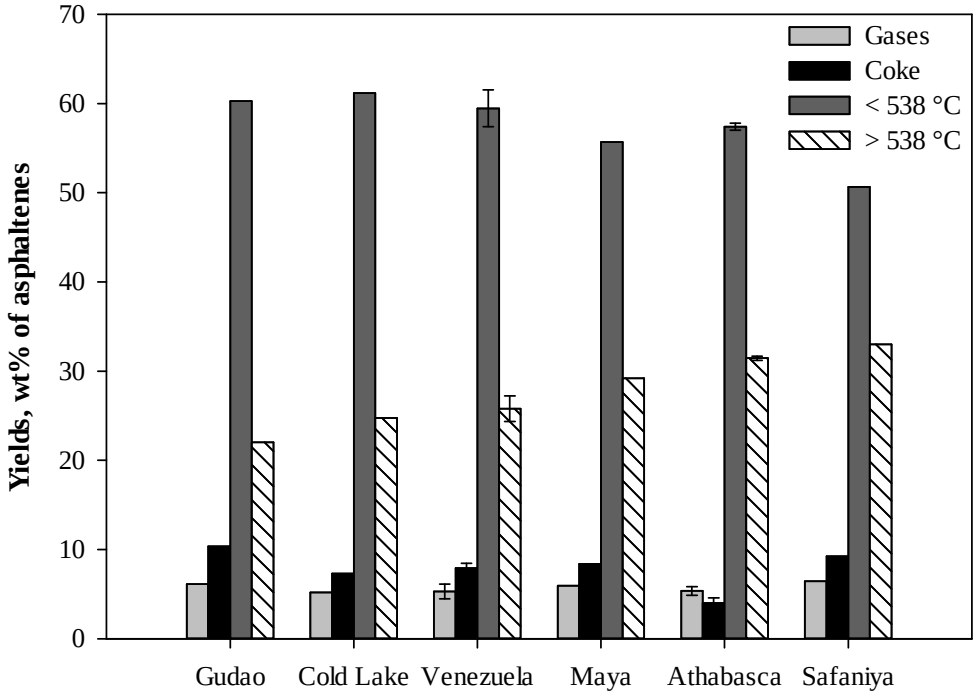

Figure 2-8. Yields from the reactions of asphaltenes from different geological regions, made by duplicate or triplicate, under conditions of 450ºC, for 3 hours, with tetralin/asphaltenes ratio of 2.5/1 and 2% catalyst

In a previous study by Karimi et al.[15], asphaltenes were reacted under thermal cracking conditions in thin films that minimized the secondary reactions of the cracked fragments. In their experiments, the yields of analyzable material, constituted by the fraction in the distillates range, were between 15 to 20%, and around 50% of the initial mass of asphaltenes ended up as coke. Therefore, the hydrogenation conditions used in this study offered a significant improvement in the yields of material in the distillates range, and in the reduction of coke in the cracking of asphaltenes.

SimDist analysis of the raw asphaltenes, and of the liquid products after the removal of tetralin, provided the boiling curves that allowed the estimation of the conversion for the vacuum residue fraction. Figure 2-9 shows the boiling curves for the liquid products from the reactions of the different asphaltenes, together with the results for Cold Lake *n*-C_7 asphaltenes, included for comparison. These results show a continuous distribution of material boiling in a wide range of temperatures, and provide evidence of the formation of lighter material from the cracking of asphaltenes. Products with boiling points below 210°C are not present in these samples because they were removed along with the tetralin solvent.

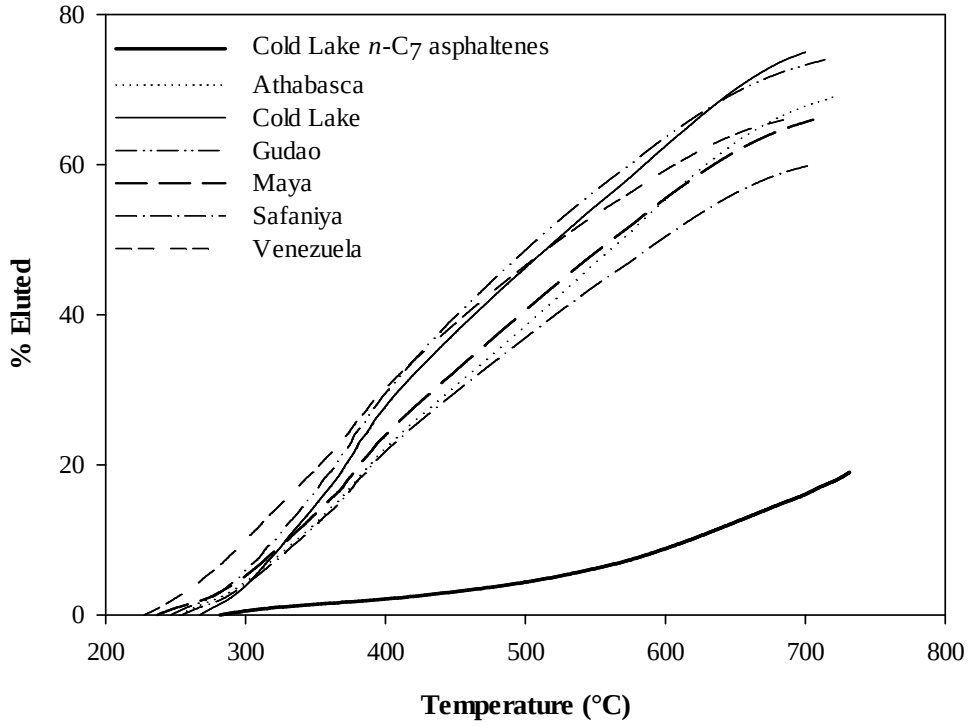

Figure 2-9. Boiling curves obtained by SimDist analysis of the liquid products from the reactions of different *n*-C_7 asphaltenes, after the removal of tetralin. The results for Cold Lake *n*-C_7 asphaltenes, before reaction, are shown for comparison.

These experiments provided a quantitative estimation of the conversion of the vacuum residue fraction, calculated as the disappearance of the > 538°C fraction. Similarly, conversions of *n*-C_7 insolubles were estimated from the results of the precipitation in presence of *n*-heptane of the samples after the reaction, and of the mixture of asphaltenes and tetralin before the reaction. MCR conversion was calculated from a balance on the amount of TGA residue, assuming coke as 100% TGA residue. These three different conversions are shown in Figure 2-10.

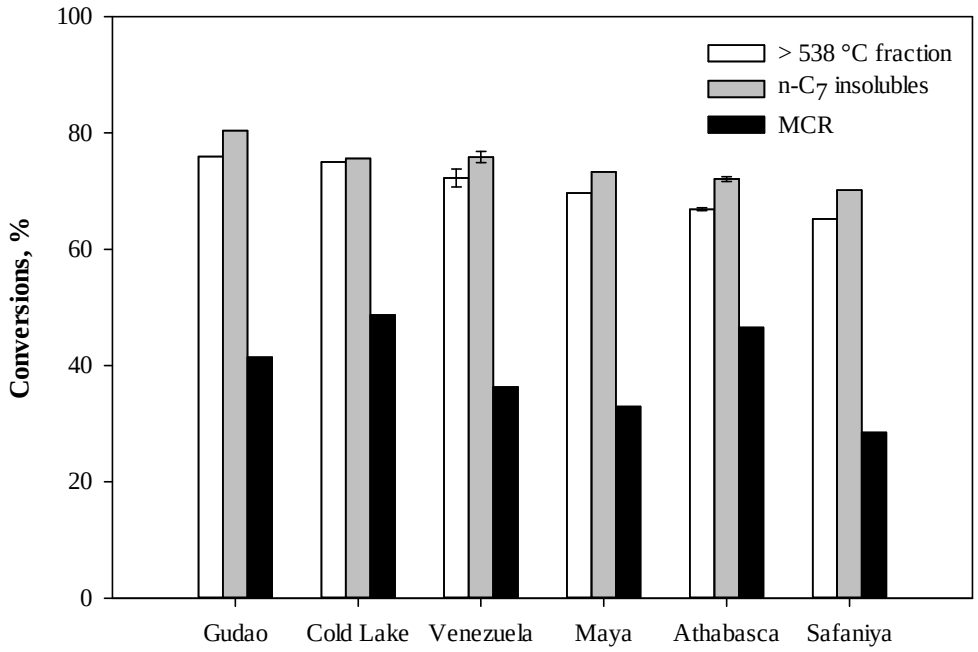

Figure 2-10. Conversions of vacuum residue fraction (> 538°C), *n*-C_7 insolubles, and MCR from the reactions of different *n*-C_7 asphaltenes reacted at 450ºC, for 3 hours, with tetralin/asphaltenes ratio of 2.5/1 and 2% catalyst

The conversions of the vacuum residue fraction and of the *n*-C_7 insolubles were very similar for each of the different asphaltenes evaluated, with values in the range between 65 to 80%. MCR conversions exhibited a different trend than the other two, and varied in the range of 30 to 55%. Safaniya *n*-C_7 asphaltenes presented the lowest values for the three different conversions.

The percentage of aliphatic sulphur determined by XPS analysis showed a high correlation with the conversion of the vacuum residue fraction, as well as with the sum of yields of coke and > 538°C fraction, as shown in Figure 2-11. Higher percentages of aliphatic sulphur led to higher conversions of the vacuum

residue fraction, and to lower yields of coke + > 538°C faction. This observation suggests that for this set of *n*-C_7 asphaltenes with comparable sulphur content, higher amounts of sulphide bonds would allow higher release of fragments because of its thermally labile character, resulting in higher conversions.

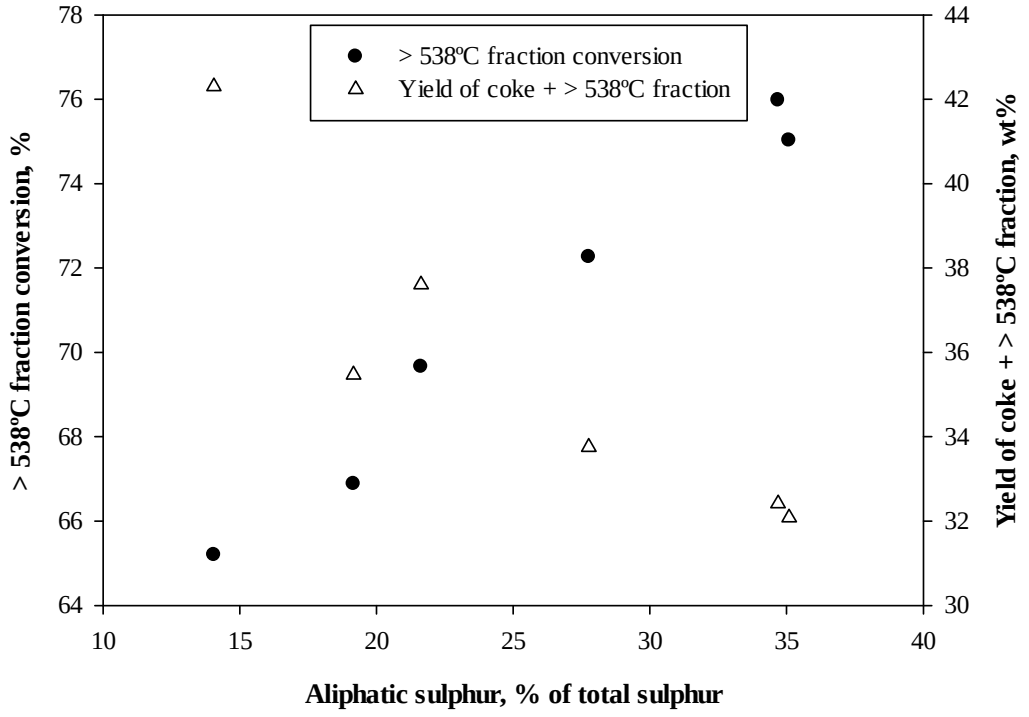

Figure 2-11. Conversion of the > 538°C fraction Vs. Percentage of aliphatic sulphur

The conversion of tetralin was estimated with the results from the GC-FID analysis of the light fractions recovered from the distillations of the total liquid products from the reactions of Athabasca and Maya *n*-C_7 asphaltenes. The amount of hydrogen transferred from tetralin to the asphaltenes was calculated based on the amount of naphthalene produced, as reported by Rahmani et al.[38]. Thus, four

atoms of hydrogen would have been transferred to asphaltenes per each molecule of naphthalene produced. These results are summarized in Table 2-7.

Table 2-7. Conversion of tetralin and hydrogen transfer in reactions of asphaltenes under hydrogenation conditions, estimated by GC-FID analysis of the boiling fraction < 343°C obtained from distillation of the total liquid products.

Asphaltenes	**Tetralin conversion (wt%)**	**Tetralin converted to naphthalene (wt%)**	**H transfer mg H / g asphaltenes**
Athabasca *n*-C_7	45.9	21.3	16.6
Maya *n*-C_7	43.3	23.5	18.3

The main product from the reaction of tetralin was naphthalene, and the other major products identified by GC-MS analysis of the light fraction included 1-methylindan, and *n*-butylbenzene, with approximate yields of 10 and 2.5 wt%, respectively. The remaining mass of tetralin that accounts for approximately 10 wt% underwent addition reactions, as observed in other studies.[38, 39]

2.3.6 Characterization of the pendant groups

Analysis of the liquid products by GC-FI-TOF HR MS provided information about the molecular structures of the molecules present in the distillates fraction (< 538°C material). Figure 2-12 shows the abundance of each one of these compounds for the six different asphaltenes evaluated in this study. The similarity observed in the composition between the different asphaltenes is remarkable. The most abundant compounds in the distillates fraction are in the

categories of saturate and 1-3 ring aromatic structures which include other subcategories of molecules, as illustrated in Figure 2-13.

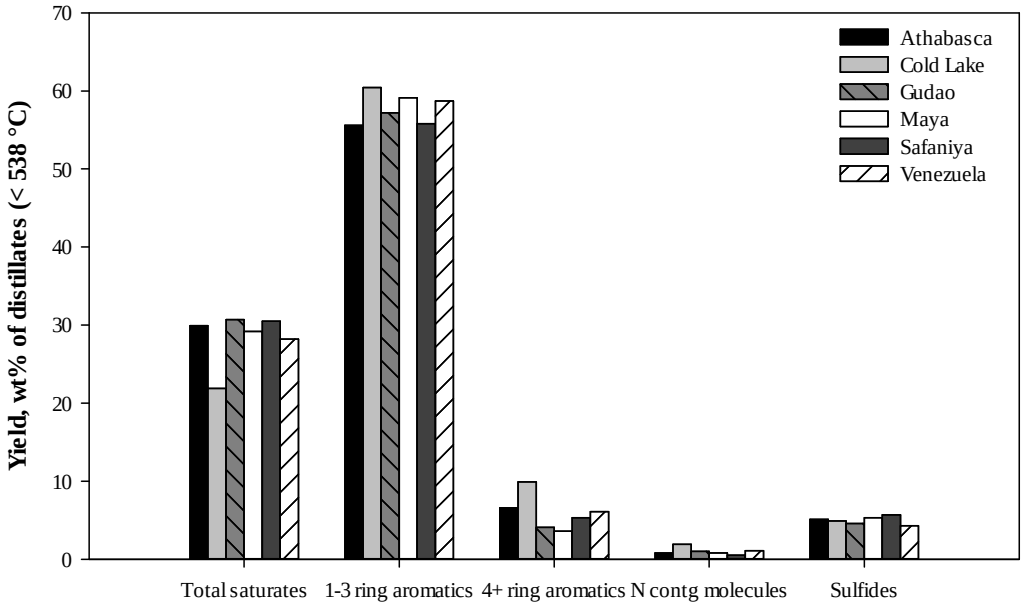

Figure 2-12. GC-FI-TOF HR MS Results for the distillates fraction (< 538ºC) from the cracking of different asphaltenes samples under hydrogenation conditions

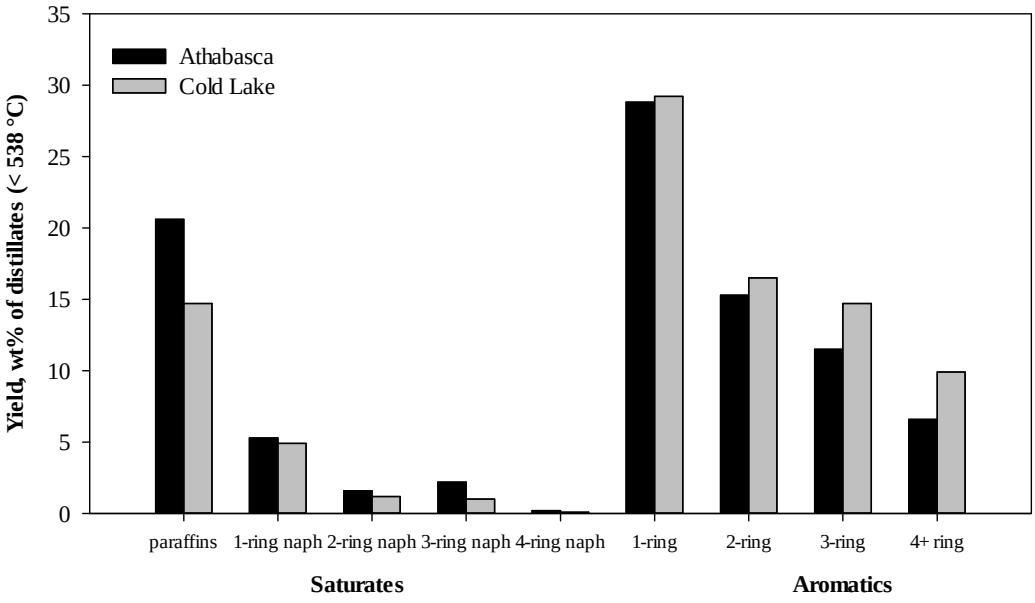

Figure 2-13. Saturate and aromatic speciation of pendant groups obtained by GC-FI-TOF HR MS analysis of the liquid products from the reaction of Athabasca and Cold Lake *n*-C_7 asphaltenes

The category of 1-ring aromatics includes olefins, thiophenes, and alkylbenzenes; benzothiophenes, naphthenobenzothiophenes, and alkylnaphthalenes are accounted for in the category of 2-ring aromatic compounds, and dibenzothiophenes are comprised in the 3-ring aromatic molecules. Figure 2-13 shows the saturate and aromatic speciation of the distillates for Athabasca and Cold Lake *n*-C_7 asphaltenes, and they provide a good representation of the abundance of these species for the set of asphaltenes evaluated, since no significant differences were observed, as shown in the summary of results obtained from the GC-MS analysis presented in Table 2-8.

Table 2-8. Molecular species identified by GC-FI-TOF HR MS analysis in the distillates

Yield, wt% of distillate	Athabasca	Cold Lake	Gudao	Maya	Safaniya	Venezuela
Total saturates	29.9	21.9	30.7	29.2	30.5	28.2
paraffins	20.6	14.7	21.6	19.7	21.2	19.0
1-ring naphthenes	5.3	4.9	5.1	5.2	5.0	5.1
2-ring naphthenes	1.6	1.2	1.3	1.8	1.7	1.8
3-ring naphthenes	2.2	1.0	2.5	2.3	2.4	2.0
4-ring naphthenes	0.2	0.1	0.2	0.2	0.2	0.3
Total 1-ring aromatics, thiophenes, and olefins	28.8	29.2	31.1	30.6	28.1	30.6
1-ring aromatics	18.7	23.3	20.2	20.9	18.8	19.7
alkyl benzenes	7.9	9.3	7.8	8.3	7.5	7.8
Total 2-ring aromatics	15.3	16.5	16.5	17.7	16.6	16.4
benzothiophenes	4.0	4.8	4.1	5.2	5.2	4.1
naphthenobenzothiophenes	1.2	1.2	1.1	1.5	1.6	1.2
naphthalenes	5.7	5.8	6.8	6.4	5.7	6.2
Total 3-ring aromatics	11.5	14.7	9.6	10.8	11.1	11.7
dibenzothiophenes	2.0	2.7	1.5	1.9	2.0	1.6
4+ ring aromatics	6.6	9.9	4.1	3.6	5.3	6.1
N-containing molecules	0.8	1.9	1.0	0.8	0.5	1.1
Sulfides	5.1	4.9	4.6	5.3	5.7	4.3

These results showed a variety of molecular structures present in the distillates recovered from the cracking of asphaltenes, including homologous series of saturate, aromatic, and heteroatomic species, which exhibited a

distribution of molecular weights below 700 Da. This variety of molecules had been previously identified by Strausz et al.,[13] Payzant et al.,[12] and Pelet and coworkers,[40] and quantitative evidence of these bridged structures was provided by Karimi et al.[15] The difference in this case is a higher yield of these building blocks from the original asphaltene fractions.

The relative abundance of molecular structures in the distillates obtained by cracking of asphaltenes under hydrogenation conditions presented higher yields of paraffins, 1-ring aromatics, and 4+ ring aromatics, compared to the results reported by Karimi et al.,[15] from the analysis of distillates obtained by thermal cracking in thin films. In contrast, other species such as 1,2, and 3-ring naphthenes, and 2-ring aromatics exhibited significantly lower yields in the distillates obtained in the present study. This comparison suggests that hydrogenation conditions, in addition to offering higher yields of analyzable material, also favored the release of large aromatic clusters, such as 4+ ring aromatics, which under thermal cracking conditions would more likely contribute to the coke yield. The abundances of 1 and 2-ring aromatics were subjected to corrections by subtraction of tetralin, naphthalene, and byproducts present in the samples; thus, some degree of uncertainty is involved in those values.

An overall view of the results, summarized in Figure 2-14, shows that the material that could not be converted to distillates and remained in the vacuum residue fraction (> 538°C), or ended up as coke, accounted for 35 to 45 wt% of the initial mass of asphaltenes. This material would be mainly constituted by polyaromatic, and large naphthenic or naphthenoaromatic clusters that cannot be

converted to distillates or gases under the reaction conditions used in this study. Examples of these structures are illustrated in Figure 2-15. As observed in the experiments with phenanthrene and 5α-cholestane, the ring structures were highly preserved, consistent with the results obtained in experiments with model compounds made by Savage and coworkers.[41]

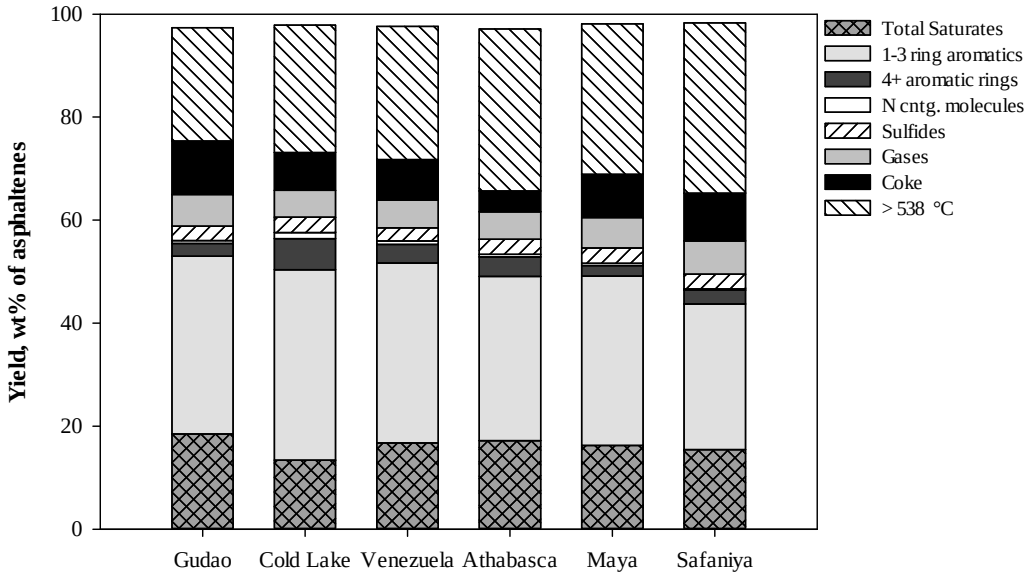

Figure 2-14. Overall yields from the cracking of different asphaltenes samples under hydrogenation conditions

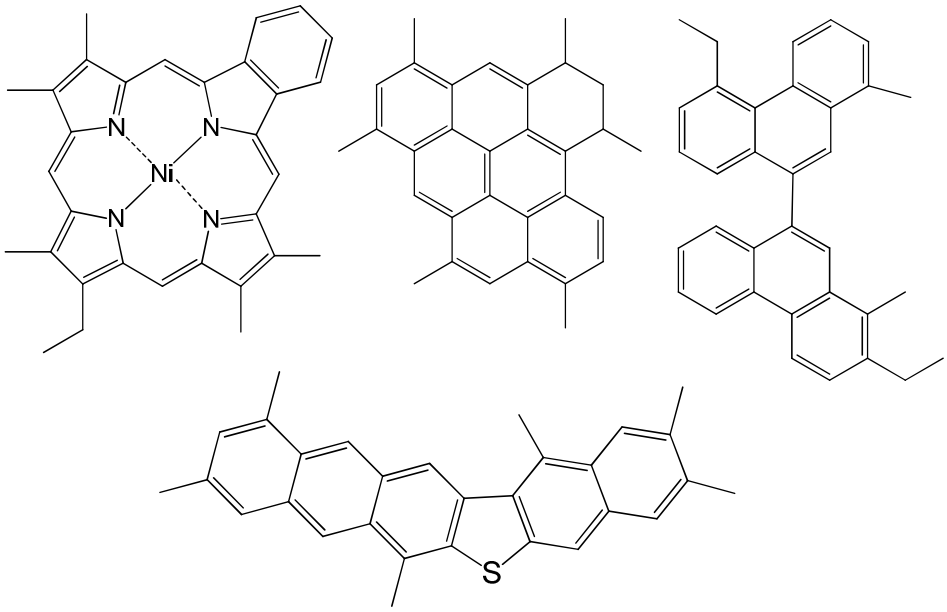

Figure 2-15. Examples of molecular structures that would survive under the reaction conditions used in this study

2.4 Implications for the molecular composition of asphaltenes

The reaction approach used in this study provided high yields of distillates which constitute the analyzable material for the characterization of the building blocks present in asphaltenes. In a previous study, Savage et al.[19] reported the benefit of introducing hydrogen-donor solvents into the reaction, as the yield of maltenes was significantly favored, and longer induction times for coke formation were observed. Similarly in this study, the hydrogenation conditions resulting from the hydrogen atmosphere, the use of tetralin as hydrogen-donor solvent, and the presence of an iron-based catalyst with low hydrogenation activity, provided favorable conditions that produced minimal coke and high yield of distillates,

while ensuring minimal change of the molecular structures in the cracked fragments.

Thus, under these hydrogenation conditions, the reaction variables were adjusted to push the yield of distillates to its maximum, and samples of asphaltenes from different geological basins in the world presented comparable yields for the different cracking products at their highest capacity to produce distillates. The high resolution GC-MS analysis of the distillable fraction also revealed a remarkable similarity in the abundance of the diverse molecular structures, including saturate, aromatic, naphthenoaromatic, and heteroatomic species.

Some of the most abundant structures identified involved saturate compounds, mainly paraffins, and also aromatic structures with 1 to 3 rings. Paraffins ranged between 9 to 13 wt% of the initial mass of asphaltenes, and the naphthenic species had individual abundances below 3.0 wt%. The aromatic structures with 1 ring presented yields between 14 to 18%, 2-ring compounds between 8 to 10%, and the 3-ring units exhibited abundances in the range between 5.5 to 9%.

Nitrogen containing molecules involved mainly alkylcarbazoles, and the sulfides referred to cyclic compounds containing aliphatic sulphur. Other sulphur species, such as thiophenic, benzothiophenic and dibenzothiophenic compounds were accounted for in the 1-ring, 2-ring, and 3-ring aromatic compounds, respectively. The GC-MS results could not provide information about the sulphur present in sulphide bridges, as the carbon-sulphur bond is thermally labile,[11] and

therefore, would most likely form H_2S during the evolution of the cracking reactions.

The abundant variety of molecular structures suggests that stochastic combinations of the individual fragments would lead to complex and diverse heterogeneity of asphaltene molecules, as previously presented by Sheremata et al.,[42] and Jaffe et al.,[43] in their efforts to obtain structural representations of asphaltenes and vacuum residue molecules, respectively.

The results from this study cannot provide any information about the structures that remained in the fraction of unconverted vacuum residue, or that formed coke. Thus, this work cannot give any information about size of the large clusters present in asphaltenes, but suggests that they would account for up to 45 wt% of the initial mass of asphaltenes, since the material remaining in the vacuum residue fraction, or that ended up in coke, would be formed not only for polyaromatic or large naphthenoaromatic structures that were originally present in asphaltenes, and are refractive under the reaction approach used in this study, but also could have arisen from condensation reactions during the process.

Likewise, these results cannot provide any inference regarding the molecular weight distribution of asphaltenes, and the number and length of bridges present in these molecules. However, the high yield of 1-3 ring aromatic molecules suggests an important presence of bridged-structures in the asphaltenes.

The samples evaluated, originally from different regions in the world including the Middle East, China, Mexico, South America, and Canada, exhibited an outstanding similarity. These results suggested that the data from this study

could be extrapolated to other asphaltene samples, however, we cannot rule out the possibility that some crude oils could contain asphaltenes which present significant differences compared to this data set.

2.5 Conclusions

1. Cracking of asphaltenes under hydrogenation conditions, involving the use of tetralin as hydrogen-donor solvent, an iron-based catalyst with modest hydrogenation activity, and hydrogen atmosphere at moderate pressures, provided favorable conditions to obtain high yields of material in the distillates range, with low production of coke, while ensuring minimal change of the ring structures of the cracked fragments, as proved with the reaction of phenanthrene and 5α-cholestane as model compounds.
2. Reaction variables of 450°C, residence time of 3 hours, hydrogen pressure of 4.1 MPa (measured at ambient temperature), tetralin/asphaltenes ratio of 2.5/1, and addition of 2% of iron-based catalyst, led to yields of distillates (< 538°C material) in the range of 50 to 60%, and coke yields below 10%.
3. Characterization of the distillates from the cracking of asphaltenes from different geological basins showed significant similarity in the abundance of the cracked fragments, suggesting a low impact of the origin on the composition of the building blocks in asphaltenes.
4. Gas chromatography – field ionization – time of flight high resolution mass spectrometry analysis identified a large variety of molecular structures present in asphaltenes ranging from saturates to aromatics and heteroatomic

compounds. Higher yields of homologous series of saturate molecules, and 1 to 3-ring aromatics were obtained compared to other species. The high yield of paraffins suggested that bridges would play an important role in the architecture of asphaltenes.

5. The material remaining in the vacuum residue fraction, together with the coke produced in the reaction, added up to 35 to 45% of the initial mass of asphaltenes. This material would account for the maximum amount of large aromatic clusters present in asphaltenes that under the cracking conditions used in this study could not be converted to lighter products.

2.6 References

1. Gray, M. R.; Tykwinski, R. R.; Stryker, J. M.; Tan, X. Supramolecular Assembly Model for Aggregation of Petroleum Asphaltenes. *Energy & Fuels* **2011**, *25*, 3125-3134.
2. Dechaine, G. P.; Gray, M. R. Membrane Diffusion Measurements Do Not Detect Exchange between Asphaltene Aggregates and Solution Phase. *Energy & Fuels* **2011**, *25*, 509-523.
3. Yen, T. F. Structure of Petroleum Asphaltene and Its Significance. *Energy Sources, Part A: Recovery, Utilization, and Environmental Effects* **1974**, *1*, 447-463.
4. Dickie, J. P.; Yen, T. F. Macrostructures of the asphaltic fractions by various instrumental methods. *Analytical Chemistry* **1967**, *39*, 1847-1852.

5. Mullins, O. C. The Modified Yen Model. *Energy & Fuels* **2010**, *24*, 2179-2207.

6. Groenzin, H.; Mullins, O. Asphaltene molecular size and structure. *J. Phys. Chem. A* **1999**, *103*, 11237-11245.

7. Groenzin, H.; Mullins, O. C. Molecular Size and Structure of Asphaltenes from Various Sources. *Energy & Fuels* **2000**, *14*, 677-684.

8. Strausz, O. P.; Safarik, I.; Lown, E. M.; Morales-Izquierdo, A. A critique of asphaltene fluorescence decay and depolarization-based claims about molecular weight and molecular architecture. *Energy & Fuels* **2008**, *22*, 1156-1166.

9. Calemma, V.; Iwanski, P.; Nali, M.; Scotti, R.; Montanari, L. Structural characterization of asphaltenes of different origins. *Energy & Fuels* **1995**, *9*, 225-230.

10. Calemma, V.; Rausa, R.; D'Antona, P.; Montanari, L. Characterization of asphaltenes molecular structure. *Energy & Fuels* **1998**, *12*, 422-428.

11. Ignasiak, T.; Kemp-Jones, A.; Strausz, O. P. The molecular structure of Athabasca asphaltene. Cleavage of the carbon-sulfur bonds by radical ion electron transfer reactions. *J. Org. Chem.* **1977**, *42*, 312-320.

12. Payzant, J. D.; Lown, E. M.; Strausz, O. P. Structural units of Athabasca asphaltene: the aromatics with a linear carbon framework. *Energy & Fuels* **1991**, *5*, 445-453.

13. Strausz, O. P.; Mojelsky, T. W.; Faraji, F.; Lown, E. M.; Peng, P. Additional Structural Details on Athabasca Asphaltene and Their Ramifications. *Energy & Fuels* **1999**, *13*, 207-227.

14. Speight, J. G. Petroleum asphaltenes - Part 1: Asphaltenes, resins and the structure of petroleum. *Oil and Gas Science and Technology* **2004**, *59*, 467-477.

15. Karimi, A.; Qian, K.; Olmstead, W. N.; Freund, H.; Yung, C.; Gray, M. R. Quantitative Evidence for Bridged Structures in Asphaltenes by Thin Film Pyrolysis. *Energy & Fuels* **2011**, *25*, 3581-3589.

16. Strausz, O. P.; Mojelsky, T. W.; Lown, E. M. The molecular structure of asphaltene: an unfolding story. *Fuel* **1992**, *71*, 1355-1363.

17. Gray, M. R. Consistency of Asphaltene Chemical Structures with Pyrolysis and Coking Behavior. *Energy & Fuels* **2003**, *17*, 1566-1569.

18. Wiehe, I. A. The Pendant-Core Building Block Model of Petroleum Residua. *Energy & Fuels* **1994**, *8*, 536-544.

19. Savage, P. E.; Klein, M. T.; Kukes, S. G. Asphaltene reaction pathways. 3. Effect of reaction environment. *Energy & Fuels* **1988**, *2*, 619-628.

20. Gray, M. R.; McCaffrey, W. C. Role of Chain Reactions and Olefin Formation in Cracking, Hydroconversion, and Coking of Petroleum and Bitumen Fractions. *Energy & Fuels* **2002**, *16*, 756-766.

21. Furimsky, E. Selection of catalysts and reactors for hydroprocessing. *Applied Catalysis A: General* **1998**, *171*, 177-206.

22. Ranganathan, R.; Denis, J. D.; Pruden, B. B. U.S. Patent 4,214,977, 1980.

23. Qian, K.; Dechert, G. J. Recent Advances in Petroleum Characterization by GC Field Ionization Time-of-Flight High-Resolution Mass Spectrometry. *Analytical Chemistry* **2002**, *74*, 3977-3983.

24. Chadha, A.; Stinespring, C. D.; Stiller, A. H.; Zondlo, J. W.; Dadyburjor, D. B. Characterization and Activity of Ferric-Sulfide-Based Catalyst in Model Reactions of Direct Coal Liquefaction: Effect of Preparation Conditions. *Ind. Eng. Chem. Res.* **1997**, *36*, 284-295.

25. Suzuki, T.; Yamada, H.; Sears, P. L.; Watanabe, Y. Hydrogenation and hydrogenolysis of coal model compounds by using finely dispersed catalysts. *Energy & Fuels* **1989**, *3*, 707-713.

26. Nuzzi M. Hydrogenation of Phenanthrene in the Presence of Nickel. I. Sequence of the Transformations Between Partially Hydrogenated Intermediate Products; Idrogenazione Del Fenantrene In Presenza Di Nichel I - Andamento Delle Trasformazioni Tra Gli Intermedi Parzialmente Idrogenati. *Rivista dei combustibili* **1986**, *40*, 219-231.

27. Benbenek, S.; Fedorynska, E.; Winiarek, P. Hydrogenation of polyaromatic coal related hydrocarbons by hydrogen transfer. *Fuel* **1994**, *73*, 1348-1353.

28. Bate, K.; Harrison, G. *Hydrogen Transfer Reactions in Model Systems Representative of Recycle Solvents;* Coal Science II; American Chemical Society: 1991; Vol. 461, pp 236-249.

29. Carlson, R. M. K.; Croasmun, W. R.; Chamberlain, D. E. *Transformations of cholestane useful for probing processing chemistry;* Proceedings of the

210th National Meeting of the American Chemical Society, August 20, 1995 - August 25; ACS: Chicago, IL, USA, 1995; Vol. 40, pp 685-690.

30. Kissin, Y. V. Catagenesis of light cycloalkanes in petroleum. *Organic Geochemistry* **1990**, *15*, 575-594.

31. Poutsma, M. L. Free-radical thermolysis and hydrogenolysis of model hydrocarbons relevant to processing of coal. *Energy & Fuels* **1990**, *4*, 113-131.

32. De Vlieger, J. J.; Kieboom, A. P. G.; Van Bekkum, H. Behaviour of tetralin in coal liquefaction: Examination in long-run batch-autoclave experiments. *Fuel* **1984**, *63*, 334-340.

33. Siskin, M.; Kelemen, S. R.; Eppig, C. P.; Brown, L. D.; Afeworki, M. Asphaltene Molecular Structure and Chemical Influences on the Morphology of Coke Produced in Delayed Coking. *Energy & Fuels* **2006**, *20*, 1227-1234.

34. Furimsky, E.; Massoth, F. E. Deactivation of hydroprocessing catalysts. *Catalysis Today* **1999**, *52*, 381-495.

35. Jimenez Mateos, J. M.; Fierro, J. L. G. X-ray photoelectron spectroscopic study of petroleum fuel cokes. *Surface and Interface Analysis* **1996**, *24*, 223-236.

36. Fukuyama, H.; Ohtsuka, K.; Terai, S.; Sawamoto, S. U.S. Patent 6,797,153, 2004.

37. Derbyshire, F.; Hager, T. Coal liquefaction and catalysis. *Fuel* **1994**, *73*, 1087-1092.

38. Rahmani, S.; McCaffrey, W. C.; Dettman, H. D.; Gray, M. R. Coking kinetics of asphaltenes as a function of chemical structure. *Energy & Fuels* **2003**, *17*, 1048-1056.

39. Khorasheh, F.; Rangwala, H. A.; Gray, M. R.; Dalla Lana, I. G. Interactions between thermal and catalytic reactions in mild hydrocracking of gas oil. *Energy & Fuels* **1989**, *3*, 716-722.

40. Pelet, R.; Behar, F.; Monin, J. C. Resins and asphaltenes in the generation and migration of petroleum. *Organic Geochemistry* **1986**, *10*, 481-498.

41. Savage, P. E.; Klein, M. T. Asphaltene reaction pathways. 4. Pyrolysis of tridecylcyclohexane and 2-ethyltetralin. *Ind. Eng. Chem. Res.* **1988**, *27*, 1348-1356.

42. Sheremata, J. M.; Gray, M. R.; Dettman, H. D.; McCaffrey, W. C. Quantitative Molecular Representation and Sequential Optimization of Athabasca Asphaltenes. *Energy & Fuels* **2004**, *18*, 1377-1384.

43. Jaffe, S. B.; Freund, H.; Olmstead, W. N. Extension of Structure-Oriented Lumping to Vacuum Residua. *Ind. Eng. Chem. Res.* **2005**, *44*, 9840-9852.

3 Evaluation of different solvents on coke formation during cracking of asphaltenes under hydrogenation conditions

3.1 Introduction

The present work employs the same catalyst and methods already described in Chapter 2 on the cracking of asphaltenes under hydrogenation conditions. Different solvents with and without hydrogen-donation capacity were evaluated based on their ability to suppress coke formation. Previous studies had shown the positive effect of the presence of hydrogen-donors during asphaltene cracking.[1-5] Significantly lower coke yields are obtained in the reactions carried out in the presence of these solvents.

Carlson et al.[6] observed that naphthenoaromatic solvents, such as 1,2,3,4-tetrahydronaphthalene, also known as tetralin, were more effective as hydrogen-donors than purely naphthenic compounds, such as decalin. They pointed out that this hydrogen transfer takes place in absence of catalyst, but the dehydrogenation products from the solvent could be regenerated and recycled to the process via catalytic hydrogenation. In their study, other solvents such as: *n*-heptane, benzene, naphthalene, and methylcyclohexane were also evaluated in order to include paraffinic, aromatic and naphthenic compounds. The cracking of a residuum sample showed that only tetralin had a significant improvement as coke

suppressor, followed by decalin. Some of the other solvents could reduce the production of coke but just marginally.

Del Bianco and coworkers[7] compared dihydrophenanthrene with other aromatic and polar solvents, including phenanthrene, 1-methylnaphthalene, quinoline, and 1-naphthol. The results showed that dihydrophenanthrene reduced significantly the coke yield, and from the other solvents tested, only phenanthrene could reduce moderately the production of coke. They suggested that reactions leading to coke formation were better controlled in presence of solvents with the capability of solvating the coke precursors.

Savage et al.[3] carried out cracking experiments under different reaction environments, involving toluene, and tetralin, in the presence and absence of hydrogen. The cracking in presence of toluene and hydrogen, and the reaction with tetralin, showed in common higher selectivities to maltenes, longer induction times for the formation of coke, and also lower reaction rates. These results suggested that toluene offered a good solubility medium for hydrogen and asphaltenes, reducing possible mass transfer limitations present in the neat reactions. Thus, with the contribution of the hydrogen participating in the reaction, the asphaltenes could preserve their hydrogen content, slowing down its transformation to coke.

Rahmani et al.[4] conducted experiments with asphaltenes in presence of different solvent mediums, including 1-methylnaphthalene, naphthalene, and tetralin. The results showed that 1-methylnaphthalene, in spite of its ability to form benzylic radicals and act as radical acceptor, did not affect the pathway for

coke formation. This study also evidenced the important influence of the chemical interactions between the asphaltenes and the solvent. The hydrogen transfer was apparently dependent not only on the concentration of the hydrogen-donor solvent, but also on the hydrogen uptake capability of the asphaltenes, which seemed to have a maximum value.

From their experiments with *n*-hexadecane and tetralin, Khorasheh et al.[8] observed a rapid abstraction of hydrogen from tetralin, and identified the participation of tetralin radicals in addition reactions with α-olefins formed as products from the cracking of the paraffin. Thus, Gray et al.[9] explained the coke suppression role of the hydrogen-donor solvents as a result of their susceptibility to react with the olefins formed during the cracking process. Consequently, instead of taking part eliminating radicals, hydrogen-donors would rather contribute in the removal of olefins which can polymerize and lead to the formation of coke. Savage et al.[3] had also attributed the coke suppression ability of these solvents to their action maintaining the solubility of the reacted asphaltenes.

Tetralin and other hydrogen-donors, such as hydrophenanthrenes, and 1,2,3,4-tetrahydroquinoline have been also studied as solvents during coal liquefaction.[10-13] Kamiya et al.,[11] for instance, concluded that three-ring hydroaromatics were more effective in coal liquefaction than tetralin. In their experiments, different solvents were evaluated in the presence of identical amounts of tetralin and 1-methylnaphthalene. Thus, the observed order of solvent conversion, as well as hydrogen-donating activity was: dihydroanthracene (DHA)

> dihydrophenanthrene (DHP) > 1,2,3,4-tetrahydroquinoline (THQ) > 1,2,3,4-tetrahydro-6-naphthol (THN) > 1,2,3,4,5,6,7,8-octahydroanthracene (OHA).

It has been also observed that during the process, tetralin not only undergoes dehydrogenation reactions, with naphthalene as the main product, but also isomerization to produce 1-methylindane, and ring-opening forming *n*-butylbenzene and other alkylbenzenes, as described by Poutsma et al.[12] The reduction of the hydrogen-donation capacity of the hydroaromatic solvents due to these molecular rearrangements was discussed by Cronauer et al.[14]

There is evidence that coke formation is preceded by phase separation.[9, 15, 16] This observation suggests that solubility plays an important role during the cracking reactions. When asphaltenes are reacted, their building blocks can be released, and the remaining structures become more aromatic. Additionally, these cracking reactions take place together with condensation and cyclization reactions that can promote the formation of high molecular weight structures. According to the phase diagram proposed by Wiehe,[17] these molecular changes that reduce hydrogen content and increase molecular weight can lead to the formation of coke. Wiehe[15] also observed that the phase separation occurred after an induction time during which these structures would concentrate until the solubility limit is exceeded. Thus, the presence of solvents in the medium can have an important impact on the phase behavior of the reaction mixture. In the case of hydrogen-donor solvents, the observed coke suppression could then be attributed to a combined ability to react with olefins[9] and maintain the solubility of the coke precursors.[3]

After the phase separation, the coke formation occurs at high reaction rates, as presented by Wiehe[15] and confirmed by Rahmani et al.[4] This also results in the formation of a separate phase, called mesophase, which exhibits the characteristics of liquid crystals.[18-20] This carbonaceous mesophase is an optically anisotropic material, which can be identified under microscopy analysis surrounded by an isotropic liquid phase. According to Hurt et al.,[21] mesophase is thought to be made up of approximately planar aromatic clusters with significant spatial order to be classified as a liquid crystal.

Bagheri et al.[19] reported the formation of liquid crystals in oil samples from different geological origins by inverted reflective microscopy. These crystalline domains, appeared in particular temperature ranges for each sample, and exhibited an amphotropic behavior; so, their formation was modified by changes in temperature and addition of solvents. These results suggested that liquid crystal analysis can provide an alternative method to get some insight into the complex phase behavior of petroleum samples.

The objective of this study was to compare different solvents based on their ability to reduce the formation of coke during the cracking of Athabasca industrial *n*-C_5 asphaltenes, in the presence of hydrogen and an iron-based catalyst. The reactions were done at 450°C and with residence time of three hours. The solvents that were compared included hydrogen-donors such as: 9,10-dihydrophenanthrene, 9,10-dihydroanthracene, tetralin, and 1,2,3,4-tetrahydroquinoline, and other aromatic solvents, such as: toluene, quinoline, pyridine, and 1-methylnaphthalene. Tetralin was used as reference to compare the

results and identify which solvents would lead to lower coke yields that could make them appropriate for studies of asphaltene molecular structures.

This study also reports the results from the optical microscopy analysis for mesophase formation of different asphaltene samples. This analysis was intended to identify some possible relation between the temperatures for liquid crystal formation and the molecular composition of the asphaltenes, based on the characterization data presented in Chapter 2. These analyses were performed in a novel hot-stage microreactor coupled to an inverted reflective microscope, as described by Bagheri et al.[18, 22]

3.2 Materials and Methods

3.2.1 Asphaltenes

Cracking reactions under hydrogenation conditions were made with an Athabasca industrial asphaltene sample that yielded 68% of *n*-C_5 asphaltenes and 59% of *n*-C_7 asphaltenes. This sample was used as received and named as Athabasca industrial *n*-C_5 asphaltenes. Cold Lake *n*-C_7 asphaltenes were provided by ExxonMobil Research and Engineering, and were used without any further treatment. Colombian and Venezuelan *n*-C_7, and Athabasca *n*-C_7 and *n*-C_5 asphaltenes were obtained by precipitation using a ratio of 40:1 of solvent (*n*-heptane or *n*-pentane) to sample (vacuum residue or Athabasca industrial *n*-C_5 asphaltenes). After the addition of the solvent, the mixture was stirred by a magnetic bar for 24 hours, afterwards the asphaltenes were filtered out under

vacuum using a 0.22 µm filter paper (Millipore), and dried at room temperature for 48 hours.

Elemental analysis of these asphaltenes samples was made in an Elementar vario MICRO CUBE unit (Elementar Americas, Inc., Mt. Laurel, NJ). The method ASTM D4530 for microcarbon residue content (MCR) was approximated by TGA analysis in a TherMax 400 Cahn Thermogravimetric Analyzer (Thermo Fisher Scientific, Waltham, MA). With argon flowing at 50 mL/min, the temperature profile consisted of an isothermal step at 21.8 ºC for 10 minutes, then the temperature was increased at a rate of 5 ºC/min up to 500 ºC, and this final temperature was maintained for 2 hours. In order to determine the ash content and report MCR on ash-free basis, the temperature program was followed by an isothermal step at 500°C for 2 hours (5 hours in the case of Cold Lake *n*-C_7 asphaltenes), with air flowing at 50 mL/min. The residual mass after this thermal analysis was reported as the ash content.

3.2.2 Catalyst and Solvents

An iron-based catalyst prepared by wet impregnation of iron sulphate ($FeSO_4.7H_2O$, ≥ 99%, from Fisher Chemical) on sub-bituminous Coal Valley was used in the cracking reactions to provide a mild hydrogenation activity. The preparation of this catalyst was described in the previous chapter, and TGA analysis had evidenced a loading of iron as metal of 10.3 wt%.

The reactions were carried out in the presence of different solvents, with and without hydrogen-donation capacity, including 1,2,3,4-tetrahydronaphthalene

(99%, ReagentPlus® from Sigma Aldrich), also known as tetralin, 1,2,3,4-tetrahydroquinoline (98%, from Aldrich), 9,10-dihydrophenanthrene (94%, from Aldrich), 9,10-dihydroanthracene (97%, from Aldrich), pyridine (≥ 99.9%, CHROMASOLV® Plus for HPLC from Sigma-Aldrich), toluene (99.9%, certified ACS from Fisher Chemical), quinoline (98%, reagent grade from Aldrich), and 1-methylnaphthalene (97%, from Acros Organics).

3.2.3 Evaluation of different solvents during the cracking of asphaltenes under hydrogenation conditions

Athabasca industrial *n*-C_5 asphaltenes were reacted in the presence of the different solvents mentioned above, ensuring the same availability of hydrogen in each case, and taking the amount of tetralin as the reference case for those solvents without hydrogen-donation capacity. The reactions were performed in 15-mL stainless steel batch microreactors, made of nominal ¾-inch Swagelok fittings, already described in our previous study, and conducted at 450°C, with residence time of 3 hours, hydrogen pressure of 4.1 MPa (measured at room temperature), and 2 wt% of catalyst. The microreactor was loaded with known amounts of asphaltenes, solvent, and catalyst, and additionally five 3/16-inch stainless steel balls to provide better mixing during the reaction. The system was leak tested, purged three to five times to displace the air, and pressurized with hydrogen.

Afterwards, the microreactor was immersed in a preheated sand bath (Tecam model SBS-4, Cole-Parmer) equipped with a mechanical system for

continuous vertical agitation, and after three hours was removed from this heating system. The gases were released, and the coke was recovered by vacuum filtration using 0.22 µm pore size filter paper (Millipore), and methylene chloride (99.9%, Stabilized HPLC grade from Fisher Chemical) as the solvent. The filter paper with the coke was dried in oven at 80°C and weighed 24 hours later.

3.2.4 Polarized-light hot-stage microscopy

The liquid crystal formation for different asphaltenes samples was monitored in-situ in a hot-stage microreactor, already described by Bagheri et al.[19, 22]. The carbonaceous mesophase formation was reported as the temperature at which the intermediate optically anisotropic phase was observed. This microreactor has a novel design that includes a view window, allowing the observation of small particles through an inverted reflective microscope (Zeiss Axio-Observer, Germany) equipped with crossed polarizers. The microreactor was loaded with few milligrams of asphaltenes and heated to a maximum temperature of 300°C by a heating tape, monitoring the temperature with a type K thermocouple. The system was purged and pressurized with nitrogen at atmospheric pressure.

The samples analyzed included Athabasca *n*-C_7, *n*-C_5 and industrial *n*-C_5, Colombian, and Cold Lake *n*-C_7 asphaltenes. Liquid crystal analysis was also done on samples of Cold Lake and Athabasca *n*-C_7 asphaltenes recovered after the reactions under hydrogenation conditions, as described in our previous study, with temperature of 450°C, residence time of 3 hours, 2 wt% of iron-based catalyst,

and tetralin/asphaltenes ratio of 2.5/1. Thus, after these reactions, the coke was filtered out, and the asphaltenes were precipitated by mixing *n*-heptane with the liquid products in a ratio of 40:1. This mixture was sonicated for one hour in an Aquasonic Ultrasonic Cleaner (VWR Scientific, Model 150HT, frequency 50/60 Hz), and vacuum filtered 24 hours later, rinsing with *n*-heptane and using 0.22 µm pore size filter paper (Millipore). The asphaltenes recovered on the filter paper were dried in an oven at 80ºC for 24 hours, and then collected for the liquid crystal analysis.

3.2.5 Polarized Optical Microscopy

A sample of coke from the cracking of Venezuelan *n*-C_7 asphaltenes, reacted under the hydrogenation conditions already described above, in presence of tetralin, hydrogen, and an iron-based catalyst, was recovered directly from the microreactor without any further solvent rinsing, polished, and analyzed under normal and cross-polarized light in the inverted reflective microscope, as already described by Bagheri et al.[22]

3.3 Results and Discussion

3.3.1 Characterization of asphaltenes samples

The elemental compositions of the asphaltenes evaluated in this study are shown in Table 3-1. All the different samples showed similar composition, except Colombian *n*-C_7 asphaltenes which exhibited significantly lower amounts of sulphur and hydrogen, and high carbon content, leading to a remarkably low H/C

molar ratio. Cold Lake *n*-C_7 asphaltenes presented low carbon content mainly due to its high ash content, as shown in Table 3-2.

Table 3-1. Elemental composition of asphaltenes samples

Asphaltenes	C	H	N	S	H/C (molar ratio)
Athabasca industrial *n*-C_5	81.6	8.5	1.4	7.7	1.25
Athabasca *n*-C_5	81.5	7.6	1.6	7.9	1.12
Athabasca *n*-C_7	81.5	7.6	1.6	8.0	1.11
Cold Lake *n*-C_7	77.6	7.6	1.6	8.3	1.17
Colombian *n*-C_7	87.3	6.9	1.8	3.1	0.95
Venezuelan *n*-C_7	81.8	8.0	2.3	6.1	1.17

Table 3-2. TGA residues under inert and oxidative atmospheres estimate MCR and ash contents of asphaltenes samples

Asphaltenes	TGA residue*, wt%	Ash content, wt%
Athabasca industrial *n*-C_5	34.0	1.0
Athabasca *n*-C_5	44.4	1.0
Athabasca *n*-C_7	46.3	0.7
Cold Lake *n*-C_7	41.3	4.8
Colombian *n*-C_7	63.2	-
Venezuelan *n*-C_7	42.2	1.3
Athabasca *n*-C_7 after reaction**	69.4	1.6
Cold Lake *n*-C_7 after reaction**	73.6	0.0

* TGA residue at 500°C approximates microcarbon residue (MCR) content determined by method ASTM D4530

** Asphaltenes after reaction were recovered from the reactions under hydrogenation conditions by precipitation from the mixture with a ratio of 40/1 n-heptane to liquid products

MCR contents for the different asphaltenes, approximated by TGA analysis, are shown in Table 3-2 as TGA residue content. Athabasca industrial *n*-C_5 asphaltenes presented the lowest TGA residue content, and most of the *n*-C_7 asphaltenes showed values in the range of 43-47 wt%, except the Colombian asphaltenes that exhibited higher TGA residue content, comparable to the reacted *n*-C_7 asphaltenes.

3.3.2 Comparison of different solvents by coke yield during the cracking of asphaltenes under hydrogenation conditions

The performance of different solvents as coke suppressors was evaluated by reacting the same amount of asphaltenes, 0.870 grams, with equivalent amounts of solvents, based on their hydrogen donation ability. Thus, the amounts of solvents were calculated to maintain the same hydrogen availability provided by tetralin in a ratio of 2/1 to asphaltenes, as shown in Table 3-3. The amounts of the solvents without hydrogen donation capacity, such as 1-methylnaphthalene, pyridine, quinoline, and toluene, were the same as in the reaction with tetralin.

Table 3-3. Hydrogen donation capacity of the solvents and their ratios to asphaltenes in the reactions

Solvents	H donation capacity (mol H/mol)	g solvent / g asphaltenes
1-methylnaphthalene	-	2.0
Pyridine	-	2.0
Quinoline	-	2.0
Toluene	-	2.0
Tetralin	4	2.0
1,2,3,4-tetrahydroquinoline	4	2.0
9,10-dihydrophenanthrene	2	5.7
9,10-dihydroanthracene	2	5.6

The amount of solvent remaining in the liquid phase under the reaction conditions was estimated for each individual case with the Peng-Robinson equation of state (VMGSim, Virtual Materials Group Inc., Calgary, CA). These estimates are presented in Table 3-4, and show that the percentage of solvent remaining in the liquid phase increases with the boiling point and critical temperature of the solvents. Thus, pyridine and toluene would be almost entirely in the vapor phase; while 9,10-dihydrophenanthrene, and 9,10-dihydroanthracene would be mainly in the liquid phase at the experimental conditions. The other solvents would be more evenly distributed between the liquid and vapor phases. The amount of liquid solvent is relevant since the reactions in the liquid phase determine the characteristics of the cracking process[9], and as observed by Rahmani et al.[4], the formation of coke is significantly influenced by the chemical interactions between the solvent and the asphaltenes.

Table 3-4. Some properties of the solvents and their percentages remaining in the liquid phase under the reaction conditions

Solvents	Solubility parameter $(MPa)^{1/2}$	Boiling point (°C)	Critical temperature (°C)	%wt solvent in liquid phase
1-methylnaphthalene	20.3[23]	240-243	498.9	63.0
Pyridine	21.7[23]	115.2	346.8	11.2
Quinoline	22.1[24]	237	509.0	61.6
Toluene	18.3[23]	110.6	318.6	8.4
Tetralin	19.4[23]	206-208	447.0	37.3
1,2,3,4-tetrahydroquinoline	22.6[24]	249	503.9	59.4
9,10-dihydrophenanthrene	-	307.8	568.9	94.1
9,10-dihydroanthracene	-	312	535.9	91.8

The reactions were made in duplicate with most of the solvents, except for 9,10-dihydrophenanthrene and 9,10-dihydroanthracene with only one reaction performed for each solvent. In the case of tetralin, four replicates of the experiment were made. The yields of coke were corrected by the amount of catalyst recovered together with the solid products from the reactions. Thus, blank reactions were made with each solvent to estimate the amount of catalyst recovered after the process. These blank reactions were made under the same conditions, but without asphaltenes, and the amounts of catalyst recovered on the filter paper were used to correct the amount of coke.

The yields of coke are compared in Figure 3-1. 1-methylnaphthalene and pyridine presented the highest yields of coke, representing approximately 25 wt% of the initial mass of asphaltenes. These results are comparable to the coke yield

reported by Karimi et al.,[25] for the same asphaltene sample, by thermal cracking in thin films. Tetralin and 1,2,3,4-tetrahydroquinoline showed comparable yields of coke, around 6-7 wt%; and 9,10-dihydrophenanthrene and 9,10-dihydroanthracene provided the lowest production of coke with values around 4.7 wt%. Quinoline and toluene exhibited intermediate yields of coke, with results of 18.6 and 14.0 wt%, respectively.

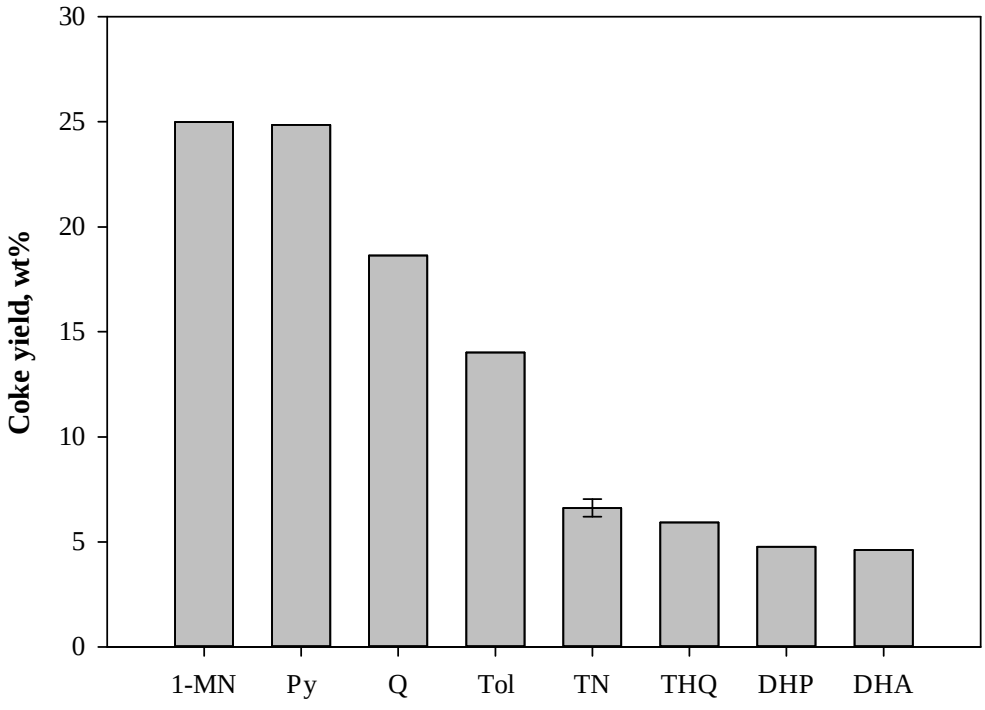

Figure 3-1. Comparison of coke yields from the cracking under hydrogenation conditions of Athabasca industrial *n*-C5 asphaltenes in the presence of different solvents: 1-MN (1-methylnaphthalene), Py (Pyridine), Q (Quinoline), Tol (Toluene), TN (tetralin), THQ (1,2,3,4-tetrahydroquinoline), DHP (9,10-dihydrophenanthrene), and DHA (9,10-dihydroanthracene).

As observed previously by Rahmani et al.[4] and by Savage et al.[3], hydrogen-donor solvents have a positive role as coke suppressors. The reactions in presence of tetralin, 1,2,3,4-tetrahydroquinoline, 9,10-dihydrophenanthrene, and 9,10-dihydroanthracene presented significantly lower coke yields than with the other solvents. Toluene exhibited lower coke yields than the other solvents without hydrogen-donation capacity, suggesting that it can provide a favorable medium for the solubility of hydrogen and asphaltenes. As shown in Table 3-4, some small differences in solubility parameter can be observed among these solvents, except for toluene that is significantly lower than the others. However, when the hydrogen-donor solvents tetralin and 1,2,3,4-tetrahydroquinoline are compared in terms of solubility parameter, the difference does not seem to have an impact on the coke yield. This could suggest that in absence of hydrogen-donation ability, the solvents that can provide a better availability of hydrogen in the reaction medium can lead to lower coke yields, as suggested by Savage et al.[3]

The hydrogen-donor solvents with three aromatic rings, 9,10-dihydrophenanthrene and 9,10-dihydroanthracene, not only presented the lowest coke yields, but also would have maintained a higher fraction in the liquid phase during the process. Furthermore, it can be observed that their reactions were made at higher ratios of solvent/asphaltenes to provide an equivalent availability of hydrogen than with tetralin. In comparison, tetralin was effective as a hydrogen-donor solvent, in terms of the significant reduction in coke yield with a low ratio to asphaltenes, and gave a lower boiling point that would make its removal for further analysis of the liquid products much simpler.

3.3.3 Liquid crystal analysis

The mesophase formation has been described as an intermediate phase formed during cracking reactions, identified by its optical anisotropy. According to the observations made with oil samples from different origins by Bagheri et al.[19], liquid crystals occur in petroleum solids as a common phenomenon with amphotropic character. The mesophase areas can coalesce to form larger mesophase domains, and this can lead to their deposition as coke.[18] Thus, liquid crystal analysis during the cracking reactions can provide some insight into the coke formation process.

Table 3-5. Temperatures for liquid crystal (LC) formation under nitrogen at atmospheric pressure

Asphaltenes	**Liquid crystal formation (°C)**
Athabasca industrial *n*-C_5	50
Athabasca *n*-C_5	75
Athabasca *n*-C_7	100
Cold Lake *n*-C_7	90
Colombian *n*-C_7	No LC formation
Athabasca *n*-C_7 (after reaction)*	No LC formation
Cold Lake *n*-C_7 (after reaction)*	No LC formation

* Asphaltenes after reaction were recovered from the reactions under hydrogenation conditions by precipitation with *n*-heptane using a ratio of 40/1 solvent to liquid products

Table 3-5 shows the onset temperatures for the observation of liquid crystal formation for different asphaltene samples. Cold Lake and Athabasca *n*-C_7

asphaltenes, recovered after reaction as described before, were analyzed using the same technique, and the formation of liquid crystals was not observed. Likewise, Colombian *n*-C_7 asphaltenes did not form liquid crystals during the analysis.

The temperature for the formation of liquid crystals seems to increase with the TGA residue content, and decrease with the H/C ratio of the asphaltenes. Similarly, the samples that did not exhibit development of crystalline domains had in common high TGA residue content, and this could also be expected to correlate with high aromatic content.[26] From the results of Chapter 2 with asphaltenes from different geological basins, we can observe that small aromatic fragments with 1 to 3 aromatic rings exhibited a very good inverse correlation with the amount of material remaining in the vacuum residue fraction and forming coke, as shown in Figure 3-2. These results would suggest that liquid crystal formation is promoted by the presence of small aromatic building blocks rather than by large aromatic clusters.[27] However, the bulk mesophase and coke would be formed by larger aromatic molecules, which would require getting together without undergoing significant crosslinking.

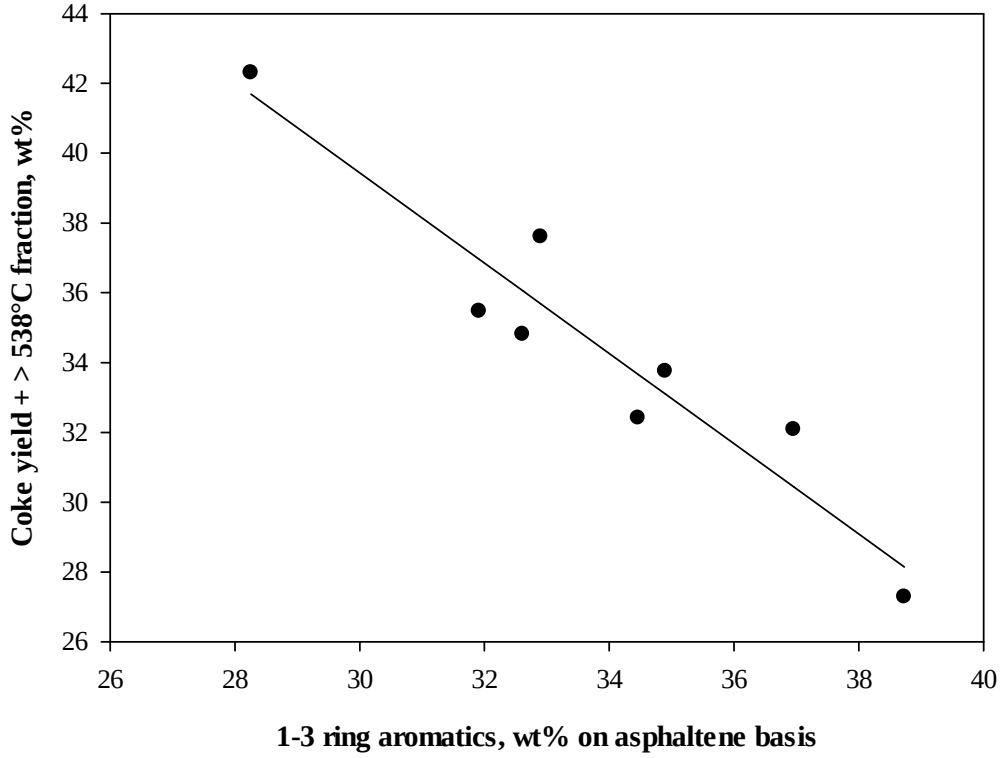

Figure 3-2. Correlation between yield of coke plus material remaining in the vacuum residue fraction, and concentration of 1-3 ring aromatic structures in asphaltenes

Figure 3-3 is presented, as example, to illustrate the mesophase observed under normal and cross-polarized light in a polished sample of coke from the reaction of Venezuelan *n*-C_7 asphaltenes. Isotropic phases are observed in black, and large anisotropic mesophase domains are identified as the white regions in the cross-polarized image. These results show that the residence time of the reactions performed in this study is long enough to give rise to the formation of large mesophase domains, as result of the arrangement of the coke material.

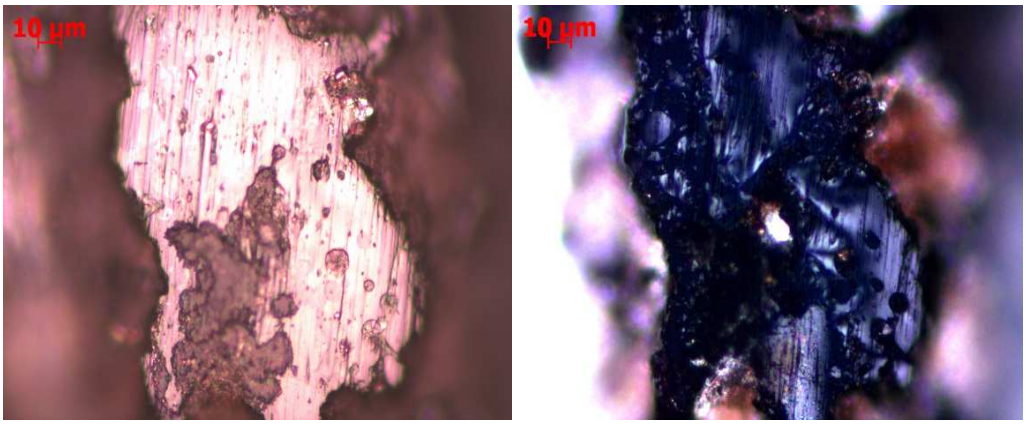

Figure 3-3. Coke from the cracking of Venezuelan *n*-C_7 asphaltenes observed under normal light (left) and cross polarized (right)*

* Bagheri et al.[22] and Qian et al.[28] reported the observation of mesophase domains by SEM analysis. Smaller anisotropic domains in the dark isotropic regions were visible under SEM, but not under optical microscopy. Thus, it could be expected to have smaller mesophase regions embedded in the isotropic liquid matrix.

3.4 Conclusions

1. Solvents with hydrogen-donation capacity showed significantly lower coke yields compared to other aromatic solvents during the cracking of Athabasca industrial *n*-C_5 asphaltenes under hydrogenation conditions. The reactions in presence of three-ring aromatic hydrogen-donors, 9-10-dihydrophenanthrene and 9,10-dihydroanthracene, presented the lowest coke formation. Although high solvent to asphaltenes ratios were used with these solvents, in order to ensure the same hydrogen availability in the reaction medium as with tetralin, it could be expected that lower ratios could

provide similar results since asphaltenes seem to have a limited hydrogen uptake capability.

2. Aromatic solvents without hydrogen donation capacity produced higher yields of coke. However, toluene and quinoline seemed to provide a more favorable medium than 1-methylnaphthalene and pyridine to prevent the deposition of reacted asphaltenes as coke.
3. The temperature for liquid crystals formation increased with the MCR content of the asphaltenes samples. Colombian *n*-C_7 asphaltenes and reacted asphaltenes obtained from the reactions under hydrogenation conditions of Cold Lake and Athabasca *n*-C_7 asphaltenes, which presented high MCR content, did not exhibit liquid crystals.
4. Microscopy analysis under cross polarized light of coke recovered from the cracking of asphaltenes showed significant large mesophase regions in the coke structure.

3.5 References

1. Ignasiak, T. M.; Strausz, O. P. Reaction of Athabasca asphaltene with tetralin. *Fuel* **1978**, *57*, 617-621.
2. Al-Samarraie, M.; Steedman, W. Pyrolysis of petroleum asphaltene in tetralin. *Fuel* **1985**, *64*, 941-943.
3. Savage, P. E.; Klein, M. T.; Kukes, S. G. Asphaltene reaction pathways. 3. Effect of reaction environment. *Energy & Fuels* **1988**, *2*, 619-628.

4. Rahmani, S.; McCaffrey, W.; Gray, M. R. Kinetics of Solvent Interactions with Asphaltenes during Coke Formation. *Energy & Fuels* **2002**, *16*, 148-154.

5. Rahmani, S.; McCaffrey, W. C.; Dettman, H. D.; Gray, M. R. Coking kinetics of asphaltenes as a function of chemical structure. *Energy & Fuels* **2003**, *17*, 1048-1056.

6. Carlson, C.; Langer, A.; Stewart, J.; Hill, R. Thermal Hydrogenation - Transfer of hydrogen from tetralin to cracked residua. *Industrial and Engineering Chemistry* **1958**, *50*, 1067-1070.

7. Del Bianco, A.; Panariti, N.; Prandini, B.; Beltrame, P. L.; Carniti, P. Thermal cracking of petroleum residues. 2. Hydrogen-donor solvent addition. *Fuel* **1993**, *72*, 81.

8. Khorasheh, F.; Gray, M. R. High-pressure thermal cracking of n-hexadecane in tetralin. *Energy & Fuels* **1993**, *7*, 960.

9. Gray, M. R.; McCaffrey, W. C. Role of Chain Reactions and Olefin Formation in Cracking, Hydroconversion, and Coking of Petroleum and Bitumen Fractions. *Energy & Fuels* **2002**, *16*, 756-766.

10. Cronauer, D. C.; Jewell, D. M.; Shah, Y. T.; Modi, R. J.; Seshadri, K. S. Isomerization and adduction of hydrogen donor solvents under conditions of coal liquefaction. *Industrial & Engineering Chemistry Fundamentals* **1979**, *18*, 368-376.

11. Kamiya, Y.; Nagae, S. Relative reactivity of hydrogen donor solvent in coal liquefaction. *Fuel* **1985**, *64*, 1242-1245.

12. Poutsma, M. L. Free-radical thermolysis and hydrogenolysis of model hydrocarbons relevant to processing of coal. *Energy & Fuels* **1990**, *4*, 113-131.

13. Whitehurst, D. D.; Mitchell, T. O.; Farcasiu, M. *Coal liquefaction: the chemistry and technology of thermal processes;* Academic Press: 1980.

14. Cronauer, D. C.; Jewell, D. M.; Shah, Y. T.; Kueser, K. A. Hydrogen transfer cracking of dibenzyl in tetralin and related solvents. *Industrial & Engineering Chemistry Fundamentals* **1978**, *17*, 291-297.

15. Wiehe, I. A. A phase-separation kinetic model for coke formation. *Ind. Eng. Chem. Res.* **1993**, *32*, 2447-2454.

16. Wang, S.; Chung, K.; Masliyah, J. H.; Gray, M. R. Toluene-insoluble fraction from thermal cracking of Athabasca gas oil: formation of a liquid-in-oil emulsion that wets hydrophobic dispersed solids. *Fuel* **1998**, *77*, 1647-1653.

17. Wiehe, I. A. A solvent-resid phase diagram for tracking resid conversion. *Ind. Eng. Chem. Res.* **1992**, *31*, 530-536.

18. Bagheri, S. R.; Gray, M. R.; Shaw, J. M.; McCaffrey, W. C. In Situ Observation of Mesophase Formation and Coalescence in Catalytic Hydroconversion of Vacuum Residue Using a Stirred Hot-Stage Reactor. *Energy & Fuels* **2012**, *26*, 3167-3178.

19. Bagheri, S. R.; Bazyleva, A.; Gray, M. R.; McCaffrey, W. C.; Shaw, J. M. Observation of Liquid Crystals in Heavy Petroleum Fractions. *Energy & Fuels* **2010**, *24*, 4327-4332.

20. Rahimi, P.; Gentzis, T.; Dawson, W.; Fairbridge, C.; Khulbe, C.; Chung, K.; Nowlan, V.; DelBianco, A. Investigation of coking propensity of narrow cut fractions from Athabasca bitumen using hot-stage microscopy. *Energy & Fuels* **1998**, *12*, 1020-1030.

21. Hurt, R. H.; Hu, Y. Thermodynamics of carbonaceous mesophase. *Carbon* **1999**, *37*, 281.

22. Bagheri, S. R.; Gray, M. R.; McCaffrey, W. C. Influence of Depressurization and Cooling on the Formation and Development of Mesophase. *Energy & Fuels* **2011**, *25*, 5541-5548.

23. Barton, A. F. M. *CRC handbook of solubility parameters and other cohesion parameters;* CRC Press: Boca Raton, FL, 1983; pp 594.

24. Wiehe, I. A. *Process chemistry of petroleum macromolecules;* CRC Press: Boca Raton, FL, 2008; pp 427.

25. Karimi, A.; Qian, K.; Olmstead, W. N.; Freund, H.; Yung, C.; Gray, M. R. Quantitative Evidence for Bridged Structures in Asphaltenes by Thin Film Pyrolysis. *Energy & Fuels* **2011**, *25*, 3581-3589.

26. Gray, M. R. Consistency of Asphaltene Chemical Structures with Pyrolysis and Coking Behavior. *Energy & Fuels* **2003**, *17*, 1566-1569.

27. Bagheri, S. R. The molecular structure of asphaltenes. **2013**.

28. Qian, Z.; Clarke, D. E.; Marsh, H. Structure in cokes from coals of different rank. *Fuel* **1983**, *62*, 1084.

4 Monte Carlo simulation of the cracking of asphaltene molecules constructed with dendritic and linear topologies

4.1 Introduction

Asphaltenes are the fraction of petroleum with the most complex and heterogeneous composition.[1] As the boiling point and molecular weight of the petroleum molecules increase, the number of isomers and different homologous series also increases significantly,[2] to the point that the probability of finding two identical asphaltene molecules would approach zero. Asphaltenes have also been found to be made up of an extraordinary variety of molecular sub-structures or building blocks involving homologous series of paraffinic, naphthenic, heteroatomic, and aromatic species.[3-6] Thus, a stochastic construction of asphaltene molecules by Monte Carlo simulation, by random selection of these identified molecular sub-structures, referred to as building blocks throughout this study, could provide a good strategy to render explicit the heterogeneity of these heavy petroleum components.

Monte Carlo simulation has shown to be a useful method that can be implemented as long as the molecular attributes or variables can be explicitly defined as probabilistic events. Thus, Monte Carlo simulation has permitted the construction of molecular representations not only of asphaltenes,[7-13] but also of coal,[14] polymers[15, 16] and lignin.[17-21]

Neurock and coworkers[8-11] presented a hierarchical construction of asphaltene molecules by random sampling of some structural attributes described by probability density functions (PDFs). The attributes included: number of unit sheets (degree of polymerization), number of aromatic and naphthenic rings, degree of substitution, and length of the aliphatic substituents. Thus, the asphaltenes were built assuming that they consist of assemblies of naphthenoaromatic cores with some aliphatic chains. The information for the construction of the PDFs was obtained from characterization data, generated by ^{1}H NMR, VPO, and elemental analysis.

Sheremata et al.[13] had reported the Monte Carlo construction of asphaltene molecules by random selections of aliphatic and aromatic groups, linked by aliphatic chains and sulphide bonds. The algorithm optimized the process to be consistent with experimental data obtained by elemental analysis, NMR spectroscopy, and molecular weight. Thus, this study paid some special attention to the carbon chemical species, and provided a quantitative molecular representation of asphaltenes. Similarly, Jaffe et al.[22] presented the method of structure-oriented lumping (SOL), where residua molecules were represented by assemblies of single core species, consisting of molecular class/homologous series described by vectors. These assemblies were linked by bridges with specified length and bond strength.

For the reaction of the molecules that were stochastically generated, the Monte Carlo studies presented by Klein and coworkers[7-9, 11, 12] applied the pathways and kinetics derived from the experimental data of model compounds,

in order to assign a reaction probability to the potential reaction sites. This approach made some assumptions to extrapolate the available data to the complex residue molecules.

In these previous simulations, the construction of asphaltene molecules used the available experimental data, but there are molecular attributes in asphaltenes that cannot be measured directly to generate a complete set of initial PDFs. Consequently, the simulation is under specified, and only for a limited number of parameters could be tuned by fitting the experimental results. One important characteristic is the molecular weight distribution; however, the nature of this distribution is a matter of considerable debate in the study of asphaltenes. The main difficulty in the measurement of the molecular weight of asphaltenes has been their tendency to aggregate in solution.[23, 24] The measurement of molecular weight by vapor pressure osmometry (VPO) is influenced by the conditions of the analysis, such as: temperature, concentration, and solvent polarity;[1, 23] thus, the reported apparent values can include significant bias due to aggregation, even when extrapolated to infinite dilution. The use of an average molecular weight would be highly misleading in this case, because asphaltenes consist of a diverse variety of molecules with a broad range of molecular weight. Measurement of the molecular weight of asphaltenes by fluorescence emission spectroscopy, as reported by Groenzin et al.,[25] suggested low molecular weights, with an average value of 750 Da, and a range of approximately 500 – 1000 Da. Strausz et al.[26] presented a critical analysis of fluorescence spectroscopy and pointed out that this analysis cannot provide quantitative information for complex

mixtures, such as asphaltenes. Similarly, the use of gel permeation chromatography (GPC) has also been reported,[27, 28] but the results suffer from the problem of agglomeration and lack of proper calibration.

Other studies have suggested that the mean molecular weight for asphaltenes would be in the range of 1000 to 2000 Da.[24, 29] For instance, Qian et al.[29] published a molecular weight distribution that was obtained from calibrated field desorption ionization mass spectrometry (FD-MS) analysis. Although field desorption ionization can generate higher molecular weight species,[29-31] these FD-MS results were validated, showing a good agreement with ESI-MS analysis,[29] and therefore, represented a good reference for the construction of populations of asphaltenes. This distribution presented an average molecular weight of 1238 Da for the asphaltenes, with minimum and maximum values circa 280 and 3500 Da, respectively, and with the distribution mode around 900 Da.

In our previous study presented in Chapter 2, favorable hydrogenation conditions enabled high conversion of asphaltenes to distillable material, with minimum production of coke, while ensuring minimal change of the ring structures during the reaction. Thus, building on the quantitative evidence for bridged structures in asphaltenes, provided in Chapter 2 and other studies,[4, 5] the objective of this approach was to create simplified Monte Carlo algorithms for the construction and cracking of asphaltene molecules that could explore the effect of the molecular architecture on the distribution of the cracking products. These simulations made use of the data for Cold Lake *n*-C_7 asphaltenes obtained in our study on cracking under hydrogenation conditions. The results obtained from

these simulations, with linear and dendritic molecular topologies, provided distributions of cracking products that were compared to the available experimental data.

4.2 Model Development

In Chapter 2, a significant amount of material from the cracking of asphaltenes was characterized. The distillates, consisting of small building blocks, also called pendant groups, were analyzed by gas chromatography - field ionization – time of flight high resolution mass spectrometry (GC-FI-TOF HR MS). The liquid products were also analyzed by simulated distillation (SimDist), after the removal of tetralin, which was used as hydrogen-donor solvent during the reaction. These available data were suitable to be transformed into PDFs that could be used as input for the stochastic construction of simplified asphaltene molecules.

One of the conclusions from Chapter 2 was that the maximum amount of large aromatic cores (large building blocks) in asphaltenes would be the sum of the coke and the material remaining in the vacuum residue range. However, the actual initial amount of large building blocks remained unknown because not only cracking reactions take place, but also reactions that build larger molecules, such as cyclization, condensation and polymerization. Therefore, the coke and the material remaining in the vacuum residue fraction could be formed not only by the initial large building blocks, but also could have arisen from smaller building blocks during the cracking reactions.[32, 33]

Keeping this in mind, this work evaluated the effect of the architecture of the linkages between the building blocks on the yields from cracking, but also included the amount of large building blocks as a variable in the construction algorithm. The construction strategy consisted of the unbiased sampling, by Monte Carlo simulation, of the type of building block from the distributions of either the distillates or the vacuum residue fraction, whose probabilities were given by the PDFs derived from the available experimental data. Two molecular architectures were considered; linear and dendritic. For the specific case of the dendritic asphaltenes, the connections between the building blocks were also randomly assigned.

The cracking reactions were also simulated by a Monte Carlo method. The information available on the constructed asphaltenes consisted of the molecular weights of their constituent building blocks, and the linkages between their building blocks. The cracking algorithm made random selections of the molecule to be cracked and the position for the breakage, without following any specific kinetics or reaction pathway. In this simplified scheme, all bridges between building blocks had the same reactivity and the same probability of breakage. The objective was to examine the distribution of products at the experimental yield of distillates. This methodology allowed the comparison of linear and dendritic populations of asphaltenes, each with the same initial molecular weight distribution.

4.2.1 Experimental data and input probability density functions (PDFs) for the simulation

In this study, the molecular weight distribution for the asphaltenes fraction was used as the main constraint in generating the population of molecules to be cracked, using the data of Qian et al.[29] for the molecular weight distribution. The maximum molecular weight in the asphaltenes distribution was 3500 Da, the minimum was around 280 Da and the mode was roughly 900 Da, as mentioned before. The data for the asphaltene fraction was available as a mass fraction distribution of the molecular weights, within the whole vacuum residue. These data were normalized and converted to a molar distribution of molecular weights, as shown in Figure 4-1, and then converted into a discrete cumulative distribution for use in the Monte Carlo construction of molecules, designated as **PDFAsph** and illustrated in Figure 4-2.

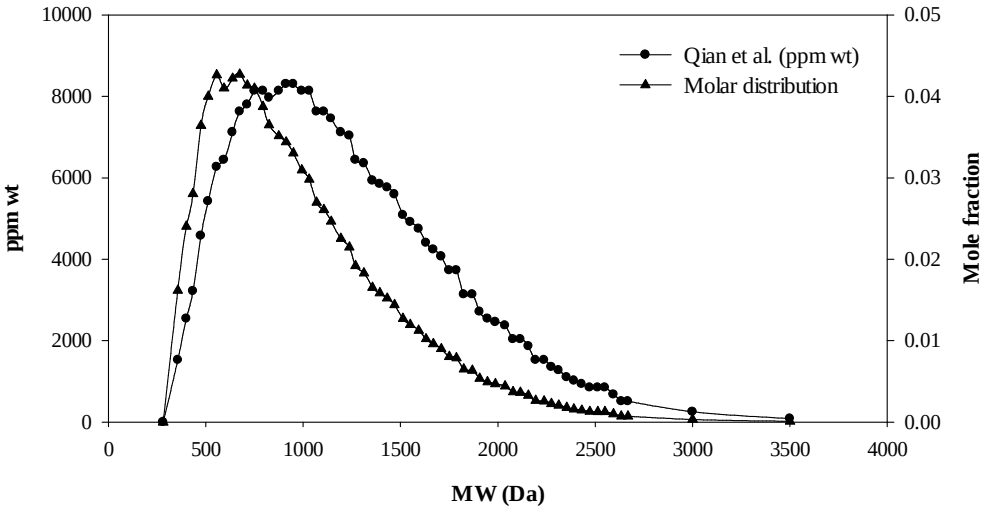

Figure 4-1. Molar distribution of MW for asphaltenes derived from data published by Qian et al.[29]

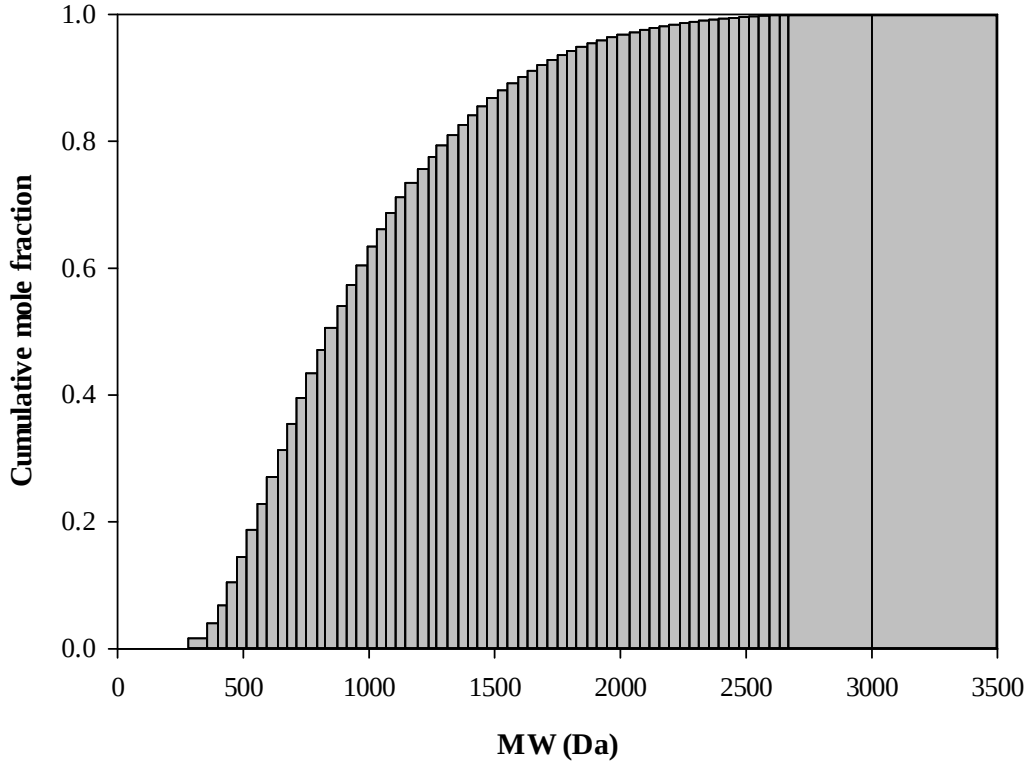

Figure 4-2. Discretized PDF of the cumulative molar distribution of MW for asphaltenes (**PDFAsph**)

The mass balance from the cracking under hydrogenation conditions of Cold Lake *n*-C_7 asphaltenes, obtained from Chapter 2, provided the corresponding yields for each product from the cracking reaction. Gas formation arises from the cracking within the building blocks as defined in this study, i.e. building blocks are defined as the ring groups with their attached alkyl groups. Given that our interest was cracking reactions that generated larger changes in molecular weight, to give rise to the formation of distillable liquids, vacuum residue, and coke, the mass balance was renormalized to remove gas yield. We assumed that the lightest

components, or gases, were generated uniformly from the other fractions of reactants. The mass balance of the reaction of Cold Lake *n*-C_7 asphaltenes, and the normalized results, are listed in Table 4-1.

Table 4-1. Mass balance from the cracking under hydrogenation conditions of Cold Lake *n*-C_7 asphaltenes (from Chapter 2), and normalized results with gases assigned uniformly to the other product fractions

Products	**Yields (wt%)**	**Normalized yields (wt%)**
Gases	4.5	0
Coke	7.5	8.1
< 538°C fraction	61.4	66.2
> 538°C fraction	23.8	25.7
Mass balance	97.2	100.0

The material converted to distillates (< 538°C) was characterized by a high resolution GC-MS analysis that provided the molar abundance for eighteen different molecular species. These results were each converted into a discrete cumulative distribution, as shown in Figure 4-3, which was used as an additional PDF, named as **PDFDist**, for the generation of the populations of asphaltene molecules.

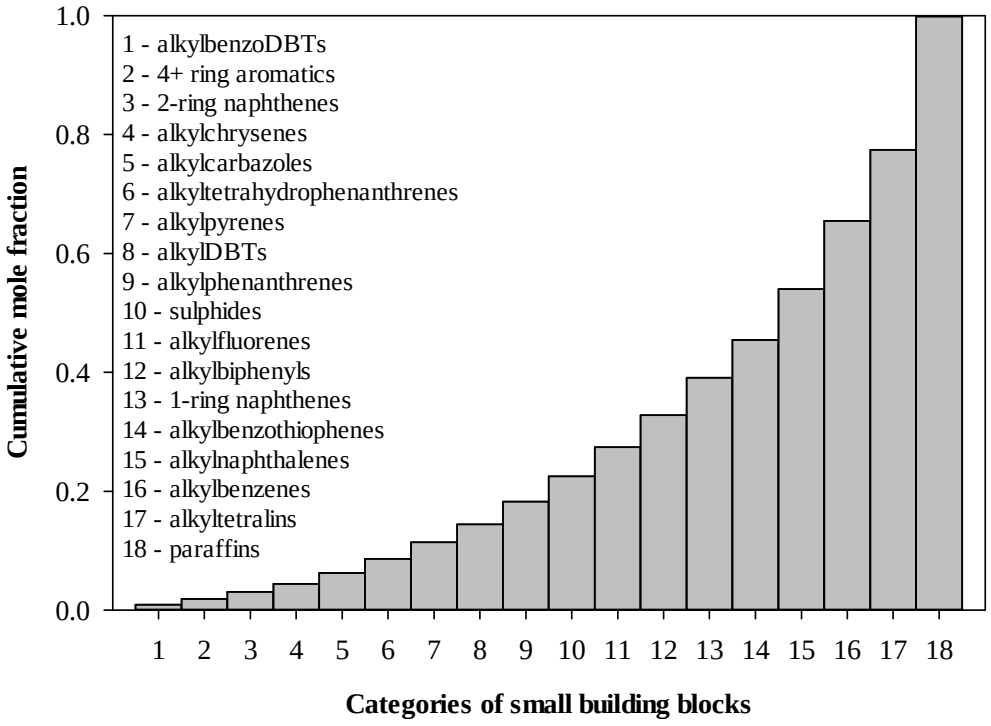

Figure 4-3. PDF of the discrete cumulative molar distribution of the categories of building blocks in the distillable fraction from the cracking of Cold Lake *n*-C_7 asphaltenes (**PDFDist**)

The same GC-MS technique also provided the molecular weight distributions for the different categories of building blocks in the distillates. The molar fractions in each category of distillable molecules were normalized, and individual discrete cumulative distributions were calculated. These distributions were named as **PDFDist1** to **PDFDist18**, and are shown in Figure 4-4 to Figure 4-6.

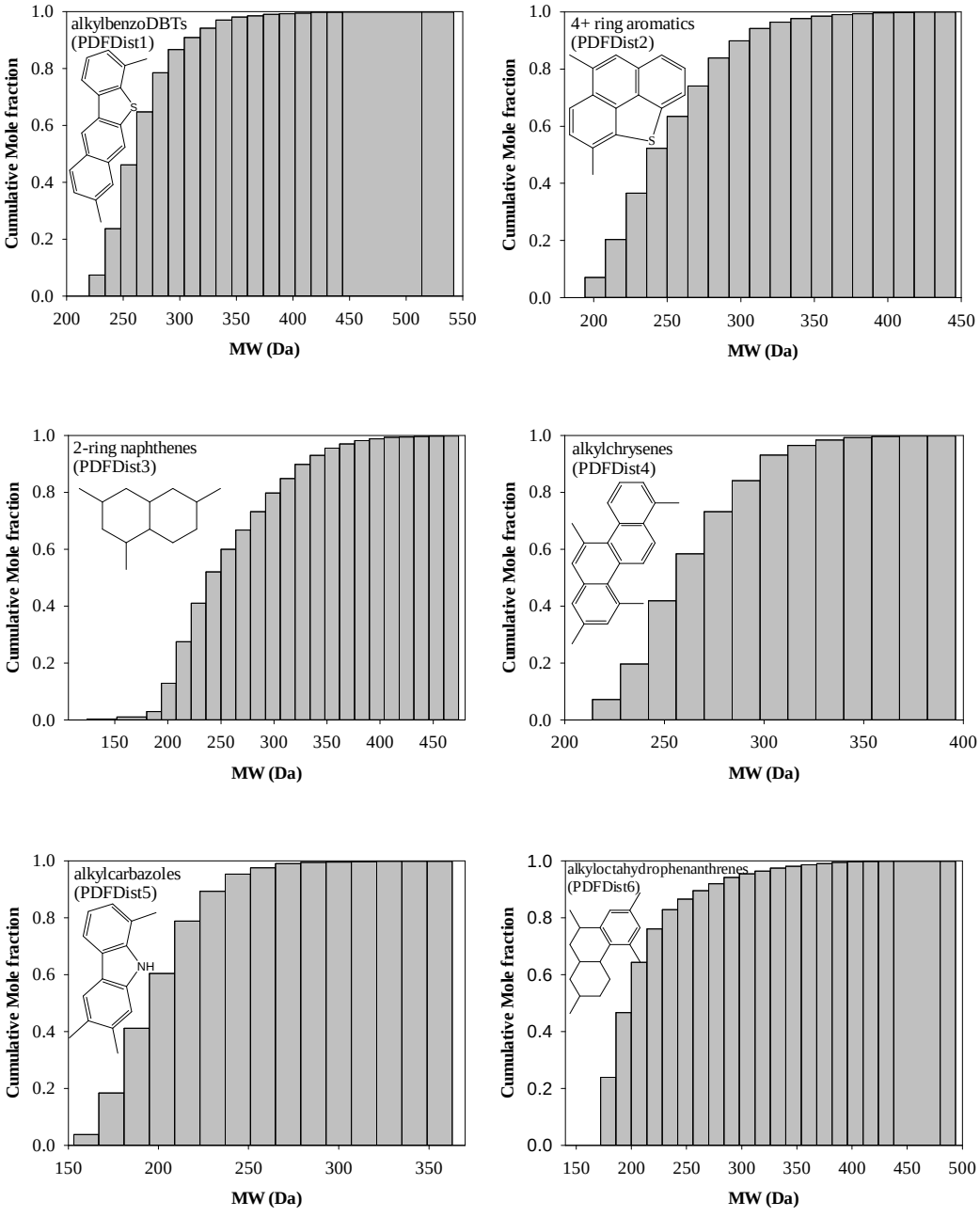

Figure 4-4. PDFs of the discrete cumulative molar distribution of molecular weights in each category of building blocks identified in the distillable fraction from the cracking of Cold Lake *n*-C_7 asphaltenes (**PDFDist1** to **PDFDist6**). The structures are representative of alkylated ring groups in each series.

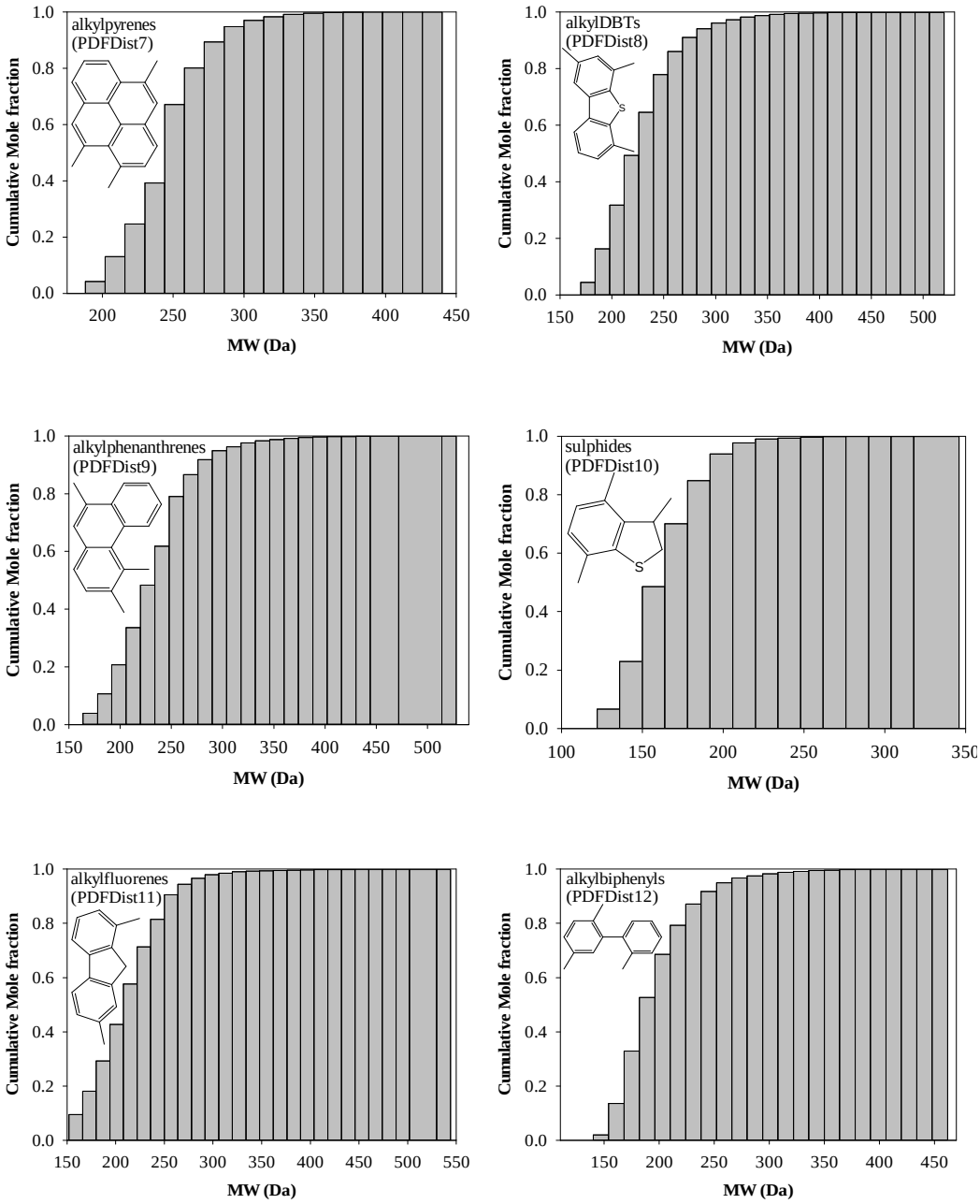

Figure 4-5. PDFs of the discrete cumulative molar distribution of molecular weights in each category of building blocks identified in the distillable fraction from the cracking of Cold Lake *n*-C_7 asphaltenes (**PDFDist7** to **PDFDist12**). The structures are representative of alkylated ring groups in each series

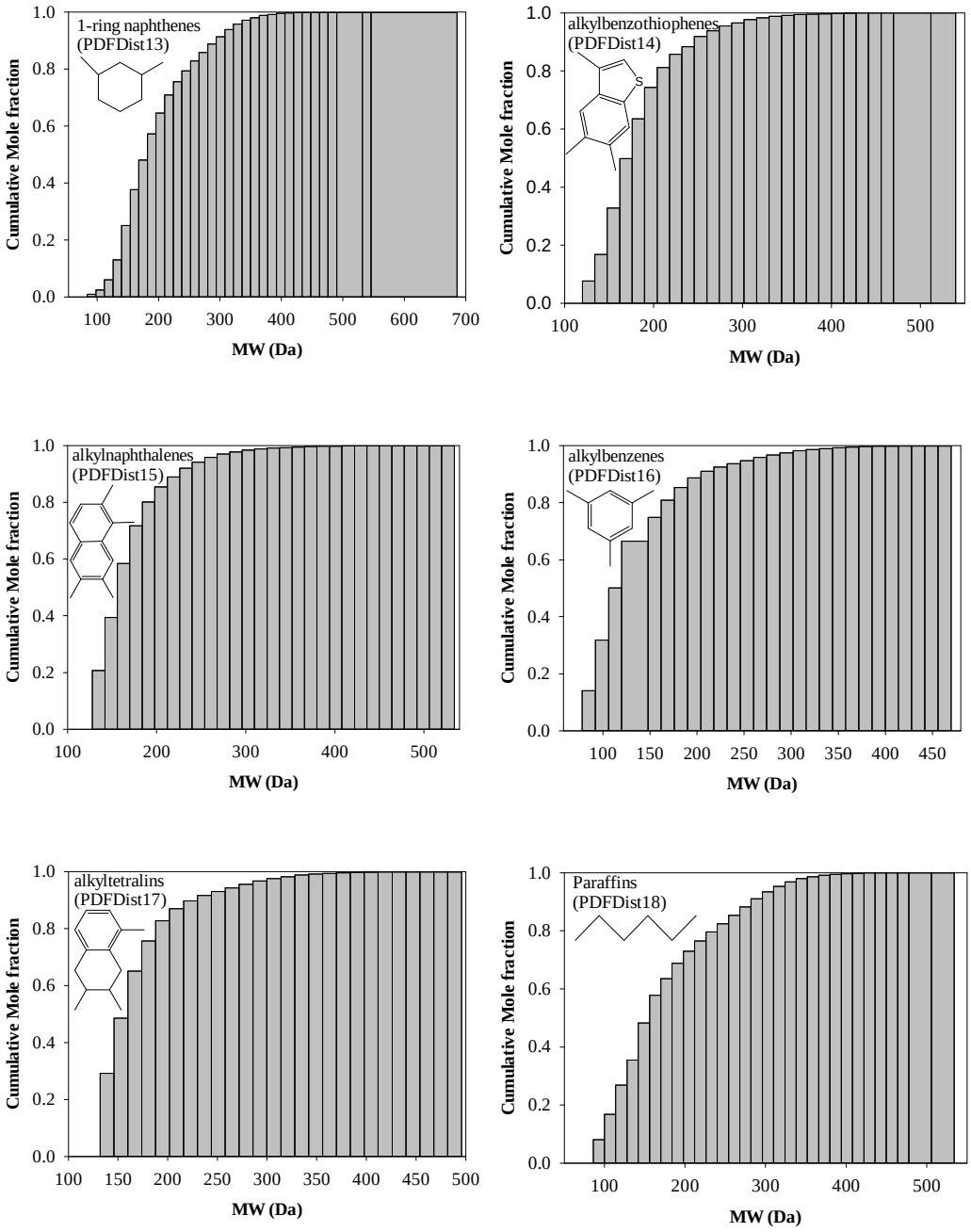

Figure 4-6. PDFs of the discrete cumulative molar distribution of molecular weights in each category of building blocks identified in the distillable fraction from the cracking of Cold Lake *n*-C_7 asphaltenes (**PDFDist13** to **PDFDist18**). The structures are representative of alkylated ring groups in each series.

The fraction of liquid products with boiling point in the vacuum residue range (> 538°C) could not be characterized by GC-MS. However, the liquid sample, obtained from the reaction, was analyzed by simulated distillation (SimDist) after removal of tetralin, which was the hydrogen-donor solvent during the process, as described in Chapter 2. The mass balance indicated that 34.5 wt% of the initial mass of asphaltenes (37.2 wt% on normalized basis without gases) was evaporated together with tetralin. The distillation curve obtained from SimDist analysis was interpolated with a cubic spline method, and then extrapolated linearly to an assumed end-point temperature of 1000°C, as illustrated in Figure 4-7.

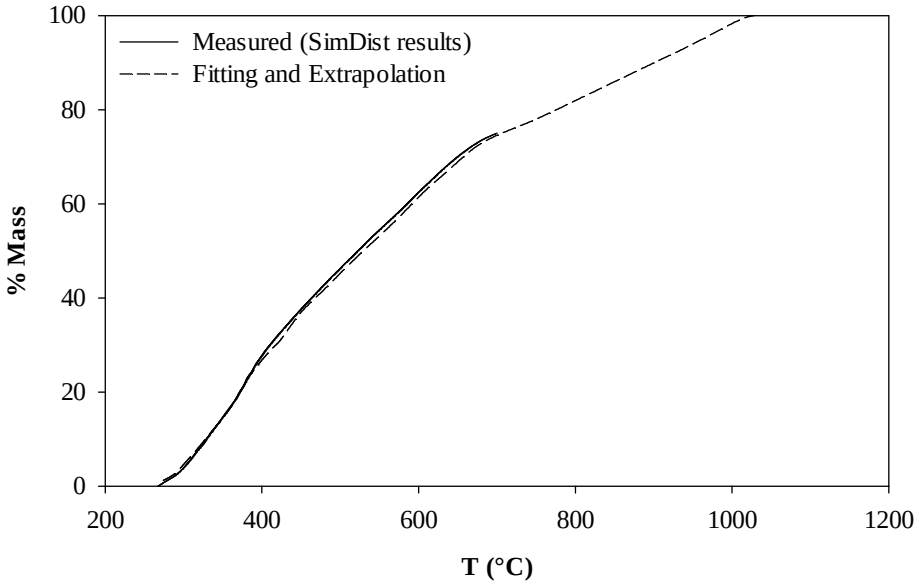

Figure 4-7. Simulated distillation results of the liquid products from the reaction of Cold Lake *n*-C_7 asphaltenes, after removal of tetralin, and fitting of the distillation curve extrapolated to 100% mass

Other methods available for extrapolation of distillation data, such as the use of probability paper, were not used because there is no evidence that these methods can give better results. Furthermore, any method used would involve uncertainty because the properties were also extrapolated as explained below.

A set of twelve pseudo-components was generated to represent this boiling curve, using VMGSim process engineering software (Virtual Materials Group, Calgary AB). It was assumed that the pseudo-components had the same UOP (or Watson) K value. Thus, the densities at 15.6°C were calculated with equation (4-1), where ABP is the average boiling point of the pseudo-component in °R, and fitted a specified bulk density at 15.6°C of 1000 kg/m^3. Figure 4-8 presents the densities estimated by this method.

$$\text{UOP K} = \frac{\sqrt[3]{\text{ABP}}}{\text{SG (15.6°C/15.6°C)}} \qquad (4\text{-}1)$$

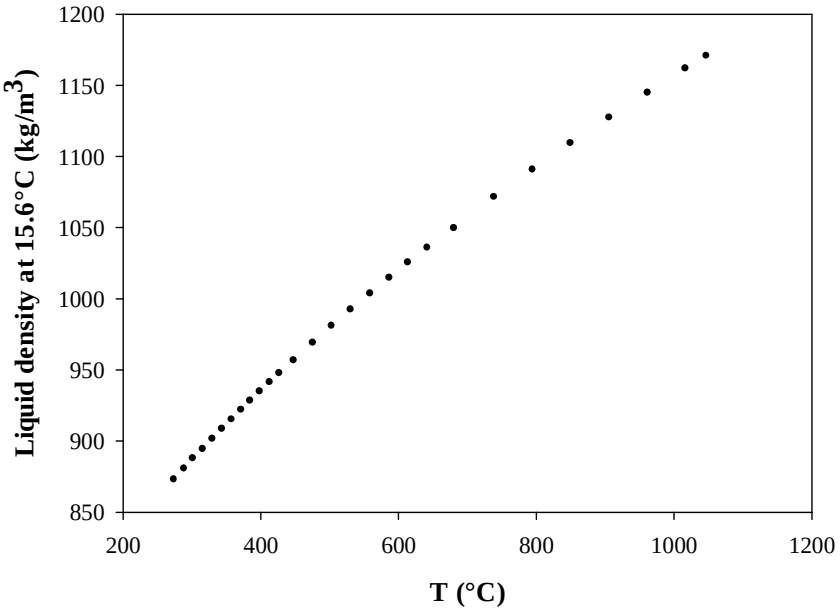

Figure 4-8. Liquid densities estimated by the constant UOP K method

The molecular weight was estimated with the Hariu-Sage method,[34] as recommended by VMGSim,[35] which uses the average boiling point and specific gravity of each pseudo-component. Thus, the uncertainty in the molecular weight estimations is higher because they are based on properties that were estimated.

The molecular weights calculated by this method were compared to the values estimated with the correlations published by Sim and Daubert,[36] White et al.,[37] Trytten and Gray,[38] Altgelt and Boduszynski,[39] and by Twu,[40] using the boiling points from Figure 4-7 and the liquid densities from Figure 4-8. The results are presented in Figure 4-9.

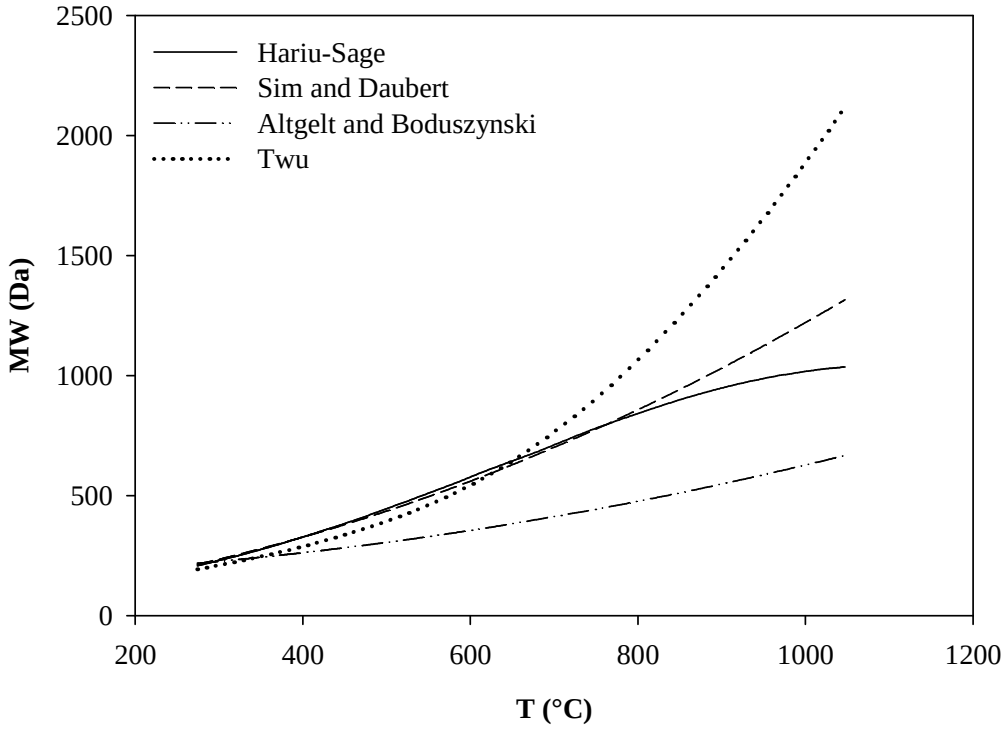

Figure 4-9. Comparison of the results obtained with different correlations available in literature for the estimation of the molecular weight distribution of the liquid products from the reaction of Cold Lake *n*-C_7 asphaltenes

The correlations proposed by White et al.,[37] and Trytten and Gray[38] were not shown in Figure 4-9, but their predictions followed the same trend than the results obtained with the correlation published by Sim and Daubert.[36] These results matched with the values estimated by the Hariu-Sage[34] method for boiling points below 800°C, but for higher boiling points some differences can be observed. The molecular weights predicted with the method proposed by Twu[40] are much higher than the values estimated with all the other methods, especially for boiling points above 700°C. On the contrary, the estimation with the correlation published by Altgelt and Boduszynski[39] underestimates the molecular weights compared to all the other methods.

Based on these results, the correlation proposed by Sim and Daubert was chosen in this study for the prediction of molecular weights because showed a good behavior with temperature and exhibited similar results with some of the other correlations. This correlation was then used to construct the PDF for the molecular weight distribution of the large building blocks that could not be characterized by GC-MS. The extrapolated distillation curve was truncated to remove material boiling below 538°C, the data were normalized, and the molar fractions were calculated to obtain the discrete cumulative distribution of large building blocks, named as **PDFCores**, illustrated in Figure 4-10.

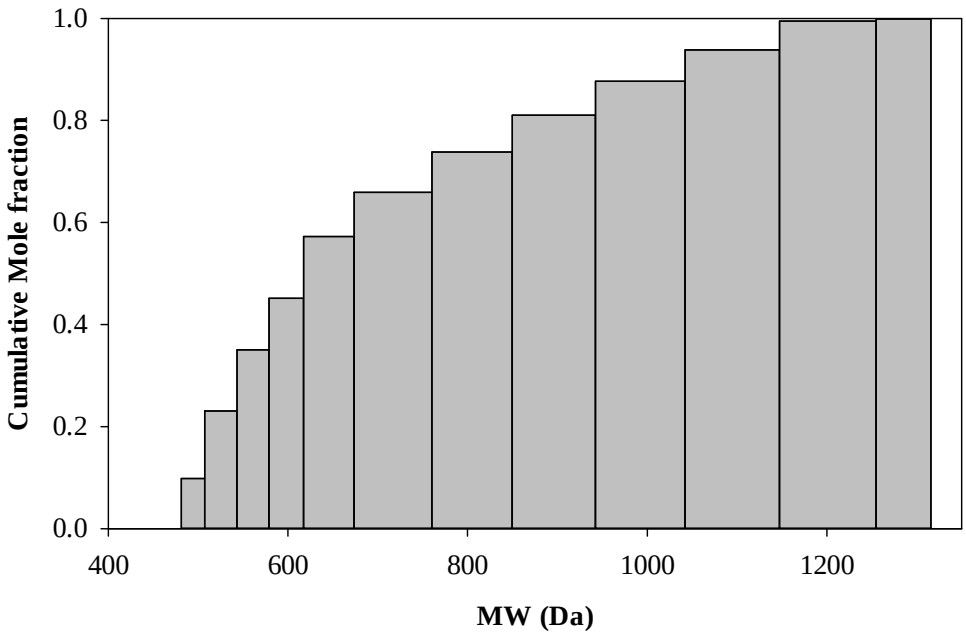

Figure 4-10. PDF of the discrete cumulative molar distribution of molecular weights for the large building blocks present in the non-distillable fraction (> 538°C) of the liquid products from the cracking under hydrogenation conditions of Cold Lake *n*-C_7 asphaltenes

4.2.2 Stochastic generation of molecules by Monte Carlo simulation

A population of ten thousand asphaltene molecules was stochastically generated by random selection of building blocks from the distributions of either cores (large building blocks) or pendant groups (small building blocks). In Chapter 2, the estimated maximum amount of large building blocks for Cold Lake *n*-C_7 asphaltenes was 31.3 wt% on initial asphaltene mass basis (33.8 wt% on normalized basis without gases). Nevertheless, the actual initial amount of large building blocks is still undetermined, and became a variable in the construction of the asphaltene molecules.

Therefore, the sub-routine for the generation of the asphaltenes populations included another PDF, identified as **PDFBlock**, which defined the probability of selecting a building block from the distributions of distillates or from the vacuum residue fraction. This binomial PDF was changed in each simulation case, assigning probabilities of 5, 15, and 25% to the large building blocks, in order to generate different populations of asphaltenes. An example of the PDF with a 15% probability for the large building blocks is shown in Figure 4-11.

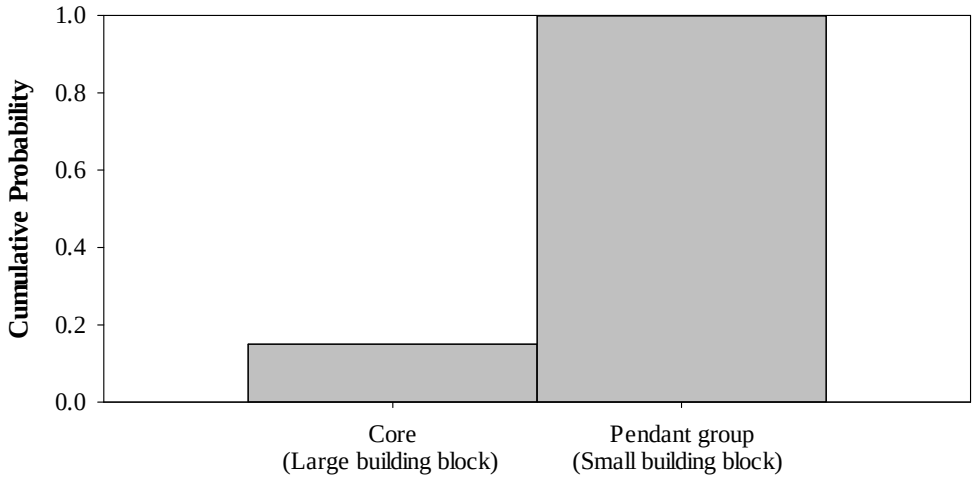

Figure 4-11. Example of PDF for the selection of the type of building block when the probability for the large building blocks is 15%

The different routines were programmed in MATLAB® (Version R2011b, The MathWorks, Inc., USA). The flowchart that describes the algorithm for the generation of a population of "n" asphaltene molecules is presented in Figure 4-12.

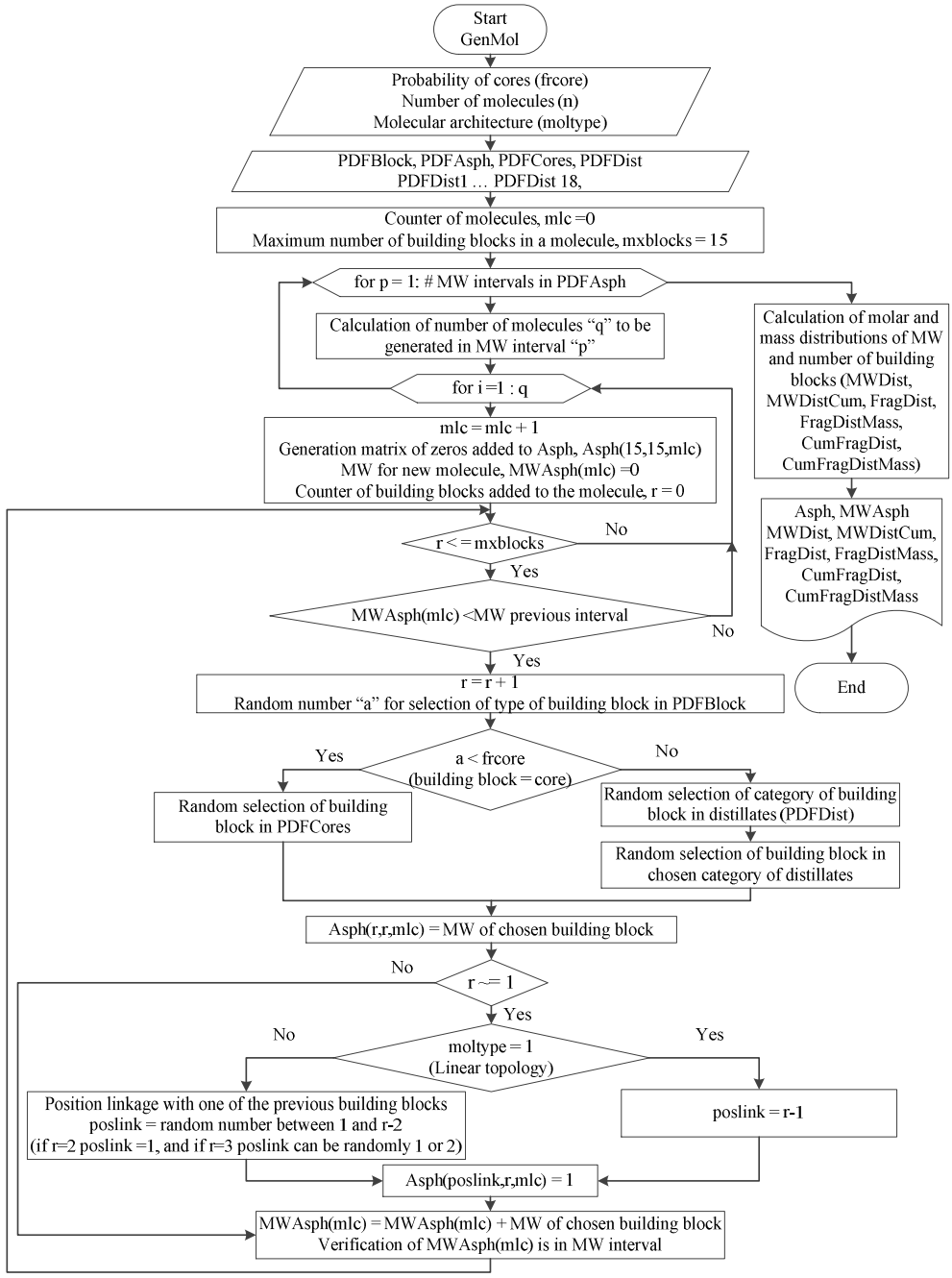

Figure 4-12. Flowchart for the generation of the population of "n" asphaltene molecules, with a given fraction of large building blocks (frcores), and defined molecular topology (linear or dendritic)

In all the simulation cases in this study, the size of the populations was ten thousand asphaltene molecules, assembled in a three dimensional matrix of dimensions 15x15x10000, named as **Asph**. Thus, each asphaltene molecule was described by a matrix of dimensions 15x15, where the building blocks, randomly selected, were placed on the main diagonal, and the connections between them were specified with ones situated above the diagonal of the matrix. For example, to connect the fourth building block to the second building block, the matrix would have "1" in the second row and fourth column, this is the position (2,4). Each new building block was allowed to be connected to only one of the previous building blocks, and the position of this linkage was defined by the variable "poslink". Therefore, at the end of the construction of the molecule, each building block would have at least one link to the rest of the molecule, defined by the position of the "1" situated on their own respective columns above the main diagonal. Additional links to a building block, also identified by "ones", were located on the same row to the right of the diagonal.

The algorithm allowed the construction of two types of molecules: linear and dendritic. In the case of linear asphaltenes, the ones were situated right above the main diagonal, indicating that each new building block was connected to the previous one. For the dendritic molecules, each new building block was randomly connected to any of the previous building blocks, but from the fourth building block, and on, the new building block was not allowed to be connected to the right previous building block in order to avoid linearity of the molecules. The variable

moltype was created to define the type of population to be generated; for linear molecules the value should be set as 1, and for dendritic should be 2.

Thus, as shown in Figure 4-12, in the general algorithm for the construction of the asphaltenes population, the percentage of large building blocks (frcore), introduced in **PDFBlock**, the type of molecules (linear or dendritic), defined by the variable moltype, and the number of molecules (n) should be specified in order to start the generation of the population. The number of molecules in each MW range was calculated with the molar distribution of molecular weights for the asphaltenes, given by **PDFAsph** (shown in Figure 4-2). Then, each molecule in the specific MW range was constructed by random selection of building blocks from the molecular weight distributions.

The first step in the construction of each molecule was the addition of a new matrix of zeros with dimension 15x15 to the three dimensional matrix **Asph**. The type of building block was randomly selected with the probability given by **PDFBlock**. If the type of building block chosen was a large building block, the molecular weight of the building block was obtained by sampling the probability density function **PDFCores**. On the contrary, if the type of building block selected was small, the algorithm would make random selections of the category of molecule from **PDFDist**, and then of the molecular weight of the building block from the probability density function of that specific type of molecule. The molecular weight of the selected building block would then be situated on the main diagonal of the matrix, starting with the position (1,1). The same procedure was followed to select each one of the new building blocks, assigning the

connections as explained before, and verifying that the final MW of the molecule was in the proper range. Linear and dendritic molecules are exemplified below.

Linear molecule

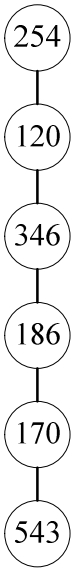

$$\begin{bmatrix}
254 & 1 & 0 & 0 & 0 & 0 & 0 & 0 & 0 & 0 & 0 & 0 & 0 & 0 & 0 \\
0 & 120 & 1 & 0 & 0 & 0 & 0 & 0 & 0 & 0 & 0 & 0 & 0 & 0 & 0 \\
0 & 0 & 346 & 1 & 0 & 0 & 0 & 0 & 0 & 0 & 0 & 0 & 0 & 0 & 0 \\
0 & 0 & 0 & 186 & 1 & 0 & 0 & 0 & 0 & 0 & 0 & 0 & 0 & 0 & 0 \\
0 & 0 & 0 & 0 & 170 & 1 & 0 & 0 & 0 & 0 & 0 & 0 & 0 & 0 & 0 \\
0 & 0 & 0 & 0 & 0 & 543 & 0 & 0 & 0 & 0 & 0 & 0 & 0 & 0 & 0 \\
0 & 0 & 0 & 0 & 0 & 0 & 0 & 0 & 0 & 0 & 0 & 0 & 0 & 0 & 0 \\
0 & 0 & 0 & 0 & 0 & 0 & 0 & 0 & 0 & 0 & 0 & 0 & 0 & 0 & 0 \\
0 & 0 & 0 & 0 & 0 & 0 & 0 & 0 & 0 & 0 & 0 & 0 & 0 & 0 & 0 \\
0 & 0 & 0 & 0 & 0 & 0 & 0 & 0 & 0 & 0 & 0 & 0 & 0 & 0 & 0 \\
0 & 0 & 0 & 0 & 0 & 0 & 0 & 0 & 0 & 0 & 0 & 0 & 0 & 0 & 0 \\
0 & 0 & 0 & 0 & 0 & 0 & 0 & 0 & 0 & 0 & 0 & 0 & 0 & 0 & 0 \\
0 & 0 & 0 & 0 & 0 & 0 & 0 & 0 & 0 & 0 & 0 & 0 & 0 & 0 & 0 \\
0 & 0 & 0 & 0 & 0 & 0 & 0 & 0 & 0 & 0 & 0 & 0 & 0 & 0 & 0
\end{bmatrix}$$

Dendritic molecule

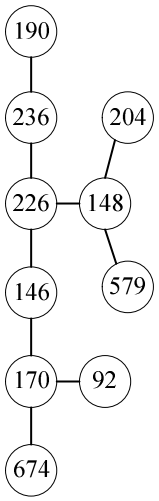

$$\begin{bmatrix}
226 & 1 & 1 & 1 & 0 & 0 & 0 & 0 & 0 & 0 & 0 & 0 & 0 & 0 & 0 \\
0 & 148 & 0 & 0 & 0 & 1 & 0 & 1 & 0 & 0 & 0 & 0 & 0 & 0 & 0 \\
0 & 0 & 146 & 0 & 1 & 0 & 0 & 0 & 0 & 0 & 0 & 0 & 0 & 0 & 0 \\
0 & 0 & 0 & 236 & 0 & 0 & 0 & 0 & 1 & 0 & 0 & 0 & 0 & 0 & 0 \\
0 & 0 & 0 & 0 & 170 & 0 & 1 & 0 & 0 & 1 & 0 & 0 & 0 & 0 & 0 \\
0 & 0 & 0 & 0 & 0 & 204 & 0 & 0 & 0 & 0 & 0 & 0 & 0 & 0 & 0 \\
0 & 0 & 0 & 0 & 0 & 0 & 674 & 0 & 0 & 0 & 0 & 0 & 0 & 0 & 0 \\
0 & 0 & 0 & 0 & 0 & 0 & 0 & 579 & 0 & 0 & 0 & 0 & 0 & 0 & 0 \\
0 & 0 & 0 & 0 & 0 & 0 & 0 & 0 & 190 & 0 & 0 & 0 & 0 & 0 & 0 \\
0 & 0 & 0 & 0 & 0 & 0 & 0 & 0 & 0 & 92 & 0 & 0 & 0 & 0 & 0 \\
0 & 0 & 0 & 0 & 0 & 0 & 0 & 0 & 0 & 0 & 0 & 0 & 0 & 0 & 0 \\
0 & 0 & 0 & 0 & 0 & 0 & 0 & 0 & 0 & 0 & 0 & 0 & 0 & 0 & 0 \\
0 & 0 & 0 & 0 & 0 & 0 & 0 & 0 & 0 & 0 & 0 & 0 & 0 & 0 & 0 \\
0 & 0 & 0 & 0 & 0 & 0 & 0 & 0 & 0 & 0 & 0 & 0 & 0 & 0 & 0
\end{bmatrix}$$

Figure 4-13. Examples of linear and dendritic molecules and their matrix representations. The numbers inside the circles represent the molecular weights of the building blocks

The verification of the molecular weight of the molecule under construction was made after every selection of a new building block although this procedure is not shown in detail in Figure 4-12. If the resulting molecular weight exceeded the upper limit of the molecular weight range, the last selected building block was not placed in the matrix, and a new building block was randomly selected. The algorithm also ensured that after adding a new building block, it was still possible to reach the target molecular weight range in the next selection step, since the smallest building block in the molecular weight distributions had a mass of 92 Da. Thus, if the resulting molecular weight of the molecule in construction was still below the lower value of the molecular weight range, the difference between the upper value and this one should be greater than 92 Da; otherwise, the last selected building block was not added to the matrix and another building block was randomly selected.

Based on this construction algorithm, once each building block was selected and placed on the diagonal of the matrix, its chemical structure was no longer relevant, only its molecular weight. In parallel with the construction of the molecular matrix, the final molecular weight of each molecule was stored in the matrix **MWAsph** of dimensions 1x10000. Once the population of molecules had been generated, the algorithm calculated the molar frequency distribution (**MWDist**), as well as their cumulative distribution (**MWDistCum**). Figure 4-14 shows the results for the case of the simulation cases of dendritic and linear molecules with 15% of large building blocks. The algorithm was able to create

populations of molecules that reproduced the molar and mass distributions obtained from the data published by Qian et al.[29]

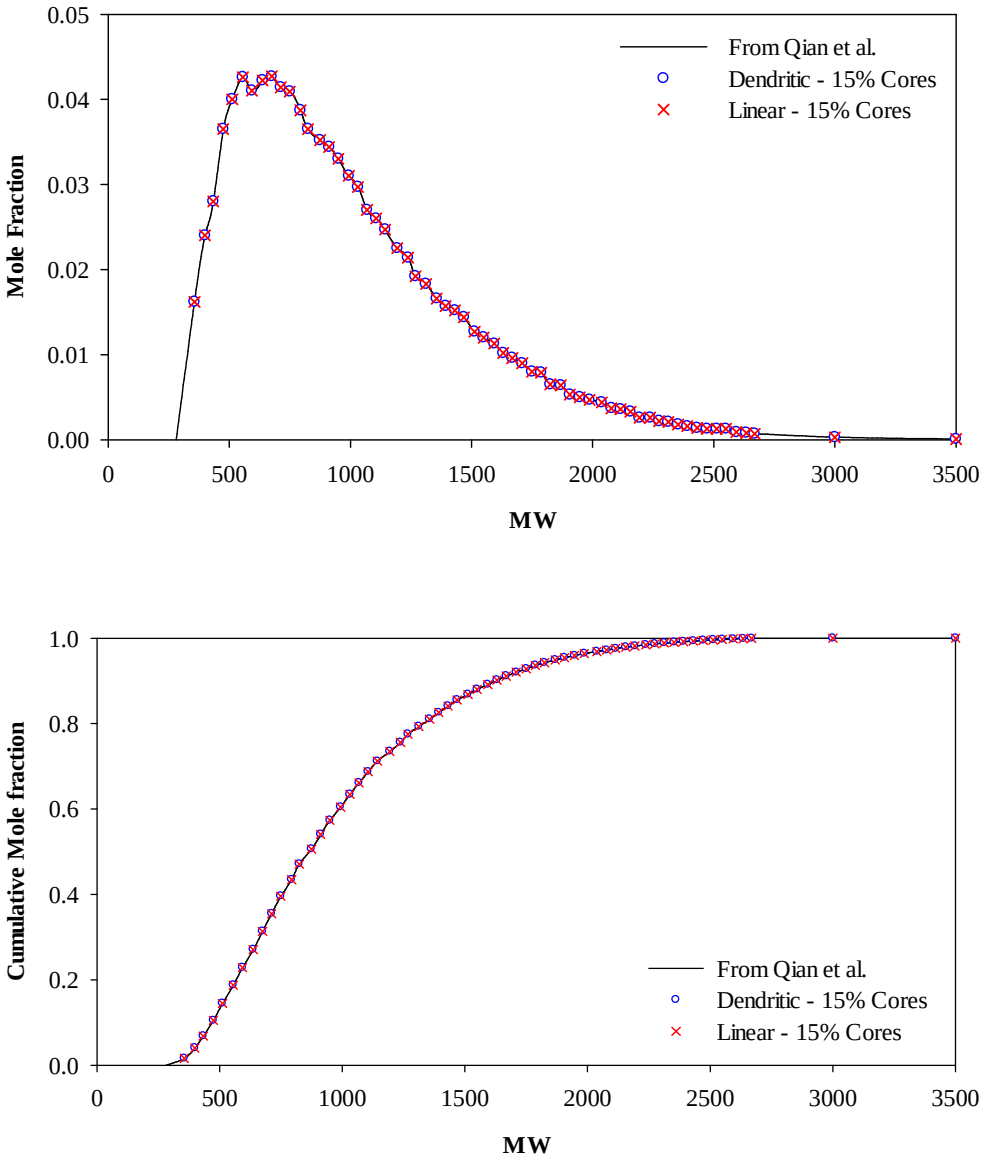

Figure 4-14. Example of molar frequency distribution, and their respective cumulative distribution, for the population of molecules generated with 15% of large building blocks. Results are compared to the data obtained from the MW distribution of asphaltenes published by Qian et al.[29]

The distributions of the number of building blocks were independent of the type of molecule, linear or dendritic, but varied with the percentage of large building blocks chosen for the construction of the populations of asphaltenes. Figure 4-15 shows these distributions for the dendritic molecules generated with 5, 15, and 25% of large building blocks. The distributions for the linear case were identical, since the connections do not affect the masses of the building blocks.

Molecules with three or less building blocks are all linear, and the data of Figure 4-15 show that the percentage of molecules with three or less building blocks were 28, 31, and 37%, respectively. Similarly, in terms of mass, 16, 20, and 25% of the total mass of the populations generated with 5, 15, and 25% of large building blocks, respectively, was constituted by molecules with three or less building blocks. Consequently, a significant fraction of the population contains so few building blocks that the architecture of their connections must be linear case.

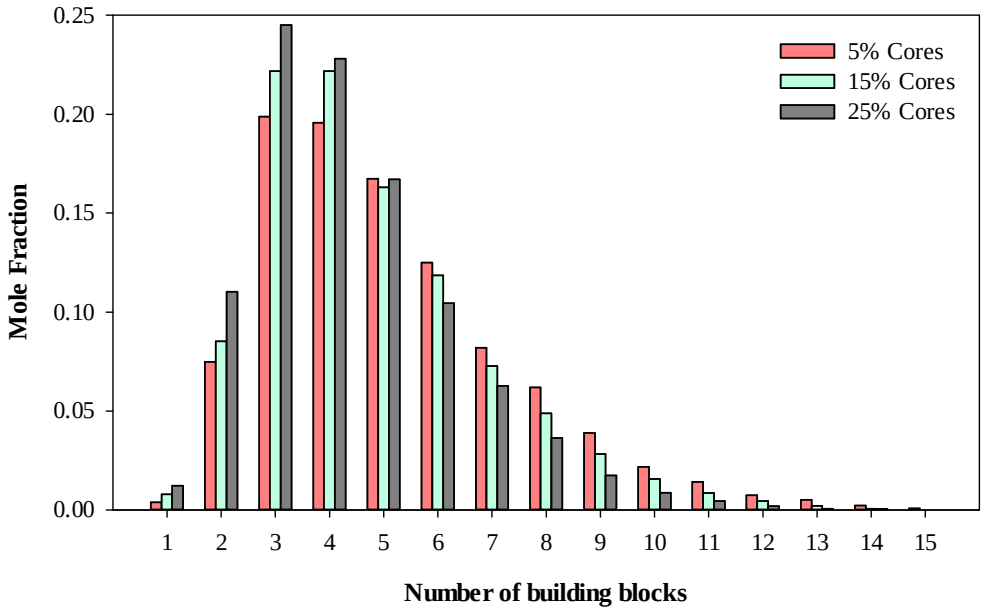

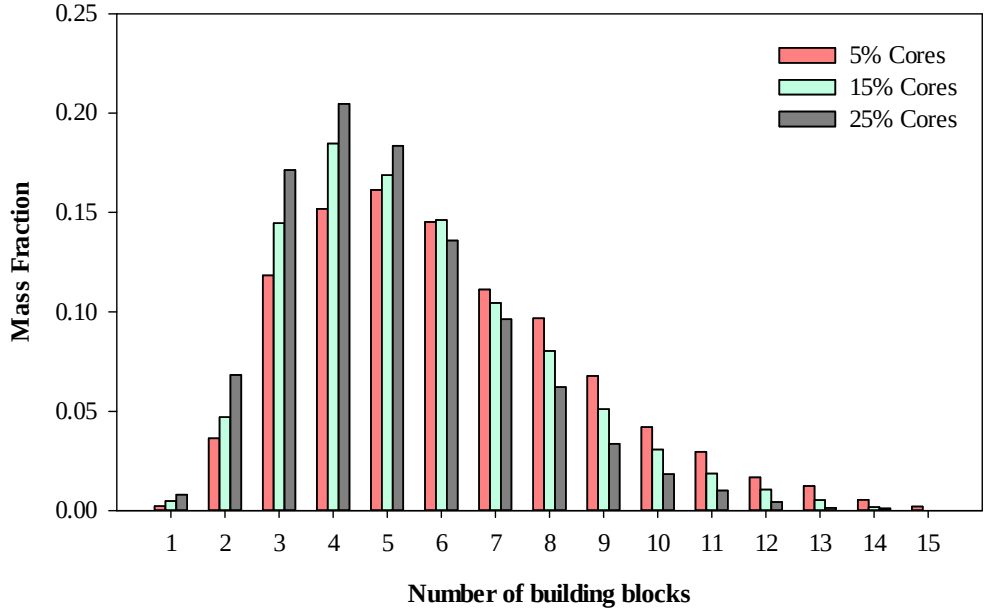

Figure 4-15. Molar and mass frequency distributions of the number of building blocks for the dendritic molecules generated with 5, 15, and 25% of large building blocks

As expected, the distributions became broader as the fraction of large building blocks was decreased. Thus, the population with 5% of large building blocks had fewer molecules with 1 to 5 building blocks than the population with 25% of these cores, but the amount of molecules with 6 or more building blocks were more abundant in the population of 5% of large building blocks compared to the others. This result is consistent with the fact that the molecules with higher amounts of large building blocks would require fewer building blocks per molecule to match the given molecular weight distribution of the asphaltenes.

Due to the random nature of the Monte Carlo simulation, the populations constructed with the same architecture and abundance of large building blocks can exhibit some differences. For example, Figure 4-16 illustrates the repeatability of the distributions of the number of building blocks for three populations of dendritic molecules generated with 15% of large building blocks.

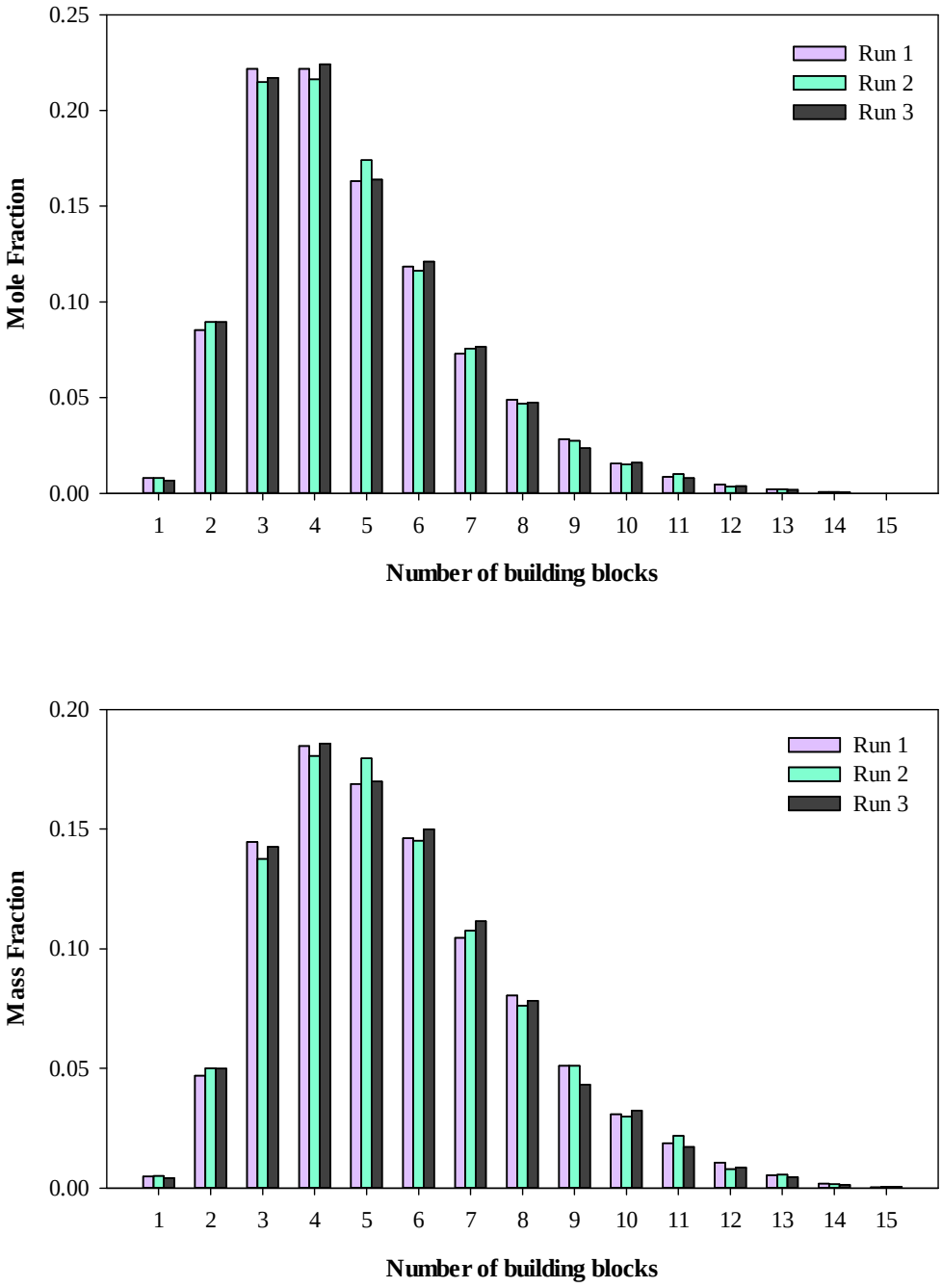

Figure 4-16. Repeatability of the Monte Carlo construction, showing molar and mass frequency distributions of the number of building blocks for three populations of dendritic molecules generated with 15% of large building blocks

The three molar distributions were evaluated with the Kolmogorov-Smirnov goodness-of-fit test, and demonstrated to be similar at a 99.99% and higher confidence levels. Likewise, these three distributions were compared with the molar distributions corresponding to 5 and 25% of large building blocks, shown in Figure 4-15, and the null hypothesis of similarity got rejected even at a confidence level of 1% in all the cases. These statistical results confirmed that the intrinsic differences derived from the Monte Carlo method are significantly smaller than the variations due to the change of the content of large building blocks in the generation of the asphaltene populations.

The mass percentage of large building blocks in the resulting populations was calculated with a separate algorithm, called MassCores (see Appendix 4). This short routine identified the building blocks with MW larger than 481 Da in the population of asphaltenes and estimated their mass fraction in the total mass of asphaltenes. This molecular weight corresponded to a boiling point of 538°C, and was calculated with the correlation given by Sim and Daubert.[36] The results indicated that 6, 17, and 26% of the total mass of the asphaltenes generated with 5, 15, and 25% of large building blocks, respectively, was constituted by clusters with molecular weights higher than 481 Da.

4.2.3 Monte Carlo simulation of the cracking of the molecules generated

The cracking reaction of asphaltenes was also simulated by the Monte Carlo method. The same cracking algorithm could be used independently of the molecular topology of the asphaltene population, and is illustrated in Figure 4-17.

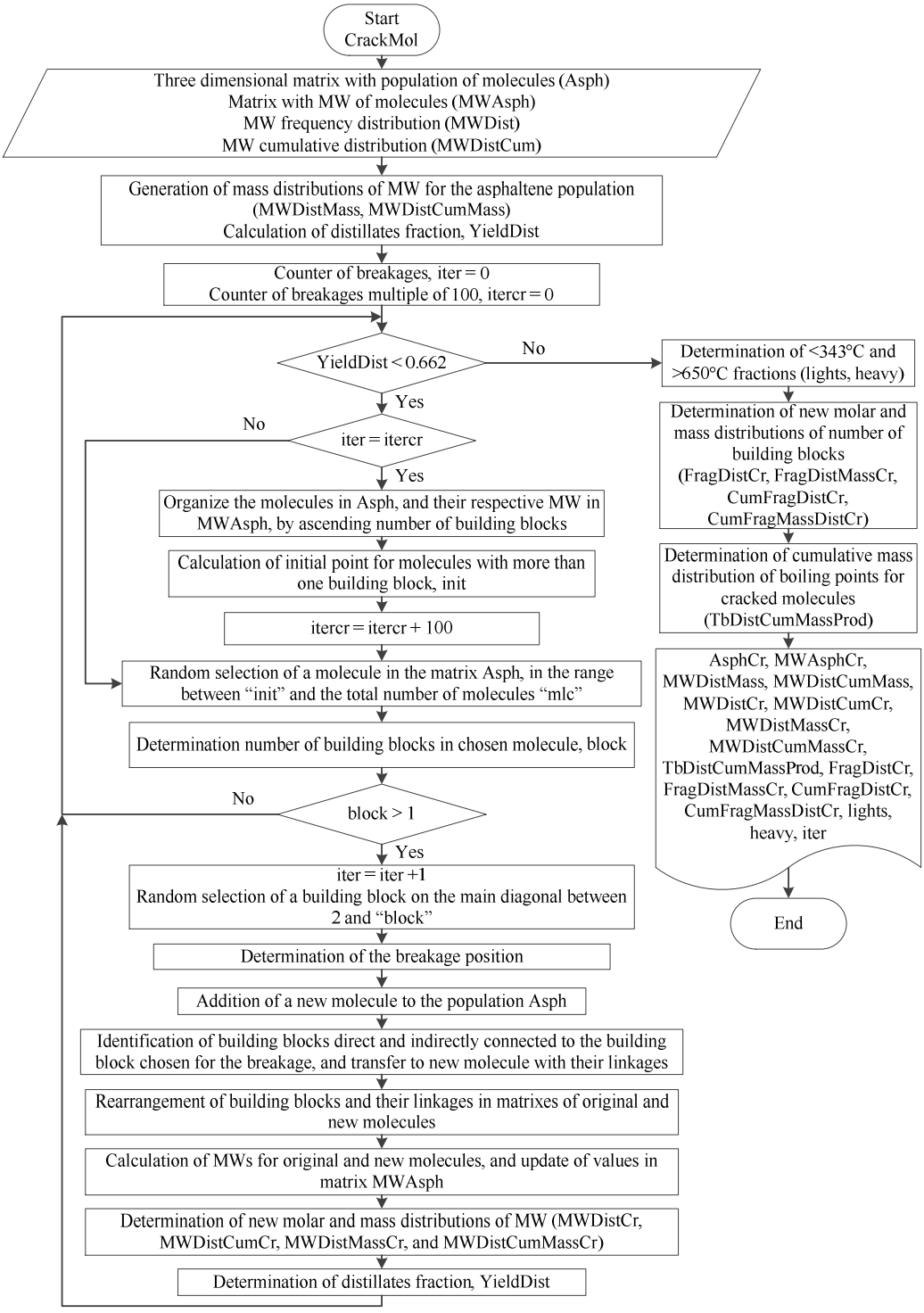

Figure 4-17. Flowchart that describes the algorithm for the cracking of a population of asphaltene molecules (**Asph**)

At each step, a molecule was randomly selected for breakage, and the point of bond cleavage was also selected randomly. The cracking reactions went on, following the same procedure, until the population reached 66.2 wt% of distillates, as experimentally found in Chapter 2.

Since only molecules with more than one building block could be cracked, the algorithm verified the number of building blocks in the selected molecule, and only went through the cracking procedure if the number of building blocks was greater than one. The simulation time was reduced if the random selection of the molecule to be cracked was restricted to only molecules with more than one building block, therefore, matrix **Asph** was reorganized by number of building blocks in the molecules, then limiting the random selection to those molecules with two or more building blocks. This reorganization of the three dimensional matrix was made after every 100 cracking steps, and was accompanied by the parallel rearrangement of the matrix **MWAsph**, which stored the molecular weight information of the respective asphaltene molecules described by **Asph**.

Once the molecule to be cracked was randomly selected, and its number of building blocks had been determined (verifying that there were more than one), the algorithm selected randomly one of its building blocks. During the construction of the molecules, each new building block had been allowed to be connected to only one of the previous building blocks located upstream on the main diagonal. Thus, each building block had only one linkage located on its own column, identified by “1”; although more “ones” could be located on its own row to identify additional linkages with building blocks downstream on the diagonal.

This configuration of the matrix allowed the selection of the bond to be cleaved by identifying the position of the linkage on the own column of the building block selected randomly.

The probabilistic selection of the building block was restricted to the range between the second and the last building block, and this last one had been previously determined with the number of blocks in the molecule. The first building block was not included in the selection since its connections were situated on its own row, and were associated to the new building blocks that had been added to the molecule.

This building block randomly selected for the breakage, and all the other building blocks that were directly or indirectly connected to it, together with the ones that described their connections, were transferred to a new matrix and deleted from the original one. Thus, the new molecule was created by adding a 15x15 matrix of zeros to the population of molecules described by the three dimensional matrix **Asph**. All the building blocks, and their connections, transferred to the new matrix, were situated in the same position that they occupied in the original matrix. Then, a separate routine was called to rearrange the original and the new matrices, in order to fill the empty positions on the main diagonal, left behind by the building blocks transferred to the new molecule, and also to ensure that the building blocks in this new matrix were situated one after another starting in the position (1,1).

Taking as example the dendritic molecule presented in Figure 4-13, if the third building block (MW = 146) was selected for the breakage, the link to be

cleaved is identified by finding the position of “1” on the third column, in this case “1” is in the first row. Thus, the matrix shows that the breakage should take place between the third and the first building block, this last one with a molecular weight of 226. The other building blocks connected to the third building block can be found on its own row, so it is observed that the only connection, represented be “1”, is on the fifth column; thus, only the fifth building block is directly connected to it. Similarly, it was found that the seventh and tenth building blocks are connected to the fifth one, and these two do not have more linkages. Consequently, the third, fifth, seventh and tenth building blocks should be transferred to the new matrix. Figure 4-18 and Figure 4-19 illustrate the molecules obtained after the cleavage, and the matrix representations of the original and new molecules, before and after the rearrangement of the building blocks.

The strategy to identify the building blocks directly and indirectly connected to the building block randomly chosen for the breakage consisted of tracking back the connections for all the building blocks, starting with the last one in the matrix. While the identified connection was with a building block located in a position of the matrix below the breakage, the algorithm would continue tracking back the connections. If the building block was connected to the building block of the cleavage, it would be transferred to the new molecule, together with the “1” located on its own column which indicates its unique connection to the previous building blocks. On the contrary, if the building block was not connected to the building block of the breakage, the algorithm would find that it was connected to some building block located above that one, and then, it would start

checking the previous building block on the diagonal following the same procedure, and so on, up to reaching the position in the matrix corresponding to the building block chosen for the breakage.

$$\begin{bmatrix}
226 & 1 & 0 & 1 & 0 & 0 & 0 & 0 & 0 & 0 & 0 & 0 & 0 & 0 & 0 \\
0 & 148 & 0 & 0 & 0 & 1 & 0 & 1 & 0 & 0 & 0 & 0 & 0 & 0 & 0 \\
0 & 0 & 0 & 0 & 0 & 0 & 0 & 0 & 0 & 0 & 0 & 0 & 0 & 0 & 0 \\
0 & 0 & 0 & 236 & 0 & 0 & 0 & 0 & 1 & 0 & 0 & 0 & 0 & 0 & 0 \\
0 & 0 & 0 & 0 & 0 & 0 & 0 & 0 & 0 & 0 & 0 & 0 & 0 & 0 & 0 \\
0 & 0 & 0 & 0 & 0 & 204 & 0 & 0 & 0 & 0 & 0 & 0 & 0 & 0 & 0 \\
0 & 0 & 0 & 0 & 0 & 0 & 0 & 0 & 0 & 0 & 0 & 0 & 0 & 0 & 0 \\
0 & 0 & 0 & 0 & 0 & 0 & 0 & 579 & 0 & 0 & 0 & 0 & 0 & 0 & 0 \\
0 & 0 & 0 & 0 & 0 & 0 & 0 & 0 & 190 & 0 & 0 & 0 & 0 & 0 & 0 \\
0 & 0 & 0 & 0 & 0 & 0 & 0 & 0 & 0 & 0 & 0 & 0 & 0 & 0 & 0 \\
0 & 0 & 0 & 0 & 0 & 0 & 0 & 0 & 0 & 0 & 0 & 0 & 0 & 0 & 0 \\
0 & 0 & 0 & 0 & 0 & 0 & 0 & 0 & 0 & 0 & 0 & 0 & 0 & 0 & 0 \\
0 & 0 & 0 & 0 & 0 & 0 & 0 & 0 & 0 & 0 & 0 & 0 & 0 & 0 & 0 \\
0 & 0 & 0 & 0 & 0 & 0 & 0 & 0 & 0 & 0 & 0 & 0 & 0 & 0 & 0
\end{bmatrix}$$

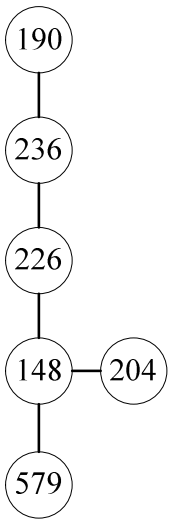

After rearrangement

$$\begin{bmatrix}
226 & 1 & 1 & 0 & 0 & 0 & 0 & 0 & 0 & 0 & 0 & 0 & 0 & 0 & 0 \\
0 & 148 & 0 & 1 & 1 & 0 & 0 & 0 & 0 & 0 & 0 & 0 & 0 & 0 & 0 \\
0 & 0 & 236 & 0 & 0 & 0 & 0 & 0 & 0 & 0 & 0 & 0 & 0 & 0 & 0 \\
0 & 0 & 0 & 204 & 0 & 1 & 0 & 0 & 0 & 0 & 0 & 0 & 0 & 0 & 0 \\
0 & 0 & 0 & 0 & 579 & 0 & 0 & 0 & 0 & 0 & 0 & 0 & 0 & 0 & 0 \\
0 & 0 & 0 & 0 & 0 & 190 & 0 & 0 & 0 & 0 & 0 & 0 & 0 & 0 & 0 \\
0 & 0 & 0 & 0 & 0 & 0 & 0 & 0 & 0 & 0 & 0 & 0 & 0 & 0 & 0 \\
0 & 0 & 0 & 0 & 0 & 0 & 0 & 0 & 0 & 0 & 0 & 0 & 0 & 0 & 0 \\
0 & 0 & 0 & 0 & 0 & 0 & 0 & 0 & 0 & 0 & 0 & 0 & 0 & 0 & 0 \\
0 & 0 & 0 & 0 & 0 & 0 & 0 & 0 & 0 & 0 & 0 & 0 & 0 & 0 & 0 \\
0 & 0 & 0 & 0 & 0 & 0 & 0 & 0 & 0 & 0 & 0 & 0 & 0 & 0 & 0 \\
0 & 0 & 0 & 0 & 0 & 0 & 0 & 0 & 0 & 0 & 0 & 0 & 0 & 0 & 0 \\
0 & 0 & 0 & 0 & 0 & 0 & 0 & 0 & 0 & 0 & 0 & 0 & 0 & 0 & 0 \\
0 & 0 & 0 & 0 & 0 & 0 & 0 & 0 & 0 & 0 & 0 & 0 & 0 & 0 & 0
\end{bmatrix}$$

Figure 4-18. Molecule resulting from the cracking of the dendritic molecule presented as example in Figure 4-13, and its matrix representations, before and after the rearrangement

$$\begin{bmatrix}
0 & 0 & 0 & 0 & 0 & 0 & 0 & 0 & 0 & 0 & 0 & 0 & 0 & 0 & 0 \\
0 & 0 & 0 & 0 & 0 & 0 & 0 & 0 & 0 & 0 & 0 & 0 & 0 & 0 & 0 \\
0 & 0 & 146 & 0 & 1 & 0 & 0 & 0 & 0 & 0 & 0 & 0 & 0 & 0 & 0 \\
0 & 0 & 0 & 0 & 0 & 0 & 0 & 0 & 0 & 0 & 0 & 0 & 0 & 0 & 0 \\
0 & 0 & 0 & 0 & 170 & 0 & 1 & 0 & 0 & 1 & 0 & 0 & 0 & 0 & 0 \\
0 & 0 & 0 & 0 & 0 & 0 & 0 & 0 & 0 & 0 & 0 & 0 & 0 & 0 & 0 \\
0 & 0 & 0 & 0 & 0 & 0 & 674 & 0 & 0 & 0 & 0 & 0 & 0 & 0 & 0 \\
0 & 0 & 0 & 0 & 0 & 0 & 0 & 0 & 0 & 0 & 0 & 0 & 0 & 0 & 0 \\
0 & 0 & 0 & 0 & 0 & 0 & 0 & 0 & 0 & 0 & 0 & 0 & 0 & 0 & 0 \\
0 & 0 & 0 & 0 & 0 & 0 & 0 & 0 & 0 & 92 & 0 & 0 & 0 & 0 & 0 \\
0 & 0 & 0 & 0 & 0 & 0 & 0 & 0 & 0 & 0 & 0 & 0 & 0 & 0 & 0 \\
0 & 0 & 0 & 0 & 0 & 0 & 0 & 0 & 0 & 0 & 0 & 0 & 0 & 0 & 0 \\
0 & 0 & 0 & 0 & 0 & 0 & 0 & 0 & 0 & 0 & 0 & 0 & 0 & 0 & 0 \\
0 & 0 & 0 & 0 & 0 & 0 & 0 & 0 & 0 & 0 & 0 & 0 & 0 & 0 & 0
\end{bmatrix}$$

After rearrangement

$$\begin{bmatrix}
146 & 1 & 0 & 0 & 0 & 0 & 0 & 0 & 0 & 0 & 0 & 0 & 0 & 0 & 0 \\
0 & 170 & 1 & 1 & 0 & 0 & 0 & 0 & 0 & 0 & 0 & 0 & 0 & 0 & 0 \\
0 & 0 & 674 & 0 & 0 & 0 & 0 & 0 & 0 & 0 & 0 & 0 & 0 & 0 & 0 \\
0 & 0 & 0 & 92 & 0 & 0 & 0 & 0 & 0 & 0 & 0 & 0 & 0 & 0 & 0 \\
0 & 0 & 0 & 0 & 0 & 0 & 0 & 0 & 0 & 0 & 0 & 0 & 0 & 0 & 0 \\
0 & 0 & 0 & 0 & 0 & 0 & 0 & 0 & 0 & 0 & 0 & 0 & 0 & 0 & 0 \\
0 & 0 & 0 & 0 & 0 & 0 & 0 & 0 & 0 & 0 & 0 & 0 & 0 & 0 & 0 \\
0 & 0 & 0 & 0 & 0 & 0 & 0 & 0 & 0 & 0 & 0 & 0 & 0 & 0 & 0 \\
0 & 0 & 0 & 0 & 0 & 0 & 0 & 0 & 0 & 0 & 0 & 0 & 0 & 0 & 0 \\
0 & 0 & 0 & 0 & 0 & 0 & 0 & 0 & 0 & 0 & 0 & 0 & 0 & 0 & 0 \\
0 & 0 & 0 & 0 & 0 & 0 & 0 & 0 & 0 & 0 & 0 & 0 & 0 & 0 & 0 \\
0 & 0 & 0 & 0 & 0 & 0 & 0 & 0 & 0 & 0 & 0 & 0 & 0 & 0 & 0 \\
0 & 0 & 0 & 0 & 0 & 0 & 0 & 0 & 0 & 0 & 0 & 0 & 0 & 0 & 0 \\
0 & 0 & 0 & 0 & 0 & 0 & 0 & 0 & 0 & 0 & 0 & 0 & 0 & 0 & 0 \\
0 & 0 & 0 & 0 & 0 & 0 & 0 & 0 & 0 & 0 & 0 & 0 & 0 & 0 & 0
\end{bmatrix}$$

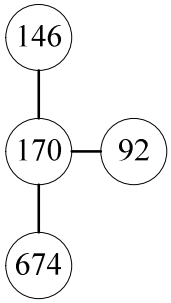

Figure 4-19. Molecule resulting from the cracking of the dendritic molecule presented as example in Figure 4-13, and its matrix representations, before and after the rearrangement

After every cracking step, the molar and mass distributions were recalculated, and were identified as the matrices **MWDistCr** and **MWDistMassCr**, with their respective cumulative distributions **MWDistCumCr** and **MWDistCumMassCr**. The mass fraction of distillates was obtained by interpolation from the cumulative mass distribution, taking into account that any molecule with a molecular weight below 481 Da could be distillable. When the target 66.2 wt% yield of distillates was reached, the algorithm converted the cumulative mass distribution of the resulting molecular population into a distillation curve (matrix **TbDistCumMassProd**), by replacing each molecular weight in the distribution with its corresponding boiling point. The conversion between boiling point and molecular weight had been used previously to transform the available SimDist data into the probability density function for the large building blocks, and was obtained from the correlation published by Sim and Daubert.[36] This curve, previously presented in Figure 4-9, was linearly extrapolated to obtain an estimation of the boiling point for the high molecular weight material.

Figure 4-20 presents the resulting distillation curves for the simulation cases with 5% of large building blocks compared to the experimental data. The SimDist curve and its extrapolation, were normalized to take into account that 37.2 wt% of the initial mass of asphaltenes, on normalized basis without gases, had been converted to distillable material lighter than tetralin, and had been lost during the removal of this solvent, and also that 8.1 wt% was converted to coke. Thus, the actual material analyzed by SimDist accounted for 54.7 wt% of the

initial mass of asphaltenes, and its boiling point curve is in the mid-range, with lighter material below and non-analyzed asphaltenes and coke above. The distillation curve for the starting population of asphaltenes, which was the same for all the simulation cases, is also shown in this figure for comparison.

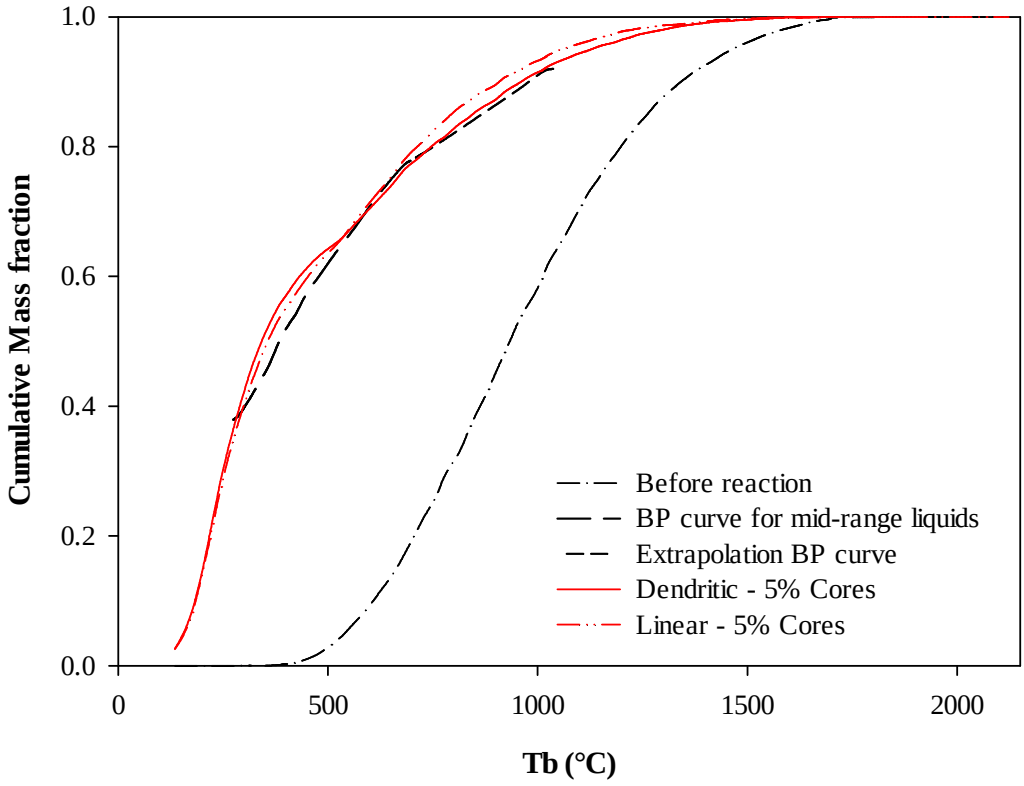

Figure 4-20. Distillation curve of the starting population of asphaltenes, and the resulting boiling point distributions after the cracking reactions for the simulation cases with 5% of large building blocks, compared with the boiling point curve for the mid-range liquids of the liquid products from the cracking under hydrogenation conditions of Cold Lake *n*-C_7 asphaltenes

The results obtained with the populations of dendritic asphaltene molecules generated with 5, 15 and 25% of large building blocks are compared in Figure 4-21. The curve for the dendritic population with 5% of large building blocks had been shown previously in Figure 4-20, so it can be used as reference to compare the results from the other simulation cases with the boiling point curve for the mid-range liquids. The molecules with 5% of large building blocks gave similar results to the curve derived from the experimental data; but as the content of these cores increases, the resulting curves differ more from the data for the mid-range liquids. We can also observe that the curves are less smooth with increasing amount of large building blocks, especially at high boiling points.

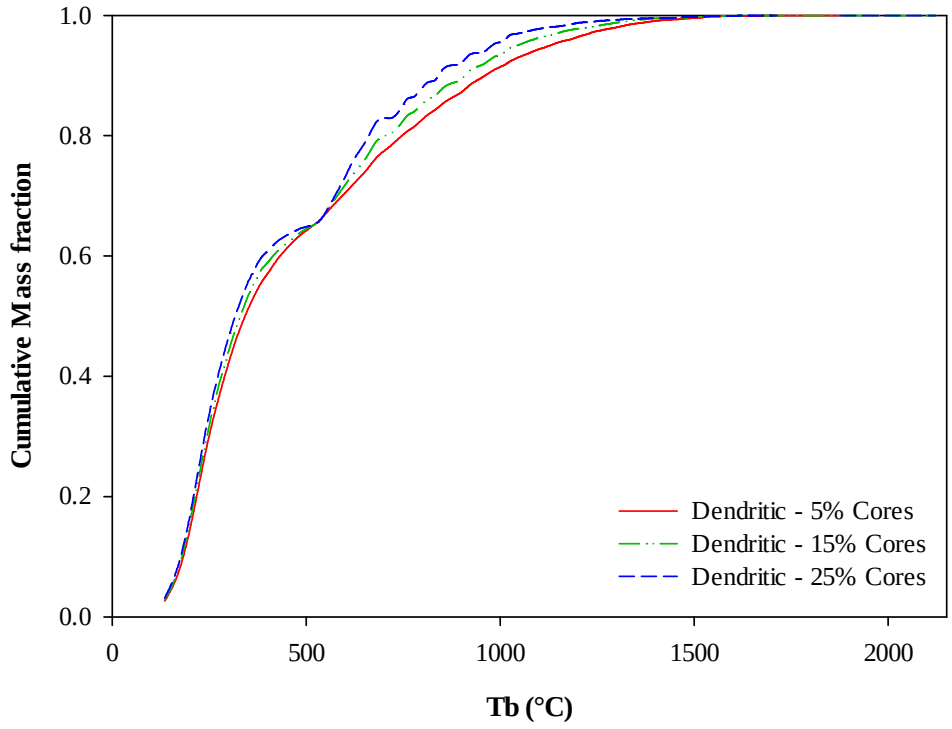

Figure 4-21. Boiling point distributions after the cracking reactions of dendritic populations of asphaltenes generated with 5, 15, and 25% of large building blocks

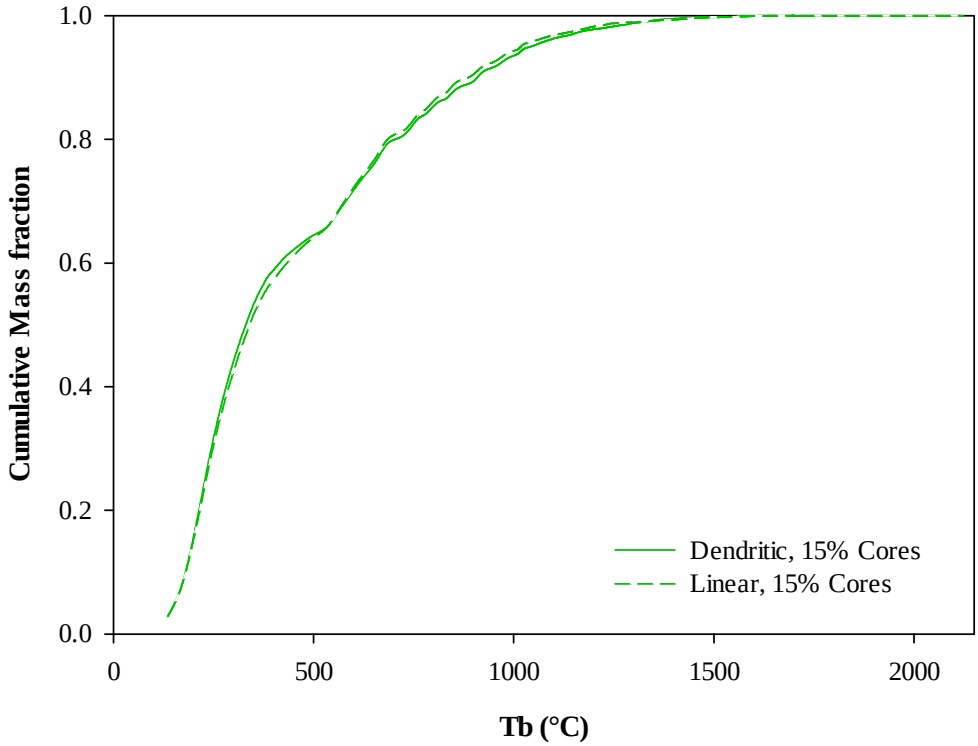

Figure 4-22. Boiling point distributions after the cracking reactions of populations of asphaltenes generated with 15% of large building blocks, with linear and dendritic molecular architectures

Figure 4-20 and Figure 4-22 show that the results are relatively independent of the topology of the molecules, since only small differences are visible between the linear and dendritic molecular architectures. However, the linear molecules fit slightly better to the distillate portion of the boiling point curve for the mid-range liquids (254-538°C), while the dendritic molecules give closer results to the high boiling point section (>538°C). The crossover of the curves takes place at the imposed yield of distillates (0.662 at 538°C), and this point also coincides with an important change in the curvature of the resulting

boiling point curves, which is especially significant as the fraction of large building blocks increases.

In order to understand better the previous results and get more information from the simulations, another parameter that was quantified from the cracking algorithm was the number of breakages, as illustrated in Figure 4-23. The results from simulations performed with 10, 20 and 30% of large building blocks have been also included in this graph, as well as the results from the repeated simulations with 15% of large building blocks and dendritic topology which can allow us to see the repeatability of the Monte Carlo method. The number of breakages can indicate which molecules can more easily yield lighter compounds, and helps to elucidate some differences based on the variation in topology and percentage of large building blocks in the construction of the molecules. Thus, asphaltene molecules with linear architecture or with lower percentages of large building blocks can yield the same amount of distillates with fewer breakages than asphaltenes with dendritic topology or with higher amounts of large building blocks, respectively. This difference in the number of cracking steps to achieve a given yield corresponds to higher reaction rates.

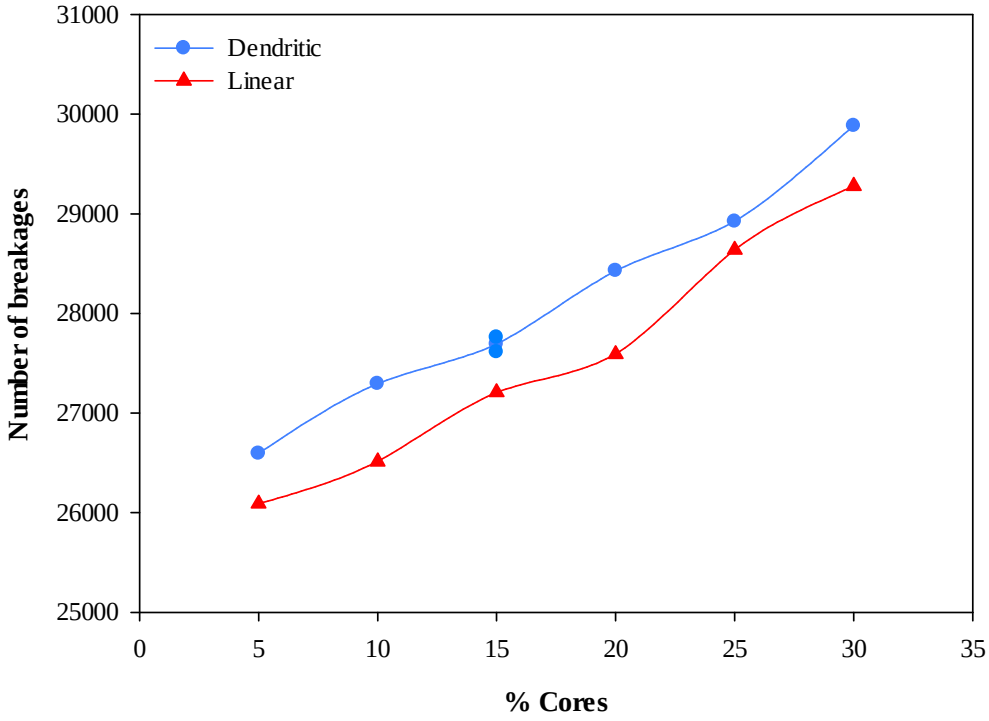

Figure 4-23. Number of breakages that the different populations of 10,000 asphaltene molecules underwent to yield 66.2 wt% of distillates

Likewise, Figure 4-24 shows that when the percentage of large building blocks increases, the molecules need to undergo more cracking reactions in order to release building blocks of low molecular weight than can compensate the larger amount of these cores. In the simulation cases with 5, 15, and 25% of large building blocks, and dendritic topology, the number of molecules in the molecular weight range between 100 to 280 Da, and 512 to 675 Da, is higher for the molecules with higher amount of large building blocks. However, in the other molecular weight ranges, 310 to 475 Da, and above 700 Da, almost consistently

there are more molecules for the population with a lower fraction of large building blocks.

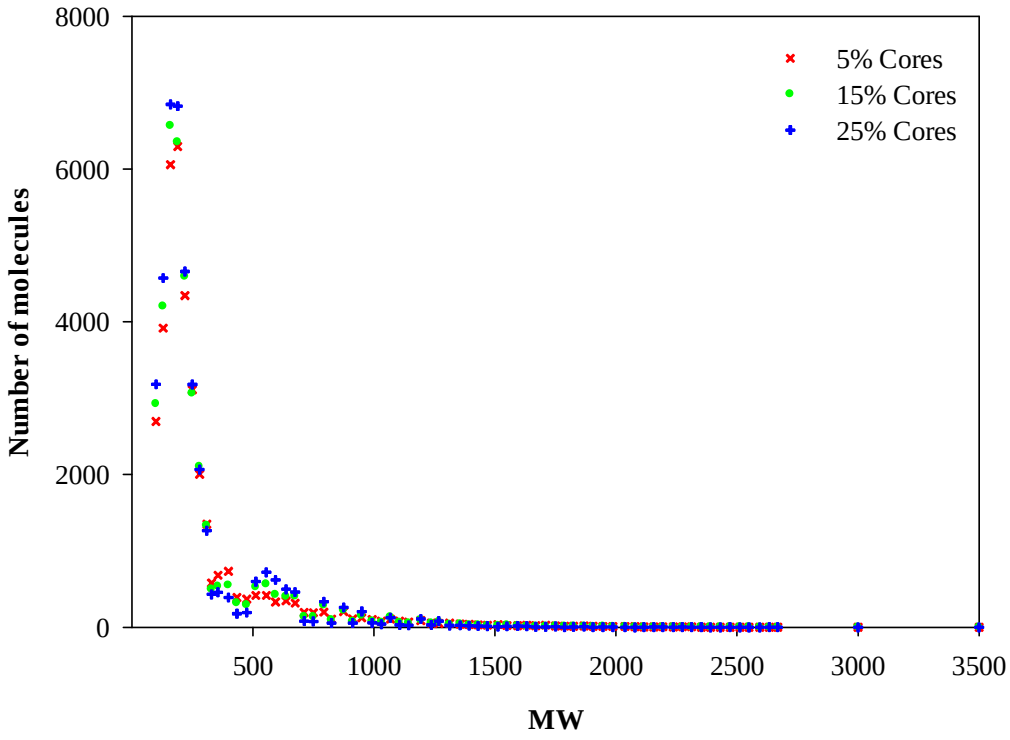

Figure 4-24. Molecular weight frequency distribution after the reaction for the populations generated with dendritic topology and 5, 15 and 25% of large building blocks

It is also remarkable that the number of molecules seems to fluctuate, becoming more significant with the increasing amount of large building blocks. This result indicates that as the molecules with more large building blocks had to undergo more breakages, they were also more extensively converted to their individual building blocks. Thus, if these individual building blocks consisted mainly of these large cores, they would not be able to undergo more breakages,

which then increased the amount of molecules in the specific molecular weight ranges of the large building blocks, which is clearly observed in these fluctuations. This means that in some ranges of molecular weight, the molecules were almost extinguished in order to yield the specified amount of distillates. These observations from Figure 4-24 can then explain the observed less smooth curves and the more significant change in their curvature at the crossover point as the amount of large building blocks increases.

These observations are also evident in Figure 4-25, which presents the molar and mass frequency distributions of the number of building blocks for the populations of dendritic molecules with 5, 15, and 25% of large building blocks after the reaction. When the amount of large building blocks increases, the number of molecules with one building block and its mass fraction also increase significantly. After the reaction, the resulting asphaltene population with 25% of large building blocks had 83 wt% of the total mass consisting of molecules with only one building block, while in the population with 5% of large cores the one-building block molecules accounted for 60 wt%.

When the molecules had been generated, the molar and mass frequency distributions of the number of building blocks were independent of the type of topology. However, after the reaction, the differences between the linear and dendritic type of molecules became more significant, as illustrated in Figure 4-26 for the single case of the populations with 15% of large building blocks. These distributions rejected the Kolmogorov-Smirnov test even at a 1% confidence level. This variation is clearly higher than the differences associated to the

stochastic nature of the simulation, which had been previously evaluated with the same method for the molar distributions of the number of fragments for three populations of dendritic molecules generated with 15% of large building blocks.

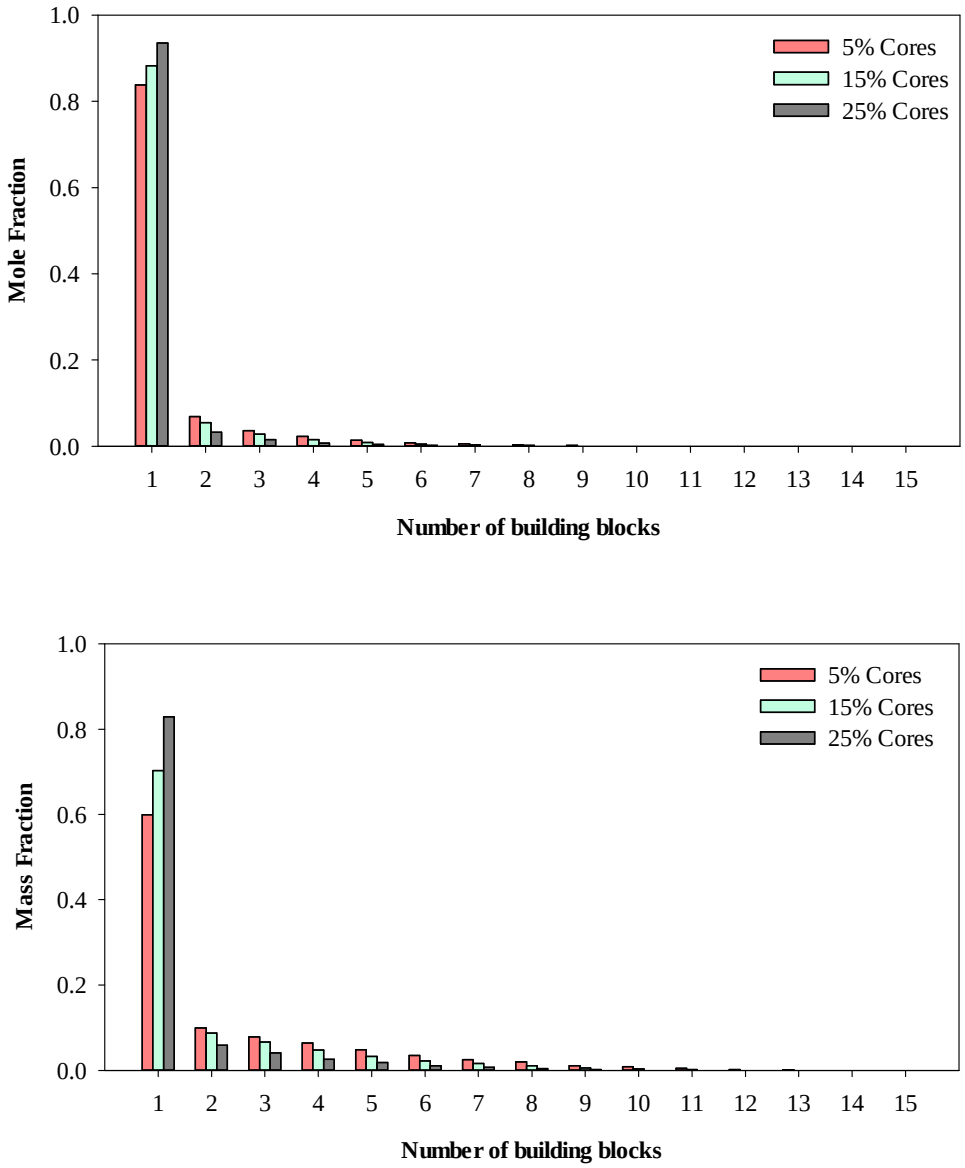

Figure 4-25. Molar and mass frequency distributions of the number of building blocks for the dendritic molecules with 5, 15, and 25% of large building blocks after the reactions that yielded 66.2 wt% of distillates

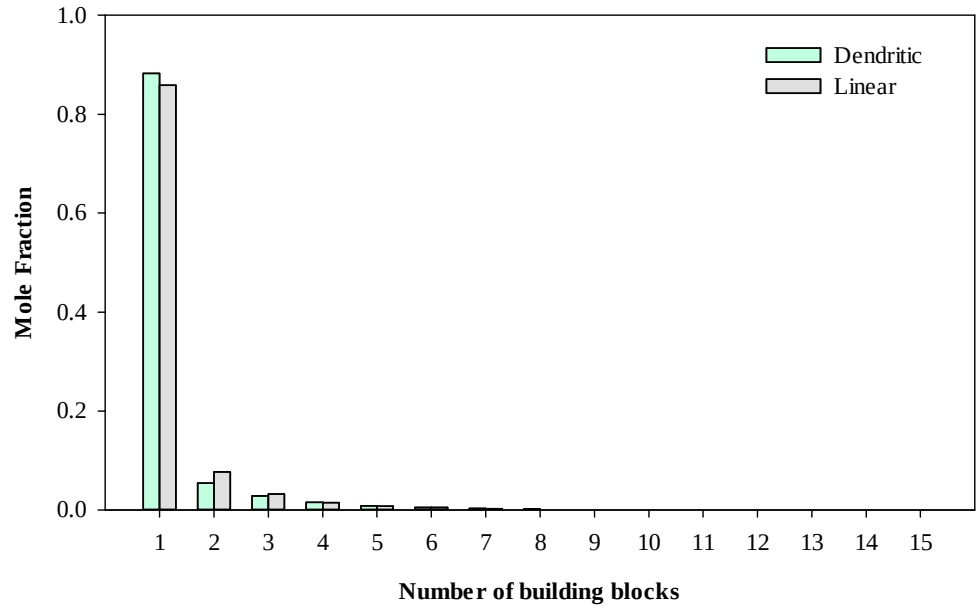

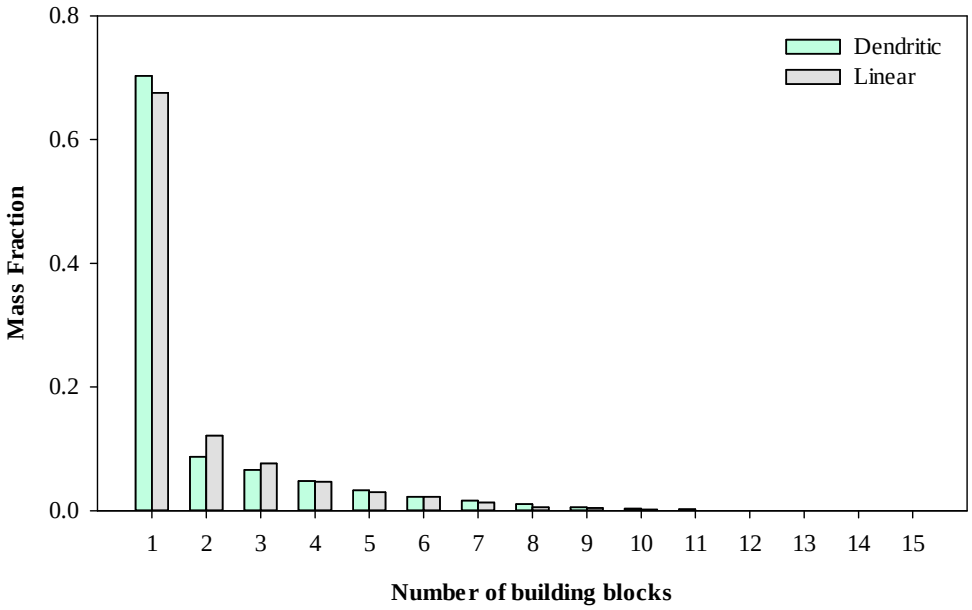

Figure 4-26. Molar and mass frequency distributions of the number of building blocks for the linear and dendritic molecules with 15% of large building blocks after the reactions that yielded 66.2 wt% of distillates

Figure 4-26 also shows that the dendritic population of asphaltenes ended up with more molecules of one building block after the reaction, which was expected based on the results presented in Figure 4-23, which was consistent with the observation that that dendritic asphaltenes underwent more breakages than linear ones, for a given yield of distillates. The simulation cases with 5 and 25% of large building blocks showed similar results, although with higher amount of large building blocks the differences came to be more significant.

Other results that were calculated in the cracking routine were the yields of the fractions < 343°C and > 650°C, and these are presented in Figure 4-27 and Figure 4-28, respectively. The results show once again that the populations generated with fewer large building blocks give a better fitting with the experimental values from the cracking of Cold Lake *n*-C_7 asphaltenes. Regarding the topology, linear molecules gave better results for the yield of the < 343°C fraction, but for the > 650°C fraction no significant differences are observed between the two different molecular topologies, except at low content of large building blocks. As pointed out in the observations from Figure 4-24, the populations with higher amount of large building blocks had to undergo more breakages in order to reach the same amount of distillates, resulting in fewer molecules with high molecular weight, and high boiling point as well, and releasing more light building blocks in order to compensate the higher amount of these large cores. This result is observed again in these two last figures, where the yields of the < 343°C and > 650°C fractions increase and decrease, respectively,

when the amount of large building blocks becomes higher in the asphaltene populations.

The experimental values reported in Figure 4-27 and Figure 4-28 were obtained from the normalized mass balance, in order to make them comparable to the results from the simulations. The < 343°C fraction included the low boiling point material lost during the evaporation of tetralin, and the value for > 650°C fraction accounted for the high boiling point material and the coke. Thus, the values for the < 343°C and > 650°C fractions estimated from the normalized experimental data were 44.4 and 25.2%, respectively.

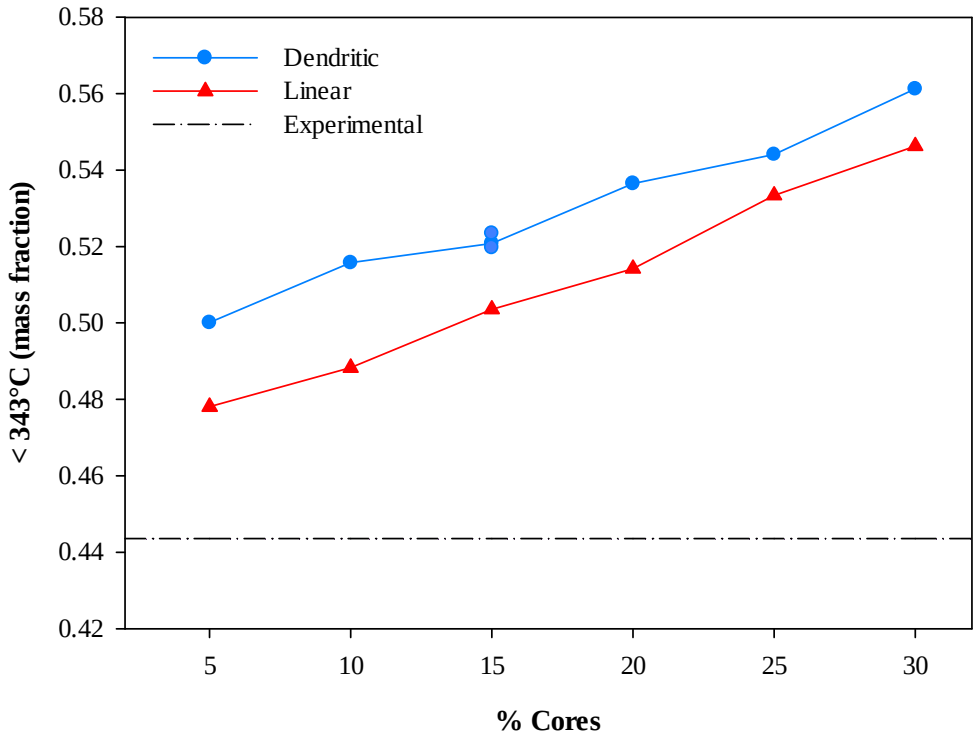

Figure 4-27. Experimental and simulated yields of < 343°C fraction, reported as weight fraction of the mass of asphaltenes

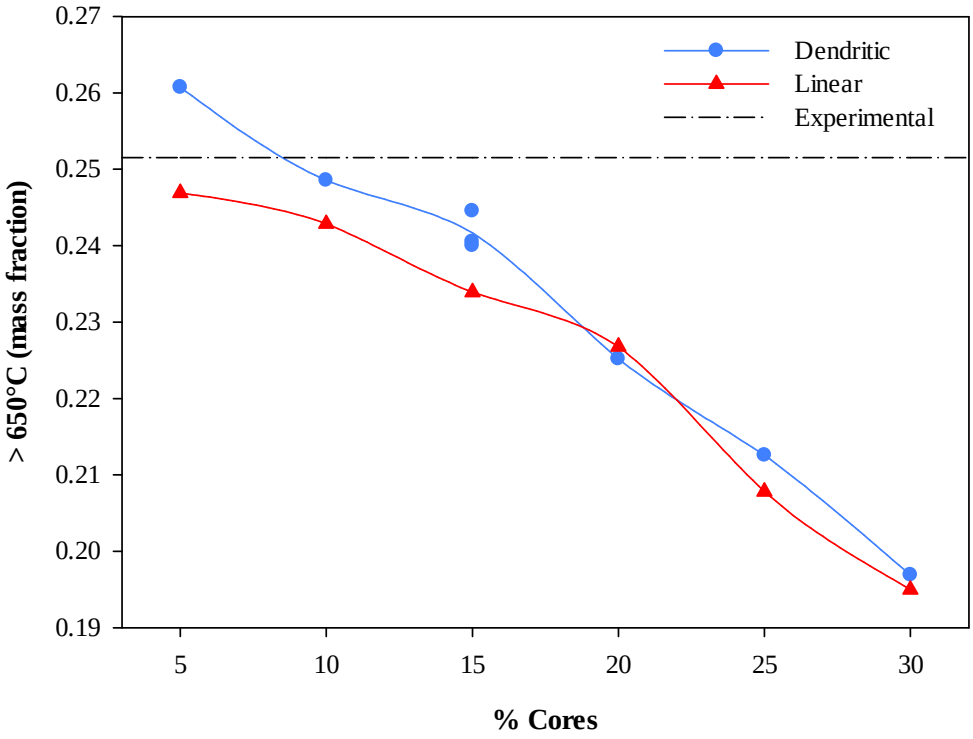

Figure 4-28. Experimental and simulated yields of > 650°C fraction, reported as weight fraction of the mass of asphaltenes

4.3 Discussion

This simulation approach was highly simplified by assuming that the strength of all the linkages between the building blocks was the same, and the probability of breakage was independent of the chemical structure of the building blocks. Another important simplification was to ignore the mass and type of bridges that would constitute the linkages. We could expect some differences in the probability of breakage depending on the length of the bridges and the presence of heteroatoms, such as S and O.[41] For example, linear carbon bridges of

three or more CH_2 groups would be less reactive than bridges with two CH_2 groups.

Similarly, the condensation and cyclization reactions that would lead to building larger molecules have not been included in the simulation. If the simulation had allowed intermolecular addition reactions to take place, we could expect that the molecules would tend to require more cracking steps to yield a given amount of distillates.

Furthermore, this simulation only explored two possible molecular topologies: linear and dendritic. In the construction algorithm the building blocks were not allowed to form macrocycles. The presence of this type of configuration would make it more difficult to yield lighter compounds, because more breakages would be required to release the small building blocks from the larger framework.

The differences observed in the distributions after cracking between linear and dendritic molecules were larger than the inherent variability of the Monte Carlo method. These two different molecular configurations showed that more breakages are required in the case of molecules with dendritic topology, in order to yield a given amount of distillates. This difference could be translated as slower rates of cracking for the dendritic molecules.

When the results were compared to the normalized experimental data for the mid-range liquids, more important differences were observed when tuning the amount of large building blocks. The results suggested that asphaltenes with lower amount of large building blocks could give better fitting of the data, and as the amount of large building blocks increased, the molecules had to pass through

more breakages to release enough building blocks with low boiling point that could compensate for the higher amount of large cores. Furthermore, as the number of breakages increased, the large cores ended up mainly as individual building blocks, resulting in less smooth curves that differed more from the reference data.

These results could suggest that the actual content of large building blocks in Cold Lake *n*-C_7 asphaltenes could be significantly lower than the 31.3 wt% estimated experimentally as the maximum content. Additionally, if we had included the addition and cyclization reactions, we could expect again that a lower fraction of large building blocks in the molecules would favor a better fitting with the target results derived from the experimental data. However, definite conclusions regarding the actual content of large building blocks in asphaltenes cannot be made based on the results of this simulation.

It is important to point out that some source of error in this work can be attributed to the lack of molecular information of the vacuum residue fraction, which hampers the generation of the probability distribution of its molecular weight. This distribution progresses to broader ranges of molecular structure as molecular weight, and complexity, become higher, as described by McKenna et al.[42] In our approach, the discrete probability density function was obtained directly from the generation of pseudo-components, based on the experimental data obtained by SimDist analysis. However, the uncertainty in the estimation of this distribution is high because part of the results were derived from extrapolated

data, and the molecular weight of each pseudo-component was estimated using density values already calculated assuming a bulk density for the sample.

The extrapolation of the distillation curve, obtained by SimDist, used an end-point of approximately 1000°C, as suggested for heavy or asphaltic oils.[35] A higher end-point value would have led to a longer tail in the curve, but would not have a major impact on the overall distribution of the bulk of the material. However, the high boiling point section of the curve is more questionable for the distributions of the simulated cracking products because it accounts for a mixture of vacuum residue and coke, and therefore, no actual boiling point data can be available in this range.

In this work the production of light ends was not included, partly because the yield of gases from the cracking of Cold Lake *n*-C_7 asphaltenes was quite low, and also because the light ends represent cracking within the building blocks as defined for this study. A different approach would be required if the objective of the simulation is to provide a complete specification for all the portions of the molecules, such as side chains and cycloalkyl rings, similar to the work of Sheremata et al.,[13] Jaffe et al.,[22] and Klein and coworkers.[9]

This work has not attempted to provide any kinetic or mechanistic study for the cracking of asphaltenes, and therefore, provides a merely stoichiometric calculation of the products distribution after the systematic random cracking of the asphaltene molecules constructed from the measured distributions of building blocks.

Extensions of this work could include the addition of other probability density functions to take into account the strength and length of the bridges. The bridges could also be allowed to include sulphide bonds, estimating the amount of sulphur in the bridges from the combined information provided by elemental analysis, XPS for sulphur speciation, and high resolution GC-MS analysis that can estimate the abundance of sulphide species, as described in Chapter 2. A probability density function able to describe the tendency of the molecules to undergo condensation reactions could also be important to get a better approximation to the experimental results.

4.4 Conclusions

1. The Monte Carlo approach used in this study for the construction and cracking of asphaltene molecules allowed to reproduce successfully a given molecular weight distribution for the asphaltenes and to evaluate differences in the distribution of products associated with the molecular topology.
2. Available analytical experimental data from the cracking under hydrogenation conditions of Cold Lake *n*-C_7 asphaltenes could be transformed into probability density functions (PDFs), which described the molecular weight distributions of the building blocks that were used as input data for the stochastic construction of asphaltene molecules.
3. The Monte Carlo simulation of the asphaltenes cracking consisted mainly of stoichiometric calculations to obtain the mass and molar distributions of the molecules after random breakages of their links. The results showed that the

distributions obtained with linear and dendritic molecules were not significantly different, but suggested that dendritic molecules would exhibit slower reaction rates, as more cracking steps were required to reach a target yield of distillable material.

4. The resulting distributions of molecules were also compared with the boiling point curve of the mid-range liquids, derived from SimDist analysis of the liquid products from the cracking of Cold Lake *n*-C_7 asphaltenes. The amount of large building blocks was used in the simulation as a tuning parameter, and better fitting was obtained when the molecules were constructed with lower amount of large building blocks.

4.5 References

1. Speight, J. G. *The chemistry and technology of petroleum;* CRC Press/Taylor & Francis: Boca Raton, FL, 2006.
2. Wiehe, I. A. *Process chemistry of petroleum macromolecules;* CRC Press: Boca Raton, FL, 2008; pp 427.
3. Pelet, R.; Behar, F.; Monin, J. C. Resins and asphaltenes in the generation and migration of petroleum. *Organic Geochemistry* **1986**, *10*, 481-498.
4. Strausz, O. P.; Mojelsky, T. W.; Faraji, F.; Lown, E. M.; Peng, P. Additional Structural Details on Athabasca Asphaltene and Their Ramifications. *Energy & Fuels* **1999**, *13*, 207-227.

5. Karimi, A.; Qian, K.; Olmstead, W. N.; Freund, H.; Yung, C.; Gray, M. R. Quantitative Evidence for Bridged Structures in Asphaltenes by Thin Film Pyrolysis. *Energy & Fuels* **2011**, *25*, 3581-3589.

6. Rueda-Velásquez, R. I.; Freund, H.; Qian, K.; Olmstead, W. N.; Gray, M. R. Characterization of pendant groups obtained by cracking of asphaltenes under favorable hydrogenation conditions. *Energy & Fuels* **2012**, *Submitted*.

7. Savage, P. E.; Klein, M. T. Asphaltene reaction pathways - V. Chemical and mathematical modeling. *Chemical Engineering Science* **1989**, *44*, 393-404.

8. Neurock, M.; Libanati, C.; Nigam, A.; Klein, M. T. Monte carlo simulation of complex reaction systems: molecular structure and reactivity in modelling heavy oils. *Chemical Engineering Science* **1990**, *45*, 2083-2088.

9. Klein, M. T.; Neurock, M.; Nigam, A.; Libanati, C. In *Monte Carlo Modeling of Complex Reaction Systems: An Asphaltene Example;* Sapre, A. V., Krambeck, F. J., Eds.; Chemical Reactions in Complex Mixtures; Van Nostrand Reinhold: New York, 1991; pp 126.

10. Neurock, M. A computational chemical reaction engineering analysis of complex heavy hydrocarbon reaction systems. (Volumes I and II), University of Delaware, United States, 1992.

11. Neurock, M.; Nigam, A.; Trauth, D.; Klein, M. T. Molecular representation of complex hydrocarbon feedstocks through efficient characterization and stochastic algorithms. *Chemical Engineering Science* **1994**, *49*, 4153-4177.

12. Wei, W.; Bennett, C. A.; Tanaka, R.; Hou, G.; Klein Jr., M. T.; Klein, M. T. Computer aided kinetic modeling with KMT and KME. *Fuel Process Technology* **2008**, *89*, 350-363.

13. Sheremata, J. M.; Gray, M. R.; Dettman, H. D.; McCaffrey, W. C. Quantitative Molecular Representation and Sequential Optimization of Athabasca Asphaltenes. *Energy & Fuels* **2004**, *18*, 1377-1384.

14. Provine, W. D.; Klein, M. T. Molecular simulation of thermal direct coal liquefaction. *Chemical Engineering Science* **1994**, *49*, 4223-4248.

15. Khorrami, P.; Radke, C. J. A random-scission model for chemical degradation of polymer solutions. *SPE Reservoir Eng* **1988**, *3*, 349-52.

16. Binder, K. Introduction to Monte Carlo simulations of polymers. *AIP Conf. Proc.* **2009**, *1091*, 55-78.

17. McDermott, J. B.; Klein, M. T. Chemical and probabilistic modelling of complex reactions: A lignin depolymerization example. *Chemical Engineering Science* **1986**, *41*, 1053-1060.

18. Landau, R. N.; Libanati, C.; Klein, M. T. Monte Carlo simulation of lignin pyrolysis: sensitivity to kinetic parameters. *Research in Thermochemical Biomass Conversion, [Ed. Rev. Pap. Int. Conf.]* **1988**, 452-463.

19. McDermott, J. B.; Libanati, C.; LaMarca, C.; Klein, M. T. Quantitative use of model compound information: Monte Carlo simulation of the reactions of complex macromolecules. *Ind. Eng. Chem. Res.* **1990**, *29*, 22-29.

20. Pen, V. P.; Pen, P. Z. Modeling of the degradation of lignin macromolecules with different topological structure. *Zh. Prikl. Khim. (S. -Peterburg)* **1999**, *72*, 1194-1198.

21. Hou, Z.; Bennett, C. A.; Klein, M. T.; Virk, P. S. Approaches and Software Tools for Modeling Lignin Pyrolysis. *Energy & Fuels* **2010**, *24*, 58-67.

22. Jaffe, S. B.; Freund, H.; Olmstead, W. N. Extension of Structure-Oriented Lumping to Vacuum Residua. *Ind. Eng. Chem. Res.* **2005**, *44*, 9840-9852.

23. Moschopedis, S. E.; Fryer, J. F.; Speight, J. G. Investigation of Asphaltene molecular weights. *Fuel* **1976**, *55*, 227-232.

24. Agrawala, M.; Yarranton, H. W. An Asphaltene Association Model Analogous to Linear Polymerization. *Ind. Eng. Chem. Res.* **2001**, *40*, 4664-4672.

25. Groenzin, H.; Mullins, O. C. Molecular Size and Structure of Asphaltenes from Various Sources. *Energy & Fuels* **2000**, *14*, 677-684.

26. Strausz, O. P.; Safarik, I.; Lown, E. M.; Morales-Izquierdo, A. A critique of asphaltene fluorescence decay and depolarization-based claims about molecular weight and molecular architecture. *Energy & Fuels* **2008**, *22*, 1156-1166.

27. Dabir, B.; Nematy, M.; Mehrabi, A. R.; Rassamdana, H.; Sahimi, M. Asphalt flocculation and deposition. III. The molecular weight distribution. *Fuel* **1996**, *75*, 1633-1645.

28. Peramanu, S.; Pruden, B. B.; Rahimi, P. Molecular Weight and Specific Gravity Distributions for Athabasca and Cold Lake Bitumens and Their

Saturate, Aromatic, Resin, and Asphaltene Fractions. *Ind. Eng. Chem. Res.* **1999**, *38*, 3121-3130.

29. Qian, K.; Edwards, K. E.; Siskin, M.; Olmstead, W. N.; Mennito, A. S.; Dechert, G. J.; Hoosain, N. E. Desorption and ionization of heavy petroleum molecules and measurement of molecular weight distributions. *Energy & Fuels* **2007**, *21*, 1042-1047.

30. Schaub, T. M.; Hendrickson, C. L.; Qian, K. N.; Quinn, J. P.; Marshall, A. G. High-resolution field desorption/ionization Fourier transform ion cyclotron resonance mass analysis of nonpolar molecules. *Analytical Chemistry* **2003**, *75*, 2172-2176.

31. McKenna, A. M.; Blakney, G. T.; Xian, F.; Glaser, P. B.; Rodgers, R. P.; Marshall, A. G. Heavy Petroleum Composition. 2. Progression of the Boduszynski Model to the Limit of Distillation by Ultrahigh-Resolution FT-ICR Mass Spectrometry. *Energy & Fuels* **2010**, *24*, 2939-2946.

32. Speight, J. G. Petroleum asphaltenes - Part 2: The effect of asphaltenes and resin constituents on recovery and refining processes. *Oil and Gas Science and Technology - Rev. IFP* **2004**, *59*, 479-488.

33. Gray, M. R.; McCaffrey, W. C. Role of Chain Reactions and Olefin Formation in Cracking, Hydroconversion, and Coking of Petroleum and Bitumen Fractions. *Energy & Fuels* **2002**, *16*, 756-766.

34. Hariu, O. H.; Sage, R. C. Crude split figured by computer. *Hydrocarbon Processing* **1969**, *48*, 143-148.

35. Virtual Materials Group Inc. *VMGSim Version 6.5 Manual;* Calgary, AB, 2011; pp 2339.

36. Sim, W. J.; Daubert, T. E. Prediction of Vapor-Liquid Equilibria of Undefined Mixtures. *Industrial & Engineering Chemistry Process Design and Development* **1980**, *19*, 386-393.

37. White, C. M.; Perry, M. B.; Schmidt, C. E.; Douglas, L. J. Relationship between refractive indices and other properties of coal hydrogenation distillates. *Energy & Fuels* **1987**, *1*, 99-105.

38. Trytten, L. C.; Gray, M. R. Estimation of hydrocracking of C-C bonds during hydroprocessing of oils. *Fuel* **1990**, *69*, 397-399.

39. Altgelt, K. H.; Boduszynski, M. M. Composition of heavy petroleums. 3. An improved boiling point-molecular weight relation. *Energy & Fuels* **1992**, *6*, 68-72.

40. Twu, C. H. An internally consistent correlation for predicting the critical properties and molecular weights of petroleum and coal-tar liquids. *Fluid Phase Equilibria* **1984**, *16*, 137-150.

41. Peng, P.; Morales-Izquierdo, A.; Hogg, A.; Strausz, O. P. Molecular Structure of Athabasca Asphaltene: Sulfide, Ether, and Ester Linkages. *Energy & Fuels* **1997**, *11*, 1171-1187.

42. McKenna, A. M.; Purcell, J. M.; Rodgers, R. P.; Marshall, A. G. Heavy Petroleum Composition. 1. Exhaustive Compositional Analysis of Athabasca Bitumen HVGO Distillates by Fourier Transform Ion Cyclotron

Resonance Mass Spectrometry: A Definitive Test of the Boduszynski Model. *Energy & Fuels* **2010**, *24*, 2929-2938.

5 Model for the prediction of the viscosity of the products from visbreaking of heavy oils

5.1 Introduction

The potential role of visbreaking for viscosity reduction of heavy oils for transportation has become more important as the depletion of light crudes has made the world turn their attention to heavy and unconventional oil resources.[1] Furthermore, visbreaking has been considered attractive for its relatively low energy consumption, simplicity, and low-cost technology that make projects more economically feasible.[2] Visbreaking can be operated at mild thermal cracking conditions, when the primary objective is the reduction of viscosity, but for increasing conversion the operation can take place at higher severities, although the fouling rates and the stability of the product become a limiting factor.[3]

Viscosity is the most important property for transportation of crude oils. In the case of heavy oils, the viscosity can be as high as 10^4 cP (1 cP = 10^{-3} Pa.s) at reservoir conditions.[4] Pipeline specifications restrict the viscosity to a maximum value, and also define certain allowable ranges for other properties, such as density, vapor pressure, bottom solids and water, among others. For instance, Enbridge specifies a maximum viscosity of 350 cSt (1 cSt = 10^{-6} m^2/s) at the reference temperature, which is set based on the pipeline temperature, and can vary depending on the time of the year.[5] Therefore, bitumen and heavy oils cannot be directly transported in pipelines, unless their viscosities are adjusted to meet the requirements. The conventional methods for transporting such viscous

materials have been the addition of diluents, such as natural gas condensate or naphtha, or by heating and insulating the pipelines.[6] Another alternative was the preparation of hydrocarbon-in-water emulsions, such as ORIMULSION™,[7] which are stable and suitable for transportation.

The reduction of viscosity of two different heavy oils through visbreaking has been explored in the present study. In order to predict the viscosity of the resulting liquid products, with limited available experimental data, a simple but consistent model is required to link composition to viscosity. Similarly, the change in distillate components due to cracking requires a kinetic model.

Dente et al.[8, 9] proposed a mathematical model for the visbreaking process and prediction of product yields and properties, such as viscosity, specific gravity, sulphur and asphaltene content, together with the estimation of some processing variables such as fouling and products stability. The kinetic mechanism was based on more than one hundred equivalent global reactions, including the radical elementary chain steps: initiation, propagation and termination of about 150 statistically grouped components, such as: paraffins, aromatics, olefins, diolefins, among others, with different methylation degree, number of rings, and other molecular characteristics. The viscosity for the products was calculated with a semi-empirical correlation that was modified to include the effect of asphaltene content and average number of carbon atoms. Bozzano et al.[10] added the effect of naphthenic components that had not been considered previously in the model by Dente et al.[8, 9] Likewise, yields, compositions and physical properties could be

predicted by the model, as well as the fouling rate and stability of the visbroken products.

The models proposed by Dente et al.[8, 9] and Bozzano et al.[10] were validated with industrial data and provided a good prediction of the process variables. However, their approach was based on the description of the feed as groups of specified chemical classes, and on the adoption of kinetics and correlations that are valid for the prediction of properties for small molecules. Therefore, these models are difficult to adapt to the study of visbreaking of heavy oils due the high complexity of their molecular composition.

Some kinetic models have also been proposed for the thermal cracking of visbreaking feeds. The inherent complexity for the development of mechanistic models for each single molecule in the feed has been approached by grouping the components based on their physicochemical properties, such as boiling points, solubility, or number of carbon atoms. These lumped kinetic models were summarized and categorized by Kataria et al.[11] into two groups: a) parallel reaction models and b) parallel-consecutive models. The models in the first group did not consider competing reactions and, in general, thermal cracking follows first order kinetics with activation energies in the range of 14 to 79 kcal/mol. The second group of models were proposed for higher severity, where coking may take place, and cracking and condensation reactions compete with each other.

For example, Di Carlo and Janis[1] proposed a kinetic model to predict the yield of distillates (<370°C) from the cracking of atmospheric residue. First order kinetics provided a good fitting for the pilot plant experimental data with three

different feedstocks. This approach could estimate the effect on viscosity reduction associated to the production of distillable material. Nonetheless, in the study of heavy oils, such simplified models can lead to shortfalls to encompass the complexity of these feeds.

Other kinetic lumped models have been proposed for thermal cracking with the same scheme: feedstock and products, such as the models proposed by Shu et al.[12] and Singh.[13] The latter paper pointed out that at low conversions, temperature and residence time are interchangeable variables in the first-order reaction model. Thus, the severity of the process, defined by these two process variables, could be achieved in a range of conditions.

Castellanos et al.[14] considered discrete pseudo-components based on true boiling point, API and molecular weight. These *n* pseudo-components were categorized according to the *i* number of carbon atoms, and each carbon atom was assumed to have two degrees of saturation: S (average degree of saturation) and O (unsaturation). It was assumed that the unsaturated molecules (O) did not undergo cracking, polymerization or condensation reactions to yield lighter diolefins or heavier hydrocarbons. Thus, 51 saturated compounds (S) were necessary to represent the feed and the products, and the total number of reactions was 1225. The parameters in the Arrhenius equation were defined in terms of the molecular weight of each S compound. The model was validated with industrial data under different operating conditions and feedstocks. In general, the calculated yields of gas, gasoline and gas oil were in good agreement with the experimental values. However, this reaction scheme, developed around the reactions of saturated

compounds, would be inappropriate for the study of cracking reactions of heavy oils, which comprise a huge variety of molecular structures and are known for their high aromatic content.

Other kinetic models have proposed lumped schemes based on boiling point fractions. For instance, Xiao et al.[15] defined the pseudo-components based on their boiling points: Gas, 210°C, 240°C, 270°C, 300°C, and 510°C. It was assumed that the cracked products did not undergo further reactions, and the conversion was defined as the total disappearance of residue to yield <510°C components.

A five lump model with consecutive-parallel reactions was proposed by Kataria et al.[11]. Six different feeds were cracked in batch reactors, and the kinetic parameters were calculated for each one of them. For a given feed (vacuum residue, 500°C +), the gas composition seemed to be independent of severity, with methane as the major component. Vacuum Gas Oil (VGO, 350-500°C) was found to undergo further cracking reactions at higher severity, while Gas (C_1-C_5), Gasoline (IBP-150°C) and Light Gas Oil (LGO, 150-350°C) fractions seemed to be more stable products.

A similar model was proposed by Singh et al.[16]. They evaluated four different feedstocks (F, vacuum residues 500°C +) in batch reactors. The selected lumps were defined based on the most value-added products, with the same boiling cuts defined by Kataria et al.[11]: Gas (G), Gasoline (GLN), Light Gas Oil (LGO) and Vacuum Gas Oil (VGO). Different lumping schemes were evaluated,

in order to find the best it of the experimental data, with all the lumps following first-order kinetics.

These different lumped kinetic models, based on boiling point fractions, were shown to be suitable and convenient for the study of thermal cracking of heavy feeds. Besides, the boiling cuts can be easily measured and provide meaningful results. However, the application of these kinetic models can be limited to a narrow range of feeds,[17] and could require validation with own experimental data, because the reported kinetic parameters and the lumped schemes are results of regression analysis of the available experimental results.

Consequently, for the kinetic study of the cracking of a given feed, a lumping scheme could be proposed and evaluated by comparing the fitting with the experimental data. In this study, the approach for the development of the model consisted of the lumping of the feed into boiling point pseudo-components, whose concentrations after the reaction could be estimated with a lumped kinetic model. The pseudo-components were defined based on their boiling points as Vacuum residue (> 524°C), Gas Oil (343-524°C), Distillates (177-343°C), and Naphtha (< 177°C). The properties of these pseudo-components were estimated, tuned with experimental values, and assumed invariable after the reaction. Thus, the viscosity of the liquid products could be calculated from the recombination of the individual properties of the pseudo-components with mixing rules available in literature.

5.2 Methods and correlations available for calculation of viscosity

Different methods and correlations have been developed for the prediction of viscosity of pure hydrocarbons (Mehrotra,[18-20]), petroleum fractions (Twu,[21, 22] Beg et al.,[23] and Mehrotra,[24]), bitumen and their mixtures (Svrcek et al.,[25] Mehrotra et al.,[26] Eastick,[27] Mehrotra,[28]), and to evaluate the effect of temperature and pressure on viscosity (Mehrotra,[29]).

Critical reviews about the calculation methods for the viscosity have been presented by Monnery et al.[30] and Mehrotra et al.[31]. The methods were classified as correlative or predictive, depending on whether model parameters must be determined experimentally or not. However, many predictive methods require viscosity data to determine either adjustable or interaction parameters. Most of the predictive methods can be used with confidence only in narrow ranges of temperature and pressure, and with a limited number of compounds; therefore extrapolation must be made with caution. For the particular case of petroleum fractions, crude oils and bitumens, different predictive and correlative methods, which can be semi-theoretical or empirical, have been reported.

5.2.1 Semi-theoretical methods

Corresponding states: This predictive method proposed by Ely and Hanley[32] is based on the principle that a dimensionless property of one substance is equal to that of another substance (reference), when both are evaluated at the same reduced conditions. The extended corresponding states method (ECS)

includes additionally the acentric factor and critical compressibility. This method can be applied from dilute gases to liquid phases, and provides good predictions when the structures of the fluids and the reference fluid are not significantly different.[30] However, methane has been widely used as reference fluid because of the availability of reliable physicochemical and thermodynamic data. A heavy hydrocarbon as reference fluid has been reported, with some modifications in the calculation of shape factors.[31] Reference fluid viscosity and density correlations are required along with critical properties, acentric factor and molar mass.

Modified Chapman-Enskog method[33]: The hard spheres method proposed by Enskog was modified to make the effective collision diameter a function of temperature and density, and then, get a better representation of "real" fluids.[30] Some input parameters are critical temperature, volume, and either acentric factor, reduced dipole moment or the empirical association factor, depending on whether the fluid is non-polar, polar or hydrogen-bonding substances, respectively.

5.2.2 Empirical methods

Some of the available empirical correlations are summarized in Table 5-1. The Andrade or de Guzman[34] equation was modified by Vogel,[35] by introducing a new parameter. Some efforts were made to generalize the parameters A, B and C, for instance, Beg et al.[23] proposed the correlations presented in equations (5-3) and (5-4).

The ASTM[36] or Walther equation[37] is a two-parameter viscosity equation that was simplified by Mehrotra[24] to obtain the single-parameter correlation

presented in equation (5-7). This last method was convenient not only for relating the single parameter to a measurable property (boiling point), but also because it was validated with viscosity data of different crude oil fractions and reported an average deviation of 2.5%.

Table 5-1. Summary of empirical correlations for the estimation of viscosity

Author(s)	**Correlation**
Andrade or de Guzman[34]	$\ln\eta=A+B/T$ (5-1)
Vogel[35]	$\ln\eta=A+B/(T+C)$ (5-2)
Beg et al.[23]	$B=\exp(5.471+0.00342* T_b)$ (5-3) $A=-0.0339 *(API)^{0.188}+0.241* \left(\frac{T_b}{B}\right)$ (5-4) Where T_b is the 50% boiling point (K)
ASTM[36] or Walther equation[37]	$\log(\log(\eta+0.7)) =b_1+b_2*\log T$ (5-5)
Mehrotra[24]	$\log(\log(\eta+0.8)) =a-3.7*\log T$ (5-6) $\log(\eta+0.8) =10^a*T^{-3.7}$ (5-7) $a = 5.489 + 0.148 *(T_b)^{0.5}$ (5-8) Where T_b is the mean boiling temperature (K)

Another approach that has been presented is the viscosity equations of state, which is based on the similarity between the P-V-T and P-η-T surfaces. Mehrotra et al.[31] pointed out the high deviations when this method is used with crude oils. Twu[21, 22] proposed another method in order to overcome the limited range of applicability of many methods when experimental data are not available.

The calculation method reported average absolute deviations (AAD) of 1.37% and 2.64% for the kinematic viscosities of hydrocarbons and petroleum fractions at 100 and 210 °F, respectively. This approach was based on a perturbation model, where *n*-paraffins were the reference fluid.

5.2.3 Viscosity mixing rules

The properties of liquid mixtures can be calculated with mixing rules. In the case of viscosity, the resulting value of this property for a liquid mixture does not correlate linearly with the individual viscosities and concentrations of the components. Therefore, different correlations have been published, and are summarized in Table 5-2.

The model of Shu et al.[12] is only valid for the simple case of two components in a mixture. ASPEN Plus™ [38] presented different correlations for multi-component mixtures. These correlations presented in equations (5-11), (5-13), and (5-14) include some binary parameters that allow an accurate representation of the viscosity of complex liquid mixtures. By default, the values for a_{ij}, b_{ij}, c_{ij}, $d_{ij,}$ k_{ij} and l_{ij} are set as zero. In the same way, the ASTM Liquid Mixture Viscosity[39] has been reported to be useful for mixture of viscous hydrocarbon components.

Table 5-2. Summary of liquid mixture viscosity equations

Author(s)	Correlation
Shu et al.[12]	$\ln\mu = X\ln\mu_A + (1-X)\ln\mu_B$ (5-9) $X = \frac{\alpha W_A}{\alpha W_A + (1-W_A)}$ (5-10) α = positive empirical constant having an upper limit of unity W_A = mass fraction of component A
ASPEN Plus™ - Aspen Liquid Mixture Viscosity[38]	$\ln\eta^l = \sum_i X_i \ln\eta_i^{*,l} + \sum_{j>i} (k_{ij} X_i X_j \ln\eta_{ij}) + \sum_i X_i \left[\sum_{j\neq i} X_j \left(l_{ij}\ln\eta_{ij}\right)^{1/3}\right]^3$ (5-11) $\ln\eta_{ij} = \frac{\left\lvert \ln\eta_i^{*,l} - \ln\eta_j^{*,l}\right\rvert}{2}$ (5-12) X_i = Mole fraction or mass fraction of component i k_{ij} = Symmetric binary parameter ($k_{ij} = k_{ji}$) l_{ij} = Antisymmetric binary parameter ($l_{ij} = -l_{ji}$) With i and j being components
ASPEN Plus™ - Viscosity quadratic mixing rule[38]	$\ln\eta^l = \sum_i X_i \ln\eta_i^{*,l} + \sum_i X_i \sum_j X_j k_{ij} (\ln\eta_i^{*,l} + \ln\eta_j^{*,l})$ (5-13)
Modified Andrade equation[38]	$\ln\eta^l = \sum_i f_i \ln\eta_i^{*,l} + \sum_i \sum_j (k_{ij} f_i f_j + m_{ij} f_i^2 f_j^2)$ (5-14) $k_{ij} = a_{ij} + \frac{b_{ij}}{T}$ (5-15) $m_{ij} = c_{ij} + \frac{d_{ij}}{T}$ (5-16) f_i, f_j = mole or mass fraction of component i or j
ASTM Liquid Mixture Viscosity[39]	$\log\left(\log\left(1000\mu_m + f\right)\right) = \sum_i w_i \log\left(\log\left(1000\mu_i + f\right)\right)$ (5-17) w_i = mass fraction of i μ_m = absolute viscosity of the mixture ($N.s/m^2$) μ_i = viscosity of component i ($N.s/m^2$) f = an adjustable parameter, typically in the range of 0.5 to 1.0
Mehrotra et al.[26]	$\log\left(\mu_m + 0.7\right) = \sum_{i=1}^{n} [x_i (M_i/\bar{M})^{0.5}] \log(\mu_i + 0.7)$ (5-18) x_i is the mole fraction of cut i, M_i is the molar mass of cut i, and $\bar{M}$ is the average mixture molar mass

5.2.4 Summary of available correlations

As observed, different prediction and correlation methods are available for the estimation of the viscosity of petroleum fractions, crude oils and bitumens. However, only a few of them could be actually considered as alternative methods for the development of the present fluid model because of the limited available data, the complexity of heavy oils, and the need to be consistent with the pseudo-component approach of this study.

The correlations proposed by Andrade or de Guzman,[34] with parameters A and B defined by Beg et al.,[23] shown in equations (5-1),(5-3), and (5-4), and the method of Mehrotra (1995),[24] given by equations (5-7) and (5-8), appear as feasible methods to approach the viscosity estimation for the fractions of heavy oils. These correlations require only density and boiling point data, which are available from the characterization of the heavy oils. Consequently, the present work has examined their accuracy with the current feeds.

For the same reasons, the mixing equations that involve additional properties, such as molar mass, do not represent practical options for the present study. Therefore, the modified Andrade equation,[38] shown in equation (5-14), was adapted by setting the interaction parameters as zero, since not enough data is available for their estimation. Thus, equation (5-14) became comparable to the equations (5-11) and (5-13) when their binary parameters are set as zero as well.

5.3 Experimental Methods

5.3.1 Visbreaking reactions

The samples of heavy oil evaluated in this study, were identified as HO# 6 and HO# 12. These samples were subjected to visbreaking reactions that provided experimental data for kinetic modelling, and the characterizations of the feed and products from the reactions were used as input data for the development of the fluid model. These thermal cracking experiments were carried out in 15-mL stainless steel batch microreactors, made up of nominal ¾ in. tube connected to Swagelok fittings, as described in Chapters 2 and 3. These microreactors are suitable to obtain enough sample for the material balance and for the analyses performed after the reaction. The isothermal conditions were provided by plunging the microreactor into a fluidized sand bath preheated to the reaction temperature. After the reaction residence time, the microreactor was removed from the sand bath and quenched in cold water.

The temperature profiles were obtained by installing a thermocouple inside the microreactor and collecting the data from one minute before introducing the microreactor into the sand bath. These temperature profiles are shown in Appendix 1for three different temperature set points: 430, 450 and 480 °C. It was observed that the temperature became stable in less than five minutes and that the actual temperature inside the microreactor was approximately 16°C below the set point.

Before the reaction, the microreactor was purged and pressurized with nitrogen at 1.38 and 0.69 MPa, respectively. Coke and liquid products were recovered and quantified for material balances. Coke was filtered out using 3.0 μm membrane filter papers (Millipore) and methylene chloride as solvent. The filter paper was dried in an oven at 80°C for 24 hours, and then weighed to quantify the amount of coke. Liquid products were quantitatively recovered after the filtration by removal of methylene chloride in a rotary evaporator. Simulated distillation (SimDist) analyses of both the heavy oil and the liquid products gave a quantitative estimation of the conversion of > 524°C fraction.

Reactions were made in duplicate, one of them was intended for mass balance, where the products were quantitatively collected, but the light ends were lost during the removal of methylene chloride by rotary evaporation, and the other reaction was made to collect the products without any further treatment, in order to minimize the loss of light ends. The samples from the second reaction were filtered with syringe filters to remove the coke, and were used for viscosity measurements and SimDist analysis.

5.3.2 Characterization of the feed and products

Heavy oil feed and liquid products were analyzed by Simulated Distillation (SimDist). A modified ASTM D6352 method was set up in a Varian 450-GC Gas Chromatogram (Bruker Ltd., Milton, ON). The temperature program for the Agilent Capillary Column WCOT Ultimetal®, L (m) x ID (mm) x OD (mm): 5 x 0.53 x 0.80, with film thickness of 0.09 μm, consisted of an initial

temperature of 40 °C ramping up to 430 °C with a heating rate of 10 °C/min, for a total heating time of 44 minutes. The initial temperature for the injector was 100 °C, followed by a heating ramp of 15 °C/min with a final temperature of 430 °C. The equipment was calibrated with a hydrocarbon mixture of paraffins from C_5 to C_{120} (ASTM D2887 Quantitative Calibration Solution, SUPELCO Analytical, 500658, C_5-C_{44}, and Polywax 655, SUPELCO Analytical, 4-8477). A lube oil from Analytical Controls Inc. (Reference Sample High Temp SimDis, Box Part No. 25650.100, Sample Part No. 56.40.202, Folio Instruments) was used as reference material. The distillation curve for this reference material was compared on a daily basis to the boiling points given by the norm in order to evaluate the performance of the equipment.

Samples were prepared in CS_2 with a dilution factor of 100, and 1 µl was injected into the chromatogram. Blank subtraction was made automatically at the end of the run by the software Galaxie Chromatography Data System Version 1.9.302.530. The integration was made using the software SimDist – Varian Galaxie Version 6.5.45, following the procedure for the method type IP 507-07 Type B (Residue), and selecting the calibration mixture High Temp ASTM DIN and IP.

The viscosities of the heavy oils and the products from their reactions were determined in a parallel plate Reologica Viscoanalyzer rheometer with diameter of 15 mm, using a gap of 1.0 mm, at three different temperatures: 15, 25, and 38°C. The density of the heavy oils was measured using a pycnometer.

5.4 Experimental Results

The thermal cracking reactions covered a range of temperatures and residence times in order to get sufficient data to evaluate the reactivity of the heavy oils, and the impact of the severity of the reaction on the final viscosity of the liquid products. The experiments and results for the thermal cracking experiments made in the batch microreactors with HO# 6 and HO# 12 are summarized in Table 5-3.

Reactions at mild conditions were duplicated. In these cases the conversion was calculated from SimDist data assuming negligible yields to coke and gas. Filtration and rotary evaporation steps were not made for the products from these reactions because coke yields were not significant.

The reaction with HO# 6 at 400 °C and with residence time of 60 minutes was repeated twice and was also made using toluene as solvent during the filtration. A good repeatability was observed and slight differences were obtained when using toluene. Liquid products were more easily filtered out with toluene than with methylene chloride.

For the reactions at 400 °C with HO# 12, two different conversions were reported. The data in brackets were obtained with SimDist results obtained in off-campus facilities. Very good reproducibility was observed between the SimDist data obtained at the University of Alberta (UofA) and at the off-campus laboratories, as shown in Figure 5-1.

Table 5-3. Thermal cracking experiments and summary of results

Heavy oil	Temperature (° C)	Residence Time (min)	Coke yield (%)	Liquids yield (%)	Conversion >524°C fraction (%)	Mass balance (%)
HO# 6	150	60‡	-	-	-0.2	-
	350	60‡	-	-	10.7	-
	400	15‡	-	-	4.1	-
		30‡	-	-	7.8	-
		40	0.8	98.6	15.6	99.7
		50	0.6	98.2	17.1	98.8
		50	0.9	98.0	19.2	98.9
		60	0.2	98.4	22.2	98.6
		60	0.5	98.5	22.0	99.0
		60*	0.4	99.1	25.1	99.6
		90	1.4	96.4	38.5	97.8
	450	15	3.6	94.3	47.3	98.0
		30ǂ	12.0	-	63.4	-
HO# 12	150	60‡	-	-	0.6	-
	350	60‡	-	-	6.4	-
	400	15‡	-	-	4.7	-
		30†	0.4	98.2	8.8 (9.4)	98.7
		40†	0.7	98.5	16.6 (13.5)	99.1
		50†	0.6	98.5	16.4 (17.5)	99.1
		60†	0.4	98.3	15.2 (17.3)	98.7
	450	15	1.3	95.9	32.3	97.3
		30	6.9	88.3	63.8	95.1

‡ Coke and gas yields were considered negligible and conversion was calculated assuming liquid yields of 100%

* Filtration with toluene instead of methylene chloride

ǂ Liquids were completely recovered but could not be weighed because part of them went through the stem that connected the microreactor to the valve when gases were released

† Conversions in brackets were calculated with SimDist data obtained in off-campus facilities

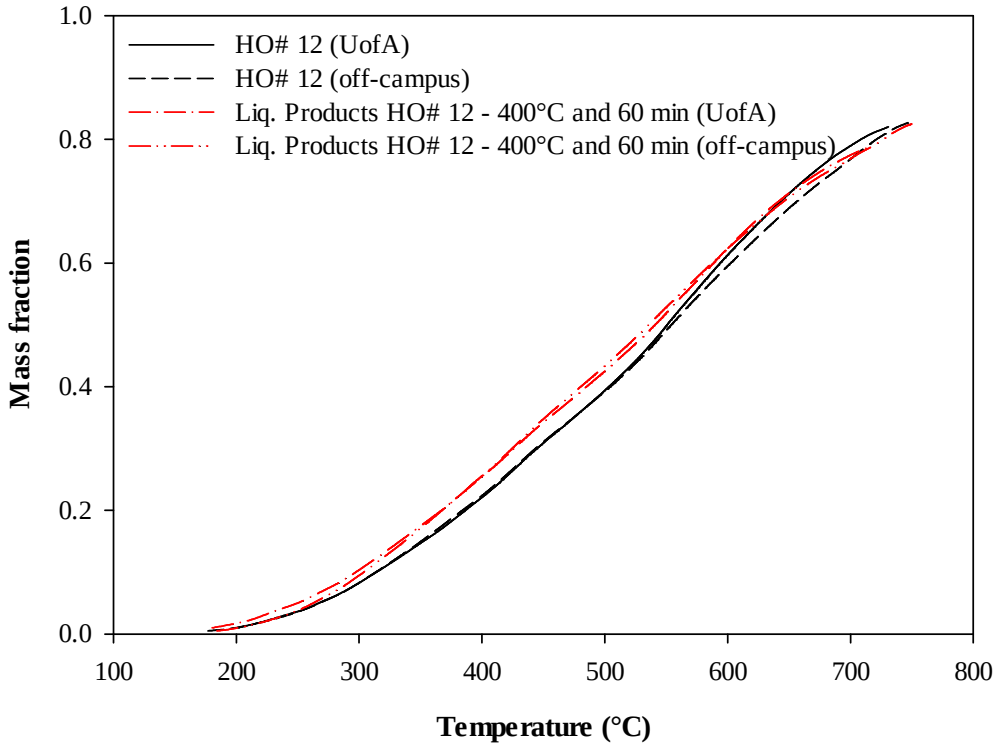

Figure 5-1. SimDist results obtained at University of Alberta and at off-campus facilities for samples of HO# 12 and the liquid products from the reaction at 400°C and 60 minutes of residence time, after rotary evaporation

Mass balances did not include the gases produced during the reaction, only accounted for the coke and the liquid products. Under the reaction conditions evaluated in the test grid, the gas yields were below 5%.

From our previous work, presented in Chapter 2 and 3, it was observed that microreactor experiments exhibit typical errors of ±1% in the yields. Another source of error in the reported results can be associated to the SimDist analysis. According to the norm ASTM D6352, SimDist data can have a maximum error of ±5% in most of the ranges of boiling points.

5.5 Fluid Model Development

A general description of the model is shown in Figure 5-2. The fluid model was developed by discretization of the feed into pseudo-components. From SimDist information and density of the feed, Riazi's method[40] provided a good fitting and extrapolation of the distillation data. Individual values of density and viscosity at different temperatures for each pseudo-component were obtained following an iterative procedure to match these values in the feed, using the boiling point of the heaviest fraction as a tuning parameter. From experimental data, the yields of the products could be obtained by lumped kinetics. Thus, the viscosity of the products could be calculated from the individual viscosities of each pseudo-component, by validated mixing rules, assuming that the properties of these fractions were invariable during the reaction. Therefore, the impact of cracking on viscosity could be evaluated as result of the variation of composition, which is function of the severity of the reaction. Reactions with higher temperatures and longer residence times would produce more light fractions, associated with higher conversion of the heavy fractions, resulting in an important reduction of the final viscosity of the liquid products.

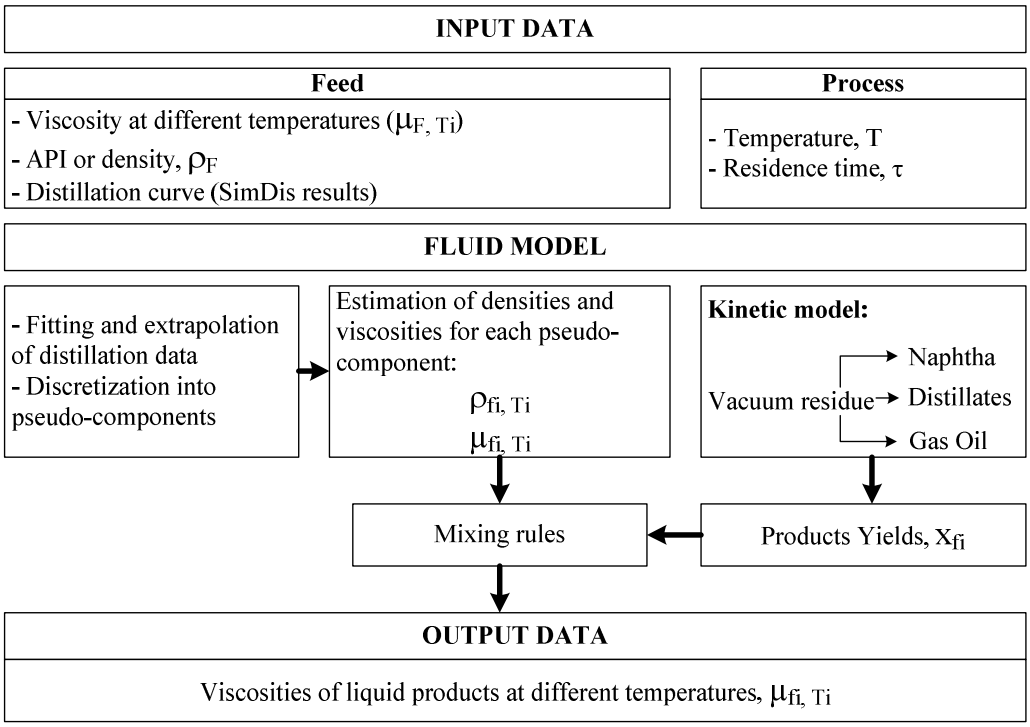

Figure 5-2. General description of the fluid model developed in this study

5.5.1 Fitting and extrapolation of distillation data

In order to calculate the properties of the individual fractions of the feed, it was necessary to find an expression that could describe the boiling points of the whole material. Riazi[40] proposed the following equation for fitting and extrapolation of distillation data:

$$T^* = \frac{T_b - T_0}{T_0} = \left[\frac{A}{B}\ln\left(\frac{1}{1-x_c}\right)\right]^{1/B} \quad (5\text{-}19)$$

Where, x_c is the cumulative weight or volume fraction and T_b is the boiling point of the respective fraction. The final boiling point remains unknown because the equation becomes undefined when $x_c = 1$.

Two different approaches were considered in this study: as suggested by Riazi,[40] the parameter B was set with a value of 1.5, and also the simultaneous

optimization of parameters A and B was evaluated to minimize the sum of squared errors (SSR).

Furthermore, the sum of squared errors (SSR) was also calculated with two different equations:

$$SSR= \sum_{i=1}^{n} \left(T_{bi,\,pred}-T_{bi,\,exp}\right)^2 \tag{5-20}$$

An alternative equation was also used:

$$SSR= \sum_{i=1}^{n} \left(T_{bi,\,pred}\left(x_{c,i}\right)-T_{bi,\,exp}\left(x_{c,i}\right)\right)^2 \tag{5-21}$$

The procedure started with the selection of a value for T_0 in equation (5-19). This boiling point temperature had to be below the minimum datum. Afterwards, parameter A, or A and B, was/were estimated to minimize the error (SSR) between the experimental data and the predicted values. It was observed that the best fitting of the distillation curve was obtained when both parameters A and B were optimized simultaneously using equation (5-20) for the estimation of the error.

When B= 1.5, the optimization of parameter A did not provide good fitting of the distillation curve. In the case of HO# 2, B=1.5 could provide a fair adjustment of the experimental results, but it was strongly dependent on the selected value for T_0. Thus, the fitting and extrapolation of the distillation curve was made with SSR calculated with equation (5-20) and with simultaneous optimization of parameters A and B. The resulting fitting curves for HO# 6 and HO# 12 are presented in Figure 5-3 and Figure 5-4, respectively.

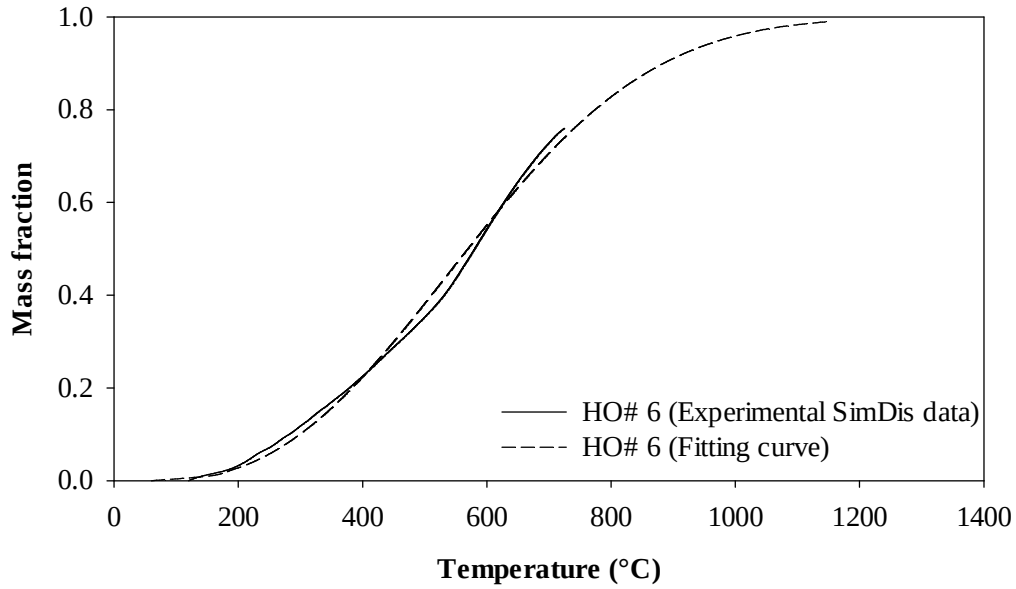

Figure 5-3. Fit and extrapolation of distillation data for HO# 6. Parameters A, B, and T_0 took values of 743.96, 2.49, and 60°C, respectively, in equation (5-19)

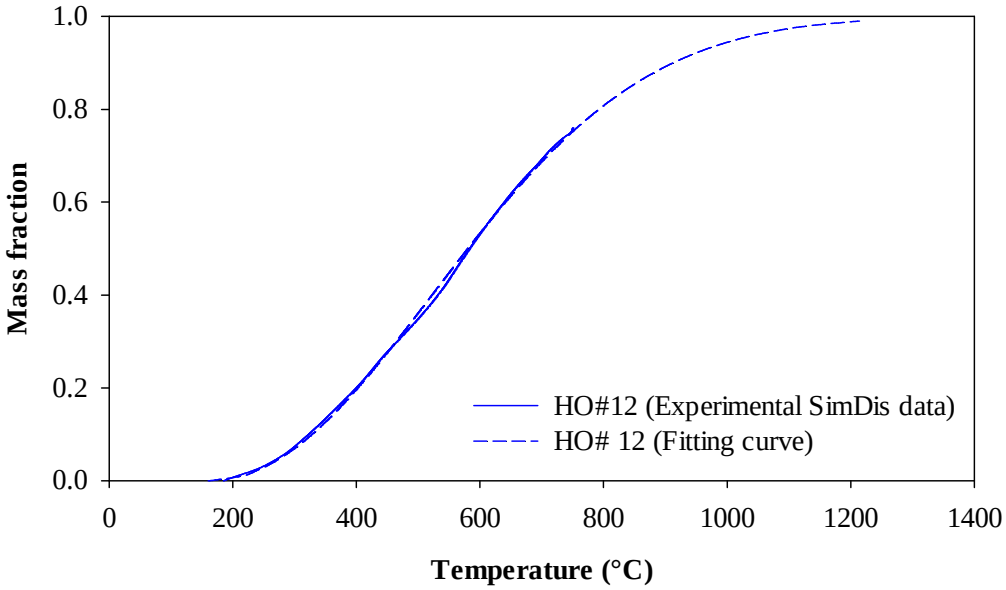

Figure 5-4. Fit and extrapolation of distillation data for HO# 12. Parameters A, B, and T_0 took values of 21.63, 2.06, and 160°C, respectively, in equation (5-19)

5.5.2 Specific gravity for each pseudo-component

For the construction of pseudo-components from the feed, two different approaches were considered. The first one consisted of the calculation of boiling points to get approximately 20 fractions, each one of 5 wt%. In the second approach the crude was divided into the fractions: Naphtha (<177°C), Distillates (177-343°C), Gas Oil (343-524°C), and Vacuum residue (>524°C).

With the value for parameter A, estimated from the boiling curve fitting, equation (5-22) could provide an estimation of the specific gravity for the different boiling fractions.

$$SG^{*} = \frac{SG-SG_0}{SG_0} = \left[\frac{A}{B}\ln\left(\frac{1}{1-x_c}\right)\right]^{1/B} \tag{5-22}$$

Riazi[40] suggested the value of 3.0 for parameter B. In this case, SG_0 is unknown, but SG_{av} must be the experimental value of density of the feed. The estimated densities for the pseudo-components must be able to satisfy equation (5-23) or equation (5-24).

$$SG_{av} = \sum_{i=1}^{n} SG_i \Delta x_{c,i} \tag{5-23}$$

Where $x_{c,i}$ is the volume fraction. Or,

$$SG_{av} = \frac{\sum_{i=1}^{n} \Delta x_{c,i}}{\sum_{i=1}^{n} \frac{\Delta x_{c,i}}{SG_i}} \tag{5-24}$$

Equation (5-24) is the alternative expression where $x_{c,i}$ is the mass fraction.

Then, the value of SG_0 was calculated by an iterative procedure to match the density of the heavy oil feed. This was made for both sets of pseudo-

components (20 components and 4 components). However, B=3.0 did not provide consistent values for the densities of the fractions. To overcome this, the value of B was estimated together with SG_0, in order to meet the density of the feed, and verifying that the densities of the respective fractions were in acceptable ranges (naphtha: 680 – 820, distillates: 800 - 920, gas oil: 900 - 980, and vacuum residue: > 940 kg/m^3).[41]

The estimated specific gravities for one of the sets of pseudo-components of HO# 6 and HO# 12 are presented in Table 5-4. The parameters B and SG_0 took values of 7.7 and 0.338, respectively, for HO# 6; and 12.9 and 0.488, for HO# 12.

Table 5-4. Specific gravity for pseudo-components of HO# 6 and HO# 12 obtained from simultaneous solution of equations (5-22) and (5-24)

Pseudo-components	**HO# 6**		**HO# 12**	
	Mass fraction	**Specific gravity**	**Mass fraction**	**Specific gravity**
< 177°C	0.02	0.700	0.00	0.784
177 – 343 °C	0.13	0.820	0.12	0.920
343 – 524 °C	0.27	0.903	0.28	0.970
> 524 °C	0.57	1.083	0.59	1.059
Specific gravity heavy oil	0.978		1.014	

The specific gravities at different temperatures for each pseudo-component were estimated by API Procedure 6A3.5[42] with equation (5-25).

$$Denl = A\,[SG^2 - (B \times SG - C + D \times MeABP)(T - E)/MeABP]^{1/2} \qquad (5\text{-}25)$$

Where:

Denl= Liquid density (lb_m/ft^3)

T = Temperature, in degrees Rankine

MeABP = Mean average boiling point, in degrees Rankine

SG= Specific gravity

A= 62.3636

B= 1.2655

C= 0.5098

D= 8.011×10^{-5}

E= 519.67

The reliability of this method has been reported with estimated errors about 0.3 percent at 1 atmosphere.[42]

5.5.3 Estimation of viscosity for pseudo-components

In spite of the multiple correlations available in literature, most of them only provide good estimations in narrow ranges of conditions. Moreover, for petroleum fractions, and more particularly for heavy oils, many of the parameters required in many of the existing methods are undefined due to their complex composition.[31] In this study, two empirical correlations were evaluated, taking into account that the only available data consisted of the distillation curve and density of the heavy oils and their pseudo-components.

The viscosity correlation of Andrade or de Guzman,[34] with parameters A and B given by Beg et al.,[23] presented in equations (5-1),(5-3), and (5-4), was one method evaluated in this study. The method of Mehrotra (1995),[24] described by equations (5-7) and (5-8), was also used to evaluate the viscosity of the pseudo-components of HO# 6 and HO# 12. It was found that the method of Andrade or de

Guzman[34] became undefined and could not provide any estimation for heavy fractions with low API. Therefore, the method of Mehrotra was used for the calculation of the viscosities. The selection of this correlation was also based on the convenience for the calculations for the pseudo-components, since it only depends on the boiling point.

For the estimation of the viscosities of the feed at different temperatures from the individual viscosity values for each pseudo-component, a simplified version of the modified Andrade Liquid mixture correlation, presented previously in equation (5-14), was used:

$$\ln\eta^{l}=\sum_{i} f_i \ln\eta_i^{*,l} \qquad (5\text{-}26)$$

Where f_i is mass fraction and the binary parameters were assumed to be zero.

The mean boiling point for the heavy fraction was unknown because the final boiling point had remained undefined from the extrapolation of the distillation curve with Riazi's method.[40] Consequently, the mean boiling point of the heaviest fraction of the crude oil could be used as a tuning parameter to fit the viscosities of the feed. Thus, the approach for the fitting of the viscosity data consisted of the estimation of the boiling point for the heavy fraction that minimized the SSR between the experimental and the predicted values for the viscosities of the heavy oils at three different temperatures: 15, 25, and 38°C. These calculations were made only for the pseudo-components based on the boiling fractions, not for the 5% mass pseudo-components. In this latter case it was necessary to set up a cut point and consider the entire heavy fraction as one

pseudo-component, otherwise the individual viscosities for the pseudo-components with high boiling points exhibited very high values, which could not be compensated by the viscosities of the light fractions to fit the experimental data. Therefore, the calculations were made only for the boiling point fractions, consisting of: naphtha, distillates, gas oil and vacuum residue, which was also more meaningful for the development of the kinetic model.

In order to account for the highly non-linear dependence of viscosity on temperature, SSR was estimated with the next three different expressions:

$$SSR= \sum_{i=1}^{n} \left(\mu_{F,Ti\ pred}-\mu_{F,Ti\ exp}\right)^2 \quad (5\text{-}27)$$

$$SSR= \sum_{i=1}^{n} \left(\ln\mu_{F,Ti\ pred}-\ln \mu_{F,Ti\ exp}\right)^2 \quad (5\text{-}28)$$

$$SSR= \sum_{i=1}^{n} \left(\frac{\ln\mu_{F,Ti\ pred}-\ln \mu_{F,Ti\ exp}}{\ln \mu_{F,Ti\ exp}}\right)^2 \quad (5\text{-}29)$$

The distribution of the error with temperature was more uniform when SSR was determined with equation (5-28). Thus, the calculation of the average boiling point of the vacuum residue fraction followed an iterative procedure to minimize the error. The estimated mean boiling points for the vacuum residue fraction of HO# 6 and HO# 12 were 657.4 and 694.7°C, respectively. As a result, the viscosities for the individual fractions could be calculated at 15, 25, and 38°C, and are shown in Figure 5-5 and Figure 5-6. These viscosities were introduced in equation (5-26), with the respective concentration of each fraction, and the viscosities of the heavy oils could be calculated. Figure 5-7 presents the parity

plot that compares these estimated viscosities with the experimental data available for the heavy oils.

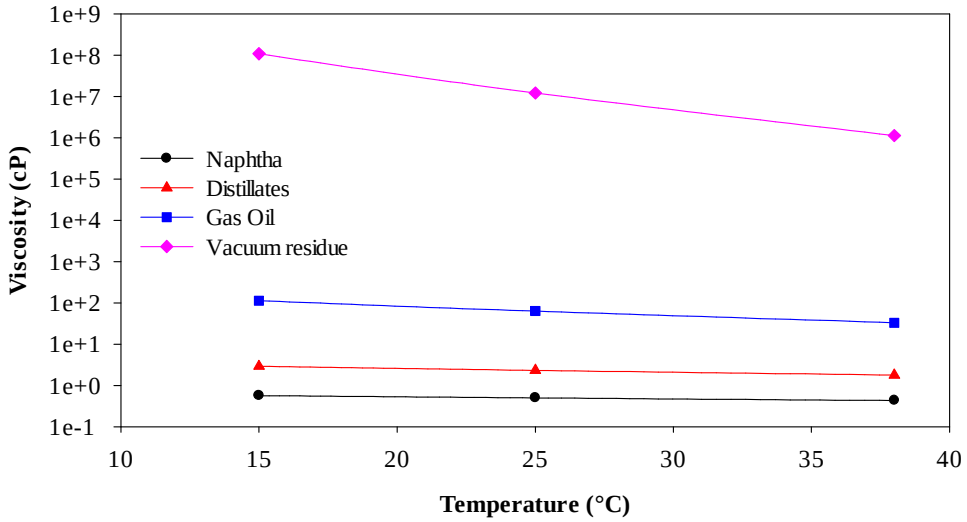

Figure 5-5. Viscosities of the boiling fractions of HO# 6 estimated with the correlation proposed by Mehrotra (1995)[24]

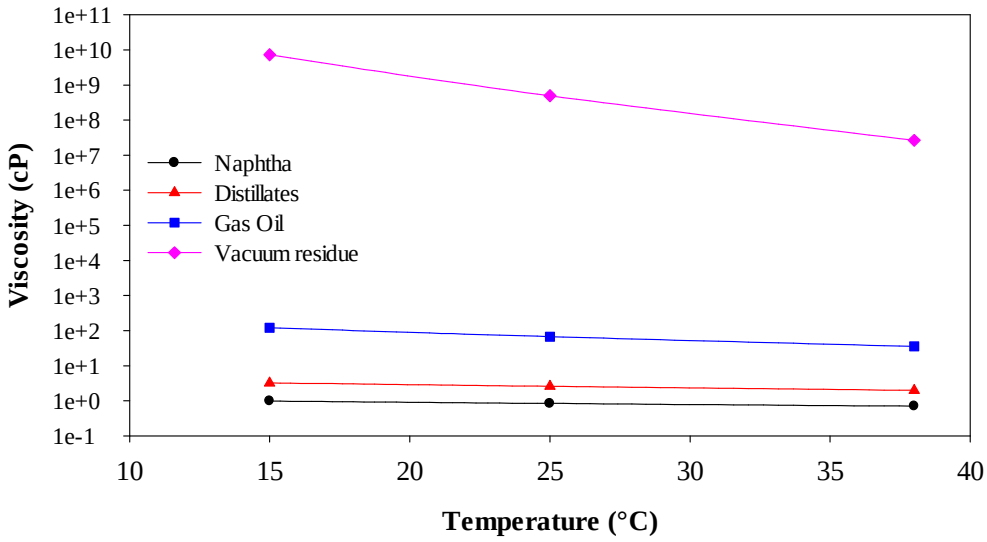

Figure 5-6. Viscosities of the boiling fractions of HO# 12 estimated with the correlation proposed by Mehrotra (1995)[24]

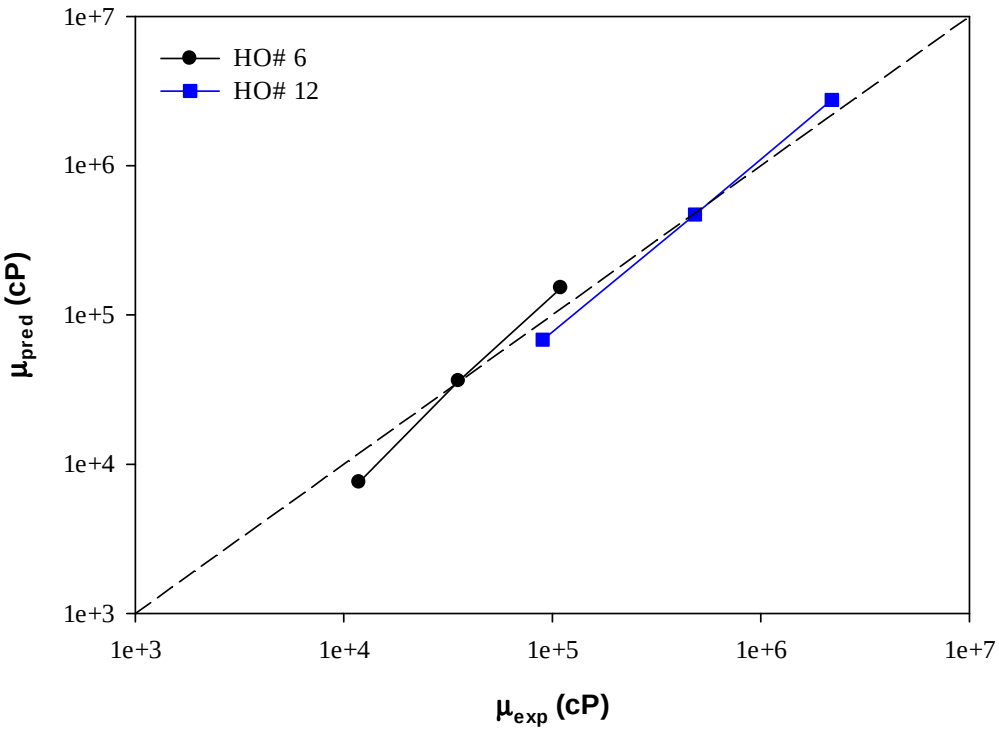

Figure 5-7. Parity plot for predicted and experimental viscosities for HO# 6 and HO# 12 at 15, 25 and 38°C

This methodology provided good fitting for the viscosity at the intermediate temperature, but underestimated the viscosity at 38°C, and overestimated it at 15°C. The average absolute deviation percentages (AAD%) for HO# 6 and HO# 12 were 25.2% and 17.6%, respectively.

This procedure provided the individual viscosities for each one of the pseudo-components, at three different temperatures. Therefore, under the assumption that the properties of each one of the pseudo-components remained invariant with reaction, the resulting viscosities of the liquid products after the reaction could be estimated by recombination of the viscosities with the mixing

rule presented in equation (5-26), and with the new mass fractions for each one of the pseudo-components obtained by SimDist analysis of the liquid products. These estimated viscosities were compared to the experimental values in order to evaluate if the assumption was valid.

The samples recovered after the reactions, without any additional treatment, were analyzed by SimDist to get the mass fractions of the pseudo-components in the products. The distillation curves for HO# 6, and HO# 12, and their liquid products, are shown in Figure 5-8 and Figure 5-9, respectively.

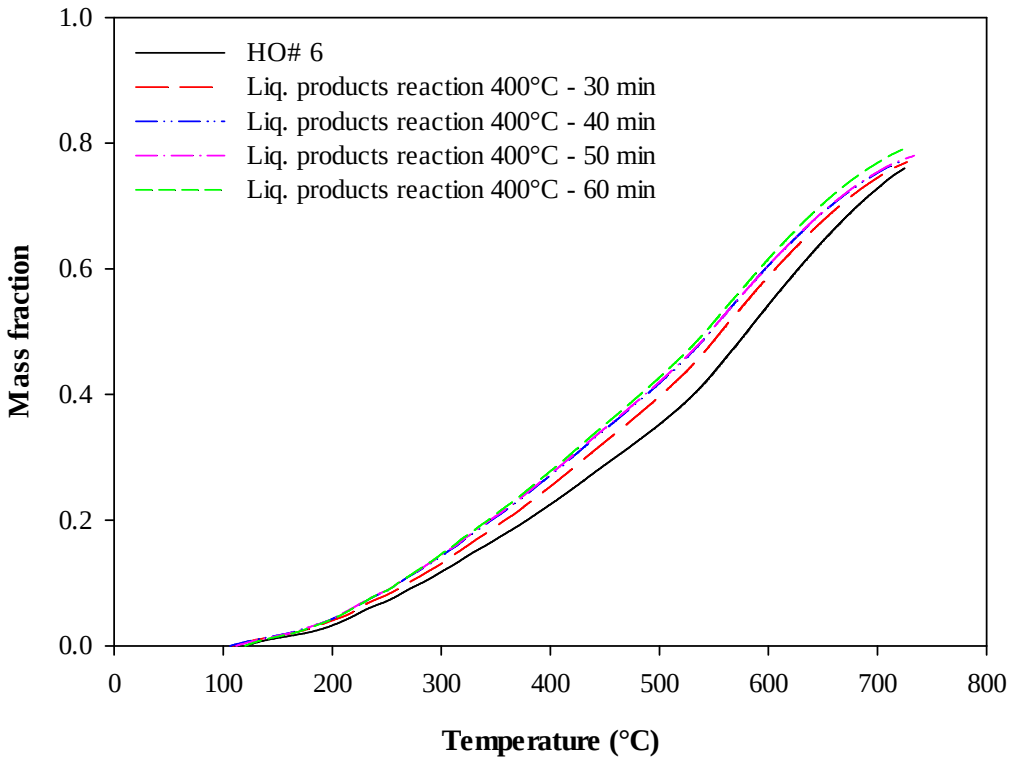

Figure 5-8. Distillation curves for HO# 6 and the liquid products from its visbreaking reactions at 400°C and different residence times

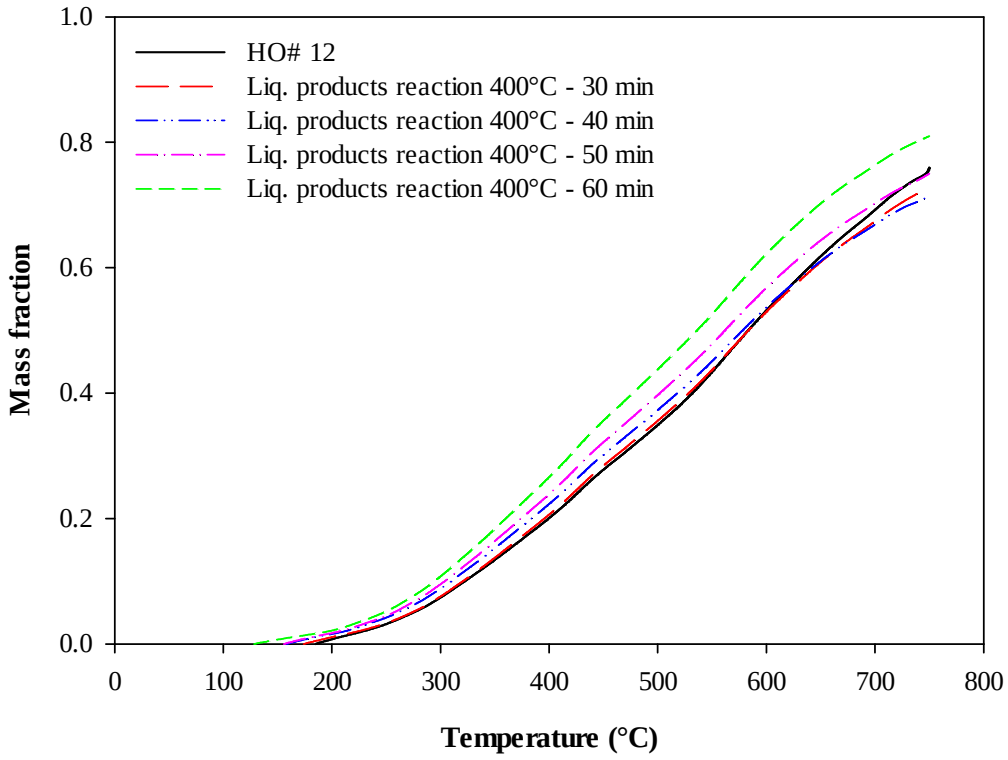

Figure 5-9. Distillation curves for HO# 12 and the liquid products from its visbreaking reactions at 400°C and different residence times

Table 5-5 and Table 5-6 summarize the mass percentages for each one of the boiling point fractions in HO# 6, HO# 12, and their liquid products. As the severity of the reaction increases, with longer residence times, the lighter fractions, which exhibit lower viscosities, increase as well; while the vacuum residue content decreases. The conversions in these reactions were in the range of 8 to around 23% for HO#6, and between 9 and 17% for HO#12.

Table 5-5. Mass percentages of the different boiling point fractions for HO# 6 and the liquid products from its reactions at 400°C and different residence times

Fraction	IBP (°C)	FBP (°C)	Mass percentages, wt%				
			Feed	Liquid Products from reactions at 400°C			
				30 min	40 min	50 min	60 min
Naphtha	-	177	2.1	2.7	2.9	2.9	2.7
Distillates	177	343	14.1	15.5	16.7	16.9	17.3
Gas oil	343	524	22.6	25.4	26.1	26.1	26.6
Vacuum residue	524	+	61.2	56.4	54.3	54.1	53.3

Table 5-6. Mass percentages of the different boiling point fractions for HO# 12 and the liquid products from its reactions at 400°C and different residence times

Fraction	IBP (°C)	FBP (°C)	Mass percentages, wt%				
			Feed	Liquid Products from reactions at 400°C			
				30 min	40 min	50 min	60 min
Naphtha	-	177	0.0	0.1	0.8	0.9	1.4
Distillates	177	343	12.5	12.7	13.5	14.5	15.8
Gas oil	343	524	26.2	26.4	26.6	28.1	30.6
Vacuum residue	524	+	61.3	60.7	59.1	56.5	52.1

The viscosity measurements for the liquid products were also performed at three different temperatures: 15, 25 and 38°C. These experimental values were compared to the predicted viscosities obtained from the recombination of the individual properties calculated for each one of the pseudo-components. In the case of HO# 6, this methodology provided a fair adjustment to the experimental measurements, but it did not work well for the case of HO# 12, as shown in Figure 5-10 and Figure 5-11.

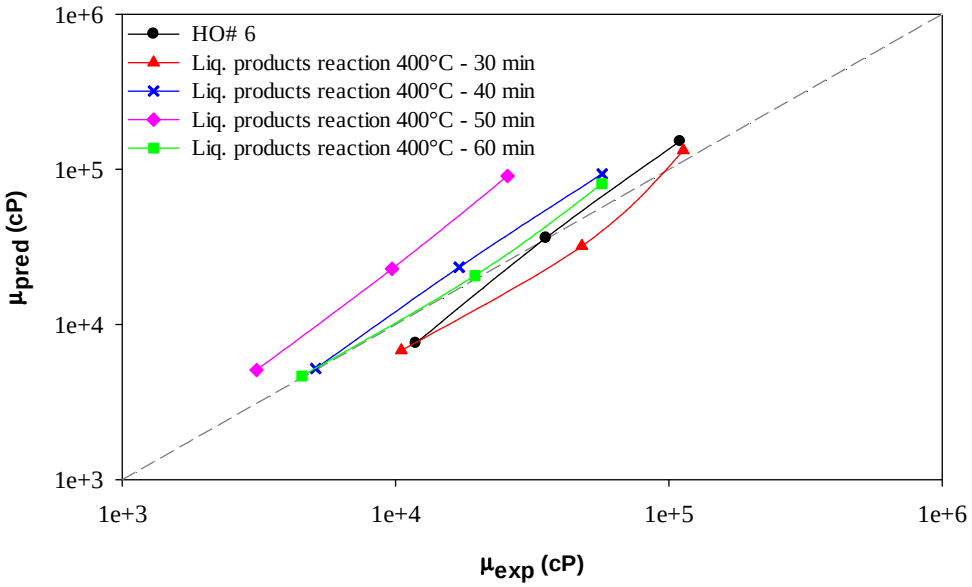

Figure 5-10. Parity plot of the experimental and predicted viscosities for HO# 6 and the liquid products from its reactions at 400°C and different residence times

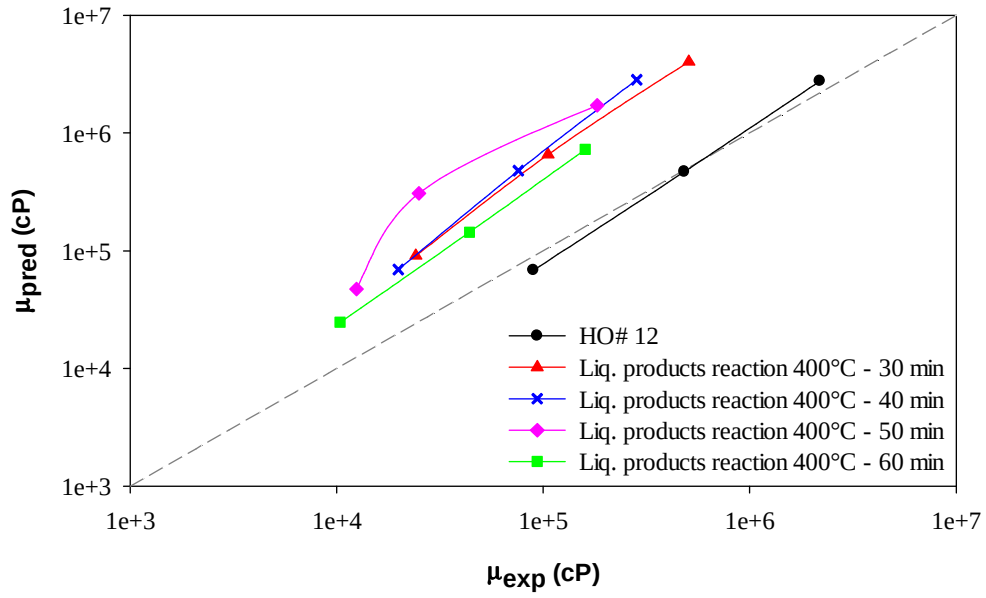

Figure 5-11. Parity plot of the experimental and predicted viscosities for HO# 12 and the liquid products from its reactions at 400°C and different residence times

The experimental measurements of the viscosities of the liquid sample obtained from the reaction of HO# 6 at 400°C and 50 minutes showed some inconsistencies. The viscosities should progressively decrease when the residence time of the reaction increases. However, as shown in Figure 5-10, this sample exhibited significantly lower viscosities when compared to the measured data for the other liquid products. Therefore, the fluid model could not provide a good prediction for this sample. Similar inconsistencies were observed for the viscosity measured at 25°C for the liquid products from the reaction of HO# 12 at 400°C and 50 minutes.

Throughout this study, the properties of the vacuum residue were used as tuning parameter to model the full heavy oil mixture. From the previous figures, we observed that the initial assumption about the invariable properties of each pseudo-component after the reactions did not provide a good estimation of the viscosities for the liquid products. Particularly for HO# 12, the predicted viscosities were considerably higher than the measured data. The most likely reason for such a breakdown in the model is changes in the viscosity of the vacuum residue due to reaction. Thus, the contribution of the vacuum residue in the calculation of the viscosities was modified with the linear expression presented in equation (5-30) to obtain a simple dependence of the viscosity on the conversion of the vacuum residue (X).

$$\mu'_{VR}=\mu_{VR}*(a+b*X) \qquad (5\text{-}30)$$

The viscosities for the liquid products were recalculated with the mixing rule given by equation (5-26), but the viscosity of the vacuum residue was replaced by the value obtained with equation (5-30). The parameters a and b were estimated to minimize the sum of errors obtained from the differences between the experimental and predicted viscosities. For HO# 6, the parameters a and b took the respective values of 1.00 and -0.23, and in this case the experimental viscosities for the liquid products from the reaction at 400°C and 50 minutes were not included because of their inconsistency. Likewise, in the case of HO# 12, the calculated values for a and b were 0.87 and -0.24, respectively, and the experimental viscosity at 25°C for the sample from the reaction at 400°C and 50 minutes was not accounted in the estimations.

The value of a = 0.87 for HO# 12 implies that the feed residue viscosity has been refitted to obtain a good agreement of the model with the viscosity measurements for the products. Thus, relying on repeatable viscosity measurements, a possible explanation for this observation is that the functionality of the vacuum residue viscosity for HO# 12 with conversion is not strictly linear.

The new predicted viscosities for HO# 6 and HO# 12 are presented in Figure 5-12 and Figure 5-13, respectively. These parity plots show a better adjustment of the estimated viscosities compared with the experimental measurements, which is more significant for the samples from HO# 12. This methodology correlated the data for the liquid products from the reactions of HO# 6 and HO# 12 with AAD of 21.7% and 21.2%, respectively.

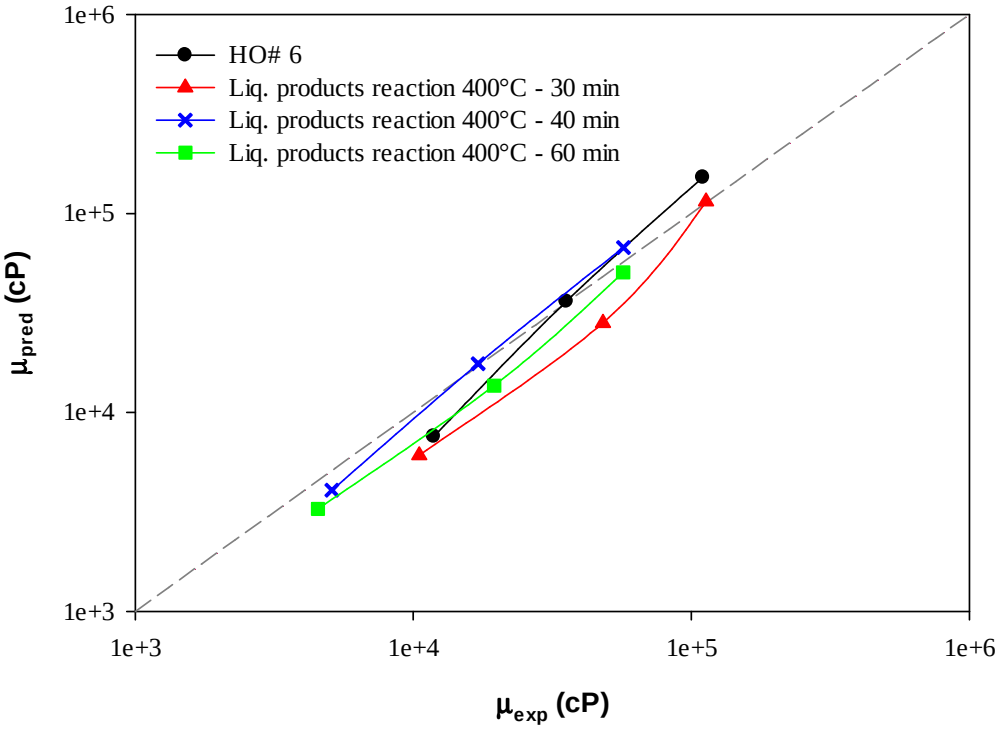

Figure 5-12. Parity plot of the experimental and predicted viscosities for HO# 6 and the liquid products from its reactions at 400°C and different residence times. Contribution of vacuum residue in the overall viscosity was modified by equation (5-30), with a = 1.00 and b = -0.23

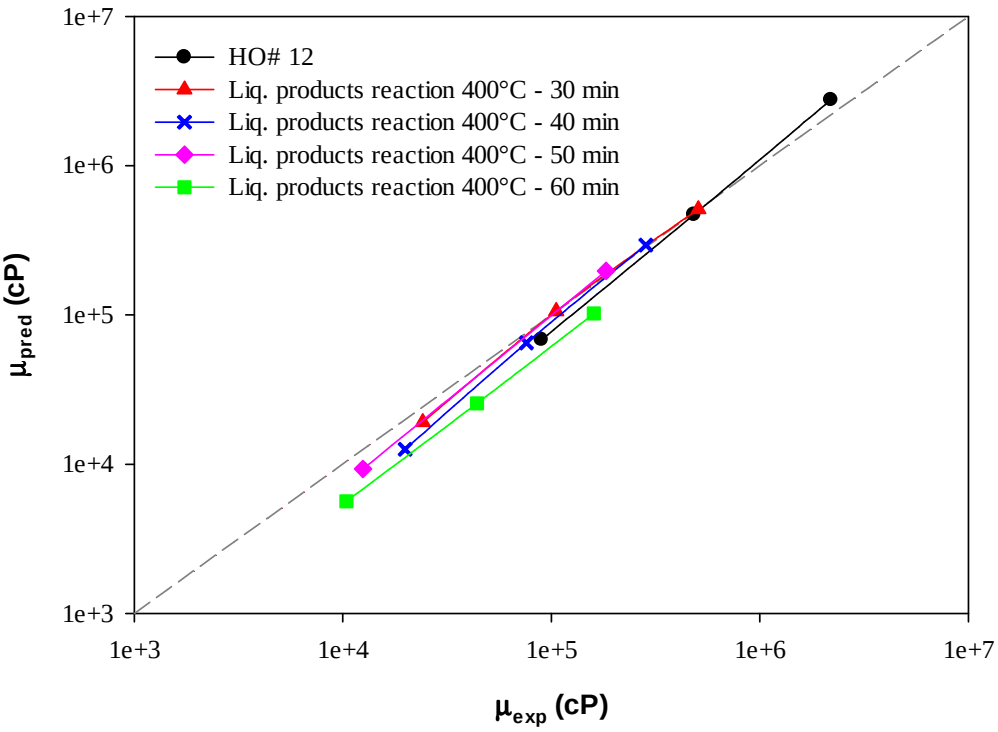

Figure 5-13. Parity plot of the experimental and predicted viscosities for HO# 12 and the liquid products from its reactions at 400°C and different residence times. Contribution of vacuum residue in the overall viscosity was modified by equation (5-30), with a = 0.87 and b = -0.24

The next step in the development of the model involved the fitting of the experimental data to a lumped kinetic model that could predict the concentrations for each one of the boiling fractions after the reaction. Thus, the viscosities of the liquid products from the reactions could be predicted from the characterization data of the feed, and the conditions of the reaction.

5.5.4 Kinetic model

The breakage of C-C bonds during thermal reactions seems to take place by free-radical mechanism,[17] and in spite of the complexity of the steps involved, they mainly exhibit an apparent overall first-order reaction order.

From the experimental data, the amounts of coke and gas produced from reactions with conversions of vacuum residue under 30% were negligible. Therefore, the lumped kinetic model could predict the yields of the different fractions in the liquid products, including naphtha, distillates, gas oil, and the remaining vacuum residue, which are of interest for the viscosity estimation, and the predictions of coke and gas could be omitted.

This lumped kinetic model assumed first order kinetics for the thermal cracking of the vacuum residue fraction. Additionally, due to the large number of molecules and the complexity of the petroleum feeds, the kinetic model has been developed on a mass basis, which is more convenient due to the uncertainties around the molecular weight of the fractions, which would be required to work on molar basis. Thus, the reaction rates were expressed in terms of the mass concentrations.

Different approaches were considered, including also the parallel cracking reaction of gas oil that exhibited some reactivity in the case of HO# 6. The kinetic parameters were estimated for the reactions made at 400°C, taking into account that the largest sets of experiments for HO# 6 and HO# 12 were made at this temperature. The experimental data from the reactions had been presented previously in Table 5-3, Table 5-5, and Table 5-6. Therefore, Table 5-7 presents

the summary of the experimental data available for the kinetic model, consisting of the overall concentrations for the boiling fractions, calculated as the product of the liquid yield and their respective concentration in the liquid products obtained from SimDist analysis.

Table 5-7. Concentrations on total mass basis of boiling fractions from the reactions of HO# 6 and HO# 12 at 400°C

Residence time (min)	**Overall mass concentration, wt%**			
	Naphtha	**Distillates**	**Gas Oil**	**Vacuum residue**
HO# 6				
15	2.6	14.5	24.2	58.7
30	2.7	15.5	25.4	56.4
40	2.9	16.5	25.7	53.5
50	2.8	16.6	25.6	53.2
60*	2.7	17.0	26.3	52.6
90	3.8	20.0	25.6	47.0
HO# 12				
30	0.6	12.0	26.0	59.7
40	0.9	13.2	26.2	58.2
50	0.9	14.2	27.7	55.7
60	1.4	15.4	30.2	51.3

* Yields for reaction of HO# 6 with residence time of 60 minutes were averaged from triplicate experiments

The parameters for the kinetic models were calculated by minimizing the sum of squared errors obtained by difference between the experimental overall

concentrations and the predicted values. Two main approaches were considered, the first one assumed that the vacuum residue was the only reactive fraction, and the second one allowed the gas oil to undergo parallel reactions to yield lighter factions.

In the first approach, the lumped kinetic model included the concept of stoichiometric coefficients introduced by Ayasse et al.[17]. Thus, the model had only one overall reaction rate, and the stoichiometric coefficients would represent the selectivities toward each one of the reaction products. This approach is illustrated in Figure 5-14.

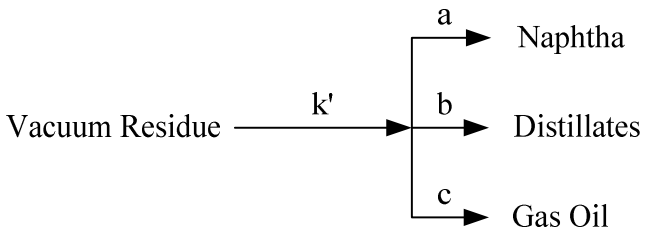

Figure 5-14. Representation of the kinetic model considered in the first approach

This reaction scheme is represented by the next set of differential equations:

$$\frac{d(VR)}{dt} = -k'*VR \quad (5\text{-}31)$$

$$\frac{d(Naphtha)}{dt} = a*k'*VR \quad (5\text{-}32)$$

$$\frac{d(Distillates)}{dt} = b*k'*VR \quad (5\text{-}33)$$

$$\frac{d(Gas\ Oil)}{dt} = c*k'*VR \quad (5\text{-}34)$$

Where:

$$a+b+c=1 \quad (5\text{-}35)$$

After integration:

$$VR=VR_0*e^{-k'*t} \quad (5\text{-}36)$$

$$Naphtha= Naphtha_0+a*VR_0*\left(1-e^{-k'*t}\right) \quad (5\text{-}37)$$

$$Distillates= Distillates_0+b*VR_0*\left(1-e^{-k'*t}\right) \quad (5\text{-}38)$$

$$Gas\ Oil= Gas\ Oil_0+c*VR_0*\left(1-e^{-k'*t}\right) \quad (5\text{-}39)$$

This approach was equivalent to the reaction scheme illustrated in Figure 5-15, which involves three independent rate constants for each one of the products from vacuum residue.

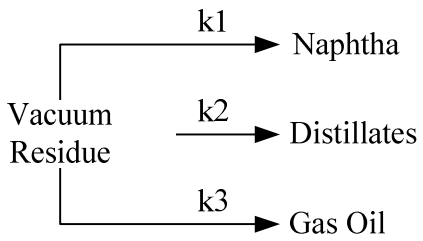

Figure 5-15. Alternative representation of the kinetic model considered in the first approach

This reaction system would be represented by the next differential equations:

$$\frac{d(VR)}{dt}=-(k_1+k_2+k_3)*VR \quad (5\text{-}40)$$

$$\frac{d(Naphtha)}{dt}=k_1*VR \quad (5\text{-}41)$$

$$\frac{d(Distillates)}{dt}=k_2*VR \quad (5\text{-}42)$$

$$\frac{d(Gas\ Oil)}{dt}=k_3*VR \quad (5\text{-}43)$$

After integration:

$$VR = VR_0 * e^{-k_{123}*t} \quad (5\text{-}44)$$

$$\text{Naphtha} = \text{Naphtha}_0 + \frac{k_1 * VR_0}{k_{123}} * \left(1 - e^{-k_{123}*t}\right) \quad (5\text{-}45)$$

$$\text{Distillates} = \text{Distillates}_0 + \frac{k_2 * VR_0}{k_{123}} * \left(1 - e^{-k_{123}*t}\right) \quad (5\text{-}46)$$

$$\text{Gas Oil} = \text{Gas Oil}_0 + \frac{k_3 * VR_0}{k_{123}} * \left(1 - e^{-k_{123}*t}\right) \quad (5\text{-}47)$$

Where:

$$k_{123} = k_1 + k_2 + k_3 \quad (5\text{-}48)$$

The sum of squared residuals (SSR) was calculated with the equation (5-49), where the index i represents the four boiling fractions, and j the number of reactions made with each heavy oil.

$$SSR = \sum_{j=1}^{n} \sum_{i=1}^{4} \left(\left(\text{Mass faction}_{i,j}\right)_{exp} - \left(\text{Mass fraction}_{i,j}\right)_{pred} \right)^2 \quad (5\text{-}49)$$

The values of the parameters obtained by minimization of the sum of squared residuals are summarized in Table 5-8. These parameters provided SSR values of 0.0018 for HO# 6 and 0.0029 for HO# 12. It can be observed that the lumped kinetic parameter k_{123} is equivalent to the rate constant k. Likewise, the ratio of the individual rate constants k_1, k_2, and k_3 show the same selectivities than the stoichiometric coefficients a, b, and c. Thus, the predicted mass concentrations with both sets of equations are the same, and are presented in Figure 5-16 and Figure 5-17.

Table 5-8. Values of parameters for the first kinetic model approach

Parameter	HO# 6	HO# 12	Parameter	HO# 6	HO# 12
k' (h^{-1})	0.156	0.117	**k_1 (h^{-1})**	0.023	0.030
a	0.15	0.26	**k_2 (h^{-1})**	0.066	0.041
b	0.42	0.35	**k_3 (h^{-1})**	0.067	0.046
c	0.43	0.39	**k_{123} (h^{-1})**	0.156	0.117

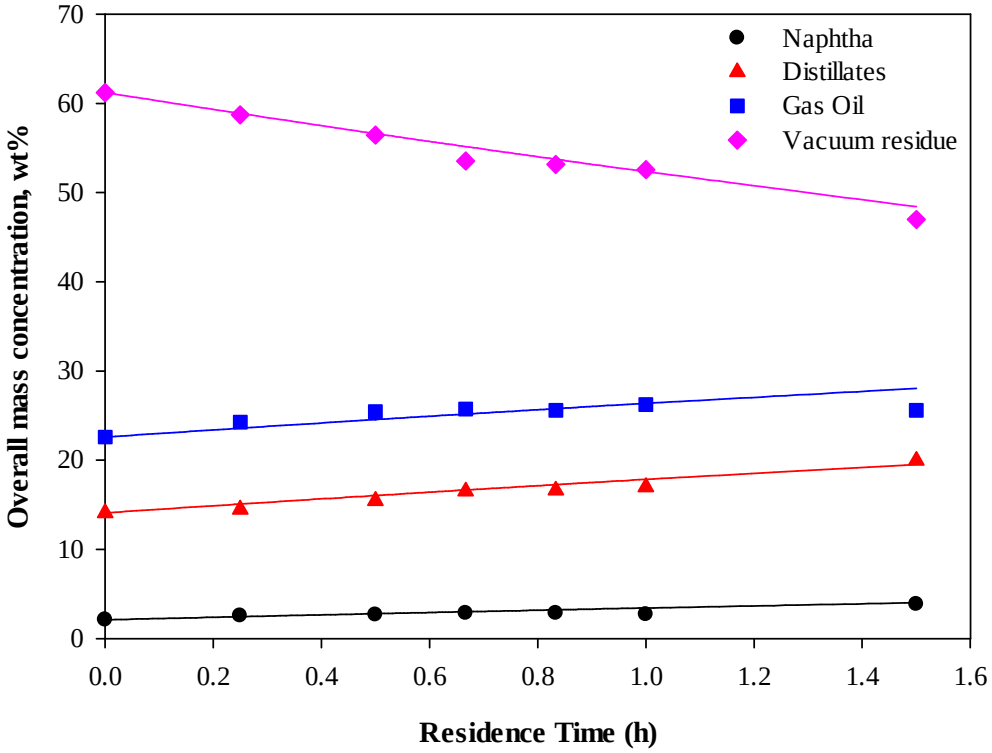

Figure 5-16. First kinetic model approach: experimental and predicted overall mass concentrations of the boiling fractions after the reaction of HO# 6 at 400°C and different residence times. The experimental data points are represented by the markers and the predictions by the continuous lines.

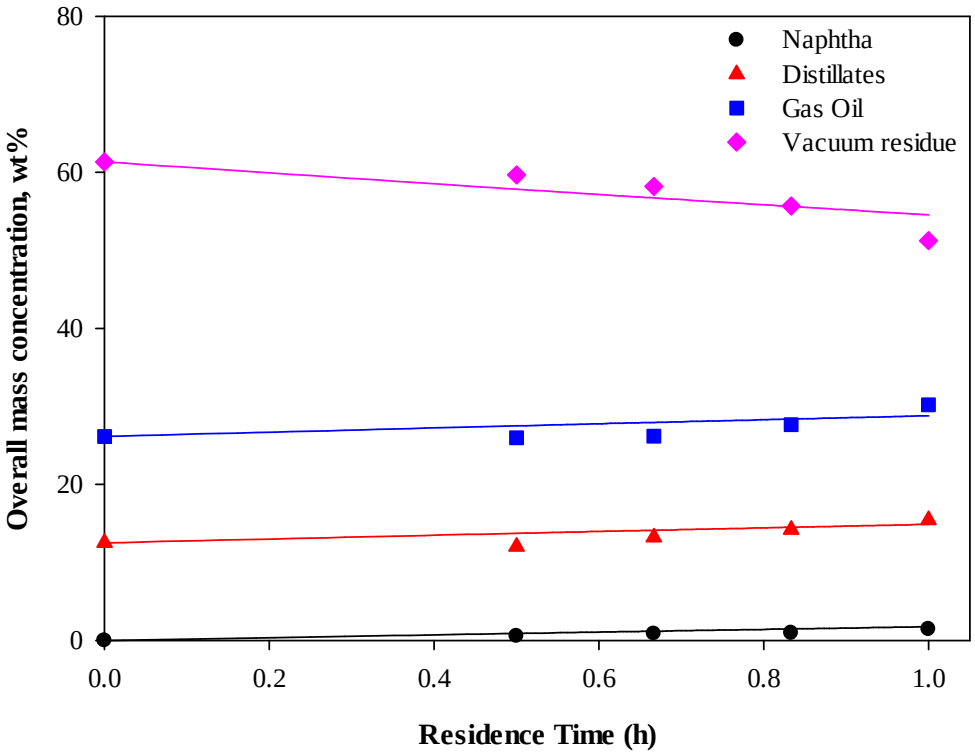

Figure 5-17. First kinetic model approach: experimental and predicted overall mass concentrations of the boiling fractions after the reaction of HO# 12 at 400°C and different residence times. The experimental data points are represented by the markers and the predictions by the continuous lines.

In the case of HO# 6, it was observed that at longer residence times the amount of gas oil decreased. Thus, in Figure 5-16, the predicted concentration of gas oil after 90 minutes of reaction is higher than the experimental value. This suggested some reactivity of the gas oil fraction that had not been considered in the first approach. Therefore, the second approach allowed cracking of the gas oil to yield naphtha and distillates, as illustrated in Figure 5-18.

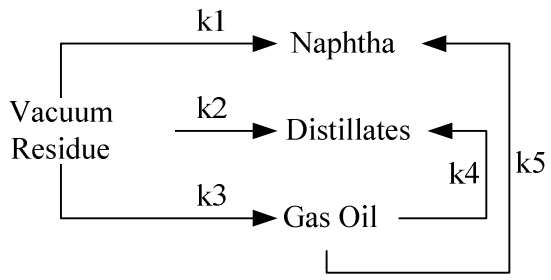

Figure 5-18. Representation of the kinetic model in the second approach

This reaction scheme is represented by the next set of differential equations:

$$\frac{d(VR)}{dt} = -(k_1+k_2+k_3)*VR \quad (5\text{-}50)$$

$$\frac{d(\text{Gas Oil})}{dt} = k_3*VR-(k_4+k_5)*\text{Gas Oil} \quad (5\text{-}51)$$

$$\frac{d(\text{Naphtha})}{dt} = k_1*VR+k_5*\text{Gas Oil} \quad (5\text{-}52)$$

$$\frac{d(\text{Distillates})}{dt} = k_2*VR+k_4*\text{Gas Oil} \quad (5\text{-}53)$$

After the integration:

$$VR = VR_0*e^{-k_{123}*t} \quad (5\text{-}54)$$

Where:

$$k_{123}=k_1+k_2+k_3 \quad (5\text{-}55)$$

Then,

$$\frac{d(\text{Gas Oil})}{dt} = k_3*VR_0*e^{-k_{123}*t}-k_{45}*\text{Gas Oil} \quad (5\text{-}56)$$

Where:

$$k_{45}=k_4+k_5 \quad (5\text{-}57)$$

Thus, rearranging this equation:

$$d(\text{Gas Oil})+k_{45}*\text{Gas Oil}*dt-k_3*VR_0*e^{-k_{123}*t}*dt=0 \quad (5\text{-}58)$$

This first order differential equation with variable coefficients was solved analytically, obtaining the next expression for the concentration of Gas Oil:

$$\text{Gas Oil}=\frac{k_3*VR_0}{k_{45}-k_{123}}\left[e^{-k_{123}*t}-e^{-k_{45}*t}\right]+\text{Gas Oil}_0*e^{-k_{45}*t} \tag{5-59}$$

Likewise, the expressions for the concentrations of naphtha and distillates were obtained:

$$\text{Naphtha}=\text{Naphtha}_0+\frac{k_1*VR_0}{k_{123}}\left[1-e^{-k_{123}*t}\right] + \frac{k_5*k_3*VR_0}{k_{45}-k_{123}}\left[\frac{1-e^{-k_{123}*t}}{k_{123}}-\frac{1-e^{-k_{45}*t}}{k_{45}}\right]+\frac{k_5*\text{Gas Oil}_0*\left[1-e^{-k_{45}*t}\right]}{k_{45}} \tag{5-60}$$

$$\text{Distillates}=\text{Distillates}_0+\frac{k_2*VR_0}{k_{123}}\left[1-e^{-k_{123}*t}\right] + \frac{k_4*k_3*VR_0}{k_{45}-k_{123}}\left[\frac{1-e^{-k_{123}*t}}{k_{123}}-\frac{1-e^{-k_{45}*t}}{k_{45}}\right]+\frac{k_4*\text{Gas Oil}_0*\left[1-e^{-k_{45}*t}\right]}{k_{45}} \tag{5-61}$$

In a similar way, when the concept of the stoichiometric coefficients was used for this second approach, as illustrated in Figure 5-19, equivalent results were obtained.

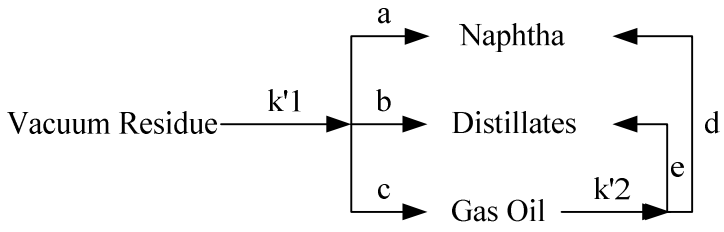

Figure 5-19. Alternative representation of the kinetic model considered in the second approach

The differential equations that represent this kinetic model are as follows:

$$\frac{d(VR)}{dt}=-k'_1*VR \tag{5-62}$$

$$\frac{d(\text{Gas Oil})}{dt} = c*k'_1*VR - k'_2*(\text{Gas Oil}) \quad (5\text{-}63)$$

$$\frac{d(\text{Naphtha})}{dt} = a*k'_1*VR + d*k'_2*(\text{Gas Oil}) \quad (5\text{-}64)$$

$$\frac{d(\text{Distillates})}{dt} = b*k'_1*VR + e*k'_2*(\text{Gas Oil}) \quad (5\text{-}65)$$

Where:

$$a+b+c=1 \quad (5\text{-}66)$$

$$d+e=1 \quad (5\text{-}67)$$

After integration:

$$VR = VR_0*e^{-k'_1*t} \quad (5\text{-}68)$$

Then,

$$\frac{d(\text{Gas Oil})}{dt} = c*k'_1*VR_0*e^{-k'_1*t} - k'_2*(\text{Gas Oil}) \quad (5\text{-}69)$$

Thus, rearranging this equation:

$$d(\text{Gas Oil}) + k'_2*(\text{Gas Oil})*dt - c*k'_1*VR_0*e^{-k'_1*t}*dt = 0 \quad (5\text{-}70)$$

The analytical solution of this first order differential equation with variable coefficients gave the next expression for the concentration of Gas Oil:

$$\text{Gas Oil} = \frac{c*k'_1*VR_0}{k'_2 - k'_1}\left[e^{-k'_1*t} - e^{-k'_2*t}\right] + \text{Gas Oil}_0*e^{-k'_2*t} \quad (5\text{-}71)$$

The concentrations for naphtha and distillates are given by the next equations:

$$\text{Naphtha} = \text{Naphtha}_0 + a*VR_0*\left[1-e^{-k'_1*t}\right] + \frac{c*d*VR_0}{k'_2 - k'_1}\left[k'_2*\left(1-e^{-k'_1*t}\right) - k'_1*\left(1-e^{-k'_2*t}\right)\right] + d*\text{Gas Oil}_0*\left[1-e^{-k'_2*t}\right] \quad (5\text{-}72)$$

$$\text{Distillates} = \text{Distillates}_0 + b*VR_0*\left[1-e^{-k'_1*t}\right] + \frac{c*e*VR_0}{k'_2 - k'_1}\left[k'_2*\left(1-e^{-k'_1*t}\right) - k'_1*\left(1-e^{-k'_2*t}\right)\right] + e*\text{Gas Oil}_0*\left[1-e^{-k'_2*t}\right] \quad (5\text{-}73)$$

With these equations, the parameters were estimated by minimizing SSR in equation (5-49). Table 5-9 summarizes the values for the rate constants in the second approach, and the estimated mass concentrations for the different fractions from the reaction of HO# 6 are compared to the experimental data in Figure 5-20.

Table 5-9. Values of parameters for the second kinetic model approach

Parameter	**HO# 6**	**HO# 12**	**Parameter**	**HO# 6**	**HO# 12**
k_1 (h^{-1})	0	0.030	**k'_1 (h^{-1})**	0.157	0.117
k_2 (h^{-1})	0	0.041	**k'_2 (h^{-1})**	0.204	0
k_3 (h^{-1})	0.157	0.046	**a**	0	0.26
k_4 (h^{-1})	0.151	0	**b**	0	0.35
k_5 (h^{-1})	0.053	0	**c**	1	0.39
k_{123} (h^{-1})	0.157	0.117	**d**	0.26	0.39
k_{45} (h^{-1})	0.204	0	**e**	0.74	0.61

For HO# 6, the estimated SSR decreased slightly compared with the first approach, and had a value of 0.0015. Parameters k_1 and k_2 that represent the reaction rate of vacuum residue towards naphtha and distillates, respectively, were set to zero by the SSR minimization process. The lumped rate constants k_{123} = 0.157 h^{-1} and k_{45} = 0.204 h^{-1} would suggest an apparent high reactivity of the gas oil fraction. Since it is known that naphtha and distillates can also be produced from vacuum residue, the restriction $k_1/k_2 = k_4/k_5$ was included in the model, and the parameters were calculated again, but the values for k_1 and k_2 were in the order of ~10^{-5}.

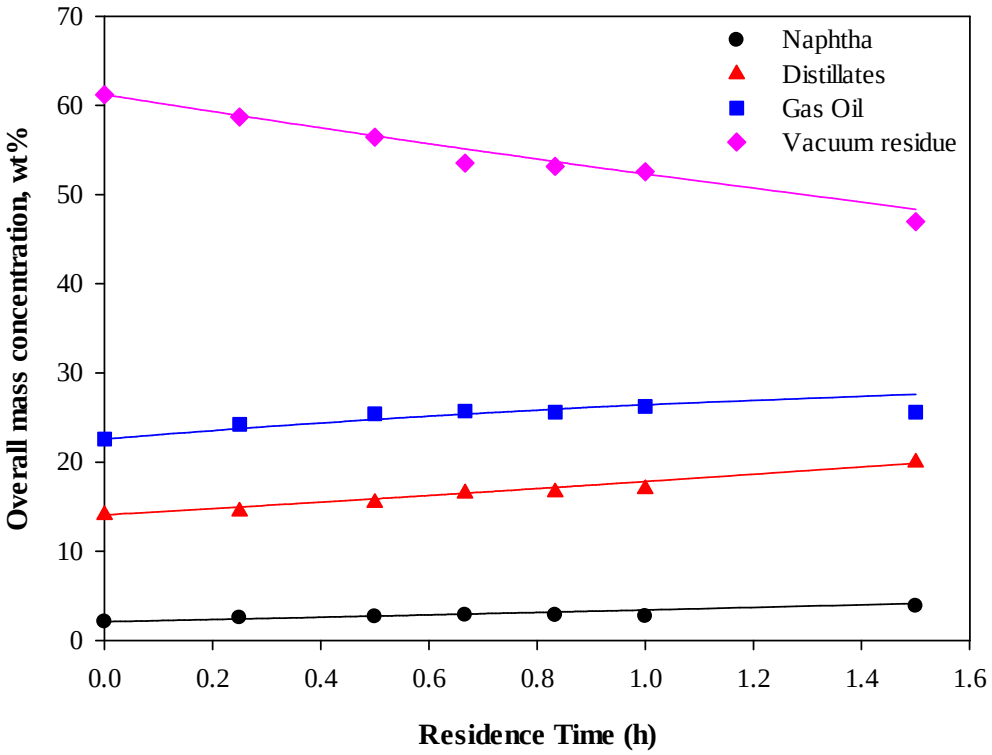

Figure 5-20. Second kinetic model approach: experimental and predicted overall mass concentrations of the boiling fractions after the reaction of HO# 6 at 400°C and different residence times. The experimental data points are represented by the markers and the predictions by the continuous lines.

The results for HO# 12 have not been plotted because the second approach provided exactly the same results than the first one. For this heavy oil, all the parameters that indicate the reactivity of the gas oil became zero after the iterative process for the minimization of SSR. These results suggested that for HO# 12 a good prediction could be obtained by neglecting the parallel reactions of gas oil, and assuming that the only reactive fraction was the vacuum residue.

In the equivalent model with stoichiometric coefficients, the values of k_1 and k_2 had the same values found for k_{123} and k_{45}, respectively. In the same way, for HO# 6, a and b were set to zero, suggesting that naphtha and distillates would be produced only from the cracking of gas oil as an intermediate. When restrictions were included in the model to force the values a and b to be different than zero, the error increased significantly, especially when the restriction $k_1 > k_2$ was used.

5.6 Discussion

These results showed that for HO# 6 a better fitting of the yields was obtained when the model was allowed to include cracking of the gas oil fraction, as previously presented in the second kinetic model approach. However, for HO# 12, the first approach provided a fair prediction of the final concentration of the boiling fractions after the reactions. When the predicted concentrations were replaced in the fluid model, the AAD was 27.7% for HO# 6, and 31.0% for HO# 12.

Some efforts can be still done in order to reduce the average absolute deviation (AAD) of the resulting predictions. The correlations available in literature, reported with low AAD, have been implemented in this study without any modification. However, the published correlations have been validated with other feeds, which would allow some adjustment of their parameters to ensure a better fitting for the own data.

As mentioned before, to meet the transportation specifications the crude oils must have a kinematic viscosity lower than 350 cSt at a given reference temperature. The kinetic and fluid model could be combined to predict the residence time of the reaction at 400°C, in order to reduce the viscosity to this point. Taking 38°C as the reference temperature, in the case of HO# 6 the target dynamic viscosity would be 337 cP, and the model estimated a residence time of 3.2 h, with a vacuum residue conversion of 39.5%. For HO# 12, the reaction residence time estimated by the model was 5.1 h, with 44.8% conversion of the vacuum residue fraction, in order to reduce the corresponding dynamic viscosity to 350 cP.

These estimations suggest that meeting the viscosity transportation requirements would demand long residence times that were not experimentally evaluated in this study. Under those conditions, significant amounts of coke would be formed, increasing the impact on the reduction of the viscosity of the liquid products. Therefore, we would expect that the target viscosity would be reached at shorter residence times than the predicted ones, due to the removal in the coke of some material that contributes to the high viscosity in the original crude. As an alternative to increasing the time, the visbreaking reaction could be performed at higher temperatures, but experimental data are required to include this variable in the kinetic model. Finally, the residence time could be selected to reach some intermediate viscosity, in such a way that less addition of diluent would be required to meet the transportation requirements.

5.7 Conclusions

1. A fluid model able to predict the viscosity of the liquid products from the visbreaking process of heavy oils has been developed. This model was based on the discretization of the feed into pseudo-components, whose concentrations after the reaction were obtained from a lumped kinetic model also developed with the available experimental data.
2. The feed was satisfactorily discretized into four pseudo-components, defined by their boiling point range as naphtha, distillates, gas oil and vacuum residue. For the development of the model we did not count with experimental data of the individual fractions; therefore, the properties of these pseudo-components were calculated with available validated correlations, and these individual values were introduced into a liquid mixing viscosity correlation to estimate the viscosity of the initial feed. This estimation was compared with the experimental data, and the fitting was improved by tuning the model with the mean boiling point of the vacuum residue fraction.
3. The attempt to keep constant the properties for the individual pseudo-components after the reaction worked well for HO# 6, but did not provide good agreement with the experimental data from HO# 12. This observation suggested some significant impact of the reactions on the chemical composition of the boiling fractions. Thus, the adjustment of the viscosity of the vacuum residue, taking into account the conversion of this fraction,

resulted in a better fitting of the viscosity predictions for the liquid products from the reactions.

4. The lumped kinetic models also differed for HO#6 and HO# 12. The gas oil fraction in HO# 6 exhibited a high reactivity, resulting in improved predictions when this fraction was allowed to undergo parallel reactions to yield the lighter fractions. In contrast, the experimental data from the reactions of HO# 12 adjusted a model scheme where the vacuum residue was the only reactive fraction. Both lumped kinetic models provided very good estimations of the resulting concentrations of the boiling fractions after the reactions.
5. The results obtained with the developed model showed that the viscosity reduction for heavy oils to meet pipeline specifications without addition of diluents would be a challenging operation. Reactors would need to work at severe conditions in order to obtain viscosity levels low enough to make the heavy oils pipelineable.

5.8 References

1. Di Carlo, S.; Janis, B. Composition and visbreakability of petroleum residues. *Chemical Engineering Science* **1992**, *47*, 2695-2700.
2. Joshi, J. B.; Pandit, A. B.; Kataria, K. L.; Kulkarni, R. P.; Sawarkar, A. N.; Tandon, D.; Ram, Y.; Kumar, M. M. Petroleum residue upgradation via visbreaking: A review. *Industrial and Engineering Chemistry Research* **2008**, *47*, 8960-8988.

3. Stratiev, D.; Kirilov, K.; Belchev, Z.; Petkov, P. How do feedstocks affect visbreaker operations? *Hydrocarbon Processing* **2008**, *87*, 105.
4. Wiehe, I. A. *Process chemistry of petroleum macromolecules;* CRC Press: Boca Raton, FL, 2008; pp 427.
5. Luhning, R. W.; Anand, A.; Blackmore, T.; Lawson, D. S. *In Pipeline Transportation of Emerging Partially Upgraded Bitumen;* Canadian International Petroleum Conference; Petroleum Society of Canada: Calgary, Alberta, 2002.
6. Chakma, A.; Islam, M. R. Modelling of visbreaking of bitumen in a jet reactor. *Chemical Engineering Science* **1990**, *45*, 2769-2775.
7. Layrisse R., I. A.; Polanco, D. R.; Rivas, H.; Jimenez G., E.; Quintero, L.; Salazar P., J.; Rivero, M.; Cardenas, A.; Chirinos, M. L.; Rojas, D.; Marquez, H. US Patent 4795478, 1989.
8. Dente, M.; Bozzano, G.; Bussani, G. The visbreaking process simulation: Products amount and their properties prediction. *Computers & Chemical Engineering* **1995**, *19*, S205-S210.
9. Dente, M.; Bozzano, G.; Bussani, G. A comprehensive program for visbreaking simulation: product amounts and their properties prediction. *Computers & Chemical Engineering* **1997**, *21*, 1125-1134.
10. Bozzano, G.; Dente, M.; Carlucci, F. The effect of naphthenic components in the visbreaking modeling. *Computers & Chemical Engineering* **2005**, *29*, 1439-1446.

11. Kataria, K. L.; Kulkarni, R. P.; Pandit, A. B.; Joshi, J. B.; Kumar, M. Kinetic Studies of Low Severity Visbreaking. *Ind. Eng. Chem. Res.* **2004**, *43*, 1373-1387.

12. Shu, W. R.; Venkatesan, V. N. Kinetics of thermal visbreaking of a Cold Lake bitumen. *Journal of Canadian Petroleum Technology* **1984**, *23*, 60-64.

13. Singh, V. D. Visbreaking Technology. *Erdoel und Kohle, Erdgas, Petrochemie vereinigt mit Brennstoff-Chemie* **1986**, *39*, 19-23.

14. Castellanos, J.; Cano, J. L.; Del-Rosal, R.; Briones, V. M.; Mancilla, R. L. Kinetic Model predicts visbreaker yields. *Oil & Gas Journal* **1991**, *89*, 76-82.

15. Xiao, J. Z.; Wang, L. J.; Chen, Q. L.; Wang, D. M. Modeling for product distribution in thermal conversion of heavy oil. *Petroleum Science and Technology* **2002**, *20*, 605-612.

16. Singh, J.; Kumar, M. M.; Saxena, A. K.; Kumar, S. Reaction pathways and product yields in mild thermal cracking of vacuum residues: A multi-lump kinetic model. *Chemical Engineering Journal* **2005**, *108*, 239-248.

17. Ayasse, A. R.; Nagaishi, H.; Chan, E. W.; Gray, M. R. Lumped kinetics of hydrocracking of bitumen. *Fuel* **1997**, *76*, 1025-1033.

18. Mehrotra, A. K. Generalized one-parameter viscosity equation for light and medium liquid hydrocarbons. *Industrial and Engineering Chemistry Research* **1991**, *30*, 1367-1372.

19. Mehrotra, A. K. Generalized viscosity equation for pure heavy hydrocarbons. *Industrial and Engineering Chemistry Research* **1991**, *30*, 420-427.

20. Mehrotra, A. K. Correlation and prediction of the viscosity of pure hydrocarbons. *Canadian Journal of Chemical Engineering* **1994**, *72*, 554-557.

21. Twu, C. H. Internally consistent correlation for predicting liquid viscosities of petroleum fractions. *Industrial & Engineering Chemistry, Process Design and Development* **1985**, *24*, 1287-1293.

22. Twu, C. H. Generalized method for predicting viscosities of petroleum fractions. *AICHE Journal* **1986**, *32*, 2091-2094.

23. Beg, S. A.; Amin, M. B.; Hussain, I. Generalized kinematic viscosity-temperature correlation for undefined petroleum fractions. *The Chemical Engineering Journal* **1988**, *38*, 123-136.

24. Mehrotra, A. K. Simple equation for predicting the viscosity of crude oil fractions. *Chemical Engineering Research and Design* **1995**, *73*, 87-90.

25. Svrcek, W. Y.; Mehrotra, A. K. One parameter correlation for bitumen viscosity. *Chemical Engineering Research and Design* **1988**, *66*, 323-327.

26. Mehrotra, A. K.; Eastick, R. R.; Svrcek, W. Y. Viscosity of Cold Lake bitumen and its fractions. *Canadian Journal of Chemical Engineering* **1989**, *67*, 1004-1009.

27. Eastick, R. R.; Mehrotra, A. K. Viscosity data and correlation for mixtures of bitumen fractions. *Fuel Process Technology* **1990**, *26*, 25-37.

28. Mehrotra, A. K. A generalized viscosity equation for liquid hydrocarbons: Application to oil-sand bitumens. *Fluid Phase Equilibria* **1992**, *75*, 257-268.

29. Mehrotra, A. K. Modeling the effects of temperature, pressure, and composition on the viscosity of crude oil mixtures. *Industrial and Engineering Chemistry Research* **1990**, *29*, 1574-1578.

30. Monnery, W. D.; Svrcek, W. Y.; Mehrotra, A. K. Viscosity: a critical review of practical predictive and correlative methods. *Canadian Journal of Chemical Engineering* **1995**, *73*, 3-40.

31. Mehrotra, A. K.; Monnery, W. D.; Svrcek, W. Y. Review of practical calculation methods for the viscosity of liquid hydrocarbons and their mixtures. *Fluid Phase Equilibria* **1996**, *117*, 344-355.

32. Ely, J. F.; Hanley, H. J. M. Prediction of transport properties. 1. Viscosity of fluids and mixtures. *Industrial & Engineering Chemistry Fundamentals* **1981**, *20*, 323-332.

33. Chung, T. H.; Lee, L. L.; Starling, K. E. Applications of kinetic gas theories and multiparameter correlation for prediction of dilute gas viscosity and thermal-conductivity. *Industrial & Engineering Chemistry Fundamentals* **1984**, *23*, 8-13.

34. Andrade, E. N. D. A theory of the viscosity of liquids - Part I. *Philosophical Magazine* **1934**, *17*, 497-511.

35. Vogel, H. The temperature dependence law of the viscosity of fluids. *Physikalische Zeitschrift* **1921**, *22*, 645-646.

36. American Society for Testing and Materials. *Annual book of ASTM standards.* ASTM: Philadelphia, PA, 1981.

37. Walther, C. The evaluation of viscosity data. *Erdöl und Teer* **1931**, *7*, 382-4.

38. Aspen Technology Inc. *Aspen Physical Property System. Physical Property Models. V7.2;* Burlington, MA, 2010.

39. Wauquier, J.; Trambouze, P.; Favennec, J. In *Petroleum refining, Vol. 1 Crude Oil, Petroleum Products, Process Flowsheets;* Éditions Technip: Paris, 1995.

40. Riazi, M. R. *Characterization and properties of petroleum fractions;* ASTM International: West Conshohocken, PA, 2005.

41. Speight, J. G.; Özüm, B. *Petroleum refining processes;* Marcel Dekker: New York, 2002.

42. American Petroleum Institute - Refining Department. *Technical data book : petroleum refining;* American Petroleum Institute: Washington, D.C, 1983.

6 Synthesis

The work presented in this thesis includes the study of two research topics that involve some challenging issues in the oil industry: the molecular structure of asphaltenes and the viscosity reduction of heavy oils.

The study of asphaltenes was covered in Chapters 2, 3, and 4, and presented important results concerning not only the composition, but also the architecture of asphaltene molecules. Chapter 2 described the cracking reactions under hydrogenation conditions that allowed asphaltenes to yield high amounts of analyzable material, with low production of coke, and also with minimal change of the ring structures. The analysis of the distillable fraction of the liquid products reported the identification and quantification of diverse homologous series of molecular species, including paraffins and naphthenic, aromatic, and heteroatomic compounds with 1 to 4 rings. Consequently, this study verified the important presence of bridged-structures in asphaltenes, because it is not feasible that these distillable molecules, or small building blocks, can be present separately in the original asphaltenes at such high concentrations.

These results reported the compositions of 50 to 60 wt% of asphaltenes from different sources around the world, and represent the largest fraction of characterized material that has been reported so far. However, there is still 35 to 45 wt% of the asphaltenes whose molecular structure is unknown because it remained in the vacuum residue fraction or ended up as coke, and therefore could not be characterized. The reaction approach that was used in this study led to suggestion that this heavy material would be constituted by the initial large

polycyclic (aromatic and naphthenoaromatic) structures present in asphaltenes, and also by products formed from condensation reactions.

The methodology used in this experimental work, consisting of cracking the asphaltenes and recovery of the products for analysis, could provide information about the molecular structures of their building blocks, but not about the architecture of how they are linked together. Thus, Chapter 4 was intended to evaluate two possible topological arrangements of these building blocks, by construction and cracking of asphaltene populations by a Monte Carlo approach. This simulation method used as inputs the probability density functions (PDFs) derived from the available experimental data from Chapter 2, and compared the distributions of the cracking products with the experimental boiling curve. The content of initial large building blocks was used as tuning parameter in the simulation since its value could not be determined experimentally.

Some simplifications were made in this simulation, regarding the description of the bridges, which were all considered equivalent in strength with no defined length, and the ignorance of reactions other than cracking. However, the reactions performed in Chapter 2 ensured minimal change of the building block ring structures as a result of hydrogenation and dehydrogenation reactions. Therefore, the main simplification in terms of the reactions that asphaltenes could undergo would be due to the absence of cyclization and condensation reactions in the simulation.

In this simulation work, the high heterogeneity of asphaltenes was represented by the generation of the molecules with random selections of building

blocks. Thus, asphaltenes were made up of small and large building blocks linked in linear or dendritic architectures. Chapter 4 provided some examples of possible representations of these molecules, and also presented distributions of the number of building blocks. These distributions showed that an important fraction of asphaltene molecules would have between 3 to 5 building blocks, and a minor amount would have only one building block (< 1.5 wt%). Thus, large building blocks could be linked to other building blocks, but could also, by themselves, be considered asphaltene molecules. This observation would suggest that "island" type of molecules could also be present in asphaltenes. For instance, some studies have suggested that porphyrins could be present in asphaltenes as a result of coprecipitation rather than chemical bonding.[1, 2] However, the experimental data obtained in the present study cannot confirm the occurrence of these structures because the high-boiling point material could not be characterized.

The results from the simulation did not indicate substantial differences between the distributions of products from the cracking of linear and dendritic asphaltenes, but suggested that dendritic molecules would exhibit lower reactivity. Additionally, better fitting with the experimental data was obtained with low contents of large building blocks. However, these results cannot be used for the estimation of the initial amount of large polycyclic structures in asphaltenes because of the simplifications and assumptions that were mentioned previously.

Chapter 3 provided some complementary experimental results. The evaluation of different solvents showed that hydrogen-donor compounds can significantly suppress the coke formation during cracking of asphaltenes under the

hydrogenation conditions described in Chapter 2. Three-ring hydrogen-donor solvents led to the lowest coke yields. However, the reactions in presence of tetralin also exhibited low coke yields, and confirmed it as a good hydrogen-donor solvent for the study of asphaltene molecular structures.

These reactions carried out under similar conditions, but varying the solvent medium, led to significant differences in coke yields. Thus, these observations are consistent with complex molecules that comprise a wide range of structures (described in Chapter 2), which can undergo different reactions depending on the solvent characteristics of the liquid. If asphaltenes consisted only of large polycyclic structures with side chains, we could not expect such variations in coke yield, and most importantly, the low coke yields observed in presence of hydrogen-donor solvents may not be achieved.

In Chapter 5, the development of a fluid model for the estimation of the viscosity of liquid products from visbreaking of two heavy oils was presented. The high complexity of these heavy materials, as evidenced in the previous chapters, required an approach that could be congruent with measurable properties. Thus, based on the distillation curve and density of the heavy oils, the model created boiling point pseudo-components, and estimated their individual properties.

The two heavy oils evaluated in this work exhibited different kinetics. Therefore, the distributions of the pseudo-components after reactions at 400°C were obtained from kinetic models that were developed for each heavy oil. This allowed the estimation of the viscosities of the liquid products with a viscosity

mixing rule, and evidenced the viscosity reduction as a result of the increasing lighter fractions and decreasing concentration of the vacuum residue. A conversion-dependent factor was used to correct the viscosity of the vacuum residue, in order to account for some changes in its composition during the reactions. The viscosity predictions at three temperatures (15, 25 and 38°C) were compared to experimental data, and showed absolute average deviations (AAD) below 31%.

The residue fraction properties were not easy to estimate due to the uncertainty in basic properties, such as the average boiling point. This fraction is mainly constituted by asphaltenes, which have been recognized in all the previous chapters as highly complex and heterogeneous materials. Thus, it is not unexpected that the modeling of the vacuum residue properties can be challenging.

The approach used in this model consisted of using the properties of this fraction to tune the model with the available experimental data. It was evidenced in Chapters 2 and 3 that asphaltenes undergo significant chemical transformations upon processing. Consequently, the need to use a conversion dependent factor to correct the residue viscosity in the products from visbreaking is in agreement with these observations.

Similarly, the differences observed between the heavy oils evaluated in Chapter 5 could arise from dissimilarities in their molecular composition. On the basis of the results presented in this work, these differences can be understood as

variations in the distributions of the diverse molecular species identified in asphaltenes.

The results obtained in this work would suggest that these building blocks, present in asphaltenes, must also constitute the other oil fractions. However, it is expected that the distributions of these compounds should exhibit differences, which would determine the properties and reactivity of every fraction. Thus, as illustrated in Figure 6-1, maltenes would be richer in low-molecular weight building blocks, while asphaltenes would comprise a wider range of structures, with low and high molecular weights, which can give rise to a much more heterogeneous and complex material.

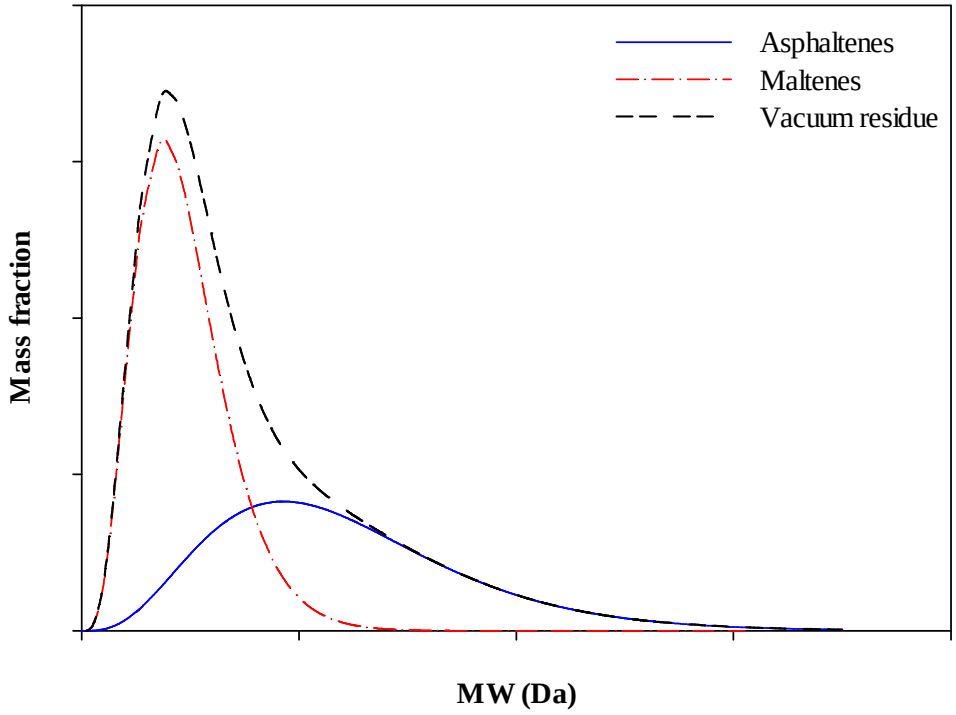

Figure 6-1. Hypothetical molecular weight distributions for the asphaltenes, resins, and the whole vacuum residue

The molecular weight distributions presented by Qian et al.,[3] obtained by FD-MS analysis, suggested that maltenes would have the same range of molecular weight than asphaltenes. However, based on the phase diagram proposed by Wiehe,[4] and the extended version presented by Gray,[5] such high molecular weight material would not be soluble in *n*-heptane, and therefore, would fall in the category of asphaltenes. Some studies have revealed possible generation of higher molecular weight species by FD-MS[3, 6, 7] which could explain the results observed with maltenes.

6.1 References

1. Beato, B. D.; Yost, R. A.; Van Berkel, G. J.; Filby, R. H.; Quirke, J. M. E. The Henryville bed of the New Albany shale—III: Tandem mass spectrometric analyses of geoporphyrins from the bitumen and kerogen. Organic Geochemistry 1991, 17, 93-105.
2. Dechaine, G. P.; Gray, M. R. Chemistry and Association of Vanadium Compounds in Heavy Oil and Bitumen, and Implications for Their Selective Removal. *Energy & Fuels* **2010**, *24*, 2795-2808.
3. Qian, K.; Edwards, K. E.; Siskin, M.; Olmstead, W. N.; Mennito, A. S.; Dechert, G. J.; Hoosain, N. E. Desorption and ionization of heavy petroleum molecules and measurement of molecular weight distributions. *Energy & Fuels* **2007**, *21*, 1042-1047.
4. Wiehe, I. A. A solvent-resid phase diagram for tracking resid conversion. *Ind. Eng. Chem. Res.* **1992**, *31*, 530-536.

5. Gray, M. R. Consistency of Asphaltene Chemical Structures with Pyrolysis and Coking Behavior. *Energy & Fuels* **2003**, *17*, 1566-1569.

6. Schaub, T. M.; Hendrickson, C. L.; Qian, K. N.; Quinn, J. P.; Marshall, A. G. High-resolution field desorption/ionization Fourier transform ion cyclotron resonance mass analysis of nonpolar molecules. *Analytical Chemistry* **2003**, *75*, 2172-2176.

7. McKenna, A. M.; Blakney, G. T.; Xian, F.; Glaser, P. B.; Rodgers, R. P.; Marshall, A. G. Heavy Petroleum Composition. 2. Progression of the Boduszynski Model to the Limit of Distillation by Ultrahigh-Resolution FT-ICR Mass Spectrometry. *Energy & Fuels* **2010**, *24*, 2939-2946.

7 Conclusions and Recommendations

7.1 Molecular structures and architecture in asphaltenes

7.1.1 Summary of conclusions

Hydrogenation conditions that involved tetralin as hydrogen-donor solvent, an iron-based catalyst (iron sulphate supported on sub-bituminous coal), and hydrogen atmosphere at mild pressures provided favorable conditions to suppress coke formation and reach high yields of analyzable material from the cracking of asphaltenes. Reaction conditions of 450°C, residence time of 3 hours, tetralin/asphaltene ratio of 2.5/1, 2 wt% of catalyst, and hydrogen pressure of 4.1 MPa (measured at room temperature) led to significant yields of distillates, in the range of 50 to 60 wt%, and coke yields below 10 wt%. Control experiments with model compounds, at the same reaction conditions, demonstrated the preservation of the ring structures.

The products were quantitatively recovered from the cracking reactions performed under the hydrogenation conditions described above, and the distillable fraction was characterized. The identification of a large variety of molecules, including saturate, aromatic and heteroatomic species, confirmed an abundant presence of bridged structures in asphaltenes. Additionally, the origin of the asphaltene samples showed a low influence on the molecular composition. Therefore, these results provided clear evidence of the presence of archipelago-type structures in asphaltenes.

The sum of non-analyzed material, which included coke and material remaining in the vacuum residue fraction, was in the range of 35 to 45 wt%. This material set an upper bound for the amount of large clusters in the asphaltenes evaluated, and would be formed by polycyclic structures originally present in the asphaltenes, and also by products from condensation reactions. Consequently, the initial amount of polyaromatic and large naphthenoaromatic species in asphaltenes remained unknown.

Different aromatic solvents were evaluated in terms of coke suppression ability in the cracking of asphaltenes under hydrogenation conditions. The coke yields from asphaltenes presented the following order: 1-methylnaphthalene ~ pyridine > quinoline > toluene >> tetralin ~ 1,2,3,4-tetrahydroquinoline > 9,10-dihydrophenanthrene ~ 9,10-dihydroanthracene. The coke yield spanned the range from 4.6 to 25.0 wt% for Athabasca industrial *n*-C_5 asphaltenes. As expected, hydrogen-donor solvents demonstrated a better coke suppression ability, and the three-ring compounds led to the lowest coke yields. Moreover, the differences observed among the solvents without hydrogen-donation ability was explained as a result of their dissimilar capability to prevent the deposition of reacted asphaltenes as coke.

The Monte Carlo simulation of the cracking of asphaltene molecules, constructed with linear and dendritic topologies, did not show a significant impact of the molecular architecture on the distribution of products. However, the molecules with dendritic linkages between their building blocks exhibited less reactivity.

7.1.2 Recommendations

The experimental work done on the characterization of asphaltene molecular structures involved samples from six different geological basins, and they all exhibited similar composition. However, the existence of significantly different samples cannot be ruled out. The evaluation of asphaltenes from additional sources under the same methodology would be required for this purpose. For instance, the analysis of asphaltenes recovered after the cracking procedure presented in this work, or asphaltenes from hydroconverted vacuum residue, could exhibit less diversity of building blocks. Similarly, evaluation of deposits from production of light crude oils could evidence some compositional differences.

The use of tetralin as a hydrogen-donor solvent in the cracking reactions added some uncertainty in the quantification of two ring species. The data was corrected by subtracting tetralin and its products from the identified molecules. It could be useful to run the reactions under comparable conditions, but using a three-ring aromatic hydrogen-donor solvent, and compare the results obtained from the characterization analyses to crosscheck the abundance of these species.

Additional experiments with different shaking rates of the microreactor could be done to evaluate possible mass transfer limitations that could affect the reaction rates.

Further work on the Monte Carlo simulation could evaluate the presence of macrocycles as an additional type of architecture. However, taking into account that we are dealing with a complex mixture, populations with combined

topological configurations could also be constructed. Other additions to be considered are the specification of the length and strength of the bonds, and the probabilistic description of condensation reactions. This additional work could provide a closer description of the cracking reactions, and evaluate if these considerations would lead to significant variances for the different molecular architectures.

The approach used to obtain the distribution of large building blocks could be eventually improved by generation of a theoretical series of polycyclic structures whose distribution could match the experimental boiling point curve. This work would provide a consistent way to represent the building blocks in both the distillable and vacuum residue fractions, and likely give smoother distributions in the heavy section of the boiling curves after cracking.

7.2 Fluid model for visbreaking of heavy oils

7.2.1 Summary of conclusions

The estimation of viscosities of the liquid products from visbreaking reactions of heavy oils was approached by the development of a fluid model based on boiling point pseudo-components. i.e. naphtha, distillates, gas oil, and vacuum residue. The estimation of the properties for each pseudo-component, with validated correlations, provided a good fit with the experimental data of the unreacted heavy oils, using the mean boiling point of the vacuum residue as a tuning parameter. Similarly, the viscosity of the vacuum residue was corrected with a factor dependent on conversion, which accounted for chemical changes

during the reaction. The distributions of pseudo-components after the reactions were obtained from the kinetic models developed for each heavy oil, which exhibited different reactivity. Thus, the viscosities of the liquid products from visbreaking reactions at 400°C were predicted with absolute average deviations (AAD) below 31%.

7.2.2 Recommendations

The parameters in the empirical correlation for viscosity, proposed by Mehrotra[1], could be tuned with current experimental data to achieve a better fit. Furthermore, the preliminary results revealed the need to consider higher conversions. Thus, experiments at higher reaction temperatures and longer residence times are recommended to produce a model that can be valid in a broader range of conditions.

7.3 References

1. Mehrotra, A. K. Simple equation for predicting the viscosity of crude oil fractions. Chemical Engineering Research and Design 1995, 73, 87-90.

Appendix 1: Heat-up curves

The heat-up curves were obtained by modifying the bottom part of the microreactor to introduce a thermocouple connected to the port of a computing system that allowed recording the temperature every four seconds. The bottom cap was replaced with a bored-through reducing union, ¾ in. x ¼ in., attached to a bored-through reducer, 1/16 in. x ¼ in. The Type K thermocouple (OMEGA KMQXL-062G-18, Cr/Ni alloy, grounded junction, and length of 18 in.) was installed by assembling on the sheath a 1/16 in. ferrule set (front ferrule/ back ferrule) with a 1/16 in. nut, ensuring that the tip of the thermocouple reached the middle part of the main body of the microreactor.

The modified microreactor was loaded with 3 grams of tetralin, and pressurized with hydrogen at 4.1 MPa at ambient temperature after the leak test. The temperature was recorded from before the microreactor was plunged into the preheated sand bath. After 60 minutes, the microreactor was taken out of the sand bath and let cool down by natural convection at room temperature without quenching. Three different temperatures were set up in the PID controller of the sand bath: 430, 450 and 480°C, as shown in Figure A1- 1.

In the test with the set point of 430°C, the system reached an average steady state temperature of 414.4°C in approximately 5 minutes after the microreactor was immersed into the sand bath, and it took 3.2 minutes to cool down to 350°C. At temperatures below 350°C the cracking reactions do not take place at significant rates. For the test with the set point of 450°C, the microreactor reached the average steady state temperature of 433.9°C in approximately 7

minutes, and it cooled down from this temperature to 350°C in 3.9 minutes. In the test with the set point of 480°C, the average steady state temperature was 462.9°C, and it was obtained in approximately 9 minutes. The system cooled down from this temperature to 350°C in 4.4 minutes.

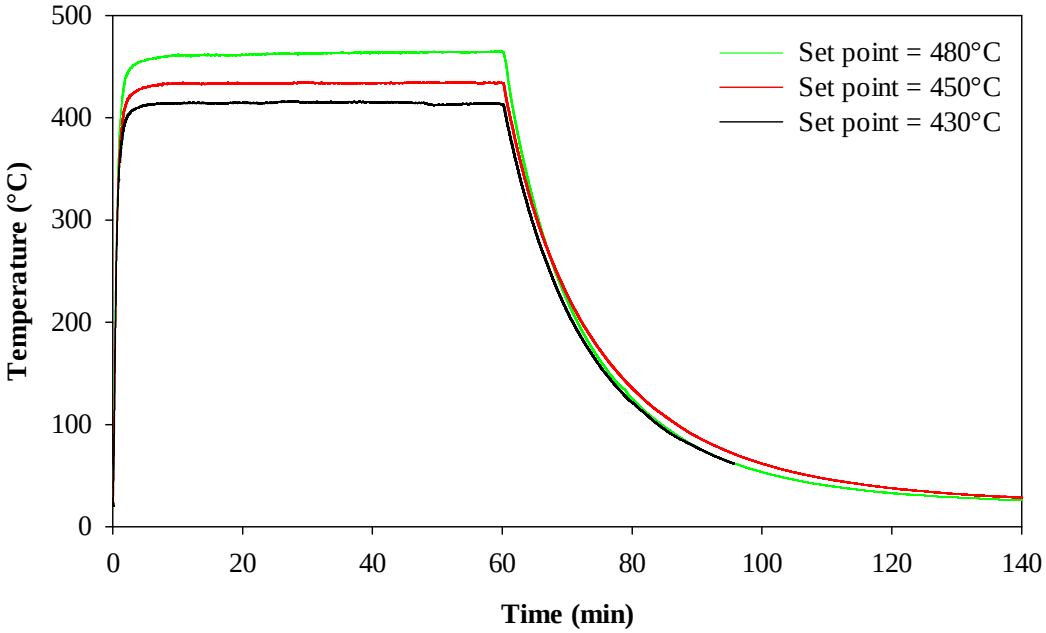

Figure A1- 1. Heat-up curves for three different temperature set points

A similar test was made with a set point of 400°C, but pressurizing the microreactor at 0.69 MPa with nitrogen at room temperature. In this particular case the microreactor was quenched in cold water in order to get the temperature profile for the reactions made with heavy oils in the viscosity study. The temperature profile is presented in Figure A1- 2.

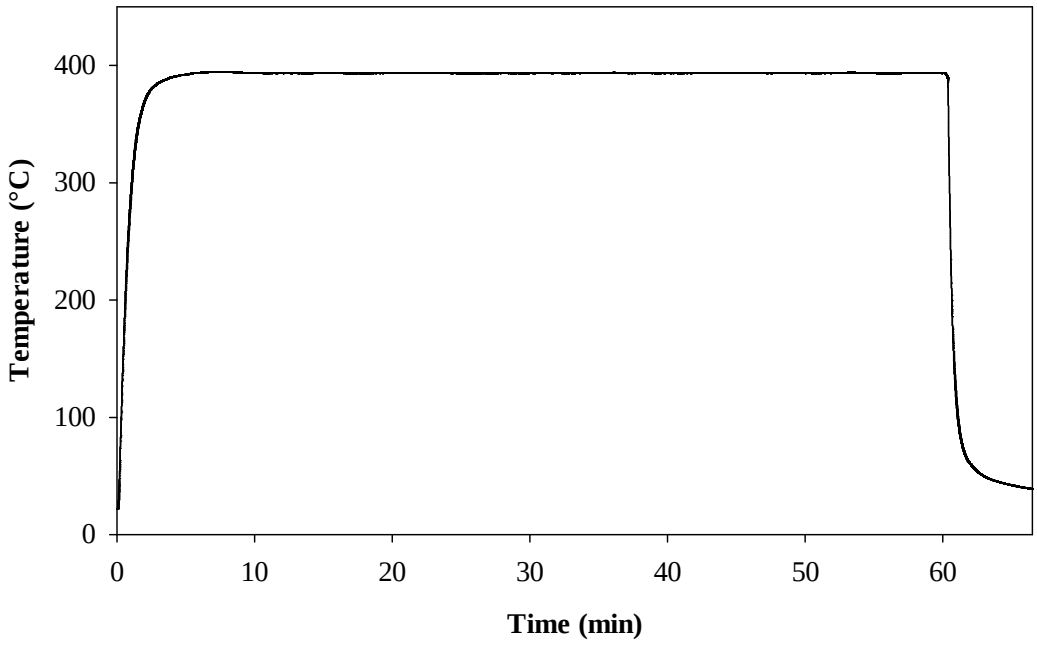

Figure A1- 2. Heat-up curve for test made with set point of 400°C and quenching the reactor in cold water

In this case, the microreactor reached an average steady state temperature of 393.5°C in 5.0 min. By immersion in cold water, the microreactor was quenched from this average temperature to 350°C in 16 seconds and approximately one minute later the temperature was below 100°C.

These different tests did not account for the heat of reaction; however, its effect on the temperature profiles should be negligible compared to the effect of heating up the microreactor which has a mass of approximately 250 grams.

Appendix 2: NMR analyses

In the first study, aromatic carbon balances could have provided a quantitative estimation of the hydrogenation degree obtained during the reactions, but NMR analyses of the liquid products and of the coke were hampered by the presence of tetralin, and catalyst, respectively. An indirect measure of hydrogen uptake, by GC-FID analysis of the light fraction obtained by distillation of the liquid products, showed that approximate amounts of 16-18 mg H/g asphaltenes were transferred from tetralin to the cracked asphaltene fragments.

Aromaticity of the total liquid products containing tetralin could not be evaluated experimentally because a high error would be introduced if the solvent was subtracted from the results. NMR analyses of the heavy fraction of the liquid products (> 343°C), obtained by distillation in the Micro Distillation System Model 800 from B/R Instrument Corporation, were performed in ExxonMobil Research and Engineering Co. These results showed aromaticity values of 63.5% for Athabasca industrial *n*-C_5 asphaltenes, and 69.2% for Cold Lake *n*-C_7 asphaltenes. These values are relatively higher than the aromaticities of 50% and 46%, reported by Karimi et al.[1] for the raw Athabasca and Cold Lake *n*-C_7 asphaltenes, respectively.

Coke samples from different reactions of Athabasca industrial *n*-C_5 asphaltenes were collected to provide enough sample for solid state ^{13}C NMR analysis that was performed in the Department of Chemistry at the University of Alberta. Spectrum data was collected with a recycle delay of 60 s and is shown in

Figure A2- 1. The catalyst, recovered with the coke sample during the filtration, had a paramagnetic behavior that affected the resolution of the spectrum. The main peak that would correspond to the aromatic and unsaturated carbons is very broad, and the peak observed around 0 ppm could not be attributed to aliphatic carbons that usually have chemical shifts in the range of 0 to 50 ppm. This last peak could be more likely considered as a side spinning band (ssb).

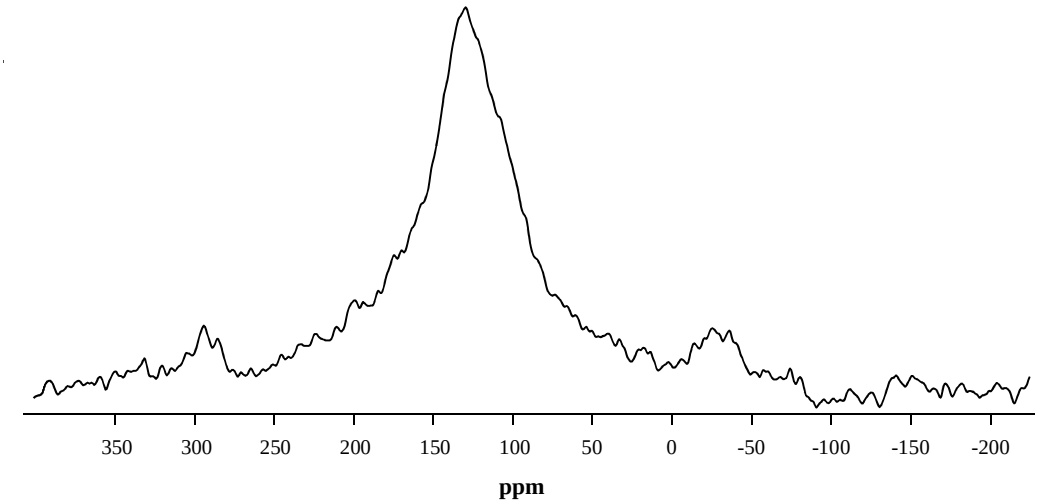

Figure A2- 1. ^{13}C NMR spectrum of coke sample from the cracking of Athabasca *n*-C_5 asphaltenes

In order to get a better NMR spectrum for the coke products, an acid treatment with a solution 0.06 M of HCl was used to remove the iron sulphate ($FeSO_4$) from the catalyst present in the sample. However, the removal was not complete, as confirmed by the results from the elemental analysis for the coke sample before and after the acid treatment.

These unsuccessful NMR analyses of both the liquid products and coke did not allow making aromatic carbon balances, and therefore, conclusions about the change of aromaticity could not be drawn.

References

1. Karimi, A.; Qian, K.; Olmstead, W. N.; Freund, H.; Yung, C.; Gray, M. R. Quantitative Evidence for Bridged Structures in Asphaltenes by Thin Film Pyrolysis. Energy & Fuels 2011, 25, 3581-3589.

Appendix 3: Correlations between variables from the reactions of asphaltene samples from different geological origins

In the first study, a large set of experimental data was obtained for asphaltene samples from different geological sources. This data was the result of characterization analyses of the asphaltene samples and of their reaction products, and from the mass balances of their cracking reactions under hydrogenation conditions.

A good correlation was found between the conversion of the vacuum residue fraction and the aliphatic sulphur (percentage of total sulphur), and also between this last variable and the sum of the yield of coke plus the vacuum residue (> 538°C) fraction after reaction. Similarly, it was pointed out a very god inverse correlation between the content of aromatic molecules with 1 to 3 aromatic rings and the percentage of material remaining in the vacuum residue fraction and forming coke.

In order to evaluate the linear correlation between different variables measured during the analysis and reaction of these diverse *n*-C_7 asphaltene samples, the Pearson correlation coefficient r was calculated for all the different combinatory options of two variables, within a total of fourteen measured variables. The correlation coefficient was calculated with the following equation:

$$r=\frac{n\sum x_i y_i - \sum x_i \sum y_i}{\sqrt{n\sum x_i^2 - (\sum x_i)^2}\sqrt{n\sum y_i^2 - (\sum y_i)^2}} \qquad \text{A3- 1}$$

The pairs of variables with squared correlation coefficients greater than 0.75 are reported in Table A3- 1.

Table A3- 1. Pearson correlation coefficients and their squares for pairs of variables obtained from the characterization and reaction of six different *n*-C_7 asphaltene samples

Variable 1	Variable 2	r	r^2
> 538°C fraction conversion	*n*-C_7 insolubles conversion	0.93	0.86
> 538°C fraction conversion	> 538°C fraction after reaction (wt%)	-0.99	0.98
> 538°C fraction conversion	< 538°C fraction after reaction (wt%)	0.87	0.76
> 538°C fraction conversion	1-3 ring aromatics (wt%)	0.89	0.79
> 538°C fraction conversion	TGA residue asphaltenes (wt%)	-0.95	0.91
> 538°C fraction conversion	TGA residue liquid products (wt%)	-0.91	0.82
> 538°C fraction conversion	H/C molar ratio	0.87	0.76
> 538°C fraction conversion	Coke yield + > 538°C fraction after reaction (wt%)	-0.87	0.76
n-C_7 insolubles conversion	> 538°C fraction after reaction (wt%)	-0.97	0.94
n-C_7 insolubles conversion	*n*-C_7 insolubles after reaction (wt%)	-0.95	0.90
n-C_7 insolubles conversion	TGA residue asphaltenes (wt%)	-0.97	0.94
n-C_7 insolubles conversion	TGA residue liquid products (wt%)	-0.89	0.79
n-C_7 insolubles conversion	H/C molar ratio	0.95	0.91
> 538°C fraction after reaction (wt%)	*n*-C_7 insolubles after reaction (wt%)	0.89	0.79
> 538°C fraction after reaction (wt%)	TGA residue asphaltenes (wt%)	0.98	0.96

> 538°C fraction after reaction (wt%)	TGA residue liquid products (wt%)	0.90	0.82
> 538°C fraction after reaction (wt%)	H/C molar ratio	-0.92	0.85
n-C_7 insolubles after reaction (wt%)	TGA residue asphaltenes (wt%)	0.88	0.78
n-C_7 insolubles after reaction (wt%)	H/C molar ratio	-0.90	0.81
< 538°C fraction after reaction (wt%)	1-3 ring aromatics (wt%)	0.95	0.90
< 538°C fraction after reaction (wt%)	TGA residue liquid products (wt%)	-0.90	0.81
< 538°C fraction after reaction (wt%)	Coke yield + > 538°C fraction after reaction (wt%)	-1.00	1.00
1-3 ring aromatics (wt%)	Coke yield + > 538°C fraction after reaction (wt%)	-0.93	0.87
TGA residue asphaltenes (wt%)	TGA residue liquid products (wt%)	0.94	0.89
TGA residue asphaltenes (wt%)	H/C molar ratio	-0.96	0.91
TGA residue liquid products (wt%)	Coke yield + > 538°C fraction after reaction (wt%)	0.92	0.85

- TGA residue was measured as an approximation to MCR content

- Mass percent (wt%) variables were given on initial asphaltene mass basis

From the mass balances, and the determination of some of these variables, it was already expected a good correlation between some of them, such as: > 538°C fraction conversion and > 538°C fraction after reaction (wt%), *n*-C_7 insolubles conversion and *n*-C_7 insolubles after reaction (wt%), and between < 538°C fraction after reaction (wt%) and Coke yield + > 538°C fraction after reaction (wt%). Some variables, such as total sulphur content (wt%), total saturates (wt%), coke yield (wt%), and MCR conversion did not have a good correlation with any of the other variables considered.

The TGA residue of the asphaltenes that approximates their MCR content, and the H/C molar ratio showed a good correlation with most of the other measured variables. From the compositional variables, it is important to highlight the direct relationship observed between the amount of aromatic molecules with 1-3 rings with the > 538°C fraction conversion, and also with the yield of distillate material (< 538°C fraction after reaction). This observation suggests than an asphaltene sample with higher content of pendant groups with 1-3 aromatic rings would more likely exhibit higher conversion, as well as higher yield of distillable material.

Appendix 4: MATLAB routines for the simulation of the cracking of asphaltenes

The third study presented the simulation of the cracking of asphaltene molecules generated with two different topologies. Five routines were programmed in MATLAB® (Version R2011b, The MathWorks, Inc., USA) for the generation of populations of asphaltene molecules, their cracking, and to perform other calculations required for the rearrangement of the matrixes and other additional estimations.

The routine for the generation of the molecules was programmed as a MATLAB function called GenMol. The user should introduce three parameters to specify the population to be generated: the fraction of cores, the number of molecules in the population, and the topology. For this last specification, the parameters 1 and 2 were used to define the linear and the dendritic topology, respectively. Thus, for instance, if we want to generate a population of 10000 asphaltene molecules with a fraction of cores of 0.05, and dendritic topology, the routine should be called from the Command Window with the next code lines:

```
[Asph,MWAsph,MWDist,MWDistCum,FragDist,FragDistMass,CumFragDist,...
CumFragMassDist]=GenMol(0.05,10000,2);
```

The outputs from this routine are specified in the square brackets, and consist of the following matrixes described in Table A4- 1.

Table A4- 1. Description of the outputs from the routine GenMol

Output	Dimensions	Description
Asph	15 x 15 x number of molecules	Three-dimensional matrix that contains the generated asphaltene molecules, with the molecular weight of their building blocks, and the connections between them
MWAsph	1 x number of molecules	This vector stores the molecular weight of the respective asphaltene molecules defined by the matrix Asph
MWDist	61 x 2	Molar discrete distribution of the molecular weight for the population of asphaltenes generated
MWDistCum	61 x 2	Molecular weight cumulative discrete distribution for the asphaltene population
FragDist	15 x 2	Molar distribution for the number of building blocks of the asphaltene molecules
FragDistMass	15 x 2	Mass distribution for the number of building blocks
CumFragDist	15 x 2	Cumulative molar distribution of the number of building blocks
CumFragDistMass	15 x 2	Cumulative mass distribution of the number of building blocks

These outputs will be available in the Workspace in MATLAB, and can be visualized in the Variable Editor window by double-clicking them. These matrixes can also be automatically displayed in the Command Window, at the end of the routine, if the semicolon is removed from the last code line. The user can modify the names of these outputs, but should be consistent in the next steps when these outputs are used as inputs in the next routines.

When the GenMol routine is executed, six figures will be displayed. Two of these figures correspond to the molar discrete distributions for the molecular weight of the population of asphaltenes, given by MWDist and MWDistCum, and are compared to the distributions obtained from the data published by Qian et al.[1] The other four figures show the molar and mass distributions of the number of building blocks in the population of asphaltenes, specified by the matrixes FragDist, FragDistMass, CumFragDist, and CumFragDistMass.

To determine the mass percentage of cores in the resulting population of asphaltenes, the function MassCores was programmed. This short routine has only one output called coresper that indicates the mass fraction of cores in the total mass of asphaltenes. This function must be called in the Command Window with the following code line:

```
[coresper]=MassCores(Asph)
```

After the generation of the population of asphaltenes, the molecules can be cracked with the routine CrackMol. The next code lines should be typed in the Command Window to call the function programmed in MATLAB:

```
[AsphCr,MWAsphCr,MWDistMass,MWDistCumMass,MWDistCr,MWDistCumCr,...
MWDistMassCr,MWDistCumMassCr,TbDistCumMassProd,FragDistCr,...
FragDistMassCr,CumFragDistCr,CumFragMassDistCr,lights,heavy,iter]=...
CrackMol(Asph,MWAsph,MWDist,MWDistCum);
```

The function CrackMol generates the outputs described in Table A4- 2.

Table A4- 2. Description of the outputs from the function CrackMol

Output	Dimensions	Description
AsphCr	15 x 15 x number of molecules after cracking	Three-dimensional matrix that contains the asphaltene molecules after cracking, with the molecular weight of their building blocks, and the connections between them
MWAsphCr	1 x number of molecules after cracking	This vector stores the molecular weight of the respective asphaltene molecules defined by the matrix AsphCr
MWDistMass	70 x 2	Mass discrete distribution of the molecular weight for the population of asphaltenes before reaction
MWDistCumMass	70 x 2	Mass cumulative distribution of the molecular weight for the population of asphaltenes before cracking
MWDistCr	70 x 2	Molar discrete distribution of the molecular weight for the population of asphaltenes after cracking
MWDistCumCr	70 x 2	Molecular weight cumulative discrete distribution for the asphaltenes after cracking
MWDistMassCr	70 x 2	Mass discrete distribution of the molecular weight for the population of asphaltenes after cracking
MWDistCumMassCr	70 x 2	Mass cumulative distribution of the molecular weight for the population of asphaltenes after cracking
TbDistCumMassProd	70 x 2	Mass cumulative distribution of the boiling point for the population of asphaltenes after cracking
FragDistCr	15 x 2	Molar distribution for the number of building blocks of the asphaltenes after cracking
FragDistMassCr	15 x 2	Mass distribution for the number of building blocks of the asphaltenes after cracking
CumFragDistCr	15 x 2	Cumulative molar distribution of the number of building blocks of the asphaltenes after cracking
CumFragDistMassCr	15 x 2	Cumulative mass distribution of the number of building blocks of the asphaltenes after cracking

lights	1 x 1	Variable that indicates the < 343°C boiling fraction in the population of asphaltenes after cracking
heavy	1 x 1	Variable for the > 650°C boiling fraction for the asphaltene population after cracking
iter	1 x 1	Variable that counts the number of breakages, and likewise, the new molecules generated. Thus, the final number of molecules is equal to the sum of the initial amount of molecules plus this variable

The execution of the function CrackMol also generates ten figures to visualize the results. Two of them are the molar (MWDistCr) and mass (MWDistMassCr) distributions of the molecular weight for the resulting population of asphaltenes after the reaction, compared with the initial distributions before the reaction (MWDist and MWDistMass, respectively). Similarly, two other graphs correspond to the cumulative molar (MWDistCumCr) and mass (MWDistCumMassCr) distributions of the molecular weight for the molecules after cracking compared with the respective distributions before the reaction, given by MWDistCum and MWDistCumMass. Two additional figures compare the cumulative mass distributions of the molecular weight (MWDistCumMassCr) and of the boiling point (TbDistCumMassProd) for the resulting asphaltene population after the reaction with the experimental results. The last four figures are again the mass and molar distributions of the number of building blocks for the asphaltene molecules after cracking, given by the matrixes FragDistCr, FragDistMassCr, CumFragDistCr, and CumFragDistMassCr.

The function CrackMol internally calls the function Rearrange that has the objective of reorganizing the building blocks and connections in the cracked molecule and in the new molecule generated. This function eliminates the empty spaces on the main diagonal of the matrix, and ensures that all the building blocks are located one after the other, starting at the position (1,1) of the matrix.

The function OrgAsph was programmed to get some additional information of the resulting population of asphaltenes after the cracking routine. This function can reorganize the matrix of asphaltenes after the reaction (AsphCr), and the respective vector with their molecular weights (MWAsphCr), by increasing ranges of molecular weight. During this operation, the function is able to calculate the number of molecules in each molecular weight range. This function has the three outputs described in Table A4- 3, and must be called from the Command Window with the next code line:

```
[Asphorg,MWAsphorg,MWmolcounter]=OrgAsph(AsphCr,MWAsphCr);
```

Table A4- 3. Description of the outputs from the function OrgAsph

Output	Dimensions	Description
Asphorg	15 x 15 x number of molecules after cracking	Three-dimensional matrix that contains the asphaltene molecules after cracking, organized by increasing ranges of molecular weight
MWAsphorg	1 x number of molecules after cracking	This vector stores the molecular weight of the respective asphaltene molecules defined by the matrix Asphorg
MWmolcounter	70 x 2	Distribution of number of molecules after cracking in each molecular weight interval

The MATLAB code for the five functions programmed for the simulation work presented in the third study is presented below.

A4- 1 Function GenMol

```
%-------------------------------------------------------------------------
%-------------------------------------------------------------------------
%            G E N E R A T I O N   OF  M O L E C U L E S
%-------------------------------------------------------------------------
%-------------------------------------------------------------------------
% MATLAB File name: GenMol.m
% Asphaltenes molecules are generated using building blocks of cores and
% distillates. PDFs are available for the cores, the different
% categories of distillable molecules, and for the asphaltenes
%-------------------------------------------------------------------------
% R o s a   I.   R u e d a - V e l á s q u e z
% U n i v e r s i t y   o f    A l b e r t a
% 2012
%-------------------------------------------------------------------------

function
[Asph,MWAsph,MWDist,MWDistCum,FragDist,FragDistMass,CumFragDist,...
    CumFragMassDist]=GenMol(frcore,n,moltype)

% The user defines the fraction of cores (frcore), the number of
molecules
% to be generated (n), and the type of molecules (moltype = 1 for linear
% molecules, and moltype = 2 for dendritic molecules)

%PDFblock - Type of building block
%Building block can be a core or a distillable molecule.
% # --- Categories
% 1 --- core
% 2 --- distillable molecules

% The fraction of cores is defined by the user with the variable frcore

PDFBlock=[frcore 1
1 2];

%-------------------------------------------------------------------------
%PDFAsph - Asphaltenes
%This PDF was obtained from the data published by Qian et al, 2007
%Data was normalized and converted to a discrete cumulative distribution
%-------------------------------------------------------------------------
PDFAsph=[0.0162 356.25
0.0402  400
0.0682  434.375
0.1047  475
0.1447  512.5
0.1873  556.25
0.2283  593.75
0.2705  637.5
0.3132  675
0.3546  712.5
0.3956  750
0.4343  793.75
0.4708  825
0.5060  875
0.5404  912.5
0.5734  950
0.6044  993.75
0.6342  1031.25
0.6612  1068.75
```

```
0.6872  1106.25
0.7119  1143.75
0.7344  1193.75
0.7559  1237.5
0.7751  1268.75
0.7934  1312.5
0.8100  1356.25
0.8258  1393.75
0.8410  1431.25
0.8554  1468.75
0.8681  1512.5
0.8801  1550
0.8914  1593.75
0.9016  1631.25
0.9112  1668.75
0.9202  1709.375
0.9282  1750
0.9361  1787.5
0.9426  1825
0.9490  1868.75
0.9543  1906.25
0.9593  1946.875
0.9640  1987.5
0.9684  2037.5
0.9721  2078.125
0.9757  2115.625
0.9790  2156.25
0.9816  2193.75
0.9842  2237.5
0.9864  2275
0.9885  2312.5
0.9903  2353.125
0.9919  2390.625
0.9933  2431.25
0.9946  2471.875
0.9959  2512.5
0.9972  2550
0.9981  2593.75
0.9989  2634.375
0.9996  2668.75
0.9999  3000
1.0000  3500];
%-------------------------------------------------------------------------
%-------------------------------------------------------------------------
% PDFCores - Cores
% This PDF was obtained from SimDist data of material recovered from the
% reaction of asphaltenes under hydrogenation conditions and after removal
% of tetralin. Data was normalized for material with boiling point > 538C,
% and cumulative distribution was generated.
% MW was determined by the correlation of Sim and Daubert
%-------------------------------------------------------------------------

PDFCores=[0.0987    507.42
0.2309  543.38
0.3507  579.04
0.4518  617.61
0.5725  673.66
0.6591  760.24
0.7380  849.80
0.8103  942.51
0.8767  1042.28
0.9380  1147.23
```

```
0.9949  1255.07
1.0000  1315.97];

%-------------------------------------------------------------------------
%-------------------------------------------------------------------------
% PDFDist - Categories of distillable molecules
% This PDF was generated from the overall mole yields for the different
% categories of distillable molecules. Data was normalized to get the
% cumulative distribution
%-------------------------------------------------------------------------
% # --- Categories
% 1 --- alkylbenzoDBTs
% 2 --- 4+ ring aromatics
% 3 --- 2 ring naphthenes
% 4 --- alkylchrysenes
% 5 --- alkylcarbazoles
% 6 --- alkyl octahydrophenanthrenes
% 7 --- alkylpyrenes
% 8 --- alkylDBTs
% 9 --- alkylphenanthrenes
% 10 -- sulfides
% 11 -- alkylfluorenes
% 12 -- alkylbiphenyls
% 13 -- 1 ring naphthenes
% 14 -- alkylbenzothiophenes
% 15 -- alkylnaphthalenes
% 16 -- alkyl benzenes
% 17 -- alkyl tetralins
% 18 -- paraffins

%-------------------------------------------------------------------------

PDFDist = [0.0092   1
0.0192  2
0.0308  3
0.0442  4
0.0624  5
0.0866  6
0.1146  7
0.1444  8
0.1825  9
0.2255  10
0.2739  11
0.3282  12
0.3911  13
0.4545  14
0.5401  15
0.6549  16
0.7742  17
1.0000  18];

%-------------------------------------------------------------------------
% PDFs for the different categories of molecules
% Experimental data had been provided in mole%.
%-------------------------------------------------------------------------
% Category # 1 --- alkylbenzoDBTs
%-------------------------------------------------------------------------
PDFDist1=[0.0742    234
0.2375  248
0.4618  262
0.6479  276
0.7855  290
```

```
0.8666  304
0.9094  318
0.9419  332
0.9704  346
0.9810  360
0.9857  374
0.9903  388
0.9925  402
0.9954  416
0.9976  430
0.9983  444
0.9991  514
1.0000  542];

%-------------------------------------------------------------------------
% Category # 2 --- 4+ ring aromatics
%-------------------------------------------------------------------------
PDFDist2=[0.0705    208
0.2031  222
0.3658  236
0.5232  250
0.6340  264
0.7410  278
0.8385  292
0.8991  306
0.9418  320
0.9637  334
0.9763  348
0.9846  362
0.9903  376
0.9938  390
0.9966  404
0.9980  418
0.9987  432
1.0000  446];

%-------------------------------------------------------------------------
% Category # 3 --- 2 ring naphthenes
%-------------------------------------------------------------------------
PDFDist3=[0.0028    152
0.0104  180
0.0298  194
0.1294  208
0.2754  222
0.4101  236
0.5206  250
0.6004  264
0.6679  278
0.7327  292
0.7975  306
0.8483  320
0.8978  334
0.9306  348
0.9561  362
0.9702  376
0.9823  390
0.9885  404
0.9935  418
0.9947  432
0.9964  446
0.9982  460
1.0000  474];
```

```
%-------------------------------------------------------------------------
% Category # 4 --- alkylchrysenes
%-------------------------------------------------------------------------
PDFDist4=[0.0715    228
0.1967  242
0.4193  256
0.5839  270
0.7321  284
0.8417  298
0.9312  312
0.9649  326
0.9840  340
0.9931  354
0.9974  368
0.9995  382
1.0000  396];

%-------------------------------------------------------------------------
% Category # 5 --- alkylcarbazoles
%-------------------------------------------------------------------------
PDFDist5=[0.0381    167
0.1838  181
0.4119  195
0.6042  209
0.7889  223
0.8935  237
0.9531  251
0.9758  265
0.9901  279
0.9945  293
0.9960  307
0.9974  321
0.9992  335
0.9996  349
1.0000  363];

%-------------------------------------------------------------------------
% Category # 6 --- alkyl octahydrophenanthrenes
%-------------------------------------------------------------------------
PDFDist6=[0.2394    186
0.4666  200
0.6432  214
0.7615  228
0.8283  242
0.8656  256
0.8949  270
0.9191  284
0.9420  298
0.9540  312
0.9637  326
0.9746  340
0.9806  354
0.9864  368
0.9904  382
0.9948  396
0.9974  410
0.9985  424
0.9994  438
0.9997  480
1.0000  494];
```

```
%-------------------------------------------------------------------------
% Category # 7 --- alkylpyrenes
%-------------------------------------------------------------------------
PDFDist7=[0.0424    202
0.1305  216
0.2471  230
0.3927  244
0.6711  258
0.8002  272
0.8935  286
0.9470  300
0.9698  314
0.9824  328
0.9915  342
0.9953  356
0.9976  370
0.9986  384
0.9988  398
0.9995  412
0.9998  426
1.0000  440];

%-------------------------------------------------------------------------
% Category # 8 --- alkylDBTs
%-------------------------------------------------------------------------
PDFDist8=[0.0441    184
0.1632  198
0.3178  212
0.4926  226
0.6456  240
0.7785  254
0.8606  268
0.9104  282
0.9406  296
0.9611  310
0.9730  324
0.9819  338
0.9876  352
0.9917  366
0.9944  380
0.9957  394
0.9966  408
0.9976  422
0.9980  436
0.9983  450
0.9988  464
0.9990  478
0.9993  492
0.9997  506
1.0000  520];

%-------------------------------------------------------------------------
% Category # 9 --- alkylphenanthrenes
%-------------------------------------------------------------------------
PDFDist9=[0.0392    178
0.1065  192
0.2067  206
0.3359  220
0.4827  234
0.6177  248
0.7907  262
0.8661  276
```

```
0.9181  290
0.9491  304
0.9629  318
0.9762  332
0.9832  346
0.9879  360
0.9918  374
0.9949  388
0.9971  402
0.9976  416
0.9978  430
0.9985  444
0.9988  472
0.9998  514
1.0000  528];

%-------------------------------------------------------------------------
% Category # 10 --- sulfides
%-------------------------------------------------------------------------
PDFDist10=[0.0664   136
0.2294  150
0.4856  164
0.7006  178
0.8482  192
0.9393  206
0.9776  220
0.9904  234
0.9934  248
0.9966  262
0.9983  276
0.9989  290
0.9995  304
0.9997  318
1.0000  346];

%-------------------------------------------------------------------------
% Category # 11 ---alkylfluorenes
%-------------------------------------------------------------------------
PDFDist11=[0.0950   166
0.1811  180
0.2926  194
0.4277  208
0.5758  222
0.7129  236
0.8146  250
0.9057  264
0.9439  278
0.9665  292
0.9790  306
0.9849  320
0.9898  334
0.9923  348
0.9940  362
0.9952  376
0.9958  390
0.9972  404
0.9976  418
0.9978  432
0.9985  446
0.9986  460
0.9988  474
0.9994  488
```

```
0.9997  502
0.9998  530
1.0000  544];

%-------------------------------------------------------------------------
% Category # 12 --- alkylbiphenyls
%-------------------------------------------------------------------------
PDFDist12=[0.0196   154
0.1361  168
0.3287  182
0.5264  196
0.6854  210
0.7928  224
0.8715  238
0.9173  252
0.9489  266
0.9669  280
0.9751  294
0.9833  308
0.9876  322
0.9918  336
0.9944  350
0.9963  364
0.9978  378
0.9988  392
0.9994  406
0.9996  420
0.9997  434
0.9999  448
1.0000  462];

%-------------------------------------------------------------------------
% Category # 13 --- 1 ring naphthenes
%-------------------------------------------------------------------------
PDFDist13=[0.0100   98
0.0243  112
0.0604  126
0.1303  140
0.2504  154
0.3764  168
0.4809  182
0.5725  196
0.6460  210
0.7090  224
0.7561  238
0.7939  252
0.8281  266
0.8579  280
0.8876  294
0.9139  308
0.9387  322
0.9575  336
0.9717  350
0.9805  364
0.9879  378
0.9921  392
0.9954  406
0.9973  420
0.9978  434
0.9985  448
0.9986  462
0.9992  476
```

```
0.9995  490
0.9996  532
0.9997  546
1.0000  686];

%-------------------------------------------------------------------------
% Category # 14 --- alkylbenzothiophenes
%-------------------------------------------------------------------------
PDFDist14=[0.0766   134
0.1678  148
0.3284  162
0.4980  176
0.6356  190
0.7432  204
0.8122  218
0.8571  232
0.8836  246
0.9190  260
0.9389  274
0.9548  288
0.9661  302
0.9764  316
0.9828  330
0.9886  344
0.9917  358
0.9941  372
0.9956  386
0.9968  400
0.9977  414
0.9985  428
0.9988  442
0.9993  456
0.9998  470
0.9999  512
1.0000  540];

%-------------------------------------------------------------------------
% Category # 15 --- alkylnaphthalenes
%-------------------------------------------------------------------------
PDFDist15=[0.2070   142
0.3945  156
0.5842  170
0.7170  184
0.8009  198
0.8538  212
0.8893  226
0.9200  240
0.9414  254
0.9584  268
0.9703  282
0.9776  296
0.9835  310
0.9877  324
0.9912  338
0.9924  352
0.9942  366
0.9960  380
0.9969  394
0.9974  408
0.9981  422
0.9983  436
0.9987  450
```

```
0.9991  464
0.9994  478
0.9995  492
0.9998  506
0.9999  520
1.0000  534];

%-------------------------------------------------------------------------
% Category # 16 --- alkyl benzenes
%-------------------------------------------------------------------------
PDFDist16=[0.1408   92
0.3184  106
0.5008  120
0.6650  148
0.7488  162
0.8085  176
0.8537  190
0.8876  204
0.9100  218
0.9253  232
0.9367  246
0.9475  260
0.9587  274
0.9674  288
0.9749  302
0.9820  316
0.9868  330
0.9899  344
0.9928  358
0.9952  372
0.9968  386
0.9979  400
0.9984  414
0.9991  428
0.9995  442
0.9998  456
1.0000  470];

%-------------------------------------------------------------------------
% Category # 17 --- alkyl tetralins
%-------------------------------------------------------------------------
PDFDist17=[0.2918   146
0.4855  160
0.6510  174
0.7564  188
0.8271  202
0.8697  216
0.8970  230
0.9159  244
0.9308  258
0.9433  272
0.9562  286
0.9670  300
0.9756  314
0.9825  328
0.9879  342
0.9917  356
0.9942  370
0.9961  384
0.9975  398
0.9985  412
0.9991  426
```

```
0.9994  440
0.9995  454
0.9998  468
0.9999  482
1.0000  496];

%-------------------------------------------------------------------------
% Category # 18 --- paraffins
%-------------------------------------------------------------------------
PDFDist18=[0.0812   100
0.1683  114
0.2687  128
0.3548  142
0.4830  156
0.5778  170
0.6357  184
0.6879  198
0.7298  212
0.7649  226
0.7965  240
0.8247  254
0.8537  268
0.8824  282
0.9102  296
0.9337  310
0.9532  324
0.9685  338
0.9795  352
0.9864  366
0.9915  380
0.9946  394
0.9970  408
0.9980  422
0.9987  436
0.9994  450
0.9996  464
0.9998  478
0.9999  506
1.0000  534];

%-------------------------------------------------------------------------
%-------------------------------------------------------------------------
% Generation of asphaltenes molecules
% With a random number, "a" selects core or distillable molecule
% Separate routines can select a building block either in the cores or in
% the distillates PDFs
% When the building block is a distillable molecule, the routine also
% selects some category of molecule, and then a specific MW in that
% category
%-------------------------------------------------------------------------
%-------------------------------------------------------------------------
% The generation of asphaltene molecules follow the distribution given
% by PDFAsph.
%-------------------------------------------------------------------------

% MWDist is the matrix that verifies the distribution of MW of the
% molecules generated
MWDist=zeros(size(PDFAsph));
MWDist(:,2)=PDFAsph(:,2);

% "n" is the number of molecules generated
% n is define by the user, n = 10000 has been used for the simulations
```

```
% "mxblocks is the size of the matrix of asphaltenes
% mxblocks= 15 was found appropriate

% moltype = Type of molecule
% 1 = lineal
% 2 = dendritic
% moltype is defined by the user

% generation of matrix of asphaltenes

% "cumole" is the cumulative mole in the distribution of asphaltenes
cumole=0;
% "mlc" is the counter of the number of asphaltenes molecules generated
mlc=0;

for p = 1:size(PDFAsph,1)
    q = (n*(PDFAsph(p,1))-n*(cumole));
    cumole = PDFAsph(p,1);
    if p==1
        MWprev=281.25;
    else
        MWprev=PDFAsph((p-1),2);
    end
    for i=1 : q
        mlc=mlc+1;
        mxblocks=15;
        Asph(:,:,mlc)=zeros(mxblocks,mxblocks);
        MWAsph(mlc)=0;
        MWCum=0;
        r=0;
        while r<15
                r=r+1;
                if MWAsph(mlc)<MWprev
                    % If MW of the molecules is lower than lower value in
                    % the range
                        a=rand(1);
                        if a < PDFBlock(1,1);
                           % Select a core building block
                           b=rand(1);
                           k=1;
                           while b > PDFCores(k,1);
                               k=k+1;
                           end
                           fragment = PDFCores(k,2);
                        else
                            % Select a distillate molecule
                            b=rand(1);
                            k=1;
                            while b > PDFDist(k,1);
                               k=k+1;
                            end
                            %Selection of specific category of distillate
                            if k==1
                                A = PDFDist1;
                            elseif k==2
                                A= PDFDist2;
                            elseif k==3
                                A= PDFDist3;
                            elseif k==4
                                A= PDFDist5;
                            elseif k==5
```

```
        A= PDFDist5;
    elseif k==6
        A= PDFDist6;
    elseif k==7
        A= PDFDist7;
    elseif k==8
        A= PDFDist8;
    elseif k==9
        A= PDFDist9;
    elseif k==10
        A= PDFDist10;
    elseif k==11
        A= PDFDist11;
    elseif k==12
        A= PDFDist12;
    elseif k==13
        A= PDFDist13;
    elseif k==14
        A= PDFDist14;
    elseif k==15
        A= PDFDist15;
    elseif k==16
        A= PDFDist16;
    elseif k==17
        A= PDFDist17;
    elseif k==18
        A= PDFDist18;
    end
    c = rand(1);
    m=1;
    while c > A(m,1);
       m=m+1;
    end
    fragment = A(m,2);
end
% Position of building block on matrix diagonal
MWCum=MWAsph(mlc);
Asph(r,r,mlc)=fragment;
MWAsph(mlc) = MWAsph(mlc) + fragment;

% assignation of links to other building blocks
if moltype ==1
    %linear molecule
    if r==1
    else
        poslink=r-1;
        Asph(poslink,r,mlc)=1;
    end
else
    % dendritic or branched molecule
    if r==1
    elseif r==2
        poslink=1;
        Asph(poslink,r,mlc)=1;
    elseif r==3
        % Building block 3 can be connected to either
        % building block 1 or building block 2
        poslink=randi([1 (r-1)]);
        Asph(poslink,r,mlc)=1;
    else
        % other build. blocks can be connected to any
       % building block except the previous one
```

```
                        % with (r-2) some linearity is avoided
                        poslink=randi([1 (r-2)]);
                        Asph(poslink,r,mlc)=1;
                    end
                end
                % Verification of MW in the range
                if MWAsph(mlc)<=PDFAsph(p,2)
                    if MWAsph(mlc)>MWprev
                        j=mxblocks;
                    else
                        %MWDiff=MWprev-MWAsph(mlc);
                        MWDiff=PDFAsph(p,2)-MWAsph(mlc);
                        if MWDiff<92
                            Asph(r,r,mlc)=0;
                            if r==1
                            else
                                Asph(poslink,r,mlc)=0;
                            end
                            r=r-1;
                            MWAsph(mlc)=MWCum;
                            mxblocks=mxblocks+1;
                        else
                        end
                    end
                else
                    Asph(r,r,mlc)=0;
                        if r==1
                        else
                            Asph(poslink,r,mlc)=0;
                        end
                        r=r-1;
                        MWAsph(mlc)=MWCum;
                        mxblocks=mxblocks+1;
                end

            end

        end

        MWAsph(mlc) = 0;
        for g=1:15
            MWAsph(mlc)=MWAsph(mlc)+Asph(g,g,mlc);
        end

        % Verification MW distribution of asphaltene molecules generated
        l=1;
        while MWAsph(mlc) > PDFAsph(l,2);
            l=l+1;
        end
        for k=1 : size(MWDist,1)
            if k==l
                MWDist(k,1)= ((MWDist(k,1))*(mlc-1)+1)/mlc;
            else
                MWDist(k,1)=((MWDist(k,1))*(mlc-1))/mlc;
            end
        end
    end
end

% Cumulative distribution
MWDistCum=zeros(size(PDFAsph));
MWDistCum(:,2)=PDFAsph(:,2);
```

```
cum=0;
for i=1:size(PDFAsph,1)
    cum= cum + MWDist(i,1);
    MWDistCum(i,1)=cum;
end
figure
plot (PDFAsph(:,2),PDFAsph(:,1),'-r',MWDistCum(:,2),MWDistCum(:,1),'--')
legend('Experimental','Simulation')
xlabel('MW')
ylabel('Cumulative mole fraction')

% Mole fractions distribution
molefractions=zeros(size(PDFAsph,1),1);
prevfrac=0;
for i=1:size(PDFAsph,1)
    molefractions(i)=PDFAsph(i,1)-prevfrac;
    prevfrac=PDFAsph(i,1);
end
MWDistsim=zeros(size(MWDist,1),1);
for i=1:size(Asph,3)
    counter=1;
    while MWAsph(i)>MWDist(counter,2)
        counter=counter+1;
    end
    MWDistsim(counter)=MWDistsim(counter)+1/size(Asph,3);
end
figure
plot (PDFAsph(:,2),molefractions(:,1),'-r',MWDist(:,2),MWDist(:,1),...
    '--b')%,MWDist(:,2),MWDistsim(:,1),':m'
legend('Experimental','MWDist')%'MWDistsim'
xlabel('MW')
ylabel('Mole fraction')


%-------------------------------------------------------------------------
% Determination of distribution of # of building blocks in molecules
% generated
%-------------------------------------------------------------------------

FragDist=zeros(15,2);
FragDist(:,1)=[1:1:15];
FragDistMass=zeros(15,2);
FragDistMass(:,1)=[1:1:15];
for i=1:mlc
    block=0;
    mxblocks=15;
    for j=1:mxblocks
        if Asph(j,j,i)~=0
            block = block+1;
        end
    end
    FragDist(block,2)=FragDist(block,2)+(1/mlc);
    FragDistMass(block,2)=FragDistMass(block,2)+MWAsph(i)/sum(MWAsph);
end
figure
plot(FragDist(:,1), FragDist(:,2))
xlabel('# Building blocks')
ylabel('Fraction of molecules')
title('Building blocks Distribution')
figure
plot(FragDistMass(:,1), FragDistMass(:,2))
xlabel('# Building blocks')
```

```
ylabel('Mass Fraction')
title('Building blocks Distribution')

%Cumulative distribution of building blocks
CumFragDist = zeros(size(FragDist));
CumFragDist(:,1)=FragDist(:,1);
CumFragMassDist = zeros(size(FragDistMass));
CumFragMassDist(:,1)=FragDistMass(:,1);
cumone=0;
cumtwo=0;
for i=1:size(CumFragDist,1)
    cumone= cumone + FragDist(i,2);
    CumFragDist(i,2)=cumone;
    cumtwo=cumtwo + FragDistMass(i,2);
    CumFragMassDist(i,2)=cumtwo;
end
figure
plot(CumFragDist(:,1), CumFragDist(:,2))
xlabel('# Building blocks')
ylabel('Cumulative Fraction of molecules')
title('Building blocks Distribution')
figure
plot(CumFragMassDist(:,1), CumFragMassDist(:,2))
xlabel('# Building blocks')
ylabel('Cumulative Mass Fraction')
title('Building blocks Distribution')
end
```

A4- 2 Function MassCores

```
%-------------------------------------------------------------------------
%-------------------------------------------------------------------------
%                  M A S S      OF      C O R E S
%-------------------------------------------------------------------------
%-------------------------------------------------------------------------
% MATLAB File name: MassCores.m
% This routine was written to determine the percentage of the total mass
% of asphaltenes that was made up of cores
%-------------------------------------------------------------------------
% R o s a   I.   R u e d a - V e l á s q u e z
% U n i v e r s i t y   o f    A l b e r t a
% 2012
%-------------------------------------------------------------------------

function [coresper]=MassCores(Asph)
mxblocks=15;
masscores=0;
masspendants=0;
for i=1:size(Asph,3)
    for j=1:mxblocks
        if Asph(j,j,i)>=481.3
            % 481.3 is the minimum mass of the cores
            masscores=masscores+Asph(j,j,i);
        else
            masspendants=masspendants+Asph(j,j,i);
    end
    end
end

totalmass=masscores+masspendants;
coresper=masscores/totalmass;
end
```

A4- 3 Function CrackMol

```
%-------------------------------------------------------------------------
%-------------------------------------------------------------------------
%              C R A C K I N G   OF   M O L E C U L E S
%-------------------------------------------------------------------------
%-------------------------------------------------------------------------
% MATLAB File name: CrackMol.m
% This function cracks asphaltene molecules generated by GenMol.m
%-------------------------------------------------------------------------
% R o s a   I.   R u e d a - V e l á s q u e z
% U n i v e r s i t y   o f    A l b e r t a
% 2012
%-------------------------------------------------------------------------

function [Asph,MWAsph,MWDistMass,MWDistCumMass,MWDistCr,MWDistCumCr,...
    MWDistMassCr,MWDistCumMassCr,TbDistCumMassProd,FragDistCr,...
    FragDistMassCr,CumFragDistCr,CumFragMassDistCr,lights,heavy,iter]...
    =CrackMol(Asph,MWAsph,MWDist,MWDistCum)

mlc=size(Asph,3);
mxblocks=15;

%-------------------------------------------------------------------------
% Any molecule with MW < 481 Da is distillable
%-------------------------------------------------------------------------
% Initial mass fraction of distillates in asphaltenes
%-------------------------------------------------------------------------

% Mole Distribution
exone=MWDist(:,2);
exone=exone';
extwo=[100 130 160 190 220 250 280 310 330 exone];
extwo=extwo';

MWDistmod=zeros ((size(extwo,1)),2);
MWDistmod(:,2)=extwo(:,1);
for i=1:size(Asph,3)
    ctm=1;
    while MWAsph(i)>MWDistmod(ctm,2)
        ctm = ctm+1;
    end
    MWDistmod(ctm,1)=MWDistmod(ctm,1)+1/size(Asph,3);
end

% Mass distribution
mass=0;
for i=1:size(MWDistmod,1)
    mass=mass+MWDistmod(i,1)*MWDistmod(i,2);
end
MWDistMass=zeros(size(MWDistmod));
MWDistMass(:,2)=MWDistmod(:,2);
for i=1:size(MWDistMass,1)
    MWDistMass(i,1)=(MWDistmod(i,1)*MWDistmod(i,2))/mass;
end

% Cumulative Mass Distribution
MWDistCumMass=zeros(size(MWDistMass));
MWDistCumMass(:,2)=MWDistMass(:,2);
cummass=0;
for i=1:size(MWDistCumMass,1)
```

```
    cummass= cummass + MWDistMass(i,1);
    MWDistCumMass(i,1)=cummass;
end
g=1;
while MWDistCumMass(g,2)<481
    g=g+1;
end
asphdist=MWDistCumMass((g-1),1)+(481-MWDistCumMass((g-1),2))*...
    (MWDistCumMass(g,1)-MWDistCumMass((g-1),1))...
    /(MWDistCumMass(g,2)-MWDistCumMass((g-1),2));

YieldDist=asphdist;

% asphdist is the initial mass fraction of distillates in the asphaltenes
%-------------------------------------------------------------------------

iter=0;
itercr=0;
while YieldDist <= 0.662

    % Rearrangement of asphaltenes matrix by number of building blocks
    % every 100 cracked molecules
    if iter==itercr
        AsphCr=zeros(size(Asph));
        MWAsphCr=zeros(size(MWAsph));
        mlcr=0;
        for i=1:size(Asph,1)
            if i==2
                init=mlcr+1;
            end
            for k=1:mlc
                bl=0;
                for j=1:size(Asph,1)
                    if Asph(j,j,k)~=0
                        bl=bl+1;
                    end
                end
                if bl==i
                    mlcr=mlcr+1;
                    AsphCr(:,:,mlcr)=Asph(:,:,k);
                    MWAsphCr(mlcr)=MWAsph(k);
                end
            end
        end
        Asph=AsphCr;
        MWAsph=MWAsphCr;
        itercr=itercr+100;
    end

    r=randi([init mlc]);
    % selection of a random molecule
    % This selection will only take into account molecules with more than
    % one building block

    block=0;
    for i=1:mxblocks
        %Determination number of building blocks in asphaltene molecule
        if Asph(i,i,r)~=0
            block = block+1;
        end
    end
```

```
% Only molecules with more than one building block can be cracked
if block > 1
    iter=iter+1;
    crpos=randi([2 block]);
    crfrag=Asph(crpos,crpos,r);
    bond=1;
    for i=1:(crpos-1)
        if Asph(bond,crpos,r)==0
            bond=bond+1;
        end
    end
    % bond indicates the bond that will be cracked
    mlc=mlc+1;
    % a new molecule is generated
    Asph(:,:,mlc)=zeros(mxblocks,mxblocks);

    % Transfering building block and its links to new molecule
    Asph(crpos,crpos,mlc)=crfrag;
    Asph(crpos,crpos,r)=0;
    Asph(bond,crpos,r)=0;

    if block>2
        linkfrg=block;
        while linkfrg > crpos
            if Asph(linkfrg,linkfrg,r)~=0
                link=1;
                for i=1:(linkfrg-1)
                    if Asph(link,linkfrg,r)==0
                        link=link+1;
                    end
                end
                origlink=link;
                if link==crpos
                    Asph(linkfrg,linkfrg,mlc)=Asph(linkfrg,linkfrg,r);
                    Asph(link,linkfrg,mlc)=1;
                    Asph(linkfrg,linkfrg,r)=0;
                    Asph(link,linkfrg,r)=0;
                else
                    while link>crpos
                        linktwo=1;
                        for i=1:(link-1)
                            if Asph(linktwo,link,r)==0
                                linktwo=linktwo+1;
                            end
                        end
                        link=linktwo;
                    end
                    if link==crpos
                        Asph(linkfrg,linkfrg,mlc)=Asph(linkfrg,linkfrg,r);
                        Asph(origlink,linkfrg,mlc)=1;
                        Asph(linkfrg,linkfrg,r)=0;
                        Asph(origlink,linkfrg,r)=0;
                    else
                    end
                end
            end
            linkfrg=linkfrg-1;
        end
    end

    % Rearrangement of building blocks in initial and new molecules
```

```
    A=Rearrange(Asph(:,:,r));
    Asph(:,:,r)=A;
    A=Rearrange(Asph(:,:,mlc));
    Asph(:,:,mlc)=A;

% Update MW in MWAsph
MWAsph(r)=0;
for i=1:15
    MWAsph(r)=MWAsph(r)+Asph(i,i,r);
end

MWAsph(mlc)=0;
for i=1:15
    MWAsph(mlc)=MWAsph(mlc)+Asph(i,i,mlc);
end

% Determination of new mole fractions
MWDistCr=zeros(size(MWDistmod));
MWDistCr(:,2)=MWDistmod(:,2);
for m=1:size(Asph,3)
    countone=1;
    while MWAsph(m)>MWDistmod(countone,2)
        countone = countone+1;
    end
    MWDistCr(countone,1)=MWDistCr(countone,1)+1/size(Asph,3);
end

% Cumulative mole distribution
MWDistCumCr=zeros(size(MWDistCr));
MWDistCumCr(:,2)=MWDistCr(:,2);
cumcr=0;
for i=1:size(MWDistCr,1)
    cumcr= cumcr + MWDistCr(i,1);
    MWDistCumCr(i,1)=cumcr;
end

%Determination of new mass fractions
MWDistMassCr=zeros(size(MWDistCr));
MWDistMassCr(:,2)=MWDistCr(:,2);
masscr=0;
for i=1:size(MWDistCr,1)
    masscr=masscr+MWDistCr(i,1)*MWDistCr(i,2);
end
% Assumes that all the molecules in each MW range have the same MW
for i=1:size(MWDistMassCr,1)
    MWDistMassCr(i,1)=(MWDistCr(i,1)*MWDistCr(i,2))/masscr;
end

% Cumulative Mass Distribution
MWDistCumMassCr=zeros(size(MWDistMassCr));
MWDistCumMassCr(:,2)=MWDistMassCr(:,2);
cummasscr=0;
for i=1:size(MWDistCumMassCr,1)
    cummasscr= cummasscr + MWDistMassCr(i,1);
    MWDistCumMassCr(i,1)=cummasscr;
end

% Mass fraction of distillates
g=1;
while MWDistCumMassCr(g,2)<481
    g=g+1;
end
```

```
    asphdistcr=MWDistCumMassCr((g-1),1)+(481-MWDistCumMassCr((g-1),2))*...
        (MWDistCumMassCr(g,1)-MWDistCumMassCr((g-1),1))...
        /(MWDistCumMassCr(g,2)-MWDistCumMassCr((g-1),2));

    YieldDist=asphdistcr;
    ConvVR=((1-asphdist)-(1-asphdistcr))/(1-asphdist);

    end
end


figure
plot(MWDistMass(:,2),MWDistMass(:,1),MWDistMassCr(:,2),MWDistMassCr(:,1))
legend('Initial','Final')
xlabel('MW')
ylabel('Mass fraction')

figure
plot(MWDistCumMass(:,2),MWDistCumMass(:,1),MWDistCumMassCr(:,2),...
    MWDistCumMassCr(:,1))
legend('Initial','Final')
xlabel('MW')
ylabel('Cumulative mass fraction')

figure
plot(MWDistmod(:,2),MWDistmod(:,1),MWDistCr(:,2),MWDistCr(:,1))
legend('Initial','Final')
xlabel('MW')
ylabel('Mole fraction')

figure
plot(MWDistCum(:,2),MWDistCum(:,1),MWDistCumCr(:,2),MWDistCumCr(:,1))
legend('Initial','Final')
xlabel('MW')
ylabel('Cumulative Mole fraction')

%-------------------------------------------------------------------------
% Cumulative mass distribution of products - compared to SimDist results
%-------------------------------------------------------------------------
% These matrixes were made as an alternative to verify previous results
%-------------------------------------------------------------------------

% Determination of mole fractions - products
    MWDistProd=zeros ((size(extwo,1)),2);
    MWDistProd(:,2)=extwo(:,1);
    for i=1:size(Asph,3)
        countm=1;
        while MWAsph(i)>MWDistProd(countm,2)
            countm = countm+1;
        end
        MWDistProd(countm,1)=MWDistProd(countm,1)+1/size(Asph,3);
    end

% Cumulative mole distribution - products
    MWDistCumProd=zeros(size(MWDistProd));
    MWDistCumProd(:,2)=MWDistProd(:,2);
    countcum=0;
    for i=1:size(MWDistProd,1)
        countcum= countcum + MWDistProd(i,1);
        MWDistCumProd(i,1)=countcum;
    end
```

```
%Determination mass fractions - products
    masspr=0;
    for i=1:size(MWDistProd,1)
        masspr=masspr+MWDistProd(i,1)*MWDistProd(i,2);
    end
    MWDistMassProd=zeros(size(MWDistProd));
    MWDistMassProd(:,2)=MWDistProd(:,2);
    for i=1:size(MWDistMassProd,1)
        MWDistMassProd(i,1)=(MWDistProd(i,1)*MWDistProd(i,2))/masspr;
    end

% Cumulative Mass cumulative - products
    MWDistCumMassProd=zeros(size(MWDistMassProd));
    MWDistCumMassProd(:,2)=MWDistMassProd(:,2);
    cummasspr=0;
    for i=1:size(MWDistCumMassProd,1)
        cummasspr= cummasspr + MWDistMassProd(i,1);
        MWDistCumMassProd(i,1)=cummasspr;
    end

%-------------------------------------------------------------------------
% SimDist results for liquid products after tetralin removal
% These results include correction for evaporation of 31% of the light
% material during rotary evaporation
% This data was processed in VMGSim to generate pseudo-components. MW was
% calculated with Sim and Daubert's correlation
%-------------------------------------------------------------------------
CLProdone=[0.3788   213.44
0.3870  225.73
0.3995  236.54
0.4137  248.71
0.4293  261.07
0.4447  273.71
0.4607  286.73
0.4810  300.01
0.5008  312.53
0.5176  326.45
0.5321  340.65
0.5458  355.16
0.5722  377.60
0.5977  408.51
0.6224  439.35
0.6471  472.77
0.6706  507.42
0.6960  543.38
0.7205  579.04
0.7426  617.61
0.7713  673.66
0.7789  701.49];
CLProdtwo=[0.7829   716.35
0.7869  731.35
0.7945  760.24
0.8182  849.80
0.8423  942.51
0.8667  1042.28
0.8916  1147.23
0.9168  1255.07
0.9191  1315.97];

figure
plot(MWDistCumMassCr(:,2),MWDistCumMassCr(:,1),...
```

```
    CLProdone(:,2),CLProdone(:,1),'r-
',CLProdtwo(:,2),CLProdtwo(:,1),'r:')
    %MWDistCumMassProd(:,2),MWDistCumMassProd(:,1),'m:',...
legend('Simulation 1','Experimental')
xlabel('MW')
ylabel('Cumulative Mass Fraction')

%--------------------------------------------------------------------------
%--------------------------------------------------------------------------
% Results are also shown in % mass vs. Tb
%--------------------------------------------------------------------------
%--------------------------------------------------------------------------
CLProdTbone=[0.3788 274
0.3870  289
0.3995  302
0.4137  316
0.4293  330
0.4447  344
0.4607  358
0.4810  372
0.5008  385
0.5176  399
0.5321  413
0.5458  427
0.5722  448
0.5977  476
0.6224  503
0.6471  531
0.6706  559
0.6960  587
0.7205  614
0.7426  642
0.7713  681
0.7789  700];
CLProdTbtwo=[0.7829 710
0.7869  720
0.7945  739
0.8182  795
0.8423  850
0.8667  906
0.8916  962
0.9168  1017
0.9191  1047];

TbDistCumMassProd=zeros(size(MWDistCumMassCr));
TbDistCumMassProd(:,1)=MWDistCumMassCr(:,1);

% Tb calculated from Sim and Daubert's correlation with SimDist data for
% asphaltenes before reaction and using MW ranges for asphaltenes

TbDistCumMassProd(:,2)=[135.5
172.1
208.8
245.4
282.0
317.5
350.8
382.4
402.5
428.0
468.3
498.6
```

```
532.8
563.0
596.7
624.7
655.8
681.9
707.0
732.1
760.0
779.5
810.0
832.2
854.2
878.8
899.8
920.1
940.1
960.1
985.7
1008.0
1023.7
1045.3
1066.8
1085.3
1103.8
1122.3
1143.8
1162.3
1183.8
1202.3
1220.8
1240.8
1260.8
1279.3
1297.8
1319.3
1337.8
1357.8
1377.8
1402.4
1422.5
1440.9
1460.9
1479.4
1501.0
1519.4
1537.9
1557.9
1576.4
1596.4
1616.4
1636.4
1654.9
1676.5
1696.5
1713.4
1876.6
2122.9];

figure
plot(TbDistCumMassProd(:,2),TbDistCumMassProd(:,1),...
    CLProdTbone(:,2),CLProdTbone(:,1),'r-',...
```

```
    CLProdTbtwo(:,2),CLProdTbtwo(:,1),'r:')
    %TbDistCumMassProd(:,2),TbDistCumMassProd(:,1),'m:',...
legend('Simulation 1','Experimental')
xlabel('Tb')
ylabel('Cumulative Mass Fraction')

%--------------------------------------------------------------------------
%--------------------------------------------------------------------------
% Determination of <343C and >650C
%--------------------------------------------------------------------------
%--------------------------------------------------------------------------

% Determination of < 343C fraction

crd=1;
while TbDistCumMassProd(crd,2)<343
    crd=crd+1;
end
lights=TbDistCumMassProd((crd-1),1)+(343-TbDistCumMassProd((crd-1),2))*...
    (TbDistCumMassProd(crd,1)-TbDistCumMassProd((crd-1),1))...
    /(TbDistCumMassProd(crd,2)-TbDistCumMassProd((crd-1),2));

% Determination of > 650C fraction

crd=1;
while TbDistCumMassProd(crd,2)<650
    crd=crd+1;
end
ligvr=TbDistCumMassProd((crd-1),1)+(650-TbDistCumMassProd((crd-1),2))*...
    (TbDistCumMassProd(crd,1)-TbDistCumMassProd((crd-1),1))...
    /(TbDistCumMassProd(crd,2)-TbDistCumMassProd((crd-1),2));
heavy=1-ligvr;

%--------------------------------------------------------------------------
% Determination of distribution of # of building blocks in molecules
%--------------------------------------------------------------------------

FragDistCr=zeros(15,2);
FragDistCr(:,1)=[1:1:15];
FragDistMassCr=zeros(15,2);
FragDistMassCr(:,1)=[1:1:15];
for i=1:mlc
    fragcr=0;
    mxblocks=15;
    for j=1:mxblocks
        if Asph(j,j,i)~=0
            fragcr = fragcr+1;
        end
    end
    FragDistCr(fragcr,2)=FragDistCr(fragcr,2)+(1/mlc);

FragDistMassCr(fragcr,2)=FragDistMassCr(fragcr,2)+MWAsph(i)/sum(MWAsph);
end
figure
plot(FragDistCr(:,1), FragDistCr(:,2))
xlabel('# Building blocks')
ylabel('Fraction of molecules')
title('Building blocks Distribution')
figure
plot(FragDistMassCr(:,1), FragDistMassCr(:,2))
xlabel('# Building blocks')
ylabel('Mass Fraction')
```

```
title('Building blocks Distribution')

%Cumulative distribution of building blocks
CumFragDistCr = zeros(size(FragDistCr));
CumFragDistCr(:,1)=FragDistCr(:,1);
CumFragMassDistCr = zeros(size(FragDistMassCr));
CumFragMassDistCr(:,1)=FragDistMassCr(:,1);
cumone=0;
cumtwo=0;
for i=1:size(CumFragDistCr,1)
    cumone= cumone + FragDistCr(i,2);
    CumFragDistCr(i,2)=cumone;
    cumtwo=cumtwo + FragDistMassCr(i,2);
    CumFragMassDistCr(i,2)=cumtwo;
end
figure
plot(CumFragDistCr(:,1), CumFragDistCr(:,2))
xlabel('# Building blocks')
ylabel('Cumulative Fraction of molecules')
title('Building blocks Distribution')
figure
plot(CumFragMassDistCr(:,1), CumFragMassDistCr(:,2))
xlabel('# Building blocks')
ylabel('Cumulative Mass Fraction')
title('Building blocks Distribution')
end
```

A4- 4 Function Rearrange

```
%-------------------------------------------------------------------------
%-------------------------------------------------------------------------
%                R   E   A   R   R   A   N   G   E
%-------------------------------------------------------------------------
%-------------------------------------------------------------------------
% MATLAB File name: Rearrange.m
% Rearrange function is able to reorganize the building blocks and
% connections to eliminate empty spaces on the main diagonal of the
% cracked molecules
% Building blocks are moved to the last empty position on the diagonal of
% the matrix, and all vertical and horizontal connections are relocated
%-------------------------------------------------------------------------
% R o s a   I.   R u e d a - V e l á s q u e z
% U n i v e r s i t y   o f    A l b e r t a
% 2012
%-------------------------------------------------------------------------

function A=Rearrange(A)
for i=1:size(A,1)
    if A(i,i)==0
        newpos=i;
        while A(newpos,newpos)==0 && newpos<size(A,1)
           newpos=newpos+1;
        end
        if A(newpos, newpos)~=0
            A(i,i)=A(newpos,newpos);
            A(newpos,newpos)=0;
            % Horizontal connections, same column but new row
            for j=(newpos+1):size(A,1)
                if A(newpos,j)==1
                    A(i,j)=A(newpos,j);
                    A(newpos,j)=0;
                end
            end
            % Vertical connection, same row but new column
            if any(A(:,newpos))==1
                newlk=1;
                while A(newlk,newpos)==0
                    newlk=newlk+1;
                end
                A(newlk,i)=A(newlk,newpos);
                A(newlk,newpos)=0;
            end
        end
    else
    end
end
```

A4- 5 Function OrgAsph

```
%-------------------------------------------------------------------------
%-------------------------------------------------------------------------
%               ORGANIZATION OF REACTED MOLECULES BY MW
%-------------------------------------------------------------------------
%-------------------------------------------------------------------------
% MATLAB File name: OrgAsph.m
% ReactAsph.m was created to check the resulting molecules after the
% cracking reaction. This routine organizes the molecules by MW range
% and counts the number of molecules in each MW range
%-------------------------------------------------------------------------
% R o s a   I.   R u e d a - V e l á s q u e z
% U n i v e r s i t y   o f    A l b e r t a
% 2012
%-------------------------------------------------------------------------

function [Asphorg,MWAsphorg,MWmolcounter]=OrgAsph(Asph,MWAsph)

MW=[100
130
160
190
220
250
280
310
330
356.25
400
434.375
475
512.5
556.25
593.75
637.5
675
712.5
750
793.75
825
875
912.5
950
993.75
1031.25
1068.75
1106.25
1143.75
1193.75
1237.5
1268.75
1312.5
1356.25
1393.75
1431.25
1468.75
1512.5
1550
1593.75
1631.25
```

```
1668.75
1709.375
1750
1787.5
1825
1868.75
1906.25
1946.875
1987.5
2037.5
2078.125
2115.625
2156.25
2193.75
2237.5
2275
2312.5
2353.125
2390.625
2431.25
2471.875
2512.5
2550
2593.75
2634.375
2668.75
3000
3500];

ranges=size(MW,1);
popl=size(Asph,3);
org=0;
MWcount=zeros(size(MW));

for i=1:ranges
    for j=1:popl
        if i==1
            if MWAsph(j)<=MW(i)
                MWcount(i)=MWcount(i)+1;
                org=org+1;
                Asphorg(:,:,org)=Asph(:,:,j);
                MWAsphorg(org)=MWAsph(j);
            end
        else
            if MWAsph(j)<=MW(i)&& MWAsph(j)>MW(i-1)
                MWcount(i)=MWcount(i)+1;
                org=org+1;
                Asphorg(:,:,org)=Asph(:,:,j);
                MWAsphorg(org)=MWAsph(j);
            end
        end
    end
end
MWmolcounter(:,1)=MW;
MWmolcounter(:,2)=MWcount;
end
```

References

1. Qian, K.; Dechert, G. J. Recent Advances in Petroleum Characterization by GC Field Ionization Time-of-Flight High-Resolution Mass Spectrometry. Analytical Chemistry 2002, 74, 3977-3983.